

Fall 8-20-2014

Submonomer Synthesis and Structure-activity Relationship Studies of Azapeptide Inhibitors of the Insulin Receptor Tyrosine Kinase

Lathamol A. Kurian
lathamol.kurian@student.shu.edu

Follow this and additional works at: <https://scholarship.shu.edu/dissertations>

 Part of the [Amino Acids, Peptides, and Proteins Commons](#), [Biochemistry Commons](#), and the [Medicinal Chemistry and Pharmaceutics Commons](#)

Recommended Citation

Kurian, Lathamol A., "Submonomer Synthesis and Structure-activity Relationship Studies of Azapeptide Inhibitors of the Insulin Receptor Tyrosine Kinase" (2014). *Seton Hall University Dissertations and Theses (ETDs)*. 1991.
<https://scholarship.shu.edu/dissertations/1991>

**SUBMONOMER SYNTHESIS AND STRUCTURE-ACTIVITY
RELATIONSHIP STUDIES OF AZAPEPTIDE INHIBITORS OF THE
INSULIN RECEPTOR TYROSINE KINASE**

*A thesis submitted to Seton Hall University in partial fulfillment of the requirements for the
degree of Doctor of Philosophy*

By

Lathamol A. Kurian

August 2014

Department of Chemistry and Biochemistry
Seton Hall University
South Orange, NJ, USA

DISSERTATION COMMITTEE APPROVALS

We certify that we have read this thesis and in our opinion it is sufficient in scientific scope and quality as a dissertation for the degree of Doctor in Philosophy.

APPROVED BY:



David Sabatino, Ph.D.
Advisor, Seton Hall University



Stephen P. Kelty, Ph.D.
Reader, Member of Dissertation Committee,
Seton Hall University



Fr. Gerald Buonopane, Ph.D.
Reader, Department of Chemistry and Biochemistry,
Seton Hall University



Nicholas H. Snow, Ph.D.
Chair, Department of Chemistry and Biochemistry,
Seton Hall University

Dedicated to my family, Iype Isac, Daniel Iype and Josha Iype

THESIS ABSTRACT

Aza-peptides are a class of peptide mimics (peptidomimetics), which have served as valuable tools for the development of peptide based therapeutic agents. The therapeutic promise of aza-peptides has been correlated to its primary sequence modification which translates into bio-active secondary structures that improves the pharmacological properties of the native peptide sequence. More specifically, aza-peptides contain a semicarbazide within the peptide backbone which restricts the peptide bond torsion angles (ϕ , ψ) into pre-organized β -turn secondary structures. Thus, aza-peptides have been shown to stabilize bio-active β -turn secondary structures responsible for high affinity and selective binding to a target receptor or enzyme in order to modulate its activity for therapeutic purpose. Moreover, aza-peptides have been found to be stable in biological media thereby improving their therapeutic indices and pharmacokinetic properties. For example, Goserelin, an aza-Gly peptide analog has received FDA approval in 1989 for the treatment of prostate and breast cancers. Therefore, the systematic substitution of aza amino acid residues within bio-active sequences (aza-amino acid scanning) has been shown to be useful in the conversion of native peptides into lead therapeutic peptidomimetics. The submonomer approach for aza-peptides synthesis has been especially useful in aza-amino acid scanning and in the production of diverse aza-peptides for structure-activity relationship studies with therapeutic targets. In this thesis, the submonomer approach for aza-peptide synthesis is put into practical use for the development of aza-peptide inhibitors of the Insulin Receptor Tyrosine Kinase (IRTK) domain.

Overexpression or unregulated signal transduction of the IRTK has been associated with increased levels of gene expression and cell proliferation that are hallmarks of tumor

progression. Thus, the inhibition of un-regulated tyrosine kinase phosphorylation of the insulin receptor may prove to be an efficient method of cancer therapy. Towards this goal, the synthetic pentapeptide, Ac-DIYET-NH₂ derived from the activation loop of the insulin receptor was found to inhibit the autophosphorylation of the IRTK to about 80% at 4 mM. Moreover, molecular docking simulation studies indicated that, Ac-DIYET-NH₂, was bound within the active site of the IRTK with a folded peptide structure that was reminiscent of a turn geometry.

In order to identify the location and importance of a turn structure on the inhibitory activity of Ac-DIYET-NH₂, aza-modifications within the IYE region were developed for structure activity relationship studies. Submonomer solid phase synthesis was used for the production of azapeptides, featuring the introduction of new aza-Ile and aza-DOPA residues. The azapeptides were analyzed and purified by reverse-phase LCMS in order to ascertain purity (>95%) and identity prior to structure-activity relationship studies. Molecular modeling and docking simulation studies revealed that the Ac-DIazaYET-NH₂ sequence, adopted a β -turn conformation that bound to the kinase domain of the IRTK. The azapeptide β -turn conformation was also proven by CD and NMR spectroscopy. The inhibitory activity of the peptides, Ac-DIYET-NH₂ vs Ac-DIazaYET-NH₂, was evaluated in a single dose experiment (400 μ M), which indicated minimal inhibitory activity (<10%) for the parent peptide, Ac-DIYET-NH₂, whereas, Ac-DIazaYET-NH₂ displayed 50% inhibition of the IRTK autophosphorylation. These results validate the importance of the peptide β -turn geometry on the inhibition of IRTK phosphorylation. This finding is not only important towards the development of potent azapeptide inhibitors of the IRTK for potential anti-cancer applications, but also in the design of novel probes for studying the mechanisms and kinetics associated with this important class of tyrosine kinases.

AKNOWLEDGEMENTS

I would like to take this time to express my gratitude for my mentor, Dr. David Sabatino. This thesis would never have been possible without his tireless efforts. His guidance, patience and support enabled this great desire in my life to become a reality. I believe no words are sufficient to express my respect and gratitude for him. It was an honor for me to be his student for the last 4 years and the knowledge that I have gained from him will help me to excel in days to come. Thank you so much Dr. Sabatino and, I wish to see you making great impact in the scientific community along with shaping the future of many students in the coming years. I would like to thank the Sabatino team for all their love and support.

I would like to thank Fr. Gerry and Professor Kelty for their help with the dissertation review. I would like to thank Professors John Sowa, Marzabadi and Wei for being a part of my dissertation committee. I would like to thank Professor Kazakevich for teaching me separation techniques. Thank you again for all the support and guidance during my stay at Seton Hall University. I would also like to thank Professors, Murphy, Snow, Antonacci and Gorun for their help during my studies at Seton Hall University. I would like to thank Maureen and Rose for all their help.

I am so delighted; I had the opportunity to be part of Seton Hall University for this great achievement. My special thanks to the Department of Chemistry and Biochemistry for admitting me into the program. I also thank the other students, who were good friends of mine at Seton Hall University.

I can't write the sacrifice my family had to go through for last 4 years without tears. It was three full time jobs for me. Though it was painful for me and my family, they were so

supportive and kind. I am so thankful to my wonderful husband, Iype Isac who encouraged me the way my mom used to do for me during my young age. My two precious kids, Daniel Iype was 5 years old and Joshua Iype was 3 years old when I started this journey. Now they have requested me to mention them as “big supporters” for this great achievement. Thank you so much epic kids for your great support!!

My great Dad, P.P. Kurian and my family assisted me to school many times during weekends. I express my thanks to my parents at this time for infecting me with the passion for education. I would like to express special thanks to my father-in law, V.I. Isac, my brother-in-law Anil Isac and my sister Lekha Mathew & family at this time for all the prayers and support. I would like to express my thanks to Sandoz (Novartis Company) and Actavis for supporting my studies. I express my sincere thanks to all my friends and other family members for their support.

I am so thankful to my Lord and Savior, the maker of heaven and earth, who walks with me and strengthens me all these days. Psalm 34:5 says - **Those who look to Him are radiant; their faces are never covered with shame. Praise God!**

TABLE OF CONTENTS

DEDICATION	iii
ABSTRACT	iv
ACKNOWLEDGEMENTS	vi
TABLE OF CONTENTS	viii
ABBREVIATIONS AND SYMBOLS	xii
LIST OF FIGURES	xvii
LIST OF TABLES	xxi
LIST OF SCHEMES	xxi

CHAPTER 1. AZAPEPTIDES: AN OVERVIEW OF THEIR SYNTHESIS, STRUCTURE AND APPLICATIONS IN MEDICINAL CHEMISTRY

1.1 ABSTRACT	1
1.2 INTRODUCTION	2
1.3 SYNTHESIS	4
1.3.1 Activation and coupling of aza-amino acids	4
1.3.2 Synthesis of azapeptides using <i>N</i> -Fmoc <i>N'</i> -alkyl carbazates	5
1.3.3 Submonomer Azapeptide Synthesis	7
1.4 CONFORMATIONAL PROPERTIES	9
1.5 MEDICINAL CHEMISTRY APPLICATIONS	14
1.5.1 Azapeptides as receptor agonists and antagonists	14
1.5.2 Azapeptides as Protease Inhibitors	17
1.6 CONCLUSIONS	19

1.7	THESIS OBJECTIVES	20
1.8	REFERENCES	23

CHAPTER 2. SOLID PHASE SUBMONOMER SYNTHESIS OF AZAPEPTIDE ANALOGS OF THE Ac-DIYET-NH₂ SEQUENCE

2.1	ABSTRACT	28
2.2	INTRODUCTION	28
2.3	CHAPTER OBJECTIVES	38
2.4	RESULTS AND DISCUSSION	39
2.5	CONCLUSIONS	45
2.6	EXPERIMENTAL SECTION	45
2.7	REFERENCES	56

CHAPTER 3. AZAPEPTIDE STRUCTURAL STUDIES BY MOLECULAR MODELING, CD AND NMR SPECTROSCOPY

3.1	ABSTRACT	58
3.2	INTRODUCTION	59
3.2.1	Azapeptide Structure and Conformation	59
3.2.2	Computational Analyses	60
3.2.3	CD Spectroscopy	61
3.2.4	NMR Spectroscopy	63
3.3	CHAPTER OBJECTIVES	64
3.4	RESULTS AND DISCUSSION	65
3.4.1	Molecular Modeling and Docking Studies	65
3.4.2	CD Spectroscopy	69
3.4.3	NMR Spectroscopy	76

3.5	CONCLUSIONS	79
3.6	EXPERIMENTAL SECTION	80
3.6.1	Materials	80
3.6.2	Computational Analysis	80
3.6.3	CD Spectroscopy	80
3.6.4	NMR Spectroscopy	81
3.6.5	Characterization Data	81
3.7	REFERENCES	85

CHAPTER 4. IRTK INHIBITORY ACTIVITY OF AZAPEPTIDES

4.1	ABSTRACT	87
4.2	INTRODUCTION	88
4.2.1	Signaling Activities of the Receptor Tyrosine Kinase	88
4.2.2	The Insulin Receptor Tyrosine Kinase	89
4.2.3	Inhibition of IRTK phosphorylation by the DIYET sequence	94
4.3	CHAPTER OBJECTIVES	95
4.4	RESULTS AND DISCUSSION	96
4.4.1	IRTK Phosphorylation Studies	96
4.4.2	Inhibition of IRTK Phosphorylation	98
4.5	CONCLUSIONS	102
4.6	REFERENCES	103
4.7	EXPERIMENTAL METHODS	104
4.7.1	Materials and Methods	104
4.7.2	Phosphorylation reactions of the IRTK	105
4.7.3	Inhibition studies of the IRTK	106

4.7.4	Western blotting	106
CHAPTER 5. CONCLUSIONS AND CONTRIBUTIONS TO KNOWLEDGE		
5.1	CONCLUSIONS AND CONTRIBUTIONS TO KNOWLEDGE MADE IN THIS THESIS	107
5.1.1	Design, Synthesis and Conformational Analyses of Azapeptide Inhibitors of the IRTK	107
5.1.2	Biological Activity of Azapeptide Analogs	110
5.1.3	Future Work	112
5.2	PUBLICATIONS AND CONFERENCE PRESENTATIONS	113
	APPENDIX A	115 - 172

ABBREVIATIONS AND SYMBOLS

A or Ala	alanine
AP	alkaline phosphatase
ATP	adenosine triphosphate
Ac ₂ O	acetic anhydride
BCIP	5-bromo-4-chloro-3-indolyl phosphate
BSA	bovine serum albumin
BTPP	tert-butylimino-tri(pyrrolidino)phosphorane
BnBr	benzyl bromide
C or Cys	cysteine
CCl ₄	carbon tetrachloride
CD	circular dichroism
CDI	carbonyldiimidazole
CGRP	calcitonin gene-related peptide
CH ₃ CN	acetonitrile
D or Asp	aspartate
DCM	dichloromethane
DIC	<i>N,N'</i> -diisopropylcarbodiimide
DIEA	diisopropylethylamine
DMF	<i>N,N'</i> -dimethylformamide
DMSO	dimethylsulfoxide
DTT	dithioreitol
EDTA	ethylenediaminetetraacetate

ESI-MS	electrospray ionization mass spectrometry
EtOH	ethanol
FA	formic acid
FDA	food and drug administration
FTIR	fourier transform infra-red
For Phe	phenylalanine
Fmoc	fluorenylmethyloxycarbonyl
G or Gly	glycine
E or Glu	glutamate
FSH	follicle-stimulating hormone
g	gram
g/mol	grams pre mole
GHRP	growth hormone releasing peptide
h	hours
HCV	hepatitis C virus
HCTU	O-(1H-6-Chlorobenzotriazole-1-yl)-1,1,3,3-tetramethyluronium hexafluorophosphate
H ₂ O	water
H or His	histidine
HepG2	human hepatoblastoma liver carcinoma cell line
I or Ile	Isoleucine
IRTK	insulin receptor tyrosine kinase
kDa	kilodalton
KCl	potassium chloride

K or Lys	lysine
KOtBu	potassium <i>tert</i> -butoxide
LH-RH	leutinizing hormone releasing hormone
LCMS	liquid chromatography mass spectrometry
L or Leu	leucine
mM	millimolar
<i>m/z</i>	mass to charge ratio
MCR	melanocortin receptor
M, Met	methionine
MeCN	acetonitrile
MeOH	methanol
MCR	melanocortin receptor
mg	milligram
MgCl ₂	magnesium chloride
MgSO ₄	magnesium sulphate
MnCl ₂	manganese chloride
mol	mole
μmol, μM	micromole, micromolar
μL	microliter
NBT	nitroblue tetrazolium
NaCl	sodium chloride
NH ₂ OH.HCl	hydroxylamine hydrochloride
Na ₂ SO ₄	sodium sulphate

NMM	<i>N</i> -methyilmorpholine
N _{2(g)}	nitrogen gas
NMR	nuclear magnetic resonance
NOE	nuclear overhauser effect
PAGE	polyacrylamide gel electrophoresis
Pd/C	palladium/carbon
PDA	photodiode array
PDB	protein data bank
PBS	phosphate buffered saline
P or Pro	proline
PSI	Peptide Scientific Inc.
PTK	protein tyrosine kinase
PVDF	polyvinylidene difluoride
R or Arg	arginine
RP-HPLC	reverse-phase high performance liquid chromatography
rpm	rotations per minute
RT	retention time
SAR	structure activity relationship
S or Ser	serine
SPPS	solid phase peptide synthesis
T or Thr	threonine
<i>t</i> -Bu	<i>tert</i> -butyl
TES	triethylsilane

TFA	trifluoroacetic acid
THF	tetrahydrofuran
TLC	thin layer chromatography
UPS	unnatural peptide synthesis
UV-Vis	ultraviolet-visible
V or Val	valine
v/v	volume per volume
W or Trp	tryptophan
Y or Tyr	tyrosine

LIST OF FIGURES

CHAPTER 1

- Figure 1.1.** Comparison of peptide and azapeptide primary structure 3
- Figure 1.2.** Azapeptide β -turn conformation defined by its ϕ and ψ dihedral angles 9
- Figure 1.3.** Structures of naturally occurring β -turn types in peptides and proteins 10
- Figure 1.4.** NOE correlations found within Boc-Ala-Phe-azaLeu-Ala-OMe 13
- Figure 1.5.** Lead RGD azapeptide mimic, **1.24**, as a selective and potent antagonist of the $\alpha\text{v}\beta_3$ receptor. 16
- Figure 1.6.** Representative azapeptide covalent inhibitors of cysteine proteases. 18
- Figure 1.7.** Macrocyclic azapeptide inhibitor, BILN 2061, of HCV NS3 serine protease. 20

CHAPTER 2

- Figure 2.1.** Submonomer synthesis of ten GHRP-6 azapeptides. Figure adapted from reference 6. 34
- Figure 2.2.** Aza-Glu GHRP-6 azapeptide binding interactions to the CD36 scavenger receptor. Figure adapted from reference 17. 35
- Figure 2.3.** Structure comparison of lysine and a constrained aza-lysine mimic. Figure adapted from reference 20. 37

Figure 2.4.	Structure of <i>N</i> -amino-imidazolin-2-one. Figure adapted from reference 21-22.	38
Figure 2.5.	Aza-amino acid scanning of Ac-DIYET-NH ₂ , 2.28 , for IRTK inhibitory activity.	39
Figure 2.6.	LCMS spectra of Ac-DIazaYET-NH ₂ , 2.36 .	42
CHAPTER 3		
Figure 3.1.	Binding model of the pentapeptide ligand, Ac-DIYET-NH ₂ , 2.28 within the active site of the IRTK.	61
Figure 3.2.	Peptide secondary structure analyses.	63
Figure 3.3.	Crystal structure of the IRTK downloaded from the Protein Data Bank (PDB ID # 1IR3).	66
Figure 3.4.	Binding models of the azapeptide Ac-DIazaYET-NH ₂ , 2.36 , for the IRTK binding domain.	68
Figure 3.5.	Binding models of the native pentapeptide Ac-DIYET-NH ₂ , 2.28 , for the IRTK binding domain.	69
Figure 3.6.	CD spectra for Ac-DazaIYET-NH ₂ , 2.38 , Ac-DazaAYET-NH ₂ , 2.37 , Ac-DazaGYET-NH ₂ , 2.39 , (20 μM) in water, at 25 °C.	70
Figure 3.7.	CD spectra for Ac-DazaIYET-NH ₂ , 2.38 , Ac-DazaAYET-NH ₂ , 2.37 , Ac-DazaGYET-NH ₂ , 2.39 , (20 μM) in phosphate buffer, at 25 °C.	71
Figure 3.8.	CD spectra for Ac-DazaIYET-NH ₂ , 2.38 , Ac-DazaAYET-NH ₂ , 2.37 ,	71

Ac-DazaGYET-NH₂, **2.39**, (20 μM) in DMSO, at 25 °C.

- Figure 3.9.** CD spectra for Ac-DIazaYET-NH₂, **2.36**, Ac-DIazaFET-NH₂, **2.40**, Ac-DIaza(DOPA)ET-NH₂, **2.41**, (20 μM) in water, at 25 °C. 72
- Figure 3.10.** CD spectra for Ac-DIazaYET-NH₂, **2.36**, Ac-DIazaFET-NH₂, **2.40**, Ac-DIaza(DOPA)ET-NH₂, **2.41**, (20 μM) in phosphate buffer, at 25 °C. 73
- Figure 3.11.** CD spectra for Ac-DIazaYET-NH₂, **2.36**, Ac-DIazaFET-NH₂, **2.40**, Ac-DIaza(DOPA)ET-NH₂, **2.41**, (20 μM) in DMSO, at 25 °C. 73
- Figure 3.12.** CD spectra for Ac-DIYazaET-NH₂, **2.42**, (20 μM) in water, at 25 °C. 74
- Figure 3.13.** CD spectra for Ac-DIYazaET-NH₂, **2.42**, (20 μM) in phosphate buffer, at 25 °C. 75
- Figure 3.14.** CD spectra for Ac-DIYazaET-NH₂, **2.42**, (20 μM) in DMSO, at 25 °C. 75
- Figure 3.15.** ¹H NMR spectra of (B) Ac-DIYET-NH₂, **2.28**, and (A) Ac-DIazaYET-NH₂, **2.36** (2 mM) in DMSO-d₆. 77
- Figure 3.16.** 2D NOESY spectrum and conformational analysis of Ac-DIazaYET-NH₂, **2.36**, (2 mM) in DMSO-d₆. 78

CHAPTER 4

- Figure 4.1.** Figurative description of the IRTK. Figure adapted from: 90
<http://grimwade.biochem.unimelb.edu.au/tutorial/s2730e.gif>.

Figure 4.2.	Phosphorylation sites of the IRTK. Figure adapted from: Hirose, M. <i>et al. Br. J. Pharm.</i> 2004 , <i>142</i> , 222 -228.	90
Figure 4.3.	Phosphorylation mechanism of the IRTK. Figure adapted from: Nelson, D.L.; Cox, M.M. <i>Lehninger Principles of Biochemistry 5 ed.</i> , 2008 , W.H. Freeman and Co. New York, NY, 440.	92
Figure 4.4.	MAP kinase signaling cascade. Figure adapted from: Nelson, D.L.; Cox, M.M. <i>Lehninger Principles of Biochemistry 5 ed.</i> , 2008 , W.H. Freeman and Co. New York, NY, 440.	93
Figure 4.5.	Western blot analyses of the IRTK phosphorylation activity.	98
Figure 4.6.	Western blot data for IRTK (200 ng/mL) phosphorylation inhibition with peptide ligands Ac- DIYET-NH ₂ (2.28), and Ac-DIazaYET-NH ₂ (2.36) at 400 μM.	99
Figure 4.7.	Western blot data for IRTK (200 ng/mL) phosphorylation inhibition with peptide ligands Ac-DIYET-NH ₂ (2.28), and Ac-DIazaYET-NH ₂ (2.36) in addition to tyrphostin inhibitor (AG1024) at 4, 40 and 400 μM.	100
Figure 4.8.	Western blot data for IRTK (200 ng/mL) phosphorylation inhibition with peptide ligands synthesized in this study at 400 μM.	101

LIST OF TABLES

CHAPTER 1

Table 1.1.	Backbone torsion angles for different types of β -turns found within azapeptides.	11
-------------------	---	----

CHAPTER 2

Table 2.1.	Characterization data of azapeptides synthesized in this study.	44
-------------------	---	----

CHAPTER 3

Table 3.1.	Binding energy calculations of Ac-DIazaYET-NH ₂ .	68
-------------------	--	----

CHAPTER 4

Table 4.1.	IRTK phosphorylation (%) in presence of peptides (400 μ M) and ATP (1000 μ M).	102
-------------------	--	-----

LIST OF SCHEMES

CHAPTER 2

Scheme 1.1.	Peptide <i>N</i> -terminus and hydrazine activation for the synthesis of azapeptides.	5
--------------------	---	---

Scheme 1.2.	Azapeptide synthesis and aza-amino acid scanning using <i>N</i> -Fmoc carbazates.	6
--------------------	---	---

Scheme 1.3.	Submonomer solid phase azapeptide synthesis method.	7
--------------------	---	---

CHAPTER 2

Scheme 2.1.	The Fmoc/Ddz-strategies for azapeptide synthesis.	30
--------------------	---	----

Scheme 2.2.	<i>N</i> -terminal isocyanate activation and carbazate coupling strategy for azapeptide synthesis.	31
Scheme 2.3.	The submonomer solid phase azapeptide synthesis method.	33
Scheme 2.4.	Copper-catalyzed <i>N</i> -arylation of semicarbazone peptide bound support. Figure adapted from reference 18.	36
Scheme 2.5.	Copper-catalyzed 1,3-dipolar cycloaddition reaction with azapropargyl glycine residues and aryl azides. Figure adapted from reference 19.	36
Scheme 2.6.	Submonomer solid-phase synthesis of Ac-DIazaYET-NH ₂ (2.36).	41
CHAPTER 4		
Scheme 4.1.	Reaction mechanism for color development using BCIP/NBT.	97

CHAPTER 1. AZAPEPTIDES: AN OVERVIEW OF THEIR SYNTHESIS, STRUCTURE AND APPLICATIONS IN MEDICINAL CHEMISTRY

1.1 ABSTRACT

Azapeptides are a class of peptide mimics (peptidomimetics), which have served as valuable tools for the development of peptide-based therapeutics. The biological activity of azapeptides has been correlated to its primary sequence and most importantly their ability to pre-organize bio-active secondary structures. Therefore, understanding the influence of azapeptide sequence and conformation on biological activity is significant for the development of selective and potent therapeutic agents. As determined by NMR, CD and IR spectroscopy, and X-ray crystallography in addition to computational analyses, the insertion of an aza-amino acid residue within a peptide sequence has been shown to pre-organize the azapeptide backbone into well folded β -turn conformations. Considering the relevance of turn structures in biologically active peptide sequences such as those belonging to the Growth Hormone Releasing Peptides (GHRPs), Oxytocin and the Leutinizing Hormone Releasing Hormone (LH-RH), azapeptide derivatives have produced enhanced peptide activity facilitating the translation of lead ligands into therapeutic agents. For example, Goserelin, an aza-Gly peptide analog has received FDA approval in 1989 for the treatment of prostate and breast cancers. Therefore, azapeptides have been adopted for the development of peptide-based drugs. At the heart of their fruitful applications are robust chemical synthesis methods which produce azapeptides by solution phase or solid phase peptide chemistry. The solution phase approach requires work-up and purification procedures following each synthetic step making the production of lengthy and more complex sequences difficult to accomplish.

Alternatively, the solid phase synthesis of azapeptides by-passes the laborious solution phase approach by employing a solid support. The first successful solid phase azapeptide syntheses involved the pre-requisite formation of the aza-amino acid building blocks in solution prior to azapeptide synthesis on solid phase. The submonomer approach introduced in 2009 circumvents any solution phase synthesis and builds azapeptides directly on solid phase. This has led to the rapid production of structurally diverse azapeptide libraries for structure-activity relationship studies with receptor targets. This chapter will highlight the role of azapeptides in biology and medicine by underscoring important contributions in synthesis and structural analyses that has enabled their widespread applications in medicinal chemistry.

1.2 INTRODUCTION

Naturally occurring peptide sequences have been isolated and synthesized for usage in biology, medicinal chemistry and pharmaceutical research. In spite of their potential, peptides are limited in their applications due to their poor stabilities in biological media, limited tissue penetration for biological activity and promiscuous binding to target receptors which restricts selectivity and potency. In an effort to mitigate these limitations, peptidomimetics have been designed to mimic naturally occurring peptides in attempts to retain the main biological function of the native sequences while enhancing their therapeutic efficacy. Many structural modifications have been incorporated within bio-active peptide sequences with the goal of producing peptide-based drugs.¹⁻³ Among these modifications, azapeptides are a class of peptide mimics which substitutes the α -carbon for a nitrogen atom in one or more amino acid producing aza-residues (**Figure 1.1**).⁴

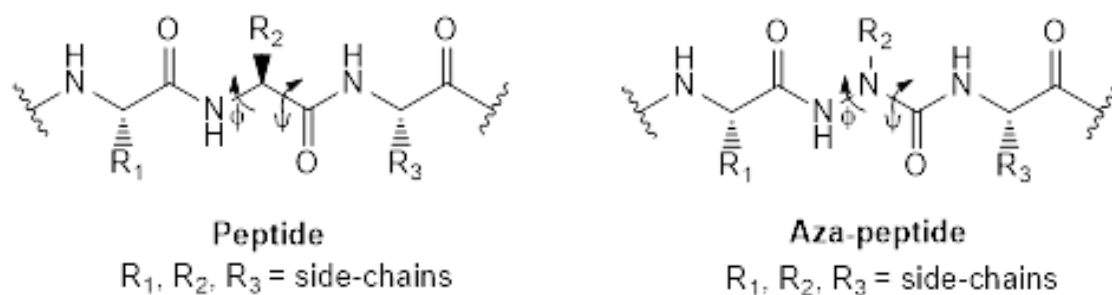


Figure 1.1. Comparison of peptide and azapeptide primary structure.

This single atom change introduces a semicarbazide into the peptide backbone which causes profound effects on configuration and structure. Replacement of an α -carbon for a nitrogen atom within the aza-residue furnishes a configurationally labile center, rapidly inverting in between two trigonal pyramidal structures. Moreover, the introduction of a N,N' -diacylhydrazine and urea moiety within the peptide backbone, constrains the φ and ψ dihedral angles producing some types of β -turn conformations as proven by CD, NMR spectroscopy, X-Ray crystallography and computational analyses.⁵

Thus, azapeptides have served to improve the structure-activity profiles of peptides by stabilizing bio-active turns which favor bioavailability, metabolic stability, receptor binding affinity and selectivity.⁴ Their fruitful applications are based on robust and efficient synthetic methods that have produced azapeptides by either solution phase or solid phase peptide synthesis. The submonomer method for azapeptide synthesis has been especially productive and has led to the generation of structurally diverse azapeptides for exploring the influence of structure on biological activity with receptor targets.⁶

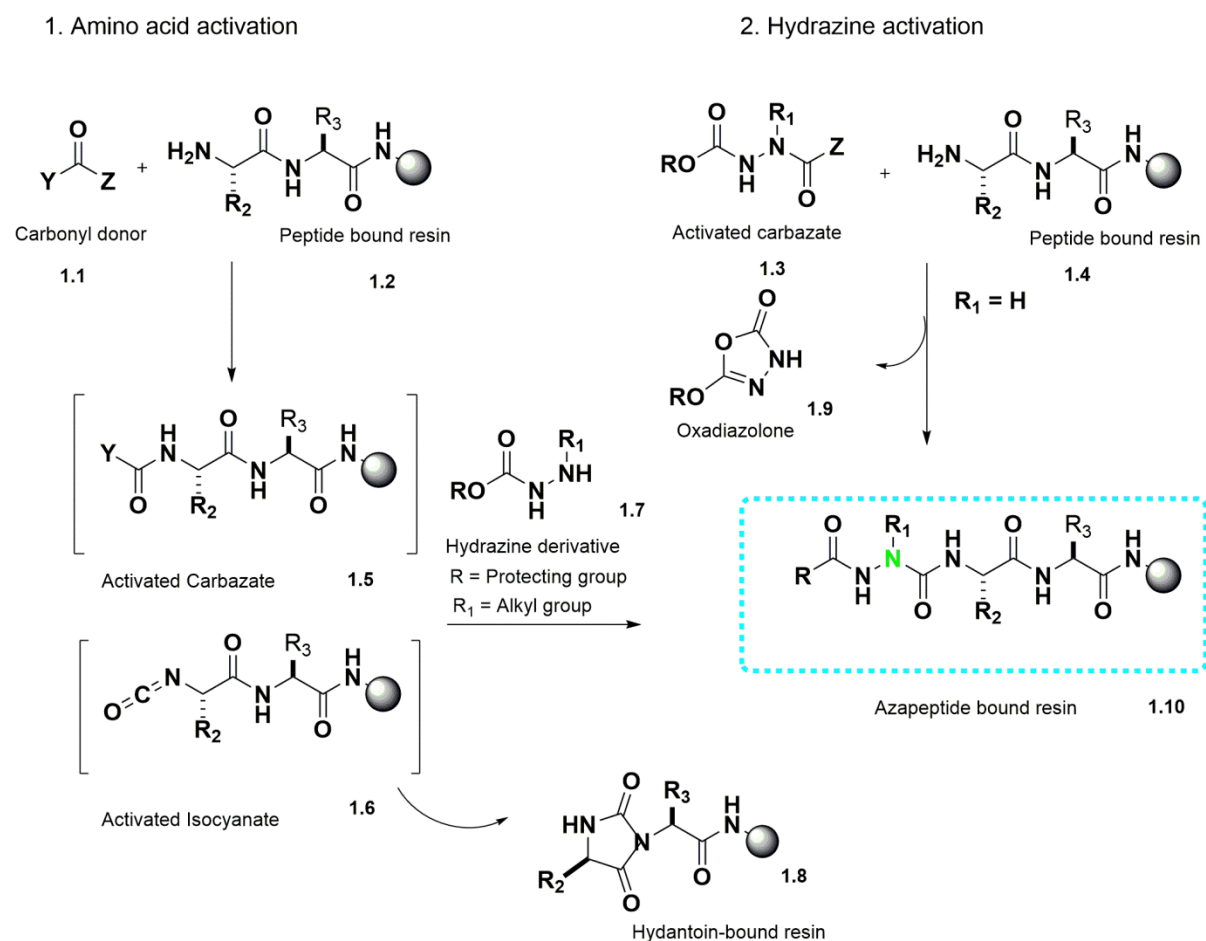
1.3 SYNTHESIS

Azapeptide synthesis is a combination of hydrazine and peptide chemistry. Azapeptides have been historically prepared by either activation of the hydrazine moiety or by activation of the peptide *N*-terminus. Following activation, a coupling step attaches the aza-amino acid building block to the peptide sequence. At this stage, conventional peptide synthesis is continued until the desired azapeptide has been produced. This strategy has been adopted in solution and on solid phase, necessitating laborious steps in the production of the aza-amino acid building blocks and in the synthesis of the coveted azapeptides. The submonomer approach has been developed to circumvent any solution phase chemistry by building the azapeptide directly on solid phase. Thus, a combination of in-solution and solid phase techniques have been crafted for making azapeptides in order to explore their structure-activity relationships.

1.3.1 ACTIVATION AND COUPLING OF AZA-AMINO ACIDS

The *N*-terminus of the growing peptide bound to a solid support has been activated with carbonyl donors, including *bis*-(2,4-dinitrophenyl)^{7,8} carbonate and carbonyldiimidazole (CDI)⁹⁻¹², *bis*(pentafluorophenyl) carbonate¹³⁻¹⁶, triphosgene¹⁷⁻¹⁹, phosgene²⁰⁻²⁴ to produce reactive isocyanates, or equivalent carbamoyl halides or active carbamates prior to coupling with a suitably protected hydrazide (**Scheme 1.1, Peptide *N*-terminus Activation**). The major drawback of this method is the intermolecular nucleophilic attack at the activated isocyanate by the secondary amide nitrogen leading to the formation of the hydantoin byproduct which prematurely terminates azapeptide synthesis. Although reversible amide bond protecting groups have been introduced to prevent hydantoin formation, these methods

require additional protection and deprotection steps lengthening the synthetic procedures.⁸ Conversely, activated carbazate intermediates have been prepared by hydrazine activation with similar carbonyl donors^{10-12,15-24} and coupled to peptide bound resin to manufacture the azapeptide on solid phase (**Scheme 1.1 Hydrazine Activation**).

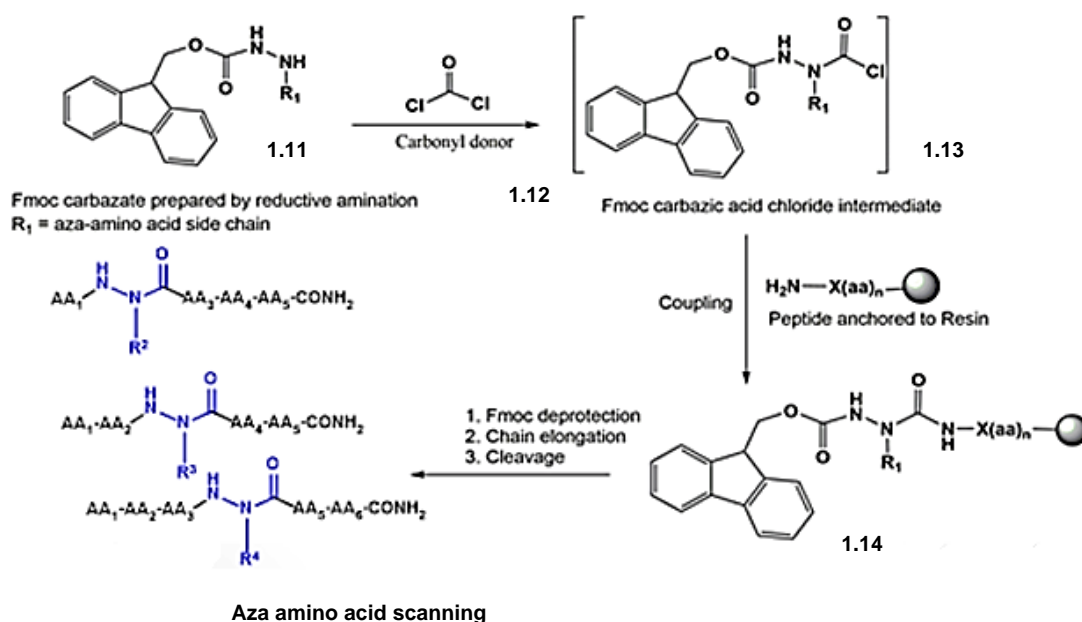


Scheme 1.1. Peptide *N*-terminus and hydrazine activation for the synthesis of azapeptides.⁷⁻²⁴

1.3.2 SYNTHESIS OF AZAPEPTIDES USING *N*-FMOC *N'*-ALKYL CARBAZATES

This hydrazine activation method was one of the first efficient strategies for scanning the importance and location of turn structures by the incorporation of aza-amino acids within bio-active peptide sequences.¹¹ The methodology (**Scheme 1.2**), aptly named, *aza-amino acid*

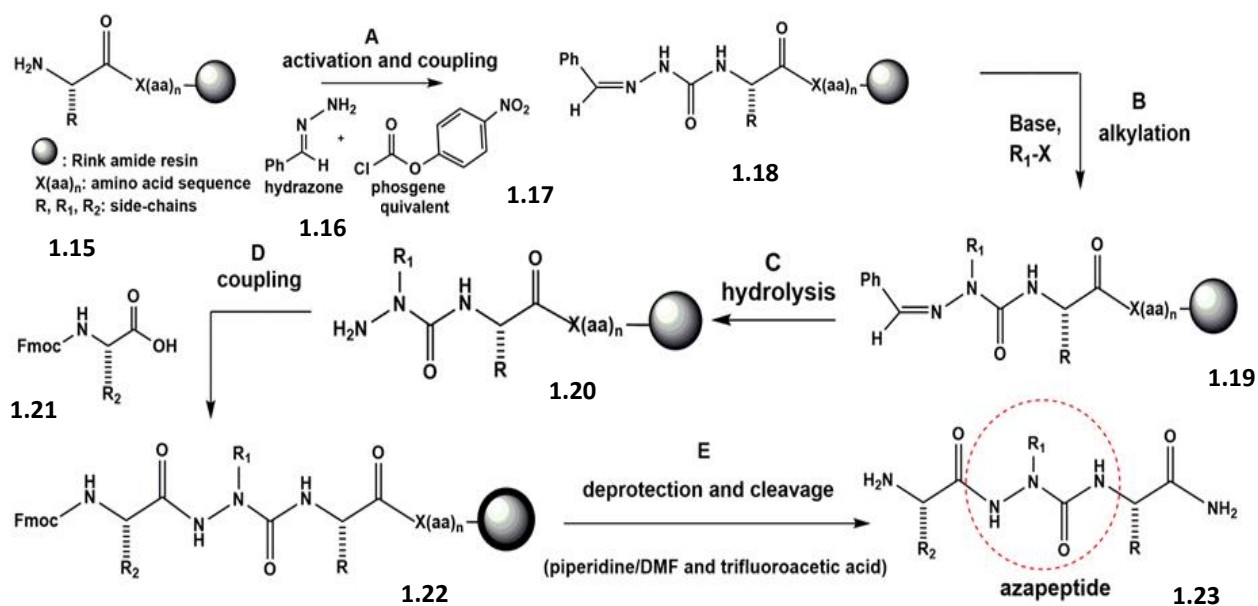
scanning, features the insertion of an *N*-Fmoc *N'*-alkyl hydrazine within conventional Fmoc-based solid phase peptide synthesis to procure the desired azapeptide for structure-activity relationship studies. The aza-amino acid monomer is produced in solution, by reductive amination of Fmoc carbazates. This alkylation step is followed by activation with phosgene which couples the Fmoc carbazic acid chloride intermediate onto the peptide bound resin. Fmoc deprotection, chain elongation and cleavage complete the synthesis of the azapeptide. This methodology was used for the generation of azapeptide analogs of the melanocortin receptor agonist, the growth hormone releasing peptide (GHRP-6) and the calcitonin gene-related peptide antagonist for exploring the effect of azapeptide structure on biological activity.²³⁻²⁵ In spite of its widespread utility, this methodology suffers from the prerequisite formation of the aza amino acid monomers by a reductive amination procedure which limits side chain diversity. To circumvent this limitation, submonomer synthesis was developed to enable the synthesis of structurally diverse azapeptides for medicinal chemistry applications.



Scheme 1.2. Azapeptide synthesis and aza-amino acid scanning using *N*-Fmoc carbazates.²³

1.3.3 SUBMONOMER AZAPEPTIDE SYNTHESIS

The submonomer approach for azapeptide synthesis has effectively extended the scope of side chain diverse azapeptides for structure-activity relationship (SAR) studies with receptor targets.^{6,26} This methodology consists of a simple 3-step procedure inserted within conventional Fmoc-based solid-phase peptide synthesis (SPPS) (**Scheme 1.3**). These include: a) hydrazone activation with 4-nitrophenylchloroformate to generate the activated carbamate intermediate and coupling onto support-bound peptide to generate the *N*-terminus semicarbazone. The activation and coupling step is followed by, b) regioselective alkylation of the semicarbazone to introduce the putative aza-side chain. Finally, c) chemoselective deprotection of the *N*-terminal semicarbazone liberates the semicarbazide for continuation of SPPS until the desired azapeptide has been made.



Scheme 1.3. Submonomer solid phase azapeptide synthesis method.^{6,26}

Moreover, the submonomer method has furnished azapeptides with un-natural side chains that were applicable to further diversification yielding *new* azapeptides. For example, aza-propargylglycine was effectively prepared for 1,3-dipolar cycloadditions with aryl azides to generate a seven compound library of [aza-1,2,3-triazole-3-alanine⁴]GHRP-6 azapeptides.²⁷ Aza-arylglycine residues have also been prepared by a copper-catalyzed monoarylation procedure during the submonomer azapeptide synthesis.²⁸ Aza-arylglycine derivatives may form a new class of potent Vancomycin analogs that may be useful in overcoming growing bacterial resistance upon antibiotic treatment. In a related application, Sonogashira coupling reactions were optimized by submonomer azapeptide synthesis for introduction of aza-aryl substituents that cyclized into *N*-amino-imidazolin-2-ones, forming a new class of Phe and Trp mimics.²⁹ The copper catalyzed coupling reaction of aza-propargylglycine residues with Mannich reagents also proved fruitful in the generation of rigid Lys mimics.³⁰ These novel aza-residues may prove to be useful substrates for exploring the influence of ionic azapeptide structure on biological activity.

The submonomer synthesis method has greatly influenced the production of azapeptides. It has effectively abolished the need for solution phase synthesis of the *N*-protected *N*⁷-alkyl hydrazides, as well as associated issues with hydantoin by-product formation. Consequently, the submonomer synthesis has significantly elaborated azapeptide structure and functional diversity. Regio-selective modifications of semicarbazone peptide on solid phase has generated novel *N*-alkylated and *N*-arylated aza-residues useful for SAR studies. Submonomer azapeptide synthesis is thus the present day method of choice for making azapeptides.

1.4 CONFORMATIONAL PROPERTIES

Stabilization of a particular conformational feature within biologically active peptides by introducing geometrical constraints may be vital for establishing therapeutic activity. In azapeptides, replacing a C_α by a N_α generates a hydrazine and a urea constituent, which restricts the bond rotation about the $-\text{CO}-\text{NH}-\text{N}_\alpha-\text{CONH}-$ peptide backbone. This conformational restraint may be characterized by the azapeptide torsion angles ϕ (phi) and ψ (psi).³¹ In principle, ϕ and ψ can have any values in between -180° and $+180^\circ$, but many values are prohibited by steric interference and stereoelectronic effects. The spacial arrangement of the peptide backbone ϕ and ψ dihedral angles define its secondary structure. The most prominent secondary structure found within azapeptides are β -turn conformations (Figure 1.2).

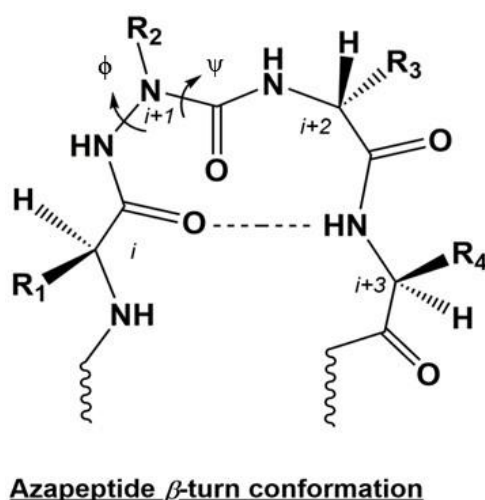


Figure 1.2. Azapeptide β -turn conformation defined by its ϕ and ψ dihedral angles.³¹

The β -turn is the simplest peptide secondary structure which involves 4 amino acid residues, with the carbonyl oxygen of the first residue at the i position forming an intramolecular hydrogen bond (H-bond) with the amino group at the fourth ($i+3$) position.

These types of structural motifs often contain glycine and proline residues that stabilize the turn conformation. Glycine is small and flexible, readily facilitating turn geometries, whereas proline is a rigid cyclic amino acid which assumes the cis configuration and locks the peptide backbone into a turn conformation. Proline and glycine have been found at the $i+1$ and $i+2$ positions, respectively, of β -turn conformations. Their influence on the ϕ and ψ dihedral angles favors different types of β -turn conformations (**Figure 1.3**).^{32,33}

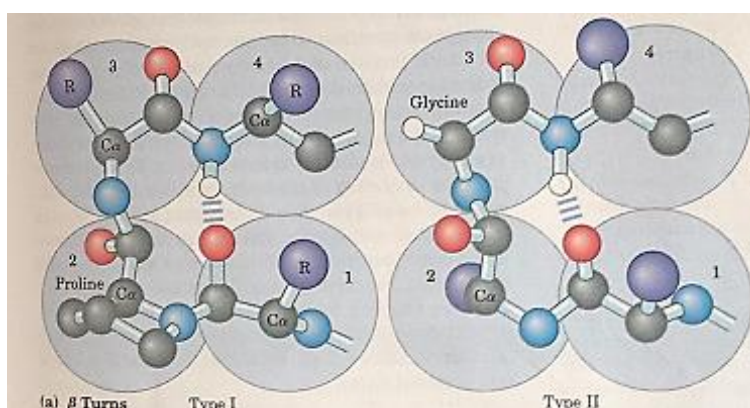
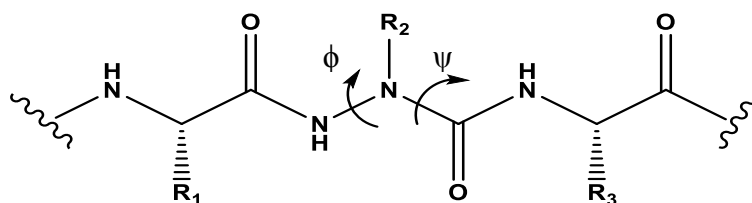


Figure 1.3. Structures of naturally occurring β -turn types in peptides and proteins.^{32,33}

Several model systems have been developed to understand the conformational properties of azapeptides. The most interesting structural variation is associated with the hydrazine moiety. The energy minimized geometry of the aza-amino acid residue is influenced by the conformational preferences of the N,N' -diacylhydrazine and urea components found within the azapeptide. For example, the conformations of hydrazine and its 1,2-diformyl derivatives, which resemble the aza-amino acid residues, were investigated by quantum mechanical computational studies.³⁴⁻³⁸ Ab initio molecular orbital calculations showed that N,N' -diacylhydrazines adopted non-planar structures in which the nitrogen lone pairs were found to be perpendicular to one another in the energy minimum conformation. Moreover, substituted N,N' -diacylhydrazines were found to be configurationally labile,

interconverting in between two mirror image nitrogen pyramids passing through a planar structure. Depending on the alkyl substitution pattern of N,N' -diacylhydrazines, a particular chiral nitrogen pyramid may be preferred at room temperature.³⁷

Insertion of N,N' -diformylhydrazines within peptide sequences results in azapeptides with torsion angles around 90° for ϕ and about 180° or 0° for ψ .³¹ These values correspond to some major types of β -turn secondary structures (**Table 1.1**). Thus, the aza-amino acid residues found within azapeptides pre-organizes β -turn secondary structures by a combination of stereoelectronic and structural effects. The N,N' -diacylhydrazine nitrogen lone pairs exhibit repulsive electrostatic interactions which bends the azapeptide backbone into an energy minimum turn conformation. Moreover, the rigid urea functions to lock the turn conformation into a privileged β -turn secondary structure.



Turn	ϕ_2 ($^\circ$)	Ψ_2 ($^\circ$)	ϕ_3 ($^\circ$)	Ψ_3 ($^\circ$)
β I	-60	-30	-90	0
β I'	60	30	90	0
β II	-60	120	80	0
β II'	60	-120	-80	0
β III	-60	-30	-60	-30
β III'	60	30	60	30
β VIa1	-60	120	-90	0
β VIa1	-120	120	-60	0

Table 1.1. Backbone torsion angles for different types of β -turns found within azapeptides.

A variety of computational, crystallographic and spectroscopic approaches have been used to investigate azapeptide conformational properties.³⁹⁻⁵⁴ The conformations of model azapeptides containing proline residues have been examined.^{43,44,46,48,50,53,54} A combination of the aza-amino acid and proline appeared to be a strong β -turn-inducing motif. Since proline is known to stabilize β -turn structures, it is uncertain about the contribution of the aza-amino acid group in such combinations. Theoretical studies on model azapeptide sequences such as, Ac-azaXaa-NH₂ (Xaa = Gly, Ala, Leu) showed that unlike naturally occurring amino acid residues, azapeptides preferred dihedral angles $\phi = \pm 90 \pm 30^\circ$, $\psi = 0$ or $\pm 180 \pm 30^\circ$. The dihedral angle ($\phi = \pm 90 \pm 30^\circ$, $\psi = 0 \pm 30^\circ$) appeared to correspond to the β -turn conformation.⁴¹ Ab initio calculations coupled to NMR spectroscopy have indicated that the preferred backbone geometries of azapeptides are similar, regardless of the side-chain functional groups on the aza-amino acid residue.⁴¹ Therefore, the conformational properties of azapeptides is contingent on the semicarbazide group, which pre-organizes the peptide backbone into a β -turn type conformation. X-ray crystallographic analyses have been performed on simple azapeptides.^{47-50,53} The majority of the azapeptides for which the X-ray data is available, contain proline or aza-proline residues, which may favor turn conformations and thereby influence the conformational properties of the aza-amino acid residue. Spectroscopic techniques such as, FT-IR, NMR and CD spectroscopy have also been used for the structural analyses. FT-IR provides the amide N-H stretching band region (3200 – 3500 cm⁻¹) which is used to distinguish the free amide protons (3400 – 3500 cm⁻¹) from the ones involved in hydrogen bonding (3200 – 3400 cm⁻¹).⁴¹ For example, the FT-IR spectrum of Boc-Ala-Phe-azaLeu-Ala-OMe in CCl₄ produced amide stretching bands at 3440, 3380, and 3320 cm⁻¹. The presence of the band at 3320 and 3380 cm⁻¹ supported the β -turn geometry, which was also validated by the NMR studies. The carbonyl C=O stretching band region

(1580 – 1720 cm^{-1}) may also provide evidence of the carbonyl groups involved in hydrogen bonds. NMR spectroscopy has also been used to study the conformation of smaller model azapeptides in solution.^{41,42,44,47,54} Distances between protons have been measured by studying through space transfer of magnetization by Nuclear Overhauser Effect (NOE) spectroscopy, to distinguish the aza-proline amide *cis*- from the *trans*-isomers. Hydrogen bonding interactions of the amide protons have also been observed by studying changes in chemical shift with variation in solvent and temperature. For example, the amide proton of Ala⁴ in Boc-Ala-Phe-azaLeu-Ala-OMe was undisturbed by the switch from CDCl_3 to DMSO-d_6 , indicative of its involvement in an intramolecular hydrogen bonding.⁴¹ 2D NOESY experiments in CDCl_3 indicated that the amide proton of azaLeu³ exhibited strong and medium NOE correlations with the α -proton of Phe² and the amide proton of Ala⁴, suggesting a type II β -turn. A weak NOE correlation in between the amide protons of Phe² and aza-Leu³ indicated that a type I β -turn was likely in equilibrium with the type II conformer (**Figure 1.4**).⁴¹

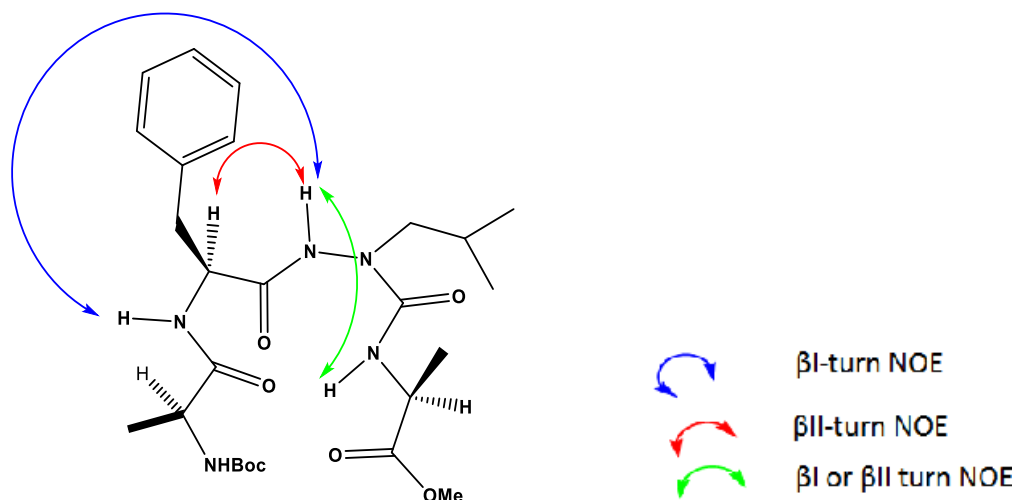


Figure 1.4. NOE correlations found within Boc-Ala-Phe-azaLeu-Ala-OMe.⁴¹

Circular Dichroism spectroscopy has also been used to study the structural characteristics of azapeptides.⁶ Azapeptide analogs which are less soluble in organic solvents can be assessed by CD spectroscopy in water and physiological buffer. For example, insertion of aza-Phe⁴ within GHRP-6 caused a change in the CD signature of the native GHRP-6 sequence from a random coil to that of a β -turn for the azapeptide. The characteristic CD bands for β -turns are characterized by negative maximum values located at around 190 and 230 nm and a positive maximum band near 215 nm.^{55,56}

1.5 MEDICINAL CHEMISTRY APPLICATIONS

Azapeptides have been shown to enhance the biological activity of the parent peptide by facilitating tissue absorption, transport and distribution, improving enzyme or receptor binding, and metabolic stability. Taken together, these attributes have led to the successful medicinal chemistry applications of azapeptides.⁴ For example, azapeptides have resisted proteolytic degradation by proteases^{11,22}, enhanced binding affinity and selectivity towards receptor targets^{6,25} in addition to demonstrating favorable pharmacodynamics which has led to the FDA approval of the first azapeptide drug, Goserelin, for the treatment of prostate and breast cancers.⁵⁷ Thus, azapeptides have proven to be useful tools for the design of drug candidates for applications in medicinal chemistry.

1.5.1 AZAPEPTIDES AS RECEPTOR AGONISTS AND ANTAGONISTS

Azapeptides have been designed and applied to regulate protein function in SAR studies that has led to important medicinal chemistry applications. The first azapeptide was designed and synthesized in 1963, as a modified angiotensin II derivative, [azaVal³]-angiotensin II (bovine) [Asp-Arg-azaVal-Tyr-Val-His-Pro-Phe], which reduced activity and

exhibited longer duration of action relative to its parent peptide in a standard blood pressure assay.⁵⁸ Azapeptide analogs of the peptide hormone oxytocin, used therapeutically to induce labor contractions have been made with varying degrees of biological activities. For example, the azaAsn⁵-oxytocin was inactive when tested within rat uterus, while azaGly⁹-oxytocin held 1.5-fold greater activity than the parent peptide.^{59,60} Azapeptide analogues of the leutinizing hormone-releasing hormone (LH-RH) [Glu-His-Trp-Ser-Tyr-Gly-Leu-Arg-Pro-Gly-NH₂], responsible for the release of the leutinizing hormone (LH) and the follicle-stimulating hormone (FSH), have been prepared and demonstrated a 100-fold enhancement relative to the parent hormone.⁶¹ An azapeptide analog, [D-Ser(*t*-Bu)⁶, azaGly¹⁰]-LH-RH (Zoladex®, Goserelin acetate, AstraZeneca Inc.) was approved for clinical use of prostate and breast cancer.⁵⁷

Azapeptide regulators of the integrin receptors α IIb β 3 and α v β 3 have been applied in platelet aggregation and pathologies such as osteoporosis, restenosis, angiogenesis and acute renal failure.²¹ The native peptide ligand, Arg-Gly-Asp (RGD), was replaced by six azapeptides substituting glycine by aza-glycine, aza-alanine or aza-sarcosine and Arg with 4-cis-guanidinocyclohexanecarboxylic acid and δ -guanidinovaleric acid. SAR studies led to the development of aminopyridine 154 (**Figure 1.5, 1.24**) which exhibited high selectivity and nanomolar binding affinity for the α v β 3 receptor.

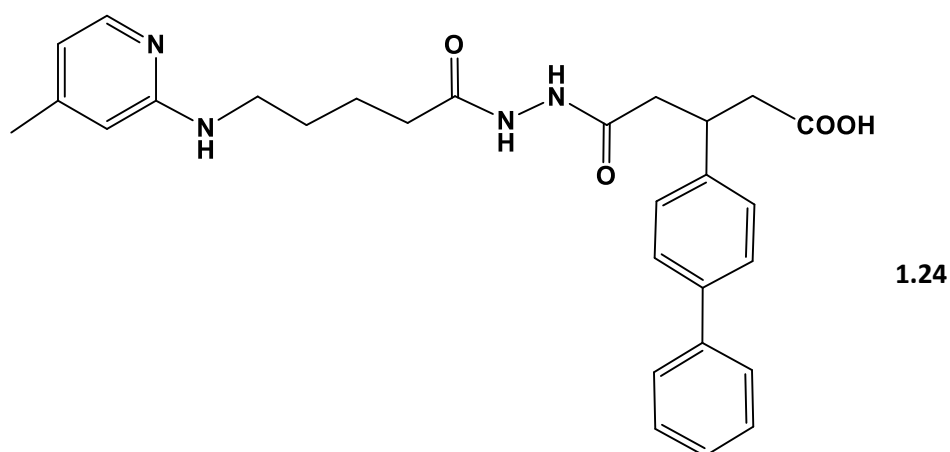


Figure 1.5. Lead RGD azapeptide mimic, **1.24**, as a selective and potent antagonist of the $\alpha v\beta 3$ receptor.

Azapeptide analogs of the Growth Hormone Releasing Peptides (GHRP-6), were also developed to improve binding selectivity and affinity to the Cluster of Differentiation 36 (CD36) scavenger receptor implicated in atherosclerosis, angiogenesis and in age-related macular degeneration.^{6,62} The native hormone, GHRP-6 exhibits dual binding activity for the Growth Hormone Secretagogue Receptor 1a (GHS-R1a) and the CD36 scavenger receptor. The pharmacophoric region of the growth hormone secretagogue GHRP-6, D-Trp-Ala-Trp, was systematically replaced by aza-amino acids residues to explore the importance of a turn conformation and side chain binding interactions on CD36 binding affinity and selectivity. An aza-Phe⁴ analog caused a 1000-fold improvement in selectivity for the CD36 receptor while reducing binding with GHS-R1a. Thus, azapeptide ligands of GHRP-6 may be useful leads in the development of selective forms of anti-atherosclerotic and anti-angiogenic treatments.

The melanocortin receptor (MCR) agonist, Ac-His-D-Phe-Arg-Trp-NH₂, has been implicated in the regulation of skin pigmentation, steroidogenesis, obesity, energy

homeostasis, and exocrine gland function. Its widespread biological activity is stimulated by its promiscuous binding to MCR subtypes mMC1R, mMC3R, mMC4R, and mMC5R. Thus, potent and selective ligands may lead to the regulation of specific metabolic signaling pathways. Towards this goal, aza-residues, for D-Phe and Arg, have been developed for stabilizing the putative bio-active β -turn found within the native sequence. These modifications caused a decrease in binding to the mMC1R and mMC4R, while substitution of Trp with aza-Nal-1, aza-Nal-2, and aza-Bip yielded analogs which displayed activity similar to the native sequence.²⁵

Aza-peptide analogs of the calcitonin gene-related peptide (CGRP) were developed to improve the inhibitory activity of this physiologically important peptide implicated in non-insulin-dependent diabetes mellitus, migraine headache, pain, and inflammation.⁶³ The insertion of aza-Gly³³ within [D₃₁,G₃₃,P₃₄,F₃₅]CGRP₂₇₋₃₇ led a 10-fold increase in inhibitory activity when compared to CGRP₂₇₋₃₇. Thus, aza-peptides have displayed an exquisite ability to modulate target receptor function with an affinity and selectivity that is absent in their naturally occurring counterparts. These favorable effects have led to the development of lead aza-peptide ligands that are currently in the pipeline for drug design and development.

1.5.2 AZAPEPTIDES AS PROTEASE INHIBITORS

Aza-peptide inhibitors of serine and cysteine proteases have also been developed for medicinal chemistry applications. Interestingly, aza-peptides possessing electrophilic aza-residues at the P1 position have been designed and developed as selective irreversible inhibitors of cysteine proteases.⁶⁴⁻⁷² A requirement for selective inhibition of cysteine over serine proteases is related to the incorporation of leaving groups, such as *p*-nitrophenolate

ion, which react preferentially with the active site cysteine thiol relative to the serine hydroxyl group. Therefore, activated esters of azapeptides *N*-Ac-Phe-azaGly-O Ph have been prepared for the rapid and effective inhibition of cysteine proteases ($>11,000 \text{ M}^{-1} \text{ s}^{-1}$).⁶⁴ More recently, azapeptides with reactive site halomethyl ketones, Michael acceptors and epoxides have all served as potent covalent inhibitors of cysteine proteases, such as the those belonging to the therapeutically relevant caspase family of cell death effector proteins (**Figure 1.6**).^{66,68-70,72} These substrates have been developed for therapeutic applications and also as biological probes for elucidating the mechanisms and kinetics associated with enzyme activity.^{73,74}

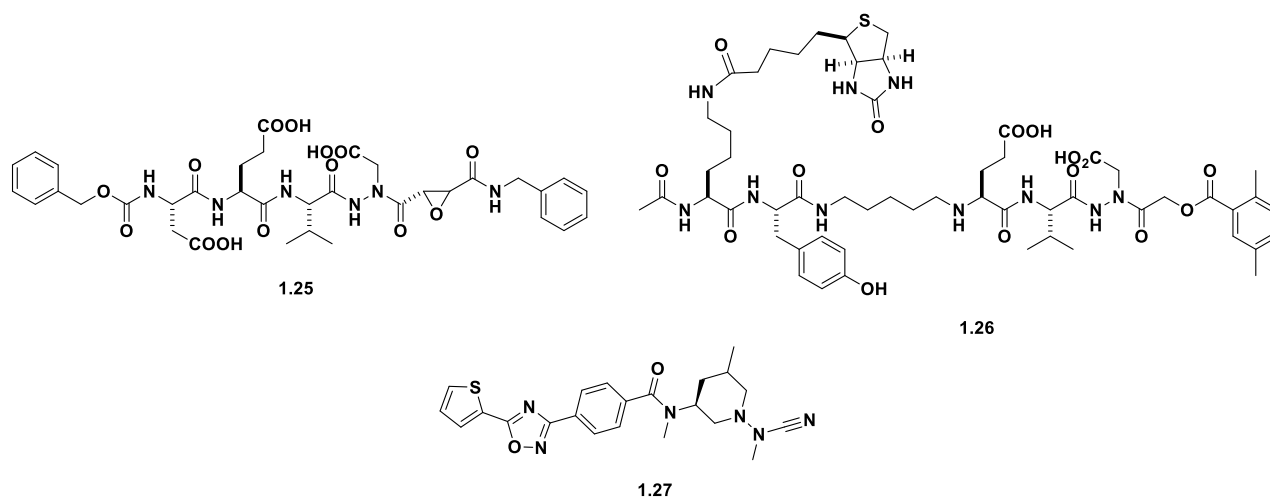


Figure 1.6. Representative azapeptide covalent inhibitors of cysteine proteases. Epoxide inhibitor, **1.25**. Acyloxymethylketone inhibitors, **1.26**, Nitrile inhibitor, **1.27**.⁶⁴⁻⁷²

Active site serine protease azapeptide inhibitors, such as the thrombin serine proteases, which plays a key role in blood coagulation, have also been developed. The ketoargininamide Boc-azaPhe-*trans*-Chx-Arg-CONH(s-PhEt) sequence was found to be the most potent inhibitor in this series.⁷⁵ A cyclic azapeptide inhibitor of HCV NS3 serine proteases has also been developed as a potential anti-viral agent. The lead macrocyclic

tripeptide, BILN 2061, displayed potent inhibition of the HCV NS3 serine protease (**Figure 1.7**).²² Furthermore, NMR spectroscopy and molecular modeling indicated that a bio-active β -turn conformation for the lead analog BILN 2061 contributed to tight binding to the active site of the HCV NS3 protease.²² Therefore, introduction of aza-amino acid residues along the backbone of bio-active peptides have provided enhanced protease inhibitor efficacy. These results are not only important for therapeutic applications, but also improve peptide metabolic stability for longer duration of action in biological media. Moreover, azapeptides own the ability to pre-organize the biologically active β -turn responsible for potent and selective regulation of enzyme targets.

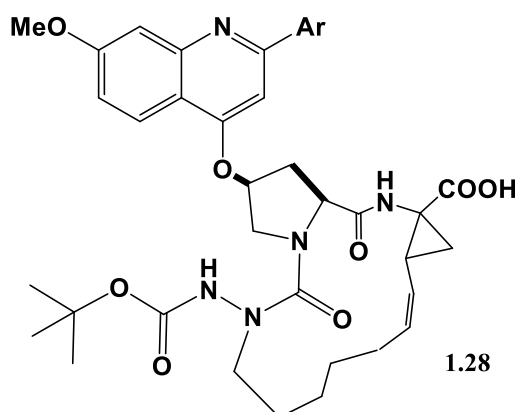


Figure 1.7. Macrocyclic azapeptide inhibitor, BILN 2061, of HCV NS3 serine protease.²²

1.6 CONCLUSIONS

Azapeptides are a special class of peptide mimics which introduce a change in configuration and a pre-organization of the peptide backbone β -turn structure found within native sequences. These structural changes are due to a combination of stereoelectronic and structural effects. The *N,N'*-diacylhydrazine moiety bends the peptide backbone into a turn

geometry due to the repulsive electrostatic effects of the nitrogen lone pairs and the rigid urea stabilizing the turn conformation. The conformational preferences of azapeptides have been observed by molecular modeling, spectroscopic and crystallographic studies. The pre-organized azapeptide β -turn structure has translated into enhanced biological activity in lead peptide sequences. In these cases, *aza-amino acid scanning* effected by the submonomer approach allows for the systematic incorporation of aza-amino acid residues along the peptide backbone for exploring the location and importance of a turn geometry on peptide activity. This methodology has enabled the rapid production of structurally diverse azapeptides for SAR studies. This has led to the development of lead azapeptide ligands as potent and selective regulators of receptor signaling activity *in-vitro* and *in-vivo*. Moreover, azapeptides have also been designed and developed as antagonists of enzyme activity. This has led to a production of azapeptide inhibitors of serine and cysteine proteases with an increase in metabolic stability which produces a longer duration of action. These substrates are also important for the better understanding of the mechanisms and kinetics of these important enzymes. Thus, azapeptides are vital tools in biological applications related to the development of potent and selective peptide-based drugs.

1.7 THESIS OBJECTIVES

In this thesis, the submonomer method is applied and optimized for the production of a small library (7) of azapeptide inhibitors of the Insulin Receptor Tyrosine Kinase (IRTK) domain. In cancer, the IRTK is overexpressed at the cell surface where it signals metabolic activity, protein expression and cell proliferation without regulation, that are all hallmarks of tumorigenesis.⁷⁶ Thus, potent and selective inhibitors of the IRTK may form the basis of effective anti-cancer agents. Towards this goal, a short pentapeptide, Ac-DIYET-NH₂,

derived from the activation loop of the IRTK has shown inhibitory activity towards IRTK autophosphorylation, albeit at high doses which limits therapeutic efficacy (80% at 4 mM).⁷⁷ Interestingly, molecular docking of the lead peptide bound to the active site of the IRTK indicated a folded peptide structure, reminiscent of a β -turn conformation. In order to evaluate whether the β -turn structure contributed to peptide activity, a series of Ac-DIYET-NH₂, azapeptides were designed to effect potent and specific inhibition of the IRTK.

In chapter 2 of this thesis, the submonomer azapeptide synthesis method is described for the production of azapeptides designed to inhibit IRTK autophosphorylation. Azapeptide modifications within the IYE pharmacophoric region are anticipated to stabilize the biologically active turn conformation. Moreover, the submonomer approach also enables the generation of novel aza-amino acid residues which contain *un-natural* side chains that may improve binding affinity and inhibitory activity. For example, a novel aza-DOPA analog is expected to be a more potent inhibitor of IRTK autophosphorylation due to the multiple hydroxyl groups at the aza-position. This is an important requirement, as Tyr residues have been attributed as the active site residues for IRTK phosphorylation which contributes to receptor signaling activity.

In Chapter 3, a conformational analysis is anticipated to provide insight into our SAR study. A molecular IRTK docking study of a lead azapeptide ligand, Ac-DIazaYET-NH₂, compared to its native sequence is expected to provide a theoretical model describing the presence and location of the putative peptide β -turn. CD and NMR spectroscopy will be used to validate the secondary structures of the azapeptides synthesized in this study.

In order to investigate the relationship between the conformational properties observed for the azapeptides and their biological activities, an IRTK inhibition assay is described in

Chapter 4. A western blot experiment is used to determine the propensity in which the azapeptides inhibit IRTK autophosphorylation in the presence of ATP. These studies are not only significant for our SAR studies, but also in the development of new azapeptide inhibitors of the IRTK. These may prove to be useful leads in the development of peptide-based anti-cancer drugs and also as valuable substrates for elucidating the mechanisms and kinetics of these important enzymes.

1.8 REFERENCES

1. Spatola, A. F. Peptide Backbone Modifications: a Structure-Activity Analysis of Peptides Containing Amide Bond Surrogates, Conformational Constraints, and Related Backbone Replacements in *Chemistry and Biochemistry of Amino Acids, Peptides and Proteins*. (Weinstein B. ed.) Marcel Dekker, Inc.: New York and Basel, **1983**, 7, 267-358.
2. (a) Gante, J. *Angew. Chem. Int. Ed. Engl.* **1994**, 33, 1699-1720; (b) Hruby, V.J. *J. Org. Chem.* **2009**, 74, 9245-9264.
3. Goodman, M.; Ro, S. Peptidomimetics for Drug Design. In *Burger's Medicinal Chemistry Principles and Practice*; 5th ed.; Wolff, M.E., Ed.; Wiley: New York, **1995**, 1, 803-861.
4. a) Gante, J. *Synthesis* **1989**, 405-413. b) Zega, A. *Curr. Med. Chem.* **2005**, 12, 589-597. c) Proulx, C.; Sabatino, D.; Hopewell, R.; Spiegel, J.; Ramos, Y.G.; Lubell, W.D. *Future Med. Chem.* **2011**, 3, 1139 - 1164.
5. (a) Lee, H. J.; Park, H. M.; Lee, K.B. *Biophys. Chem.* **2007**, 125, 117-126. (b) Hammerlin, C.; Cung, M.T.; Boussard, G. *Tetrahedron Lett.* **2001**, 42, 5009-5012. (c) Andre, F.; Boussard, G.; Marraud, M.; Didierjean, C.; Aubry, A. *Tetrahedron Lett.* **1996**, 37, 183-186. (d) Benatalah, Z.; Aubry, A.; Boussard, G.; Marraud, M. *Int. J. Pept. Protein Res.* **1991**, 38, 603-606.
6. (a) Sabatino, D.; Proulx, C.; Klocek, S.; Bourguet, C.B.; Boeglin, D.; Ong, H.; Lubell, W.D. *Org. Lett.* **2009**, 11, 3650- 3653, (b) Sabatino, D.; Proulx, C.; Pohankova, P.; Ong, H.; Lubell, W.D. *J. Am. Chem. Soc.* **2011**, 133, 12493-12506.
7. Gray, C.J.; Quibell, M.; Baggett, N.; Hammerle, T. *Int. J. Peptide Protein Res.* **1992**, 40, 351-362.
8. Liley, M.; Johnson, T. *Tetrahedron Lett.* **2000**, 41, 3983-3985.
9. Ahn, I.A.; Kim, S.W.; Ro, S. *Mol. Divers.* **1998-1999**, 4, 23-24.
10. Verhelst, S.H.; Witte, M.D.; Arastu-Kapur, S.; Fonovic, M.; Bogyo, M. *Chembiochem.* **2006**, 7, 943-950.
11. Wiczerzak, E.; Drabik, P.; Łankiewicz, L.; Ołdziej, S.; Grzonka, Z.; Abrahamson, M.; Grubb, A.; Brömme, D. *J. Med. Chem.* **2002**, 45, 4202-4211.
12. Mhidia, R.; Melnyk, O. *J. Pept. Sci.* **2010**, 16, 141-147.

13. Han, H.; Janda, K.D. *J. Am. Chem. Soc.* **1996**, *118*, 2539-2544.
14. Han, H.; Yoon, J.; Janda, K.D. *Bioorg. Med. Chem. Lett.* **1998**, *8*, 117-120.
15. Hansen, T.K. *Tetrahedron Lett.* **1999**, *40*, 9119-9120.
16. Randolph, J.T.; Zhang, X.; Huang, P.P.; Klein, L.L.; Kurtz, K.A.; Konstantinidis, A.K.; He, W.; Kati, W.M.; Kempf, D.J.. *Bioorg. Med. Chem. Lett.* **2008**, *18*, 2745-2750.
17. Frochot, C.; Vanderesse, R.; Driou, A.; Linden, G.; Marraud, M.; Thong Cung, M. *Lett. Pept. Sci.* **1997**, *4*, 219-225.
18. Andre, F.; Boussard, G.; Bayeul, D.; Didierjean, C.; Aubry, A.; Marraud, M. *J. Pept. Res.* **1997**, *49*, 556-562.
19. Zega, A.; Mlinsek, G.; Sepic, P.; Golic Grdadolnik, S.; Solmajer, T.; Tschopp, T.B.; Steiner, B.; Kikelj, D.; Urleb, U. *Bioorg. Med. Chem.* **2001**, *9*, 2745-2756.
20. Gibson, C.; Goodman, S.L.; Hahn, D.; Holzemann, G.; Kessler, H.; *J. Org. Chem.* **1999**, *64*, 7388-7394.
21. Sulyok, G.A.G.; Gibson, C.; Goodman, S.L.; Holzemann, G.; Wiesner, M.; Kessler, H.; *J. Med. Chem.* **2001**, *44*, 1938-1950.
22. Randolph, J.T.; Zhang, X.; Huang, P.P et al. *Bioorg. Med. Chem. Lett.* **2008**, *18*(8), 2745-2750
23. Boeglin, D.; Lubell, W.D. *J. Comb. Chem.* **2005**, *7*, 864-878.
24. Freeman, N.S.; Hurevich, M.; Gilon, C. *Tetrahedron* **2009**, *65*, 1737-1745.
25. Boeglin, D.; Xiang, Z.; Sorenson, N.B.; Wood, M.S.; Haskell-Luevano, C.; Lubell, W.D. *Chem. Biol. Drug Des.* **2006**, *67*, 275-283.
26. Kurian, L.; Silva, T.; Sabatino, D. *Bioorg. Med. Chem. Lett.* **2014**, *asaps*.
27. Proulx, C.; Lubell, W.D. *J. Org. Chem.* **2010**, *75*, 5385-5387.
28. Proulx, C.; Lubell, W.D. *Org. Lett.* **2010**, *12*, 2916-2919.
29. Proulx, C.; Lubell, W.D. *Org. Lett.* **2012**, *14*, 4552-4555.
30. Zhang, J.; Proulx, C.; Tomberg, A.; Lubell, W.D. *Org. Lett.* **2014**, *16*, 298-301.
31. Thormann, M.; Hofmann, H.J. *J. Mol. Struct. (Theochem)*. **1999**, *469*, 63-76.
32. Richardson, J.S. *Adv. Protein Chem.* **1981**, *34*, 167-339.

33. Hutchinson, E.G.; Thornton, J.M. *Protein Sci.* **1994**, *3*, 2207-2216.
34. Ramondo, F.; Bencivenni, L. *J. Chem. Soc. Perkin Trans.* **1995**, *2*, 1797-1804.
35. Reynolds, C.H.; Hormann, E. *J. Am. Chem. Soc.* **1996**, *118*, 9395-9401.
36. Bishop, G.J.; Price, B.J.; Sutherland, I.O. *J. Chem. Soc. Chem. Commun.* **1967**, *14*, 672-674.
37. Fletcher, J.R.; Sutherland, I.O. *J. Chem. Soc. Chem. Commun.* **1969**, *13*, 706-708.
38. Lee, H.J.; Lee, M.H.; Choi, Y.S.; Park, H.M.; Lee, K.B. *J. Mol. Struct. (Theochem)*. **2003**, *631*, 101-110.
39. Lee, H.J.; Ahn, I.A.; Ro, S.; Choi, K.H.; Lee, K.B. *J. Pept. Res.* **2000**, *56*, 35-46.
40. Ro, S.; Yoon, C. *J. Phys. Chem.* **2000**, *214*, 1699-1706.
41. Lee, H.J.; Choi, K.H.; Ahn, I.A.; Ro, S.; Jang, H.G.; Choi, Y.S.; Lee, K.B. *J. Mol. Struct.* **2001**, *569*, 43-54.
42. Lee, H.J.; Song, J.W.; Choi, Y.S.; Park, H.M.; Lee, K.B. *J. Am. Chem. Soc.* **2002**, *124*, 11881-11893.
43. Lee, H.J.; Jung, H.J.; Kim, J.H.; Park, H.M.; Lee, K.B. *Chem. Phys.* **2003**, *294*, 201-210.
44. Lee, H.J.; Park, H.M.; Lee, K.B. *Biophys. Chem.* **2007**, *125*, 117-126.
45. Zhang, W.J.; Berglund, A.; Kao, J.L.; Couty, J.P.; Gershengorn, M.C.; Marshall, G.R. *J. Am. Chem. Soc.* **2003**, *125*, 1221-1235.
46. Che, Y.; Marshall, G.R. *J. Org. Chem.* **2004**, *69*, 9030-9042.
47. André, F.; Vicherat, A.; Boussard, G.; Aubry, A.; Marraud, M. *J. Pept. Res.* **1997**, *50*, 372-381.
48. Lecoq, A.; Boussard, G.; Marraud, M.; Aubry, A. *Biopolymers* **1993**, *33*, 1051-1059.
49. Marraud, M.; Aubry, A. *Pept. Sci.* **1996**, *40*, 45-83.

50. Benatalah, Z.; Aubry, A.; Boussard, G.; Marraud, M. *Int. J. Pept. Protein. Res.* **1991**, *38*, 603-605.
51. Gante, J.; Krug, M.; Lauterbach, G.; Weitzel, R.; Hiller, W. *J. Pept. Sci.* **1995**, *1*, 201-206.
52. Hemmerlin, C.; Cung, M.T.; Boussard, G. *Tetrahedron Lett.* **2001**, *42*, 5009-5012.
53. André, F.; Marraud, M.; Boussard, G. *Tetrahedron Lett.* **1996**, *37*, 183-186.
54. Bac, A.; Rivoal, K.; Cung, M.; Boussard, G.; Marraud, M.; Soudan, B. Tetaert, D.; Degand, P. *Lett. Pept. Sci.* **1997**, *4*, 251-258.
55. Kelly, S.M.; Jess, T.C.; Price, N.C. *Biochim. Biophys. Acta.* **2005**, *1751*, 119-139.
56. Bush, C.A.; Sarkar, S.K.; Kopple, K.D. *Biochemistry* **1978**, *17*, 4951-4954.
57. (a) Tyrrell, C.J.; Altwein, J.E.; Klippel, F.; Varenhorst, E.; Lunglmayr, G.; Boccardo, F.; Holdaway, I.M.; Haefliger, J.M.; Jordaan, J.P. *J. Urol.* **1991**, *146*, 1321-1326; (b) Taylor, C.W.; Green, S.; Dalton, W.S.; Martino, S.; Rector, D.; Ingle, J.N.; Robert, N.J.; Budd, G.T.; Paradelo, J.C.; Natale, R.B.; Bearden, J.D.; Mailliard, J.A.; Osborne, C.K. *J. Clin. Oncol.* **1998**, *16*, 994-999.
58. Hess, H.J.; Marchand, W.T.; Laubach, G.D. *J. Am. Chem. Soc.* **1963**, *85*, 4040-4041.
59. Niedrich, H. *J. Prakt. Chem.* **1972**, *314*, 769-779.
60. Niedrich, H.; Oehme, C. *J. Prakt. Chem.* **1972**, *314*, 759-768.
61. Dutta, A.S.; Furr, B.J.A.; Giles, M.B.; Morley, J.S. *Clin. Endocrinol.* **1976**, *5*, S291-S298.
62. Proulx, C.; Picard, É.; Boeglin, D.; Pohankova, P.; Chemtob, S.; Ong, H.; Lubell, W.D. *J. Med. Chem.* **2012**, *55*, 6502-6511.
63. Boeglin, D.; Hamdan, F.F.; Melendez, R.E.; Cluzeau, J.; Laperriere, A.; Héroux, M.; Bouvier, M.; Lubell, W.D. *J. Med. Chem.* **2007**, *50*, 1401-1408.
64. Magrath, J.; Abeles, R.H. *J. Med. Chem.* **1992**, *35*, 4279-4283.
65. Asgian, J.L.; James, K.E.; Li, Z.Z.; Carter, W.; Barrett, A.J.; Mikolajczyk, J.; Salvesen, G.S.; Powers, J.C. *J. Med. Chem.* **2002**, *45*, 4958-4960.

66. James, K.E.; Asgian, J.L.; Li, Z.Z.; Ekici, O.D.; Rubin, J.R.; Mikolajczyk, J.; Salvesen, G.S.; Powers, J.C. *J. Med. Chem.* **2004**, *47*, 1553–1574.
67. Ovat, A.; Muindi, F.; Fagan, C.; Brouner, M.; Hansell, E.; Dvorak, J.; Sojka, D.; Kopacek, P.; McKerrow, J.H.; Caffrey, C.R.; Powers, J.C. *J. Med. Chem.* **2009**, *52*, 7192-7210.
68. Ekici, O.D.; Li, Z.Z.; Campbell, A.J.; James, K.E.; Asgian, J.L.; Mikolajczyk, J.; Salvesen, G.S.; Ganesan, R.; Jelakovic, S.; Grutter, M.G.; Powers, J.C. *J. Med. Chem.* **2004**, *49*, 5728-5749.
69. Sexton, K.B.; Kato, D.; Berger, A.B.; Fonovic, M.; Verhelst, S.H.L.; Bogyo, M. *Cell Death Diff.* **2007**, *14*, 727-732.
70. Ekici, O.D.; Gotz, M.G.; James, K.E.; Li, Z.Z.; Rukamp, B.J.; Asgian, J.L.; Caffrey, C.R.; Hansell, E.; Dvorak, J.; McKerrow, J.H.; Potempa, J.; Travis, J.; Mikolajczyk, J.; Salvesen, G.S.; Powers, J.C. *J. Med. Chem.* **2004**, *47*, 1889-1892.
71. Gotz, M.G.; James, K.E.; Hansell, E.; Dvorak, J.; Seshadri, A.; Sojka, D.; Kopacek, P.; McKerrow, J.; Caffrey, C.R.; Powers, J.C. *J. Med. Chem.* **2008**, *51*, 2816-2832.
72. Ganesan, R.; Jelakovic, S.; Campbell, A.J.; Li, Z.Z.; Asgian, J.L.; Powers, J.C.; Grutter, M.G. *Biochemistry* **2006**, *45*, 9059-9067.
73. Kato, D.; Verhelst, S.H.L.; Sexton, K.B.; Bogyo, M. *Org. Lett.* **2005**, *7*, 5649-5652.
74. Lee, J.; Bogyo, M. *Chem. Biol.* **2010**, *5*, 233–243.
75. Semple, J.E.; Rowley, D.C.; Brunck, T.K.; Ripka, W.C. *Bioorg. Med. Chem. Lett.* **1997**, *7*, 315-320.
76. Blume-Jensen, P.; Hunter, T. *Nature* **2001**, *411*, 355–365.
77. Kato, M.; Abe, M.; Kuroda, Y.; Hirose, M.; Nakano, M.; Handa, T. *J. Pept. Sci.* **2009**, *15*, 327–336.

CHAPTER 2. SOLID PHASE SUBMONOMER SYNTHESIS OF AZAPEPTIDE ANALOGS OF THE Ac-DIYET-NH₂ SEQUENCE

2.1 ABSTRACT

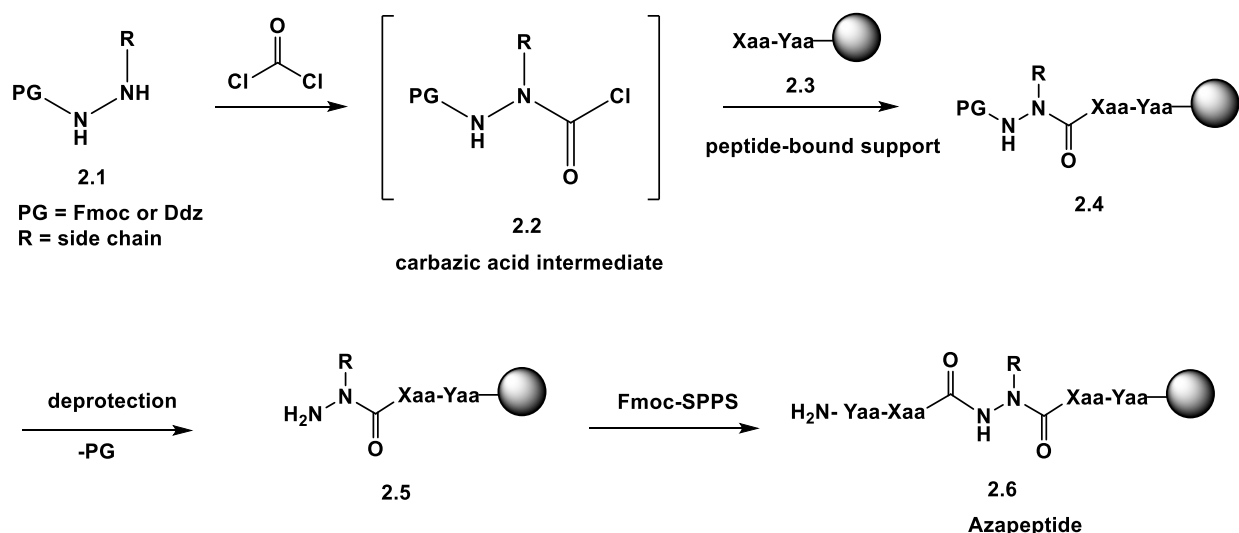
A small library (7) of azapeptide derivatives of the Ac-DIYET-NH₂, **2.28**, sequence has been prepared by submonomer azapeptide synthesis in an effort to explore the importance of a turn conformation on peptide activity. The synthetic pentapeptide, Ac-DIYET-NH₂, **2.28**, was found to inhibit the autophosphorylation of the insulin receptor tyrosine kinase (IRTK) domain to about 80% at 4 mM, making it a potential lead in the development of novel peptide-based anti-cancer drugs. The submonomer method for making azapeptide derivatives of the Ac-DIYET-NH₂, **2.28**, sequence featured a modified three step procedure, (a) activation and coupling, (b) alkylation and (c) deprotection, inserted within conventional Fmoc-based solid phase peptide synthesis. Aza-amino acid residues were built within the IYE pharmacophoric region of Ac-DIYET-NH₂, **2.28**, including new aza-Ile and aza-DOPA residues. Azapeptides were prepared in sufficient isolated yields (36% - 55%) and purities > 95% for structure activity relationship (SAR) studies (Chapters 3 and 4).

2.2 INTRODUCTION

Azapeptides are a special class of peptide mimics formed by the incorporation of aza-amino acid monomers within a peptide sequence.¹ The site-specific insertion of aza-amino acid residues along a peptide sequence (*i.e.* aza-amino acid scanning) has been used to identify the importance and location of β -turn-conformations on peptide biological activity.² Thus, azapeptides have enhanced binding affinity and selectivity against biological targets³ and have improved pharmacokinetic properties for the translation of biologically active

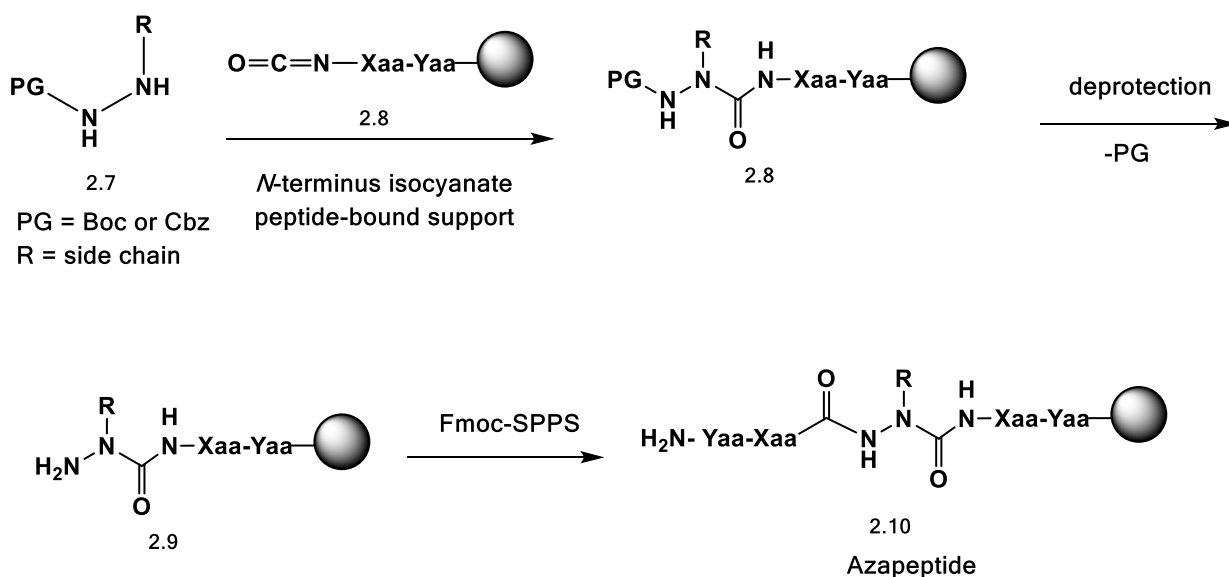
peptides into azapeptide drugs.⁴ Enabling their utility in biological and medicinal applications are more than 50 years of method development. These have involved a combination of solution phase hydrazine and peptide chemistry⁵ and evolved into the present day submonomer approach for azapeptide synthesis.⁶

Historically, azapeptide synthesis has necessitated the pre-requisite formation of activated hydrazine precursors in solution prior to their incorporation within a peptide sequence on solid phase. Among the most common aza-amino acid building blocks prepared for the solid phase synthesis of azapeptides are the *N*-Fmoc protected *N'*-alkyl hydrazine⁷ and *N*-Boc aza-dipeptide fragments⁸, as well as *N*-Fmoc-⁹ and *N*-2-(3,5-dimethoxyphenyl)propan-2-yloxy-carbonyl (Ddz)¹⁰-protected aza-amino acid chlorides. The Fmoc/Ddz-strategies (**Scheme 2.1**) have been especially useful in producing small libraries of azapeptides for exploring SAR studies with receptor targets.^{9,10} These methods required the solution phase preparation of the *N*-Fmoc or *N*-Ddz-protected *N'*-substituted carbazates, **2.1**. These aza-amino acid building blocks were prepared by reductive amination, followed by a phosgene treatment which generated the activated aza-amino acid chloride, **2.2**, for coupling to the resin bound peptide, **2.3**. In spite of their utility in aza-amino scanning, these methods have limited widespread applicability due to the difficulties associated with the synthesis of the aza-amino acid monomers and the restricted side chain diversity produced by reductive amination.



Scheme 2.1. The Fmoc/Ddz-strategies for azapeptide synthesis.^{9,10}

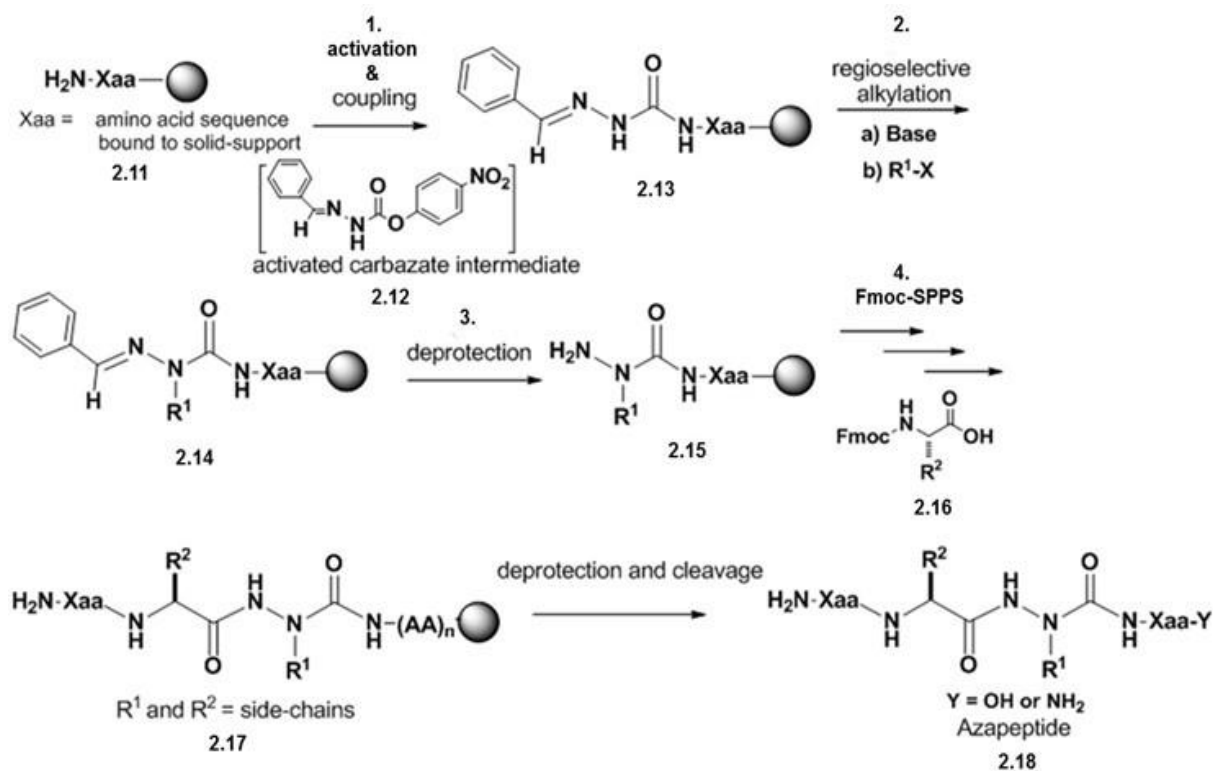
A variety of methods have also been developed for preparing azapeptides by activating the *N*-terminal amino group of a resin bound peptide into an isocyanate and coupling with a suitable aza-amino acid monomer (**Scheme 2.2**). For example, aza-tri, dipeptide and amino acid fragments have been prepared in solution and coupled onto the activated *N*-terminus of peptide bound resin.^{8,11} In these approaches, multiple steps were required to make the aza amino acid building blocks and the synthesis method was contaminated with significant amounts of hydantoin. Reversible amide bond protecting groups have since then been introduced to surmount the issues of hydantoin formation, albeit with additional steps for the introduction and removal of the protecting group.¹² Thus, aza-amino acid or *N*-terminus peptide activation have been successfully employed for making bio-active azapeptides. However, these methods are limited in their ability for producing a combinatorial library of structurally diverse azapeptides for studying SARs with biological targets.



Scheme 2.2. *N*-terminal isocyanate activation and carbazate coupling strategy for azapeptide synthesis.^{8,11}

The previously described methods necessitated the preparation of the aza-amino acid monomers in solution prior to their incorporation within azapeptide sequences by conventional solid phase peptide synthesis (SPPS).⁷⁻¹² A more direct and versatile approach would be to build the aza-amino acid residue during the course of the azapeptide synthesis method. Inspired by the un-natural peptide synthesis (UPS) approach developed by O'Donnell¹³ and applied by others¹⁴, the submonomer azapeptide synthesis strategy⁶ circumvents the need for monomer preparation and does not require stereo-chemical control for building the aza-residue on solid phase. Instead, the construction of the aza-amino acid residue during SPPS requires the efficient introduction of a suitably protected aza-glycine residue, its chemo-selective alkylation, deprotection and chain extension reactions. In the submonomer approach (**Scheme 2.3**), aza-glycine has been incorporated at the *N*-terminus of the peptide bound support by treating benzaldehyde hydrazone with *p*-nitrophenyl

chloroformate and coupling the activated carbazate to form the *N*-terminal semicarbazone. Regioselective semicarbazone alkylations introduced varying side chain groups at the azaglycine position. Semicarbazone deprotection and conventional SPPS¹⁵ were continued until the desired azapeptides were produced. Thus, the submonomer azapeptide synthesis method followed a three-step procedure inserted within the SPPS cycle (**Scheme 2.3**). The method consisted of (1) activation and acylation of peptide bound resin with an activated benzylidene carbazate, **2.12**, formed *in-situ* upon the reaction of benzaldehyde hydrazone and *p*-nitrophenyl chloroformate, (2) alkylation of the *N*-terminal semicarbazone, **2.13** and (3) its deprotection yielded semicarbazide, **2.15**, ready for (4) conventional Fmoc-based SPPS.⁶ Following step 3, the submonomer method may be repeated producing azapeptides with several aza-residues within the sequence or the fully functionalized azatides.¹⁶ Completion of the solid phase synthesis produced the protected azapeptides bound to their solid supports. Azapeptide deprotection and cleavage from solid phase were finally accomplished for analysis and purification which led to structure-function studies. In a nutshell, the submonomer method was created to simplify azapeptide synthesis while providing greater opportunity for the combinatorial library preparation of side chain diverse azapeptides for SAR studies.



Scheme 2.3. The submonomer solid phase azapeptide synthesis method.⁶

The submonomer approach has led to the solid phase synthesis of 10 aza-analogs of GHRP-6 built from support bound aza-glycine alkylations with primary and secondary alkyl halides (**Figure 2.1**).⁶ Among this series, the conformational and biological properties of [aza-Phe⁴]-GHRP-6 evaluated by CD spectroscopy and receptor binding studies respectively demonstrated a stable β -turn favored selective CD36 receptor binding. Considering the anti-angiogenic properties of GHRP-6 ligands that favor selective CD36 scavenger receptor binding, [aza-Phe⁴]-GHRP-6 may become a promising lead for the development of treatments for angiogenic disorders, such as age-related macular degeneration.

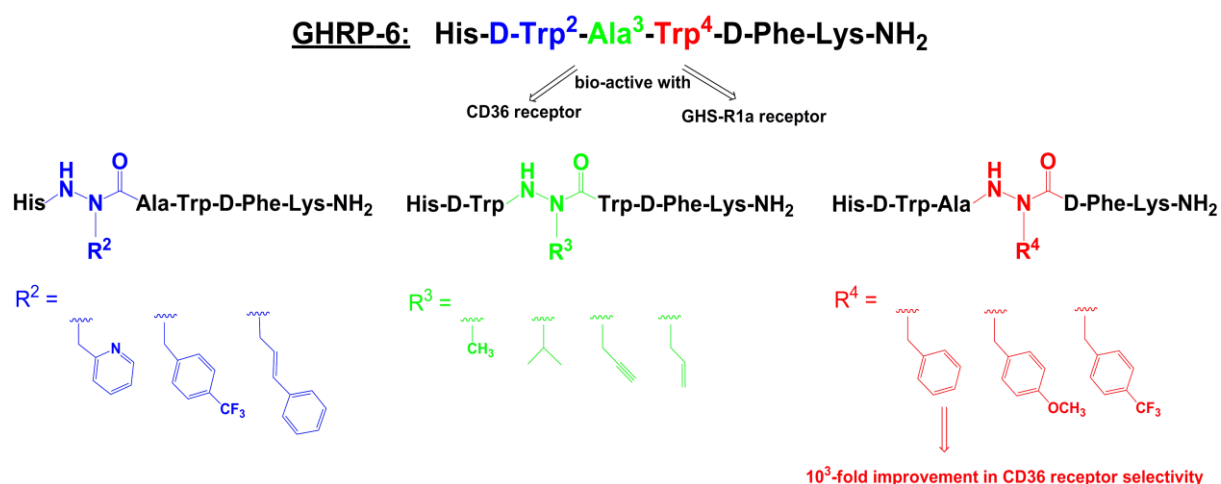


Figure 2.1. Submonomer synthesis produced ten GHRP-6 azapeptides, from which the [aza-Phe⁴]-GHRP-6 analog exhibited a 1000-fold increase in CD36 scavenger receptor binding relative to the growth hormone secretagogue receptor (GHS-R1a). Figure adapted from reference 6.

Expanding on the alkylation step, Michael additions of electron deficient olefins and conjugate addition-elimination reactions of activated allylic acetates have produced aza-Glu surrogates to explore the influence of turn conformation and carboxylate interactions on azapeptide activity (**Figure 2.2**).¹⁷ Fifteen aza-Glu derivatives of GHRP-6 were prepared by the submonomer approach, effectively expanding the repertoire of side chain diverse azapeptides for SAR studies with receptor targets. Moreover, aza-pyrroglutamate and pyrrolidine GHRP-6 analogs were prepared upon intramolecular cyclization of aza-Michael acceptors with the *N*-terminal amine of the peptide sequence. Structural studies of the aza-Glu peptides by NMR and CD spectroscopy demonstrated folded azapeptide conformations which translated into varying degrees of CD36 receptor binding affinities, none of which outperformed the [aza-Phe⁴]-GHRP-6 analog.

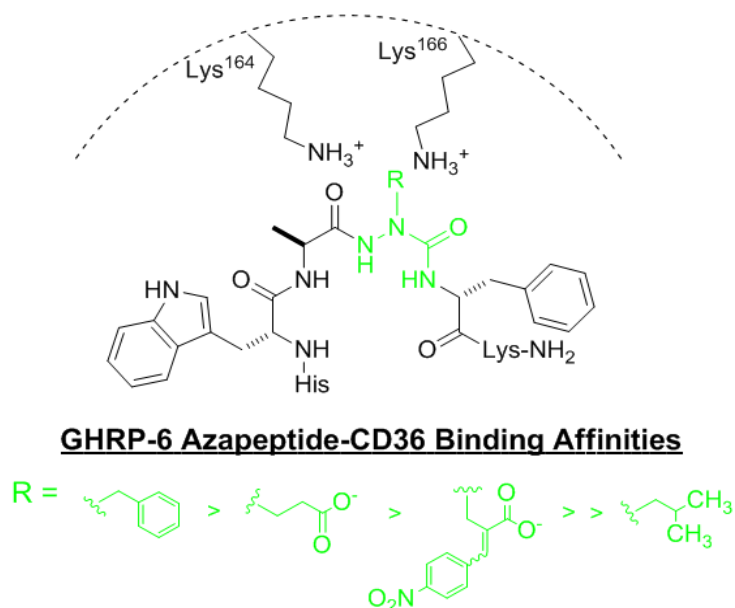
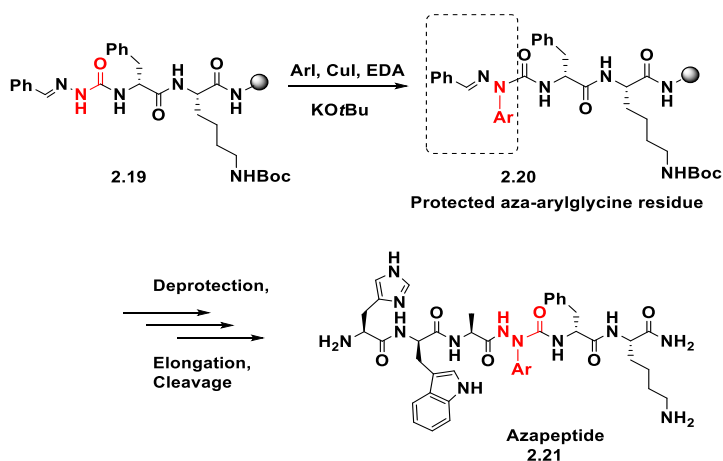


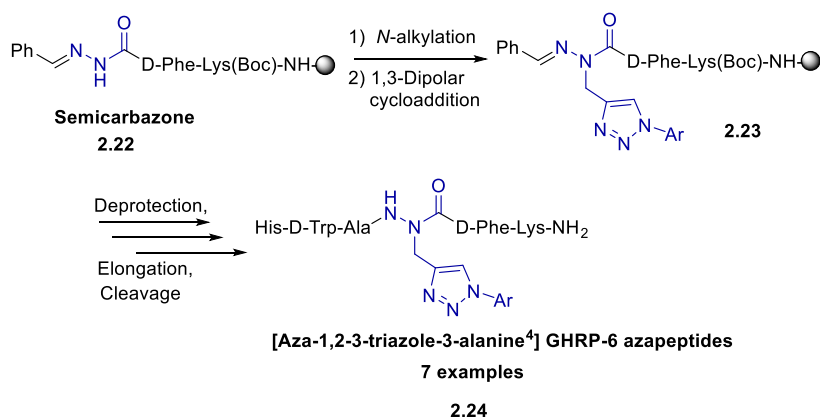
Figure 2.2. Aza-Glu GHRP-6 azapeptide binding interactions to the CD36 scavenger receptor. Figure adapted from reference 17.

Submonomer azapeptide synthesis has also produced 13 aza-arylglycine GHRP-6 analogs by copper-catalyzed *N*-arylation of semicarbazone peptide bound support.¹⁸ The use of aryl and heteroaryl iodides furnished azapeptides with side chains bearing resemblance to the aza-Phe, aza-Tyr, aza-Trp and aza-His residues (**Scheme 2.4**). Substitution of the Trp⁴ position with aza-arylglycine residues induced a β -turn conformation which may favor CD36 binding affinity and selectivity.



Scheme 2.4. Copper-catalyzed *N*-arylation of semicarbazone peptide bound support. Figure adapted from reference 18.

Seven new GHRP-6 azapeptides containing aza-1,2,3-triazole-3-alanine residues were prepared on aza-propargylglycine residues by a copper-catalyzed 1,3-dipolar cycloaddition reaction with aryl azides (**Scheme 2.5**).¹⁹ This libraries-from-libraries methodology featured further diversification of the aza-residues and led to the generation of new azapeptides that may be useful for structure-activity studies.



Scheme 2.5. Copper-catalyzed 1,3-dipolar cycloaddition reaction with azapropargyl glycine residues and aryl azides. Figure adapted from reference 19.

The azapropargyl glycine residue was also used for the production of constrained aza-lysine peptides (**Figure 2.3**). Their synthesis was accomplished by a copper catalyzed coupling of Mannich reagents to aza-propargylglycine residues. Eighteen aza-Lys GHRP-6 analogs were produced by the so-called A(3)-coupling reaction.²⁰

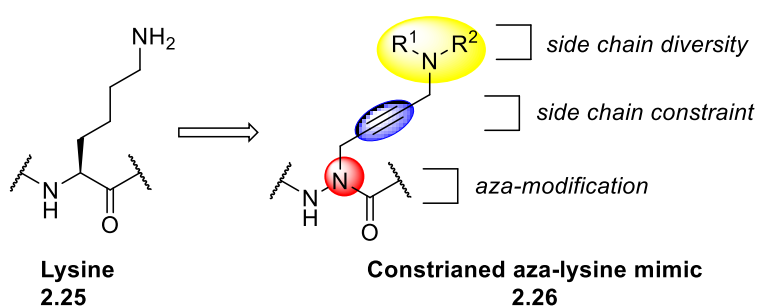


Figure 2.3. Structure comparison of lysine and a constrained aza-lysine mimic. Figure adapted from reference 20.

The submonomer method has also been used to modify the azapeptide backbone. For example, 4-substituted *N*-amino-imidazolin-2-one peptides were synthesized by a base-promoted cyclization of aza-propargylglycine residues.²¹ Further diversification of the *N*-amino-imidazolin-2-one scaffold was accomplished by a tandem Sonogashira cross-coupling and cyclization reaction with aryl and heteroaryl iodides to modify the 4-position of the imidazolin-2-one. These peptide mimics revealed a type II' β -turn conformation according to X-ray crystallography and circular dichroism spectroscopy supported the presence of a turn conformation. This privileged structure led to tight binding affinity for the CD36 receptor, and inhibitory activity on MAP kinase JNK phosphorylation, that are all indicative of modulating scavenger receptor activity. In a related application, *N*-amino-imidazolidin-2-one peptidomimetics have also been achieved by alkylation and cyclization of the urea nitrogen

of a semicarbazone using ethylene bromide. The syntheses and isolation of 25 *N*-amino-imidazolidin-2-one peptidomimetics have been developed by an extension of the submonomer azapeptide synthesis method.²²

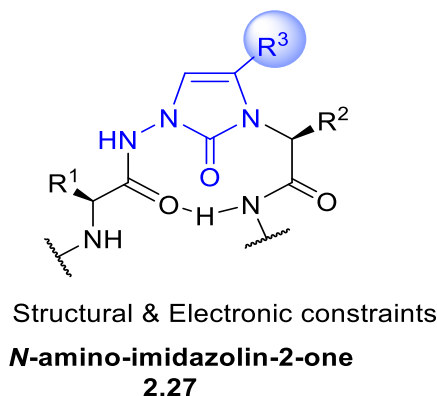


Figure 2.4. Structure of *N*-amino-imidazolin-2-one. Figure adapted from reference 21-22.

Thus, submonomer solid phase azapeptide synthesis has effectively expanded the repertoire of side chain diverse azapeptides useful in studying the effects of the α -nitrogen configuration, backbone conformation and side chain structure on biological activity.

2.3 CHAPTER OBJECTIVES

In this chapter, the synthesis and characterization of a new class of azapeptide inhibitors of the insulin receptor tyrosine kinase (IRTK) will be described.²³ The azapeptide ligands are derived from the activation loop of the IRTK which encompass the Ac-DIYET-NH₂, **2.28**, sequence. Submonomer azapeptide synthesis will be employed to develop a small library of azapeptide analogs of the native sequence to identify the influence and location of turn structure on IRTK inhibitory activity. Specifically, the IYE pharmacophoric region of **2.28** will be systematically replaced with aza-amino acid residues to facilitate our aza-amino acid

scanning strategy (**Figure 2.5**). Following azapeptide synthesis, LCMS analyses and purification, the isolated azapeptides will be employed for SAR studies (Chapters 3 and 4).

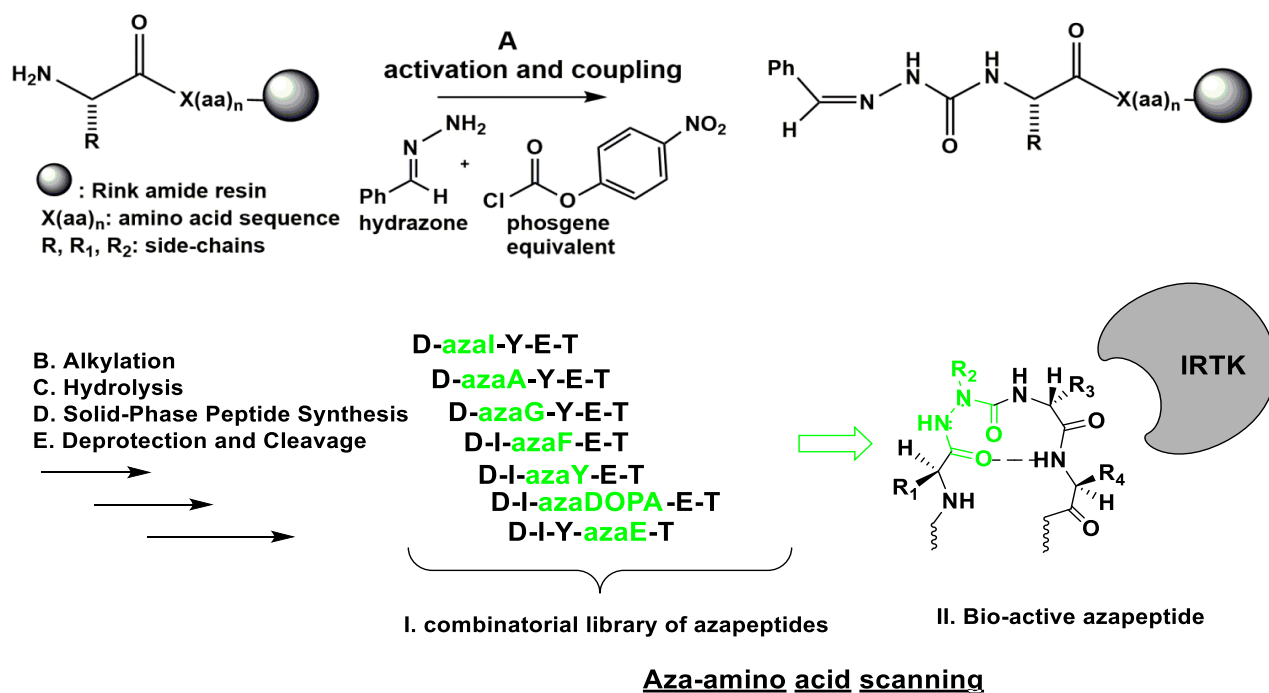


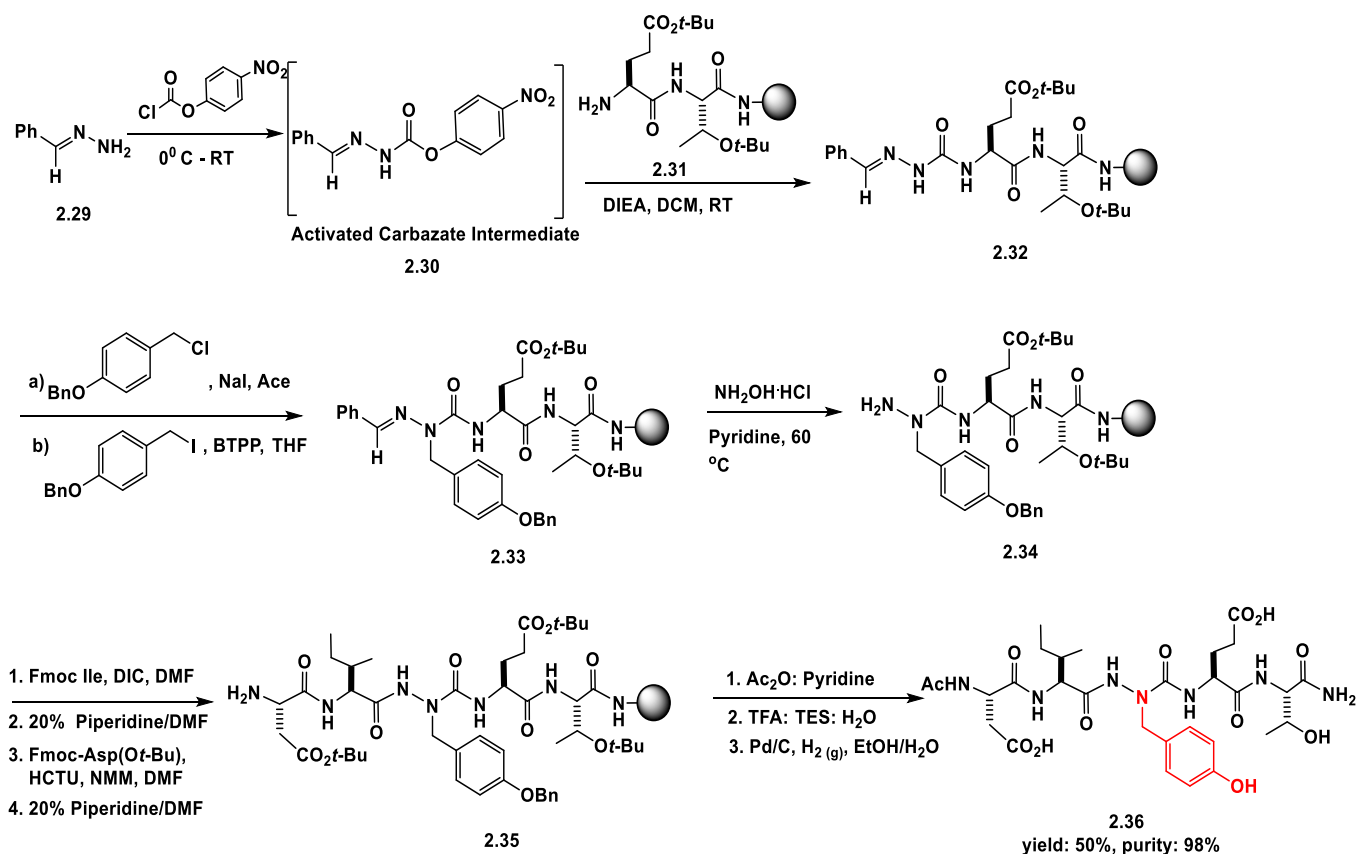
Figure 2.5. Aza-amino acid scanning of Ac-DIYET-NH₂, **2.28**, for IRTK inhibitory activity.²³

2.4 RESULTS AND DISCUSSION

The native sequence Ac-DIYET-NH₂ **2.28** and an analog Ac-DIFET-NH₂ **2.43** were synthesized by SPPS using Rink amide AM resin in 75% isolated yields. The submonomer approach was adopted and optimized for the preparation of azapeptide analogs of the Ac-DIYET-NH₂, **2.28**, sequence. Reaction conditions were initially developed for Ac-DIazaYET-NH₂, **2.36**. This methodology consisted of an activation and coupling step, which facilitated the introduction of an activated carbamate intermediate, **2.30**, onto the peptide

bound support, **2.31**, to generate the *N*-terminal semicarbazone, **2.32**. Regioselective alkylation was next accomplished by a tandem halogen exchange and alkylation reaction. Halogen exchange of 4-benzyloxybenzyl chloride and sodium iodide²⁴ resulted in the formation of 4-benzyloxybenzyl iodide *in-situ*. The more reactive benzyl iodide was used as alkylating reagent with the non-ionic Schwesinger phosphazene-base, *tert*-butylimino-tri(pyrrolidino)phosphorane, BTPP²⁵ to generate the alkylated semicarbazone, **2.33**. No alkylation was observed by the reaction of 4-benzyloxybenzyl chloride, BTPP and the semicarbazone bound support, highlighting the importance of the halogen exchange step to yield the more reactive 4-benzyloxybenzyl iodide electrophile. Following alkylation, transamination of the *N*-terminal semicarbazone, **2.33**, to generate semicarbazide, **2.34**, was completed in a pre-set incubator (60 °C, 100 rpm, 12 h) by treating the resin in a solution of hydroxylamine hydrochloride buffered in pyridine (1.5 M). These mild conditions were found to be chemo-selective for the removal of the semicarbazone group while leaving the side chain protecting groups intact and minimizing the premature cleavage of the azapeptide from the solid support. Following semicarbazone deprotection, conventional solid phase peptide synthesis¹⁵, was used to complete the partially protected azapeptide, **2.35**. Attempts for the removal of the aza-Tyr benzyl protecting group from the azapeptide bound support were unsuccessful on solid phase, resulting in minor deprotection yields and concomitant side product formation. Therefore, the azapeptide was cleaved from the Rink amide-linked polystyrene solid support²⁶ and deprotection of the acid-labile side chain protecting groups were accomplished in TFA with H₂O and TES scavenging the reactive tetrabutyl carbonium ion species.²⁷ The removal of the aza-Tyr benzyl protecting group was next accomplished in solution by a Pd/C catalyzed hydrogenolysis reaction⁸ which finally afforded the desired Ac-DIazaYET-NH₂, **2.36**, (Scheme 2.6). Following purification and characterization by RP-

LCMS, **2.36**, was isolated in yields of 50% and purities >95% as ascertained by RP-LCMS (Figure 2.6).



Scheme 2.6. Submonomer solid phase synthesis of Ac-DIazaYET-NH₂ (**2.36**).

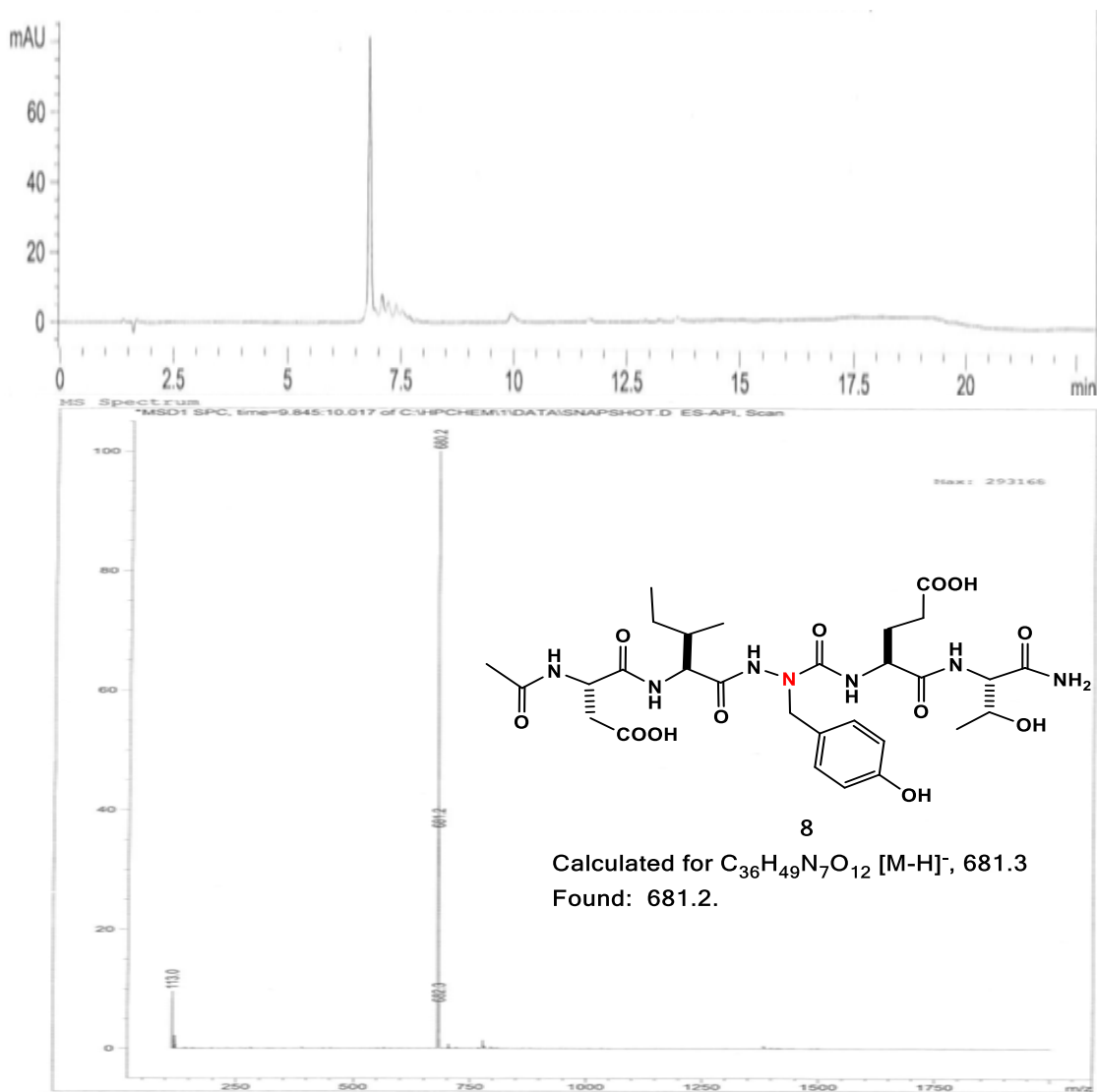
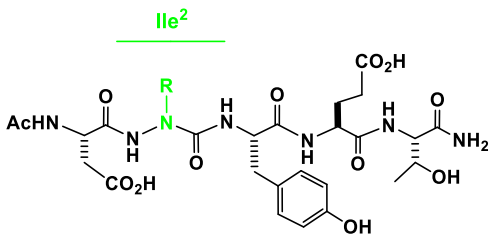
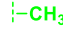


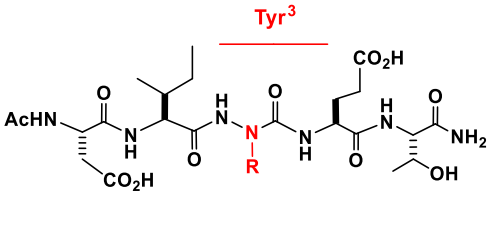
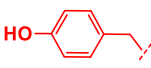
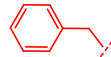
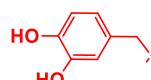
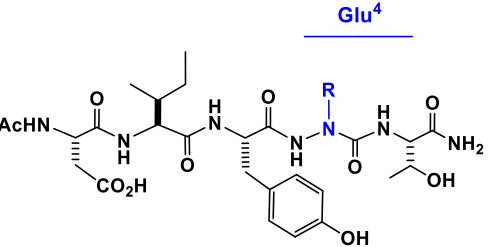
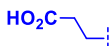


Figure 2.6. LCMS spectra of Ac-DIazaYET-NH₂, **2.36**.

Azapeptide analogs targeting the IYE pharmacophoric region of the parent pentapeptide Ac-DIYET-NH₂, **2.28**, were next prepared by the established submonomer synthesis method (**Scheme 2.6**) and characterized by RP-LCMS (**Table 2.1**). At the 2 position, [aza-Ile²] and [aza-Ala²] residues were introduced respectively by alkylation with 2-iodobutane and methyl iodide in the presence of BTPP. The [aza-Gly²]-residue was recovered without alkylation to generate azapeptides (**2.37-2.39**) in isolated yields of 51-55% and

purities > 95%. Of note, the aza-Ile residue was synthesized in racemic form due to the achiral 2-iodobutane used as alkylating reagent. However, a single azapeptide diastereomer for **2.38** was isolated by RP-LCMS for structure-activity relationship studies. Moving to the 3 position, the [aza-Phe³] residue was constructed with KOtBu as base and benzyl bromide as alkylating reagent to produce the Ac-DIazaFET-NH₂, **2.40**, analog, in good yields (43%) and isolated purities (96%) according to RP-LCMS analyses. In the case of [aza-Tyr³], and [aza-DOPA³], halogen exchange reactions²⁴ converting the alkylating reagents 4-benzyloxybenzyl chloride and 3,4-dibenzyloxybenzyl chloride, respectively, to their corresponding alkyl iodides in the presence of BTPP improved yields (36-50%) and purities >95% for the desired azapeptides (**2.36**, **2.41**). At the 4 position, [aza-Glu⁴] was installed using Michael addition chemistry¹⁷ with KOtBu and *tert*-butyl acrylate to generate Ac-DIYazaET-NH₂, **2.42**, in isolated yields of 42% and 96% purity.

Table 2.1. Characterization data of azapeptides synthesized in this study.

	entry	R	crude purity ^a	isolated purity ^b	isolated yield ^c	mass ^d	RT (min) ^e	RT (min) ^f
 <p>Ile²</p>	2.37		73%	96%	51%	638.2(638.3)	7.42	5.26
	2.38		74%	95%	55%	680.2(680.3)	6.97	5.13
	2.39		63%	96%	55%	624.2(624.2)	6.99	5.04
 <p>Tyr³</p>	2.36		44%	98%	50%	681.2(681.3)	9.95	6.68
	2.40		61%	96%	43%	666.3(666.2)	11.76	7.76
	2.41		22%	95%	36%	698.2(698.3)	8.90	6.33
 <p>Glu⁴</p>	2.42		58%	96%	42%	680.3(680.2)	9.61	6.41

^aCrude purity by RP-LCMS at 214 nm using 2-90% MeOH in H₂O with 0.1% FA over 15 min. ^bIsolated purity by RP-LCMS at 214 nm using 2-90% MeOH in H₂O with 0.1% FA over 15 min. ^cCalculated from resin loading. ^dObserved mass (expected mass) as [M+H]⁺ or [M-H]⁻ by ESI-MS in positive or negative mode. Retention times (min) by RP-LCMS at 214 nm using 2-90% ^eMeOH or ^fMeCN in H₂O with 0.1% FA over 15 min.

2.5 CONCLUSIONS

In conclusion, a new class of azapeptide analogs of the Ac-DIYET-NH₂, **2.28**, sequence were constructed by submonomer synthesis. Submonomer solid phase synthesis furnished a small library (7) of azapeptides featuring the introduction of new aza-Ile and aza-DOPA residues. Halogen exchange reactions were found to be particularly well suited for the introduction of aza-Tyr and aza-DOPA residues at the Tyr³ position. These reactions were used to convert the poorly reactive benzyl chlorides to the more reactive iodides which furnished azapeptide, **2.36** and **2.41** in 50 and 36% yields, respectively. The aza-isoleucine analog was synthesized using racemic 2-iodobutane as alkylating agent in the presence of BTPP. Although this resulted in diastereomeric Ac-DazaIYET-NH₂, **2.38**, RP-LCMS purification and analysis provided a single diastereomer, suitable for SAR studies. Azapeptides were isolated in sufficient yields (36-55%) and good purities (>95%) following submonomer synthesis and RP-LCMS purification. Thus, the submonomer approach for azapeptide synthesis proved to be an efficient methodology for the combinatorial preparation of azapeptides useful for structure-function studies. With purified constructs in hand, opportunity now exists for exploring influence of azapeptide configuration, conformation and side chain interactions on IRTK binding and inhibitory activity (Chapters 3 and 4).

2.6 EXPERIMENTAL SECTION

Materials. Fmoc-Asp(OtBu), Fmoc-Ile, Fmoc-Tyr(*t*-Bu), Fmoc-Glu(*t*-Bu) and Fmoc-Thr (*t*-Bu) and Fmoc-Phe were purchased from Novabiochem™ (EMD Millipore) and used as received. Polystyrene Rink Amide AM resin (0.79 mmol/g) was purchased from Novabiochem™ (EMD Millipore), and the manufacturer's reported loading of the resin was used in the calculation of the yields of the final products. Reagents used for the submonomer

solid phase synthesis of azapeptides include, *tert*-butyl acrylate (TCI), 3,4-dibenzyloxybenzyl chloride (Acros), hydroxylamine hydrochloride (Alfa Aesar), potassium *t*-butoxide (Aldrich), *N,N*-diisopropylcarbodiimide, DIC (TCI), *N*-methyilmorpholine, NMM (Acros), piperidine, *N,N*-diisopropylethylamine, DIEA (Aldrich), triethylsilane, TES (Alfa Aesar), benzyl bromide BnBr (TCI), 4-nitrophenyl chloroformate (Alfa Aesar), palladium 10% weight on activated carbon, Pd/C (Aldrich), acetic anhydride, Ac₂O (Mallinckrodt) hydrazine hydrate (Alfa Aesar), trifluoroacetic acid TFA (Alfa Aesar), pyridine (Alfa Aesar), 2-iodobutane (TCI), 4-benzyloxybenzyl chloride (Aldrich), iodomethane (Alfa Aesar), *tert*-Butylimino-tri(pyrrolidino)phosphorane, BTPP (Aldrich), *N,N*-dimethylformamide DMF (Macron), formic acid FA (Aldrich), dichloromethane DCM (Macron), methanol MeOH (Macron), acetone Ace (Macron), acetonitrile MeCN (Macron), tetrahydrofuran THF (BDH) and *O*-(1H-6-Chlorobenzotriazole-1-yl)-1,1,3,3-tetramethyluronium hexafluorophosphate HCTU (Creosalus).

Fmoc-based Solid Phase Peptide Synthesis.

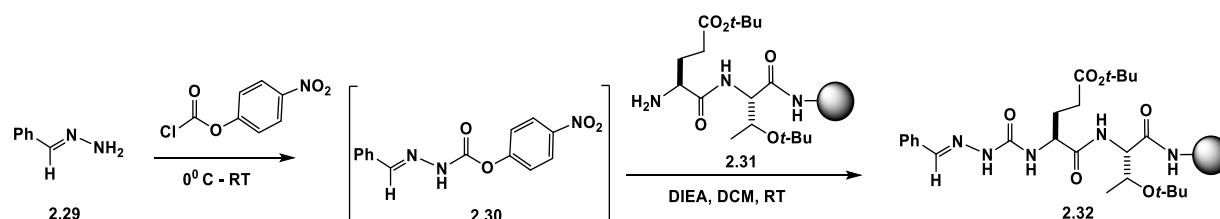
Peptide syntheses were performed under standard Fmoc-SPPS conditions¹⁵ on a PSI 200C Peptide Synthesizer (Peptide Scientific, New York NY) using Polystyrene Rink Amide AM resin (0.79 mmol/g). Couplings of amino acids (3 equiv.) were performed in DMF using HCTU (3 equiv.) as coupling reagent and NMM as base (6 equiv.). About 5 equiv. of amino acids and HCTU and 10 equiv. of NMM were used for the coupling of the first amino acid [Fmoc Thr(*t*-Bu)] to the resin. Fmoc deprotections were performed by treating the peptide bound resin with 20% piperidine in DMF for 20 min. The resin was washed after each coupling and deprotection steps with DMF (3 x 10 mL). *N*-terminal acetylation was performed by addition of acetic anhydride (0.1 mmol, 50 equiv. 472 μ L) and pyridine (400

μL) in DMF (1.5 mL). The reaction was continued for about 20 minutes on an overhead shaker. The peptide bound resin was vacuum filtered and washed with DMF (3 x 10 mL), MeOH (3 x 10 mL), THF (3 x 10 mL), and DCM (3 x 10 mL). The purity of di-, [Glu-Thr-CONH₂] tri-, [Tyr-Glu-Thr-CONH₂] & [Phe-Glu-Thr-CONH₂] and tetra- [Ile-Tyr-Glu-Thr-CONH₂] & [Ile-Phe-Glu-Thr-CONH₂] peptide fragments were ascertained by molecular weight confirmation using ESI-LCMS following cleavage and deprotection of small aliquots of resin. After each step during the synthesis of control sequences as well as azapeptides, reaction monitoring and verification of the products, were performed by LCMS.

Cleavage test of resin-bound peptide. A small portion of the peptide bound resin (3-5 mg) was treated with a freshly made solution of TFA/H₂O/TES (95:2.5:2.5, v/v/ v, 0.5 mL) for about 30 min at room temperature. The cleavage mixture was filtered and then concentrated under air or nitrogen and crude peptide was precipitated with cold ether (1.5 mL). Crude peptide samples were agitated on a vortex shaker, and spun in a centrifuge followed by decantation of the supernatant which left a pellet that was dissolved in 50% MeCN/H₂O (about 1 mg/mL) and injected in LCMS for analyses.

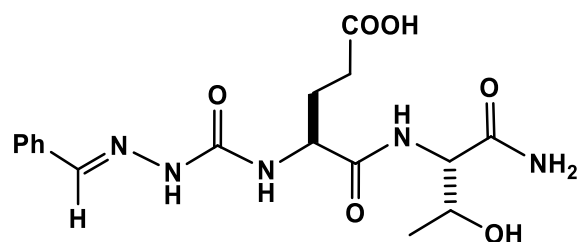
Submonomer azapeptide synthesis.

Representative protocol for aza-Gly peptide synthesis, preparation of semicarbazone-azaGly-Glu(*t*-Bu)-Thr(*t*-Bu) Rink amide AM resin (2.32).



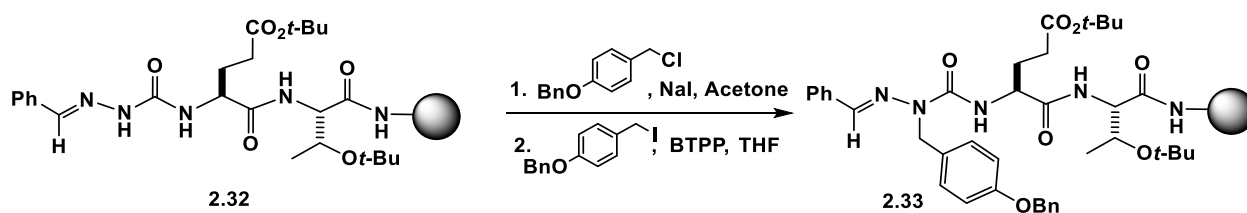
To a stirred solution of EtOH (1.5 mL) in a vial equipped with a magnetic stirrer at 0 °C, was added hydrazine hydrate (56 µL, 1.8 mmol). To this reaction mixture, dropwise addition of benzaldehyde (61 µL, 0.6 mmol) was added. The reaction progress was tracked by TLC, [(2:1 Hexane:EtOAc), R_f (benzaldehyde): about 0.7 and R_f (benzaldehyde hydrazone): about 0.6] which indicated complete reaction in about 15 min. The reaction mixture was quenched in H₂O (5 mL) and the desired benzaldehyde hydrazone was extracted with DCM (3 x 5 mL). The organic phase was dried with anhydrous MgSO₄ or Na₂SO₄, concentrated to yield the crude product (70 mg, 98%) that was employed without further purification.

Benzaldehyde hydrazone (70 mg, 0.6 mmol, 3 equiv.) was dissolved in DCM (1 mL) and added dropwise over 15 min to a solution of *p*-nitrophenyl chloroformate (123 mg, 0.61 mmol, 3.2 equiv.) in DCM (1 mL) at 0 °C. The reaction mixture was warmed to room temperature (22 °C) and stirred for an additional 1.5 h under nitrogen. Complete conversion of the starting material to the activated carbamate intermediate, **2.30**, was confirmed by TLC [(2:1 Hexane:EtOAc), R_f: 0.75]. DIEA (210 µL, 1.2 mmol, 6 equiv.) was added to neutralize the reaction mixture (20 min at 0°C) and the suspension was added to the resin for the coupling reaction. This reaction was mixed on an automated shaker for 16 h at room temperature. The next day, the resin was filtered and washed under vacuum with DMF (3 x 10 mL), MeOH (3 x 10 mL), THF (3 x 10 mL), and DCM (3 x 10 mL). The reaction conversion was monitored by analyzing a small sample of resin (~3 mg) by LCMS following peptide cleavage and deprotection [1 mL, TFA/TES/H₂O (95:2.5:2.5, v/v/v)] from the solid support.



Benzaldehyde semicarbazone-azaGly-Glu-Thr-CONH₂ (2.32). ESI-LCMS [2-90% MeOH in H₂O (0.1% FA), 15 min] RT = 6.5 min; Calculated for C₁₃H₂₃N₅O₆ [M+H]⁺ 394.1 found *m/z* 394.1.

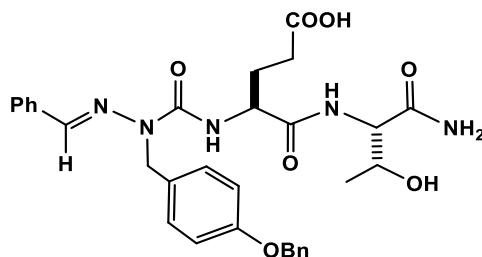
Representative alkylation of aza-Gly, preparation of semicarbazone-azaTyr(OBn)-Glu(*t*-Bu)-Thr(*t*-Bu) Rink amide AM resin (2.33).



For benzyl chloride derivatives, Finkelstein reactions²⁴ were performed by dissolving 4-benzyloxybenzyl chloride (140 mg, 0.1 mmol, 6 equiv.) and NaI (180 mg, 1.2 mmol, 12 equiv.) in acetone (1 mL). The reaction was refluxed overnight (16 h) for the production of 4-benzyloxybenzyl iodide. The reaction mixture was quenched with water (3 mL) and extracted with ether (2 x 10 mL). The ether layer was isolated and dried over anhydrous MgSO₄ and the solution was evaporated to dryness under vacuum.

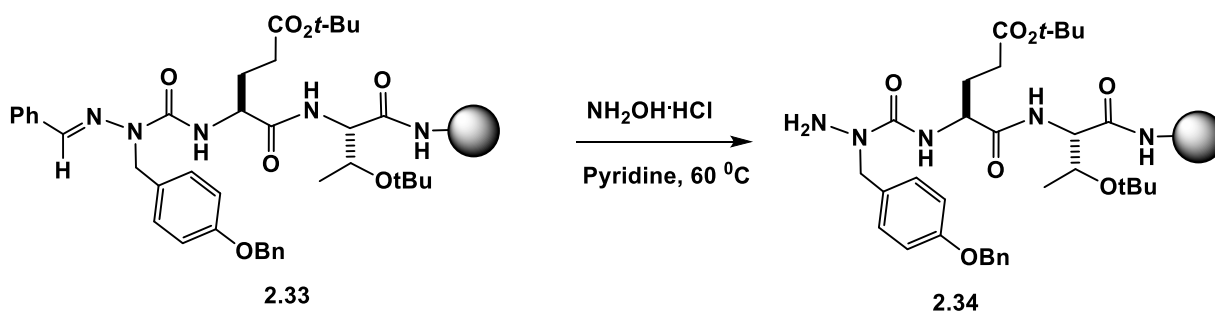
The semicarbazone peptide bound resin **2.32** (0.1 g, 67 μmol) was swollen in THF (1 mL), and BTPP (92 μL, 0.1 mmol, 3 equiv.) was added to activate the semicarbazone for the alkylation reaction. The mixture was agitated on an automated shaker for about 20 min, and then treated with 4-benzyloxybenzyl iodide (196 mg, 0.1 mmol, 3 equiv.) at room

temperature for an additional 16 h. The resin was filtered, then washed with DMF (2 x 10 mL), MeOH (2 x 10 mL), THF (2 x 10 mL), and DCM (2 x 10 mL) and dried under vacuum. The extent of reaction was monitored by sampling an aliquot (~3 mg) of resin which was subjected to 1 mL of TFA/TES/H₂O (95:2.5:2.5, v/v/v) for cleavage and deprotection of the crude peptide.



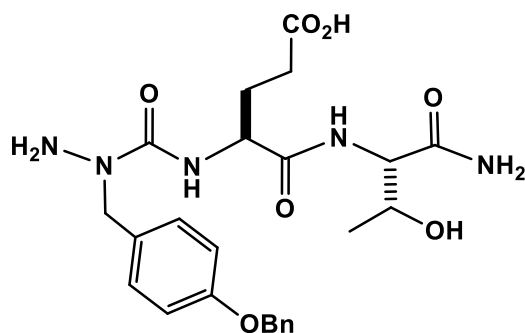
Benzaldehyde semicarbazone-azaTyr(OBn)-Glu-Thr-CONH₂ (2.33). ESI-LCMS [2-90% MeOH in H₂O (0.1% FA), 15 min] RT = 12.5 min; Calculated for C₃₁H₃₅N₅O₇ [M+H]⁺, 590.2 found *m/e* 590.2.

Representative protocol for semicarbazone removal, preparation of azaTyr(OBn)-Glu(*t*-Bu)-Thr(*t*-Bu) Rink amide AM resin (2.34).



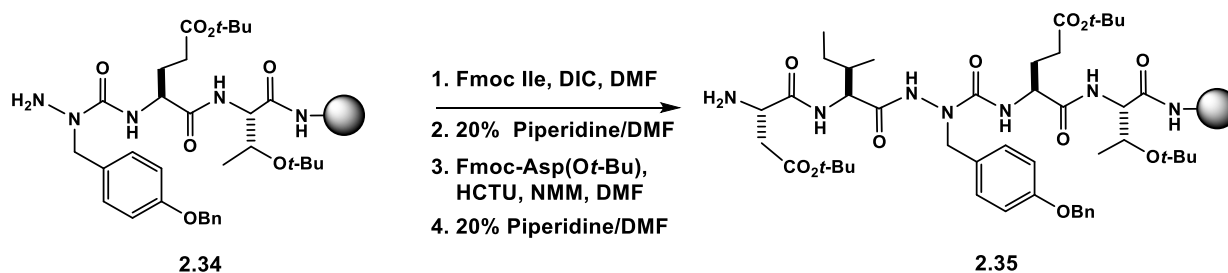
The resin-bound semicarbazone **2.33** (0.1 g, 67 μmol) was treated with a solution of 1.5 M NH₂OH·HCl in pyridine (2.5 mL) and the semicarbazone transamination reaction was completed in a pre-set incubator (60 °C, 100 rpm, 12 h) to liberate the resin bound

semicarbazide **2.34**. The resin was filtered and washed under vacuum with DMF (3 x 10 mL), MeOH (3 x 10 mL), THF (3 x 10 mL), and DCM (3 x 10 mL). The extent of the reaction was monitored by ESI-LCMS, by cleaving and deprotecting an aliquot (~3 mg) of resin with TFA/TES/H₂O (1 mL, 95:2.5:2.5, v/v/v).



azaTyr(OBn)-Glu-Thr-CONH₂ (2.34). ESI-LCMS [2-90% MeOH in H₂O (0.1% FA), 15 min] RT = 8.5 min; Calculated for C₂₄H₃₁N₅O₇ [M+H]⁺, 502.2 found *m/z* 502.2.

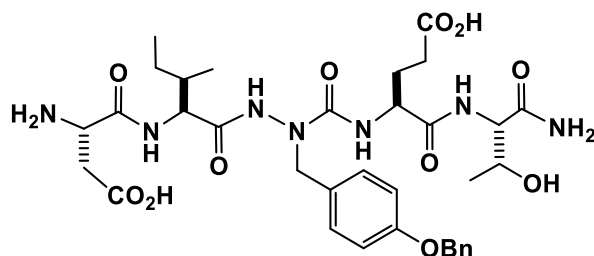
Preparation of Asp(*t*-Bu)-Ile-azaTyr(OBn)-Glu(*t*-Bu)-Thr(*t*-Bu) Rink amide AM resin (2.35).



Fmoc-Ile (353 mg, 0.67 mmol, 10 equiv.) and diisopropylcarbodiimide (77 μ L, 0.34 mmol, 5 eq) in DCM (1 mL) were reacted for 20 min on ice. The suspension was then concentrated *in vacuo*, dissolved in DMF (1 mL), and added to semicarbazide peptide resin **2.34** (0.1 g, 67 μ mol) for the coupling reaction. This reaction was continued for an additional 16 h at room temperature (22 °C) and the resin was filtered and washed under vacuum with DMF (3 x 10

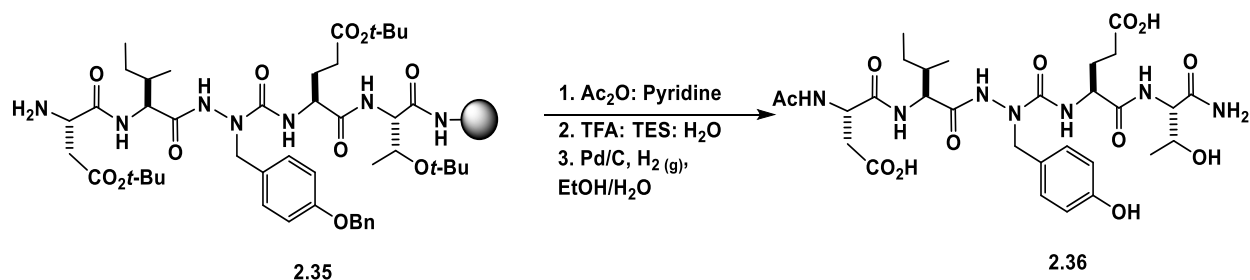
mL), MeOH (3 x 10 mL), THF (3 x 10 mL), and DCM (3 x 10 mL). Fmoc deprotection was performed by addition of 20% piperidine in DMF (2 mL) and the reaction was continued on an overhead shaker for 20 minutes at 22° C. Upon completion of the Fmoc deprotection reaction, the azapeptide bound resin was vacuum filtered, washed with DMF (3 x 10 mL), MeOH (3 x 10 mL), THF (3 x 10 mL), and DCM (3 x 10 mL).

Fmoc-Asp(*t*-Bu) (123 mg, 0.3 mmol, 3 equiv.), HCTU (124 mg, 0.3 mmol, 5 equiv.) and NMM (66 μ L, 0.6 mmol, 6 equiv.) were dissolved in DMF (1 mL) and added to the resin. The reaction was agitated on an overhead shaker for 30 min. The resin was then filtered and washed under vacuum with DMF (3 x 10 mL), MeOH (3 x 10 mL), THF (3 x 10 mL), and DCM (3 x 10 mL). Fmoc deprotection was then performed as previously described. The sample crude purity was analyzed by ESI-LCMS by subjecting an aliquot (~3 mg) of resin to the cleavage and deprotection conditions [1 mL, TFA/TES/H₂O (95:2.5:2.5, v/v/v)].

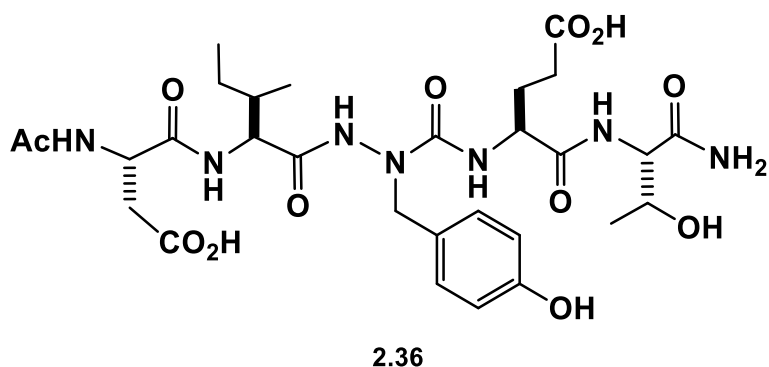


Asp-Ile-azaTyr(OBn)-Glu-Thr-CONH₂ (2.35). ESI-LCMS [2-90% MeOH in H₂O (0.1% FA), 15 min] RT = 8.5 min; Calculated for C₂₄H₃₁N₅O₇ [M+H]⁺, 615.3 found *m/z* 615.3.

Preparation of Ac-Asp-Ile-azaTyr-Glu-Thr-CONH₂ (2.36).



N-terminal acetylation was performed by addition of acetic anhydride (0.1 mmol, 50 equiv. 472 μ L) and pyridine (400 μ L) in DMF (1.5 mL). The reaction was continued for about 20 minutes on an overhead shaker. The peptide bound resin was vacuum filtered and washed with DMF (3 x 10 mL), MeOH (3 x 10 mL), THF (3 x 10 mL), and DCM (3 x 10 mL). The extent of reaction was monitored by subjecting an aliquot (~3 mg) of resin to cleavage conditions [1 mL, TFA/TES/H₂O (95:2.5:2.5, v/v/v)] and analyzing the crude by LCMS. The azapeptide (0.2 mmol) was then dissolved in ethanol:water (1 mL, 50:50 v/v) and 10% Pd/C catalyst (20 mg) was added to the solution. A hydrogen filled balloon was placed over the reaction vessel and the reaction was continued overnight at room temperature (22 °C). The solution was filtered and lyophilized to a dry powder followed by LCMS analysis as previously described.



Ac-Asp-Ile-Aza-Tyr-Glu-Thr-CONH₂ (2.36). ESI-LCMS [2-90% MeOH in H₂O (0.1% FA), 15 min] RT = 10.1 min; Calculated for C₃₆H₄₉N₇O₁₂ [M-H]⁻, 681.3 found *m/z* 681.2.

Complete deprotection and cleavage of azapeptides (2.36-2.42) from the resin.

The Rink resin-bound azapeptides were deprotected and cleaved from the support using freshly made solutions of TFA/H₂O/TES (95:2.5:2.5, v/v/v, 20 mL/g of peptide resin) at room temperature for 2.5 h. The resin was filtered and rinsed with 1 mL of TFA. The filtrate and rinses were concentrated under a flow of N_{2(g)} until a crude oil persisted. Cold ether (10-15 mL) was then added to crude oil to precipitate the peptide. Following centrifugation (1200 rpm for 10 min.), the supernatant was removed and the crude peptide was taken up in aqueous MeCN or MeOH (10% v/v in water) and freeze-dried to a white solid prior to analysis.

Analyses and purification of azapeptides (2.36-2.42).

Analyses and characterization of crude azapeptides were accomplished on either an AgilentTM Technologies 1100 Series LCMS instrument with ESI ion-source, single quadrupole mass detection and positive or negative mode ionization or a Waters Alliance HPLC system equipped with a photodiode array detector (PDA) for azapeptide analyses at 214 nm. Azapeptide samples were dissolved in 50% H₂O in acetonitrile or methanol (1 mg/mL). The LCMS analyses were performed on a Symmetry Shield C₁₈ reverse-phase column (150 × 4.60 mm, 3.5 μm), using binary solvent system consisting of 0.1% formic acid in H₂O (Mobile phase A), and 0.1% formic acid in methanol (Mobile phase B) at a flow rate of 1.0 mL/min and UV detection at 214 nm. Linear gradients of the mobile phase (0.1% formic acid in methanol, 2-90% over 15 min) were used for analyses of the crude azapeptides.

Purification of azapeptides was conducted on a WatersTM PrepLC instrument equipped with a reverse-phase YMC pack ODS A column (250 × 20 mm, 5 μm), using binary solvent system consisting of 0.1% formic acid in H₂O, and 0.1% formic acid in methanol at a flow rate of 15 mL/min and UV detection at 214 nm. Linear gradients of the mobile phase (0.1% formic acid in methanol, 2-90% in 15 min) were used for purifications of azapeptides. Fractions containing pure azapeptides were combined, freeze-dried and lyophilized to a white powder. Purified azapeptide samples were analyzed for purity by LCMS with a Symmetry Shield C₁₈ reverse-phase column (150 × 4.60 mm, 3.5 μm), with a flow rate of 1.0 mL/min using a 2-90% gradient from water (0.1% FA) to CH₃CN (0.1% FA) or to MeOH (0.1% FA) as previously described.

2.7 REFERENCES

1. Gante, J. *Synthesis* **1989**, 405-413.
2. Jamieson, A.G.; Boutard, N.; Sabatino, D.; Lubell, W.D. *Chem. Biol. Drug Des.* **2013**, *81*, 148-165.
3. Proulx, C.; Sabatino, D.; Hopewell, R.; Spiegel, J.; Ramos, Y.G.; Lubell, W.D. *Future Med. Chem.* **2011**, *3*, 1139 – 1164.
4. Zega, A. *Curr. Med. Chem.* **2005**, *12*, 589–597.
5. Hess, H.J.; Marchand, W.T.; Laubach, G.D. *J. Am. Chem. Soc.* **1963**, *85*, 4040-4041.
6. Sabatino, D.; Proulx, C.; Klocek, S.; Bourguet, C.B.; Boeglin, D.; Ong, H.; Lubell, W.D. *Org. Lett.* **2009**, *11*, 3650- 3653.
7. Quibell, M.; Turnell, W.G.; Johnson, T. *J. Chem. Soc. Perkin Trans. 1*, **1993**, 2843-2849.
8. Melendez, R.E.; Lubell, W.D. *J. Am. Chem. Soc.* **2004**, *126*, 6759-6764.
9. Boeglin, D.; Lubell, W.D. *J. Comb. Chem.* **2005**, *7*, 864-878.
10. (a) Freeman, N.S.; Hurevich, M. and Gilon, C. *Tetrahedron* **2009**, *65*, 1737-1745, (b) Freeman, N.S.; Tal-Gan, Y.; Klein, S.; Levitzki, A.; Gilon, C. *J. Org. Chem.* **2011**, *76*, 3078-3085.
11. Gray, C. J.; Quibell, M.; Bagget, N.; Hammerle, T. *Int. J. Pept. Protein Res.* **1992**, *40*, 351-362.
12. Liley, M.; Johnson, T. *Tetrahedron Lett.* **2000**, *41*, 3983.
13. O'Donnell, M.J.; Zhou, Changyou, Z.; Scott, W.L. *J. Am. Chem. Soc.* **1996**, *118*, 6070-6071.
14. (a) Zhao, L.; Li, C-J. *Angew. Chem. Int. Ed.* **2008**, *47*, 7075-7078, (b) Zhao, L.; Basle, O.; Li, C-J. *Proc. Natl. Acad. Sci. USA* **2009**, *106*, 4106-4111, (c) Ooi, T.; Kameda, M.;

- Maruoka, K., *J. Am. Chem. Soc.* **1999**, *121*, 6519-6520, (d) Ooi, T.; Tayama, E.; Maruoka, K. *Angew. Chem. Int. Ed. Engl.* **2003**, *42*, 579-582.
15. Collins, J.M.; Porter, K.A.; Singh, S.K.; Vanier, G.S. *Org. Lett.* **2014**, *16*, 940-943.
16. Han, H.; Janda, K.D. *J. Am. Chem. Soc.* **1996**, *118*, 2539-2544.
17. Sabatino, D.; Proulx, C.; Pohankova, P.; Ong, H.; Lubell, W.D. *J. Am. Chem. Soc.* **2011**, *133*, 12493-12506.
18. Proulx, C.; Lubell, W. D. *Org. Lett.* **2010**, *12*, 2916-2919.
19. Proulx, C.; Lubell, W. D. *J. Org. Chem.* **2010**, *75*, 5385-5387.
20. Zhang, J.; Proulx, C.; Tomberg, A.; Lubell, W.D. *Org. Lett.* **2014**, *16*, 298-301.
21. (a) Proulx, C.; Lubell, W.D. *Org. Lett.* **2012**, *14*, 4552-4555, (b) Proulx, C.; Lubell, W.D. *Biopolymers* **2014**, *102*, 7-15.
22. Doan, N.D.; Hopewell, R.; Lubell, W.D. *Org. Lett.* **2014**, *16*, 2232-2235. Kurian, L.; Silva, T.; Sabatino, D. *Bioorg. Med. Chem. Lett.* **2014**, *manuscript in revision*.
24. Conant, J.B.; Kirner, W.R.; Hussey, R.E. *J. Am. Chem. Soc.* **1925**, *47*, 488-501.
25. Schwesinger, R.; Willaredt, J.; Schlemper, H.; Keller, M.; Schmitt, D.; Fritz, H.; *Chem. Ber.* **1994**, *127*, 2435-2454.
26. Rink, H.; *Tetrahedron Lett.* **1987**, *28*, 3787-3790.
27. King, D.S.; Fields, C.G.; Fields, G.B. *Int. J. Pept. Protein Res.* **1990**, *36*, 255-266.

CHAPTER 3: AZAPEPTIDE STRUCTURAL STUDIES BY MOLECULAR MODELING, CD AND NMR SPECTROSCOPY

3.1 ABSTRACT

The structural characterization of the azapeptide analogs (**Table 2.1, sequence no. 2.36-2.42**) of the Ac-DIYET-NH₂, sequence were performed by molecular modeling and docking simulations, circular dichroism (CD) and NMR spectroscopy. Computational analyses were initially performed to determine the structural differences between the azapeptide analog, Ac-DIazaYET-NH₂, sequence **2.36** and its parent sequence, **2.28**. Interestingly, the azapeptide sequence, **2.36**, was found to maintain a turn-type geometry which translated into tight binding affinity ($< 5\text{\AA}$) within the active site of the insulin receptor tyrosine kinase (IRTK) domain. The structural properties of the azapeptides synthesized in this study (**Chapter 2, Table 2.1**) were further analyzed by CD spectroscopy to determine trends in peptide folds in aqueous media (H₂O and phosphate buffered saline, PBS) and organic solvent (dimethyl sulfoxide, DMSO). The peptides were found to exhibit secondary structural features which contained both random and turn conformations that were contingent on solvent, sequence and position of the aza-amino acid substitutions. Specifically, the CD spectrum of the parent peptide Ac-DIYET-NH₂ (**2.28**), was compared to that of the azapeptide, Ac-DIazaYET-NH₂ (**2.36**). The insertion of the [aza-Tyr³] residue within the $i+2$ position of the native sequence was found to stabilize a β -turn conformation. NMR spectroscopy confirmed the azapeptide β -turn structure by providing evidence of the intramolecular hydrogen bonding interaction in between the CO at the i and the NH at the $i+3$ position. Moreover, 2D NOESY correlation studies supported the azapeptide fold, highlighting the influence of the [aza-Tyr³] residue in locking the turn-type geometry. In light

of the stable azapeptide folded structures which may translate into IRTK binding and inhibitory activity, a structural study is presented within this chapter and concluded with the biological activity of the azapeptides in Chapter 4 of this thesis.

3.2 INTRODUCTION

3.2.1 AZAPEPTIDE STRUCTURE AND CONFORMATION

Introduction of an aza-amino acid within a peptide sequence provides a unique conformational change within the peptide backbone, resulting in a stable turn-type secondary structure.¹ Several model systems were designed and examined to understand the conformational properties of azapeptides. For example, the conformations of a 1,2-diacylhydrazine, which mimics the semicarbazide moiety found within azapeptides, were investigated by computational analyses. These studies indicated that the 1,2-diacylhydrazine adopted a nonplanar global minimum structure in which the nitrogen lone pairs were essentially perpendicular to one another.²⁻⁶ Azapeptide conformation is dictated by the dihedral angles φ (NH-N $_{\alpha}$) and ψ (N $_{\alpha}$ – CO). A variety of computational, spectroscopic and crystallographic methods have been used to study the conformational properties of azapeptides. These studies have shown that azapeptides prefer a narrow range of dihedral angle values ($\varphi = 90^{\circ} \pm 30^{\circ}$ or $-90^{\circ} \pm 30^{\circ}$ and $\psi = 0^{\circ} \pm 30^{\circ}$ or $180^{\circ} \pm 30^{\circ}$) which correspond closely to different types of β -turn secondary structures (**Figure 1.2, Table 1.1**).⁷ Introduction of a semicarbazide residue within a peptide chain causes significant restriction of the peptide backbone favoring nonlinear conformations which mimics several known types of β -turn structures found in naturally occurring peptides and proteins.⁸ Significantly, the stabilized β -turn conformations found within azapeptides have translated into improved peptide biological activity, underscoring their potential in medicinal chemistry applications.⁹⁻¹¹

3.2.2 COMPUTATIONAL ANALYSES

Computational docking experiments of the pentapeptide, Ac-DIYET-NH₂, **2.28**, with the IRTK binding domain were performed with DOCK 6 and its accessories programs.¹² These binding simulations illustrated a folded peptide structure reminiscent of a turn conformation which may contribute to binding affinity (**Figure 3.1**).¹² The docking studies showed that binding site occupied by Ac-DIYET-NH₂, **2.28**, consisted of an ATP binding site and the catalytic loop. Two key residues, Asp 1132 and Arg 1136, found within the catalytic loop of the insulin receptor played a crucial role in the IRTK phosphorylation reactions and may be considered optimal locations for peptide inhibitory activity. According to the IRTK binding studies, the pentapeptide ligand, Ac-DIYET-NH₂, **2.28**, was found near the catalytic site, with the threonine residue interacting with Asp 1132 and Arg 1136 of the IRTK, presumably through hydrophobic and H-bonding interactions. The binding interactions of Ac-DIYET-NH₂, **2.28**, with these 2 key IRTK binding site residues may prevent the entry of ATP substrate to the catalytic site of the receptor. Consequently, IRTK autophosphorylation and activation of its signaling pathways are inhibited. Thus, peptide analogs that may stabilize the bio-active conformation responsible for IRTK binding may lead to the generation of more potent inhibitors of this important receptor.

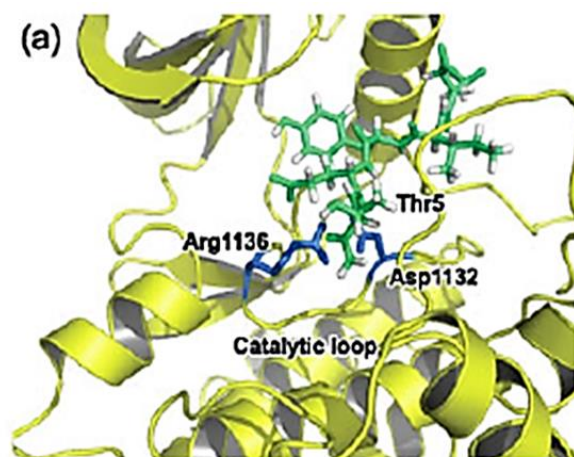


Figure 3.1. Binding model of the pentapeptide ligand, Ac-DIYET-NH₂, **2.28** within the active site of the IRTK. Figure adapted from reference Kato, M. *et al. J. Pept. Sci.* **2009**, *15*, 327.¹²

3.2.3 CD SPECTROSCOPY

Circular Dichroism (CD) spectroscopy is a powerful method in structural biology, useful for the conformational analysis of peptides and proteins. CD spectroscopy is a measure of the difference in light absorption of right versus left-handed polarized light.¹³ When asymmetric molecules such as peptides absorb circularly polarized light, a CD signal that is characteristic of the peptide conformation (ellipticity) as a function of wavelength in the UV (190 - 350 nm) region is generated. Therefore, the CD spectrum provides a unique trace that is contingent on the nature of the chromophores and the asymmetric structure of the peptide.

More specifically, CD spectroscopy is an excellent tool for the rapid evaluation of peptide secondary structures. It may also be useful in determining the various folding patterns of peptides and their mimics, the stabilities of their secondary structures and may also provide valuable information on their binding properties with ligands and receptor targets.¹⁴ Thus, CD spectroscopy is a useful characterization technique for studying peptide secondary

structures in order to gain greater insight into their structure-activity relationships. Although other methods may also be used to evaluate peptide structures, including computational analyses¹⁵, mass spectrometry¹⁶, nuclear magnetic resonance (NMR) spectroscopy¹⁷ and X-ray crystallography¹⁸, the CD study retains the ability to produce quick spectra for a wide range of peptide samples in solution relative to these other laborious techniques.^{13,14} This is because CD spectroscopy provides a non-destructive method for sample analyses while providing opportunity for exploring peptide structure, bio-physical and biological properties.

The chirality of the peptides along with their ability to absorb electromagnetic radiation in the far (190 – 260 nm) and near (260 – 350 nm) UV region make them well suited for conformational analysis by CD spectroscopy. The CD spectrum in this region is dominated by the $n \rightarrow \pi^*$ (C=O) and $\pi \rightarrow \pi^*$ (N-CO) transitions of the amide groups and are reflective of the peptide backbone geometry. The electronic transitions of the peptide functional groups in the far UV-region and the asymmetric peptide geometry produces a CD spectrum that is contingent on the peptide secondary structure. Peptide coils, helices, sheets and turn conformations have all been characterized by CD spectroscopy (**Figure 3.2, i**).^{13,14} A random coil has a broad positive $n \rightarrow \pi^*$ electronic absorption transition at 210 nm and a negative $\pi \rightarrow \pi^*$ transition at 190 nm. The β -sheet peptide secondary structure has a negative $\pi \rightarrow \pi^*$ transition from 230 - 210 nm and a positive $n \rightarrow \pi^*$ transition at 196 nm. Peptide turns have positive $n \rightarrow \pi^*$ transitions in between 220 and 200 nm and a negative band at 190 nm. The CD spectra for α -helices have negative bands at 222 nm and 208 nm and a positive band near 190 nm. In addition to these characteristic electronic absorptions, CD spectroscopy provides information on the asymmetric peptide backbone geometry, that is dictated by the ϕ and ψ torsion angles (**Figure 3.2, ii**).^{13,14,19}

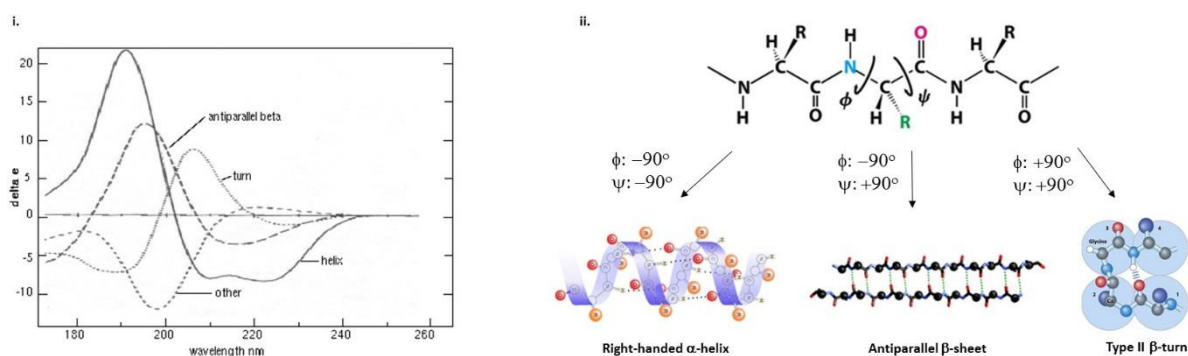


Figure 3.2. Peptide secondary structure analyses **i.** Far UV (180 – 260 nm) CD spectra associated with peptide secondary structures: solid curve, α -helix; long dashes, anti-parallel β -sheet; dots, type I β -turn; dots and short dashes, random coil. **ii.** Peptide dihedral angles (ϕ , ψ) associated with the α -helix, β -sheet and β -turn peptide secondary structures.^{13,14,19}

3.2.4 NMR SPECTROSCOPY

NMR spectroscopy has been used to determine the primary sequences and to study the secondary structures of short model peptides in solution.²⁰⁻²⁴ This is primarily due to the interaction of radiofrequency radiation in an oriented magnetic field with nuclei (^1H , ^{13}C , ^{15}N) that are sensitive to NMR spectroscopy. Considering peptides contain an abundance of NMR sensitive nuclei for analyses, various direct detection (^1H and ^{13}C NMR) and correlation experiments (^1H - ^1H COSY, ^1H - ^1H TOCSY, ^1H - ^1H NOESY, ^1H - ^{13}C HMQC, ^1H - ^{15}N HSQC) have been used to sequence the amino acid residues found within peptides and for mapping their secondary structures. Deuterated solvents are used in NMR spectroscopy to calibrate the instrument to the radiofrequency for detection and to minimize the overlap of solvent signals with sample. Moreover, deuterated solvents (*i.e.* DMSO- d_6 or CDCl_3 / DMSO- d_6 mixtures) that minimize exchange of deuterium with sample protons that are acidic or protic in nature (*e.g.* $-\text{OH}$, $-\text{COOH}$, $-\text{NH}_2$) have been used to characterize peptide

secondary structures. In these deuterated solvent systems, peptide H-bonding interactions that maintain their secondary structures may be detected. Moreover, protons that are solvent exposed and not implicated in peptide folds will produce larger chemical shift changes that are sensitive to solvent and temperature changes. For example, in the NMR study of a model azapeptide, Boc-Ala-Phe-azaLeu-Ala-OMe, the amide proton of Ala⁴ was undisturbed by the switch from chloroform to DMSO-d₆, indicative of its involvement in an intramolecular hydrogen bond.²⁴ Additionally, 2D NOESY experiments may also be used to characterize the nature of the peptide fold by determining which protons are within close NOE (< 5 Å) contact distances. In CDCl₃, the model azapeptide indicated that the amide proton of the [azaLeu³] residue exhibited strong and medium NOE, respectively with the α -proton of [Phe²] and the amide proton of [Ala⁴], suggesting a type II β -turn with the aza-residue located in the *i*+2 position (**Figure 1.5**).²⁴

3.3 CHAPTER OBJECTIVES

Azapeptide analogs of the Ac-DIYET-NH₂ sequence, **2.28**, presented in Chapter 2 will be further investigated in this chapter to determine their structural properties. The structural studies will be initially performed by computational analyses. Molecular modeling will be used to explore the influence of the aza-amino acid residue on azapeptide conformation *in silico*. The Ac-DIazaYET-NH₂ sequence, **2.36**, and its parent peptide, Ac-DIYET-NH₂, **2.28** will be used in a proof-of-concept study to explore the influence of the [aza-Tyr³] residue on peptide backbone configuration and secondary structure. Following conformational analyses of **2.28** a molecular docking simulation study will be conducted to determine the likelihood azapeptide, **2.36**, will bind to the active site of the IRTK. As suitable controls, these binding experiments will be performed in comparison to the parent

pentapeptide, Ac-DIYET-NH₂, **2.28**, and the natural ATP ligand of the IRTK. These simulation experiments will pave the way for structure-activity relationship studies of the azapeptides. CD and NMR spectroscopy will be used to confirm the azapeptide structures in solution. These techniques are especially useful for the rapid and precise elucidation of peptide conformational properties which will serve to validate the computational studies. Moreover, these spectroscopic studies will be useful in supporting the putative β -turn secondary structures found within the azapeptide analogs of the Ac-DIYET-NH₂, **2.28**, sequence. These azapeptides may prove to be useful ligands for the IRTK and related tyrosine kinases for studying enzyme kinetics, mechanisms of action and in regulating their biological activity for therapeutic applications (Chapter 4).

3.4 RESULTS AND DISCUSSION

3.4.1 MOLECULAR MODELING AND DOCKING STUDIES

The binding model of the parent pentapeptide Ac-DIYET-NH₂, **2.28**, with the IRTK has shown that the peptide ligand is positioned near ASP 1132 and ARG 1136, two key residues found within the catalytic loop of the receptor and involved in the autophosphorylation reactions.¹² Molecular docking studies were performed to gain a better understanding of the binding model of the azapeptide analog, Ac-DIazaYET-NH₂, **2.36**, for the kinase domain of the insulin receptor.

The crystal structure of the IRTK domain (Ser⁹⁸¹- Lys¹²⁸³) bound with ATP and a peptide (KKKLPATGDYMNMSVGD) was available from Protein Data Bank (PDB ID # 1IR3, and downloaded from the website (**Figure 3.3**)).²⁵

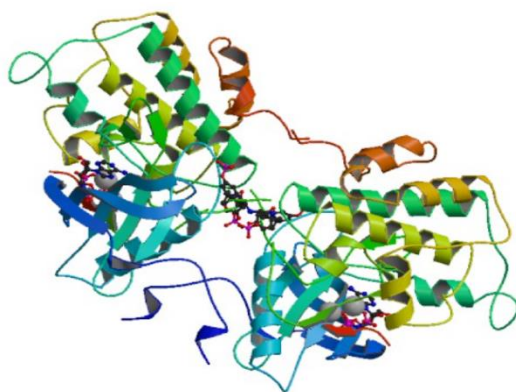


Figure 3.3. Crystal structure of the IRTK downloaded from the Protein Data Bank (PDB ID # 1IR3).²⁵

The crystal structure of the IRTK was saved as a PDBQT file and transported within AutoDock Tools to generate grid functions for the docking simulation studies. A molecular docking study was performed with the azapeptide analog Ac-DIazaYET-NH₂, **2.36**, in relation to the native peptide Ac-DIYET-NH₂, **2.28**, to visualize the binding interactions of the modified peptide with the catalytic loop of the IRTK. An interface between the molecular graphics system PyMOL and the molecular docking suite AutoDock Vina²⁶ was used to demonstrate the combination of docking and visualization models. AutoDock tools were used to generate the PDBQT files of the receptor and the ligands. Vina is the program which performed the docking and its output files were in PDBQT format. The output files were visualized using PyMOL for evaluation of the binding models. The ligand was enclosed in a box with a number of grid points in x, y, z directions, 20 x 22 x 16 and a grid spacing of 1.0 Å. The center of the grid was set to -23.906, 30.439 and 12.466. Vina has generated 9 possible models of the azapeptide analog Ac-DIazaYET-NH₂, **2.36**, binding to the catalytic loop of IRTK. The affinity of these candidates at 37 °C and the probability of their docked conformations were computed according to the Arrhenius equation (**Table 3.1**). The first three candidates were found to be very similar in probability, differing by only about 2.5%.

The visualization of the binding models by PyMOL displayed similar docking locations for the azapeptide, **2.36**. For the docking studies, the lowest energy docked conformation, according to the AutoDock scoring function was selected as the binding model. The results indicated that the proposed Ac-DIazaYET-NH₂, **2.36**, ligand also binds to the catalytic loop of the IRTK, and in closer proximity ($< 5\text{\AA}$) to the key Asp 1132 and Arg 1136 residues, relative to the parent peptide (**Figures 3.4 and 3.5**). Specifically, the azapeptide ligand, Ac-DIazaYET-NH₂, **2.36**, was found to respectively position the threonine amide and the aspartate side chain groups near ($< 5\text{\AA}$) the Asp 1132 and Arg 1136 IRTK residues (**Figure 3.4**). It may be suggested that a combination of hydrogen bonding and ionic interactions were associated with the azapeptide:IRTK binding model. Moreover, the Ac-DIazaYET-NH₂, **2.36**, sequence was found to project a turn-type conformation bound to the IRTK domain that may contribute to binding affinity.

The same grid points were used for the generation of the binding models for the Ac-DIYET-NH₂, **2.28**, sequence. The native peptide was positioned further ($> 5\text{\AA}$) from Asp 1132 and Arg 1136 within the catalytic loop of the IRTK (**Figure 3.5**). Moreover, the parent pentapeptide was found to project a random conformation at the IRTK binding site. Thus, the azapeptide ligand Ac-DIazaYET-NH₂, **2.36**, may confer a stable turn geometry that may translate into tighter IRTK binding and enhanced inhibitory activity relative to the native sequence.

Binding energy calculations for Ac-DIazaYET-NH₂ sequence based on Autodock Vina Output files

Candidate	Affinity (kcal/mol)	(-a/RT)	Affinity at 37 °C (kcal/mol)	Probability
1	-6.5	10.552462	38271.5	0.16668
2	-6.4	10.390116	32536.5	0.14170
3	-6.4	10.390116	32536.5	0.14170
4	-6.3	10.227771	27660.8	0.12047
5	-6.3	10.227771	27660.8	0.12047
6	-6.2	10.065425	23515.7	0.10241
7	-6.1	9.903080	19991.8	0.08707
8	-6.0	9.740734	16996.0	0.07402
9	-5.7	9.253697	10443.1	0.04548

Table 3.1. Binding energy calculations of Ac-DIazaYET-NH₂

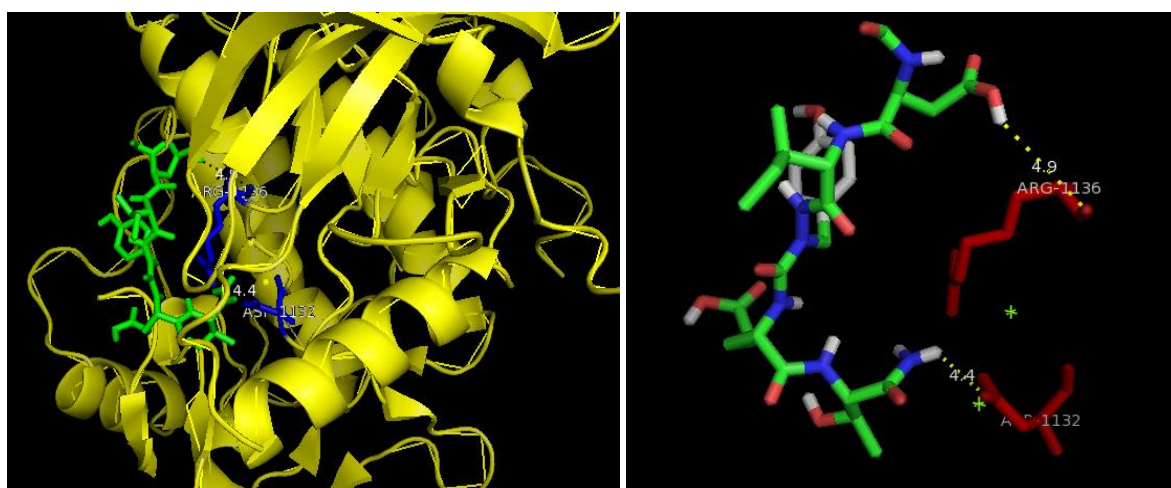


Figure 3.4. Binding models of the azapeptide Ac-DIazaYET-NH₂, **2.36**, for the IRTK binding domain. The spatial distances in between the azapeptide *N*-terminal Asp and the *C*-terminal Thr with the IRTK Arg 1136 and Asp 1132 were respectively found at 4.9 and 4.4 Å.

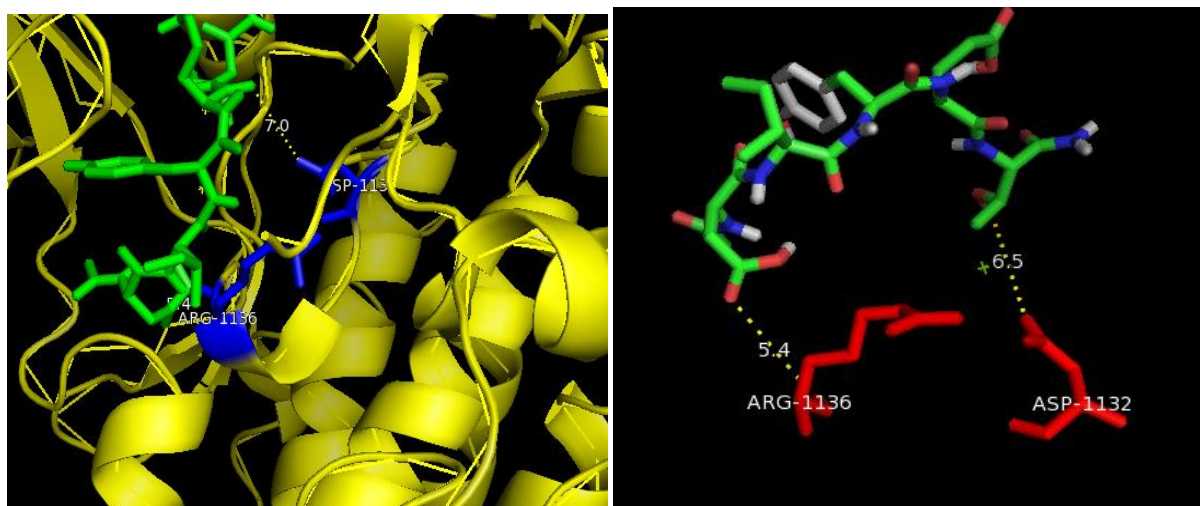


Figure 3.5. Binding models of the native pentapeptide Ac-DIYET-NH₂, **2.28**, for the IRTK binding domain. The spatial distances in between the peptide *N*-terminal Asp and the *C*-terminal Thr with the IRTK Arg 1136 and Asp 1132 were respectively found at 5.4 and 6.5 Å.

3.4.2 CD SPECTROSCOPY

CD spectroscopy was used to determine the propensity for azapeptides to adopt the putative β -turn structure which may contribute to enhanced IRTK binding and inhibitory activity. The main objective of this study was to compare the conformational trends of the parent pentapeptide sequence, Ac-DIYET-NH₂, **2.28**, and its related azapeptide analogs. The CD study was conducted in aqueous conditions (H₂O, phosphate buffered saline, PBS) to determine the influence of salt on peptide conformation. Moreover, the CD spectrum of the peptides was also collected in DMSO, to support the NMR data acquired for the azapeptides dissolved in deuterated DMSO. The conformational study of the azapeptides (**Table 2.1**, **sequence no. 2.37 – 2.42**) was used to determine the influence of the aza-substitution on peptide structure.

The CD spectra of the peptides were measured on an Aviv 62A DS CD Spectrophotometer using a 1.0 cm path-length quartz cell containing peptide (20 μM) dissolved in water, phosphate buffer at pH 7.2 and DMSO at room temperature in the far UV range (190 - 260 nm). The CD spectra were plotted as changes in molar ellipticities (θ) vs. wavelength (nm) **Figures 3.6-3.14**.

In order to assess the influence of solvent on peptide structures, the CD spectrum of the parent peptides Ac-DIYET-NH₂, **2.28**, and Ac-DIFET-NH₂, **2.43**, was compared to the azapeptides (**Table 2.1, sequences 2.37 – 2.42**). At the 2 position, the [aza-Ile²], [aza-Ala²] and the [aza-Gly²]-residues exhibited CD spectra that were respectively associated with random coil in water (**Figure 3.6**), a combination of helical and turn geometries in phosphate buffer (**Figure 3.7**) and folded conformations in DMSO (**Figure 3.8**).¹³ Thus, the solvent conditions were found to impact the azapeptide folds, indicating the influence of solvent and aza substitutions at the *i+1* position on the peptide conformations.

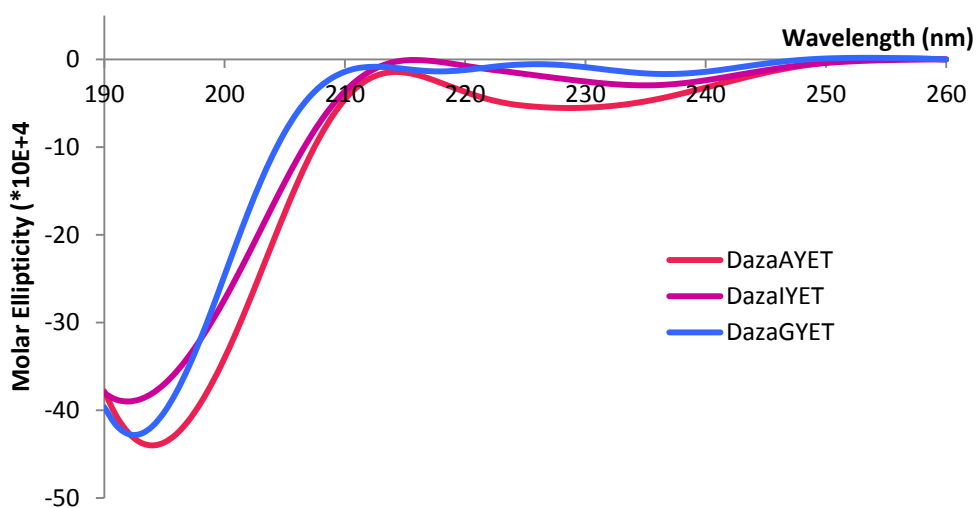


Figure 3.6. CD spectra for Ac-DazaIYET-NH₂, **2.38**, Ac-DazaAYET-NH₂, **2.37**, Ac-DazaGYET-NH₂, **2.39**, (20 μM) in water, at 25 °C.

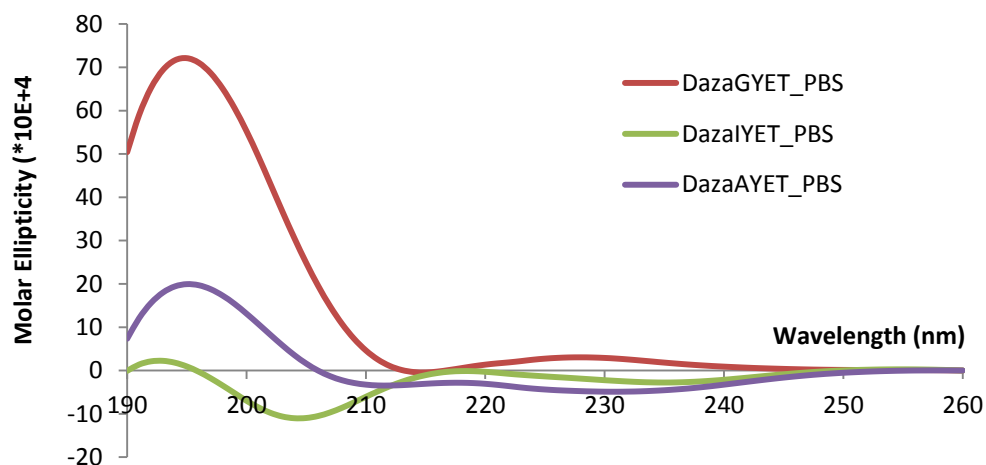


Figure 3.7. CD spectra for Ac-DazaIYET-NH₂, **2.38**, Ac-DazaAYET-NH₂, **2.37**, Ac-DazaGYET-NH₂, **2.39**, (20 μM) in phosphate buffer, at 25 °C.

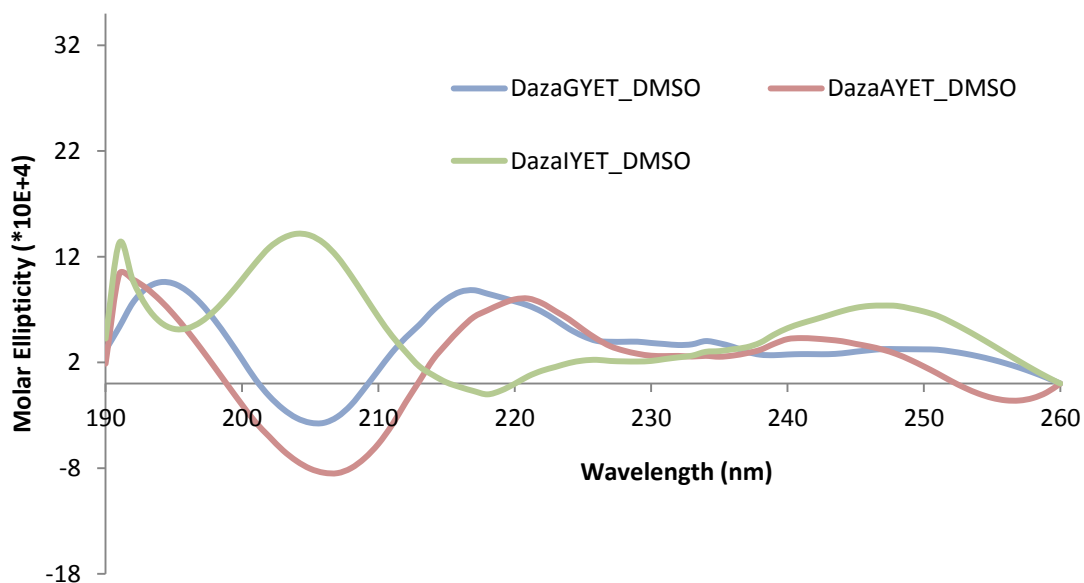


Figure 3.8. CD spectra for Ac-DazaIYET-NH₂, **2.38**, Ac-DazaAYET-NH₂, **2.37**, Ac-DazaGYET-NH₂, **2.39**, (20 μM) in DMSO, at 25 °C.

Moving along to the 3 position of the Ac-DIYET-NH₂, **2.28**, sequence, [aza-Tyr³], [aza-DOPA³] and [aza-Phe³] modifications at the *i*+2 position were studied by CD spectroscopy (Figures 3.9-3.11). The CD curve for the parent peptide was typical of a random coil or a disordered structure, characterized by the strong negative band at 190 nm.¹³ Conversely, the CD curve for the azapeptides in water were found to exhibit a change in conformation, characterized by a positive band near 215 nm and two negative ones near 230 and 190 nm. The observed structure is indicative of a β -turn geometry, with some proportion of random coil due to the sharp negative minima observed near 190 nm (Figure 3.9).^{7,9,10,19,20} The observed β -turn geometry was also maintained for the azapeptide dissolved in phosphate buffer (Figure 3.10), whereas peptide folds were observed in DMSO (Figure 3.11). Thus, the insertion of aza-residues at the *i*+2 position of the native sequence was found to stabilize a turn conformation about the peptide backbone geometry.

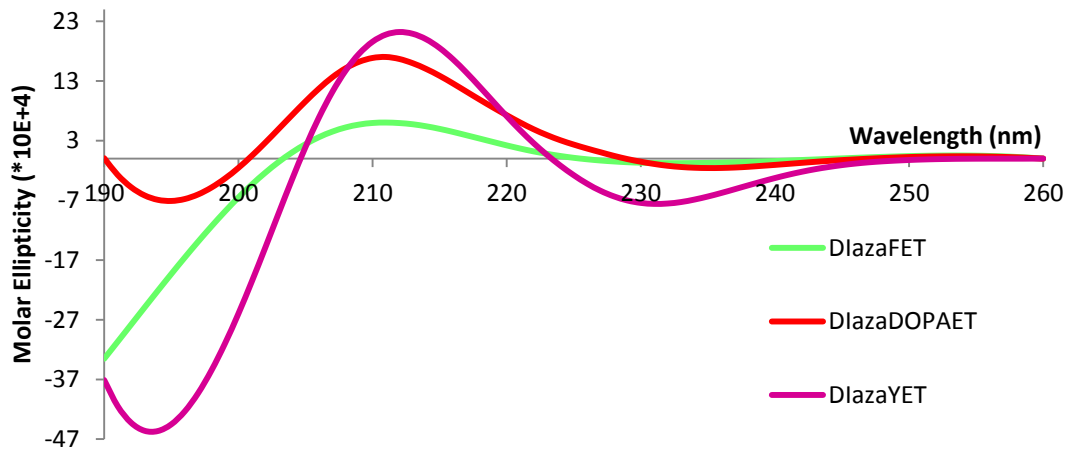


Figure 3.9. CD spectra for Ac-DIazaYET-NH₂, **2.36**, Ac-DIazaFET-NH₂, **2.40**, Ac-DIaza(DOPA)ET-NH₂, **2.41**, (20 μ M) in water, at 25 $^{\circ}$ C.

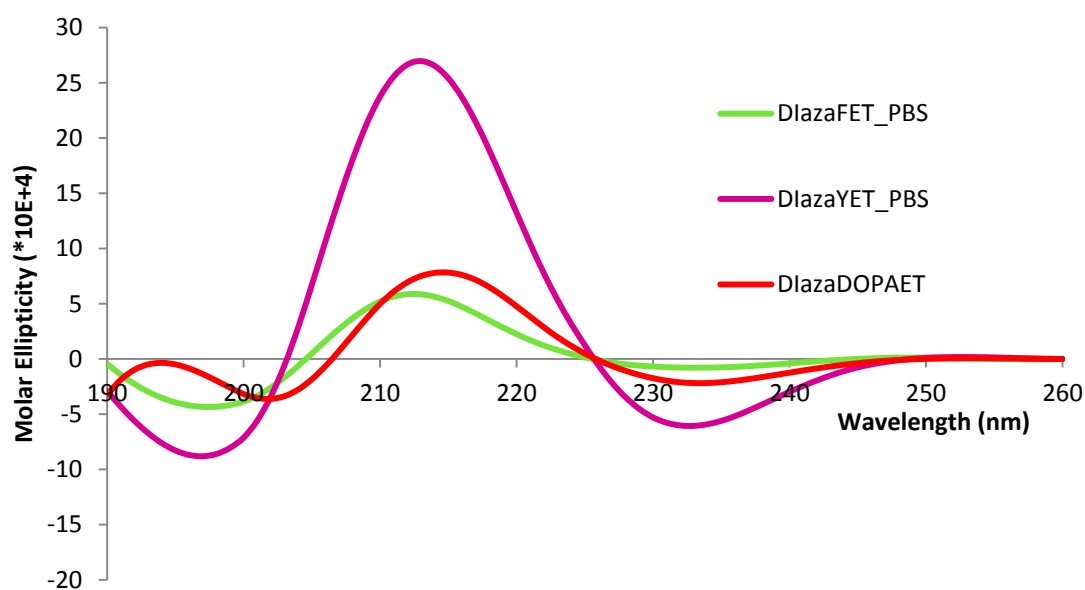


Figure 3.10. CD spectra for Ac-DlazaYET-NH₂, **2.36**, Ac-DlazaFET-NH₂, **2.40**, Ac-Dlaza(DOPA)ET-NH₂, **2.41**, (20 μM) in phosphate buffer, at 25 °C.

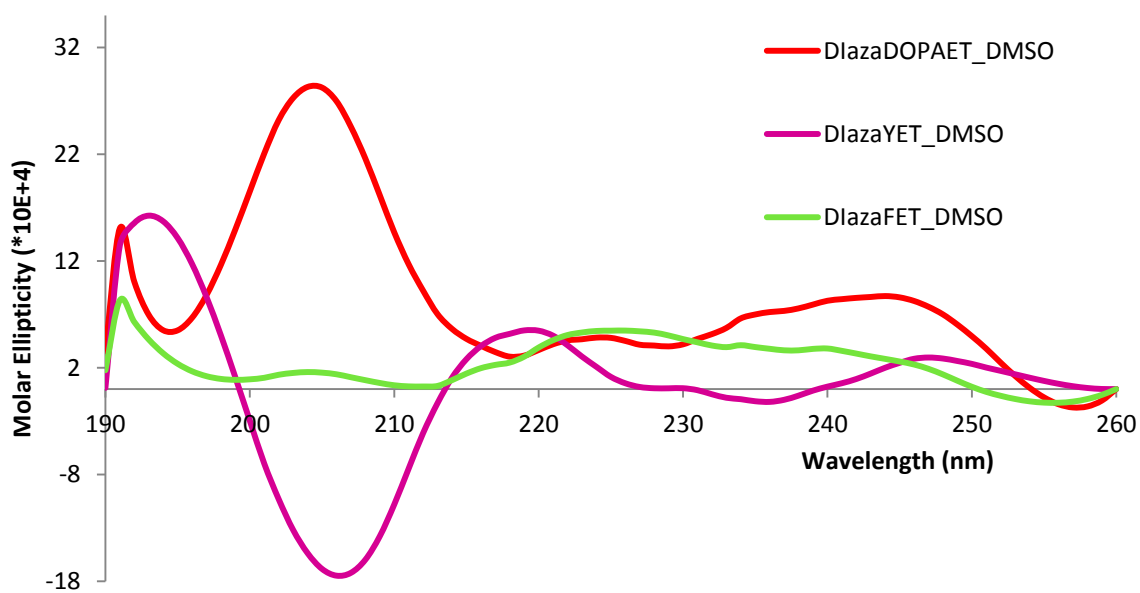


Figure 3.11. CD spectra for Ac-DlazaYET-NH₂, **2.36**, Ac-DlazaFET-NH₂, **2.40**, Ac-Dlaza(DOPA)ET-NH₂, **2.41**, (20 μM) in DMSO, at 25 °C.

At the 4 position, Ac-DIYazaET-NH₂, **2.42**, displayed a CD spectrum in water, PBS and DMSO that failed to stabilize a peptide turn conformation. These results were based on the large proportion of random coil observed in water and characterized by the negative minimum band at 190 nm (**Figures 3.12**). In phosphate buffer, the azapeptide displayed a large positive band near 190 nm, that are typically consistent with helical type structures (**Figure 3.13**).¹³ In DMSO, a poorly folded peptide geometry indicated that the aza-Glu modification at the 4 position of the sequence weakly stabilized the peptide secondary structure (**Figure 3.14**).

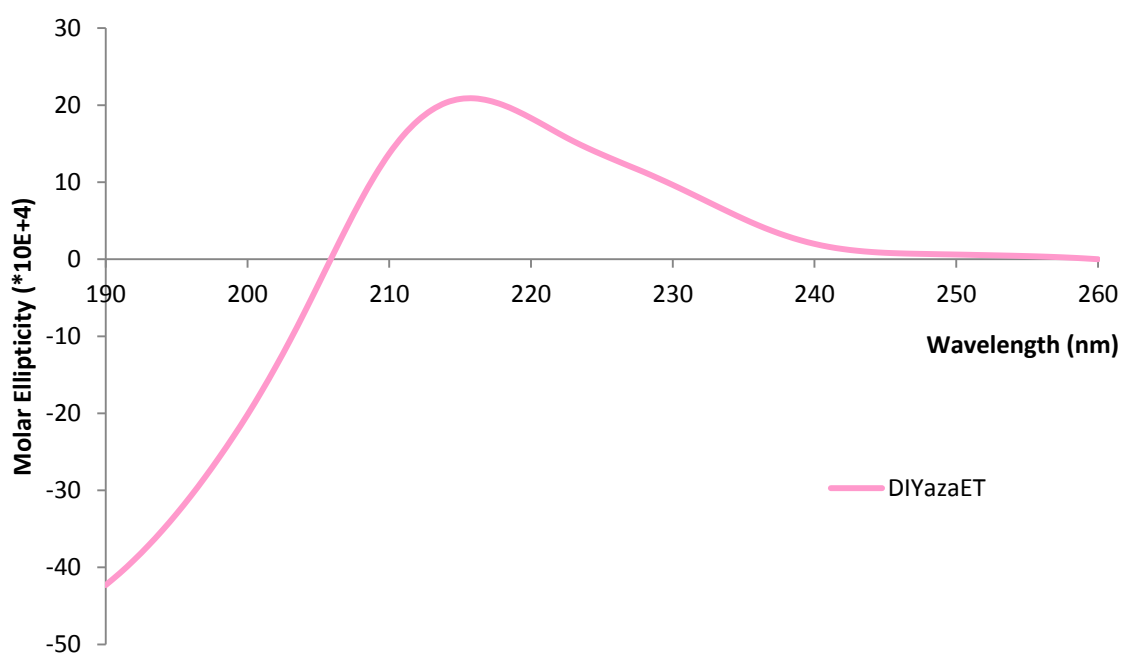


Figure 3.12. CD spectra for Ac-DIYazaET-NH₂, **2.42**, (20 μ M) in water, at 25 °C.

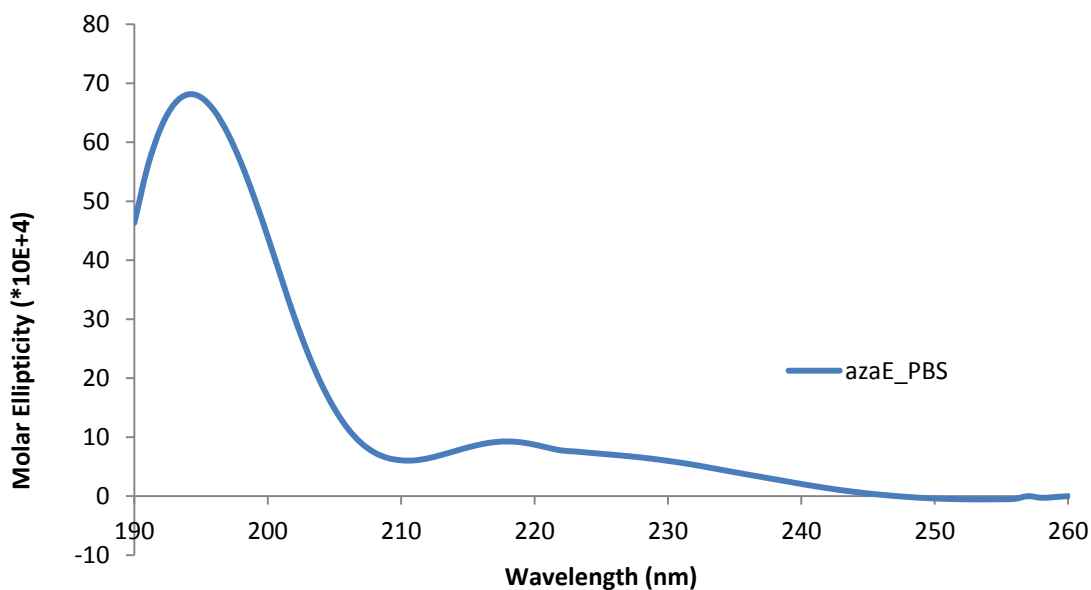


Figure 3.13. CD spectra for Ac-DIYazaET-NH₂, **2.42**, (20 μM) in phosphate buffer, at 25 °C.

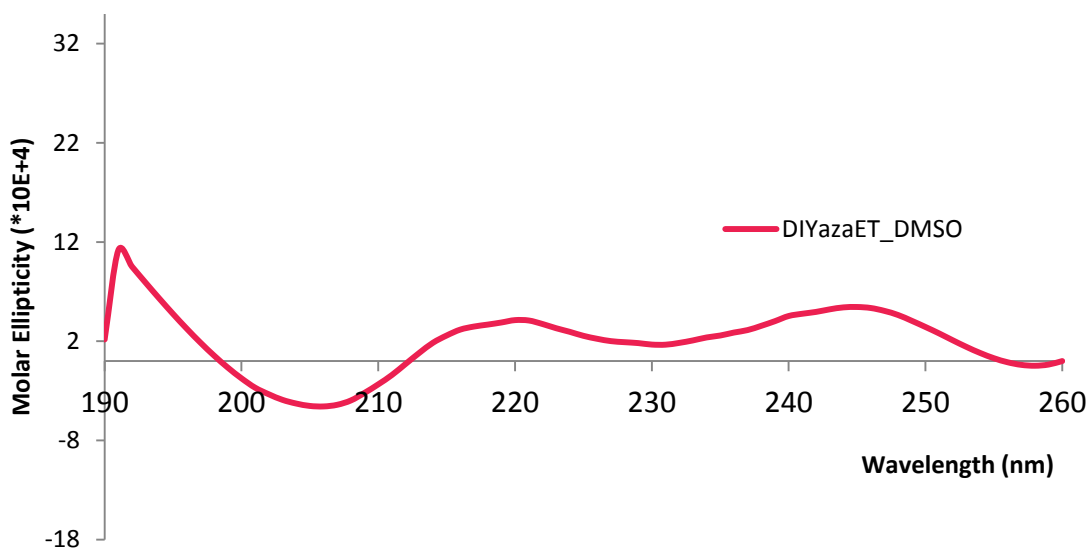


Figure 3.14. CD spectra for Ac-DIYazaET-NH₂, **2.42**, (20 μM) in DMSO, at 25 °C.

In sum, azapeptides (**2.36** – **2.42**) displayed conformations that were found to vary with the location and nature of the aza-residue in aqueous media (water and phosphate buffer) and organic (DMSO) solvents illustrating rich peptide structures that may contribute to biological activity.

3.4.3 NMR SPECTROSCOPY

NMR spectroscopy was next performed to support the observed azapeptide turn conformation in Ac-DIazaYET-NH₂, **2.36**. The NMR spectrum of the parent pentapeptide Ac-DIYET-NH₂, **2.28** was compared to azapeptide, **2.36**, in deuterated water and DMSO. In DMSO, the azapeptide exhibited an NMR spectrum that was consistent with a β -turn structure. The azapeptide secondary structure was characterized by the disappearance of the Glu NH and down-field chemical shift of the Ile NH (δ : 8.2 vs 7.6) when compared to the parent peptide (**Figure 3.15 A and B**, respectively). This observation is consistent with the hydrogen bonding interaction found in between the carbonyl group of the Asp residue at the *i* position and the amino group of the Glu residue at the *i*+3 position to generate the turn conformation that is stabilized by the aza-Tyr residue at the *i*+2 position. Moreover, 2D NOESY confirmed successive NOE correlations that were consistent with an organized azapeptide turn geometry found within Ac-DIazaYET-NH₂, **2.36**, and absent within Ac-DIYET-NH₂, **2.28**, whose protons appeared to be solvent exposed with fewer NOE correlations (**Figure 3.16**).²⁰⁻²⁴

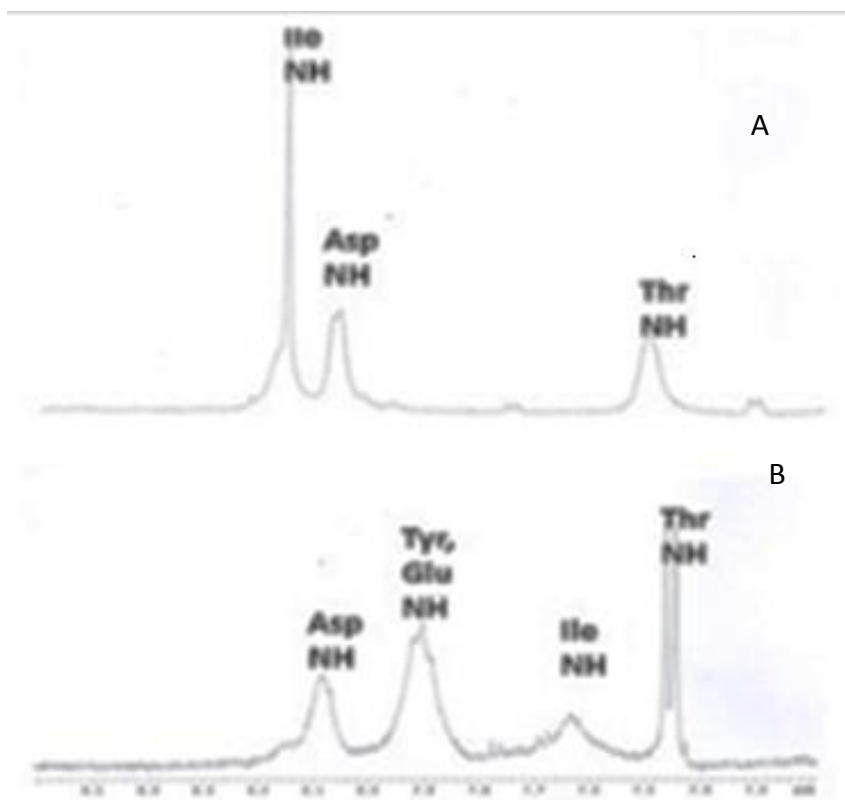


Figure 3.15. ¹H NMR spectra of (B) Ac-DIYET-NH₂, **2.28**, and (A) Ac-DIazaYET-NH₂, **2.36**, (2 mM) in DMSO-d₆.

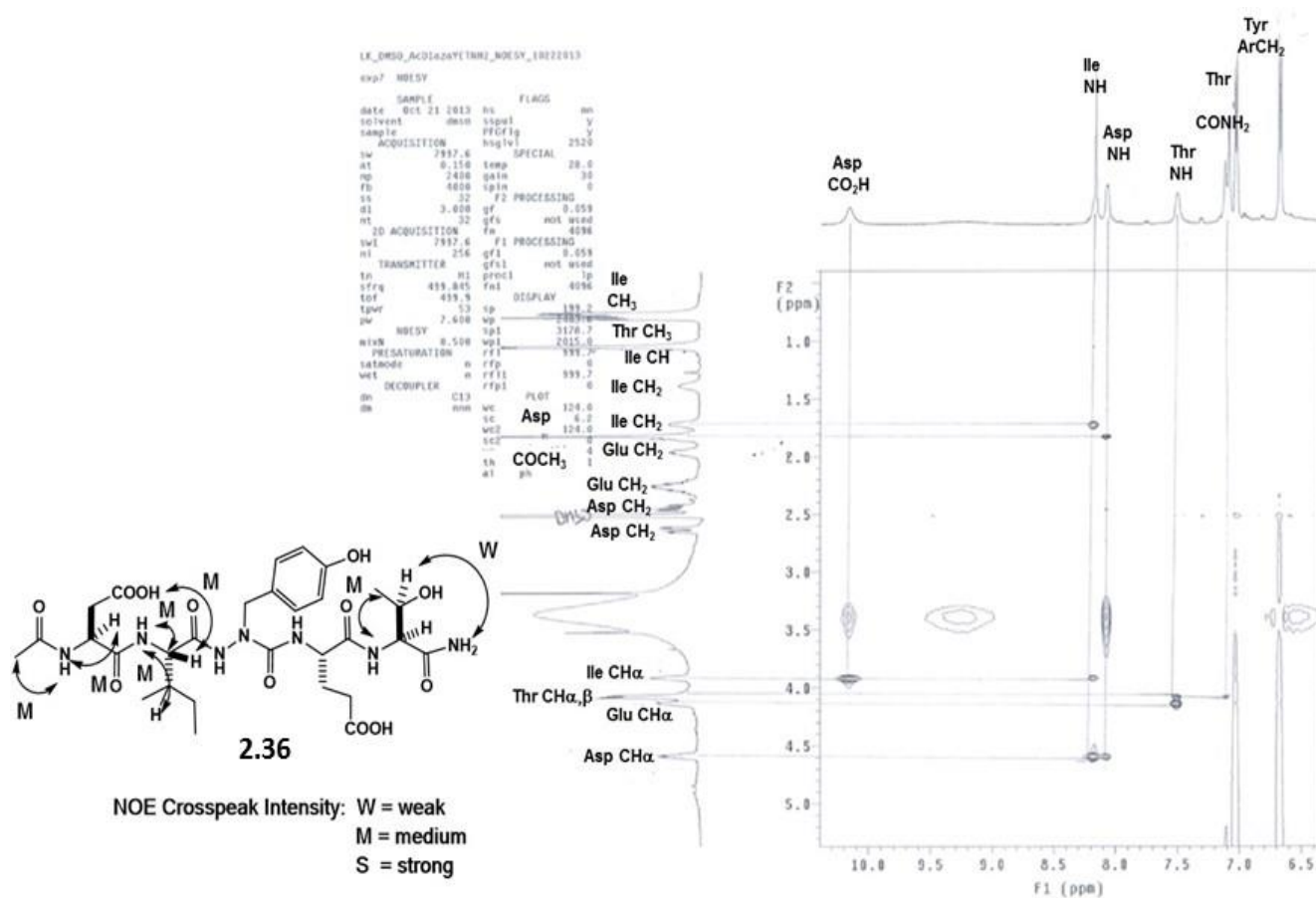


Figure 3.16. 2D NOESY spectrum and conformational analysis of Ac-DlazaYET-NH₂, **2.36**, (2 mM) in DMSO-d₆.

3.5 CONCLUSIONS

In this chapter a conformational study of the azapeptides (**Table 2.1, sequences 2.36-2.42**) belonging to the Ac-DIYET-NH₂, **2.28**, sequence was conducted to explore the influence of the aza-substitutions on peptide backbone geometry. A computational study was initially investigated to determine the molecular structure of a selected azapeptide sequence, Ac-DIazaYET-NH₂, **2.36**, and its correlation with IRTK binding. Molecular modeling and docking studies displayed a folded azapeptide turn geometry which translated into tight IRTK binding ($< 5 \text{ \AA}$) at the active site of the target receptor. Thus, a β -turn conformation was observed *in silico* with the Ac-DIazaYET-NH₂, **2.36**, sequence. In order to validate azapeptide structures in solution, CD and NMR spectroscopy indicated that the azapeptide folds were contingent on solvent, location and nature of the aza-residues found within the Ac-DIYET-NH₂, **2.28**, sequence. Significantly, aza-substitutions at the $i+2$ position, Tyr³, were found to stabilize the β -turn structure in water, phosphate buffer and DMSO. Thus, aza-modifications at this position may be useful in studying the influence of the β -turn trajectory and side chain interactions on IRTK binding affinity and inhibitory activity. The latter is a focal point of the biological studies reported in Chapter 4 of this thesis, in order to gain insight into the SARs in between the putative azapeptide ligands and their IRTK target receptor.

3.6 EXPERIMENTAL SECTION

3.6.1 MATERIALS

Sodium chloride, potassium chloride, disodium phosphate, monobasic potassium phosphate and deuterated solvents were all purchased from Aldrich (Milwaukee, WI) and used without further purification.

3.6.2 COMPUTATIONAL ANALYSIS

The crystal structure of the IRTK domain (Ser⁹⁸¹-Lys¹²⁸³) bound with ATP and a peptide ligand (KKKLPATGDYMNMSVGD) was available for download from the Protein Data Bank (PDB ID # 1IR3). A molecular docking study was then performed with a selected azapeptide Ac-DIazaYET-NH₂ and compared with the native peptide sequence Ac-DIYET-NH₂ to visualize the binding model of the peptides on the catalytic loop of the IRTK. An interface between the molecular graphics system PyMOL and the molecular docking suite AutoDockVina was used to demonstrate the docking and visualization models. The peptide ligands were enclosed in a box with the number of grid points in x, y, z directions, 20 x 22 x 16 correlating with a grid spacing of 1.0 Å. The center of the grid was set to -23.906, 30.439 and 12.466. For the docking simulation studies, the lowest energy docked conformation, according to the AutoDock scoring function was selected as the binding model.

3.6.3 CD SPECTROSCOPY

The CD spectra of the peptides were collected in the far UV range (190 - 260 nm). The CD spectra of the peptides were collected and blank corrected with the corresponding solvent. All CD spectra were recorded on an Aviv 62A DS CD Spectrophotometer using a 1.0 cm path-length quartz cell containing 20 µM of peptide dissolved in water, phosphate buffer (0.005 M Na₂HPO₄, 0.14 M KCl and 0.001 M MgCl₂ at pH 7.2) and DMSO at room

temperature. The CD spectra were transported to Microsoft Excel and plotted as changes in molar ellipticities (θ) vs. wavelength (nm).

3.6.4 NMR SPECTROSCOPY

^1H NMR spectra were recorded on a Varian Oxford NMR spectrometer (500 MHz) with samples (2 – 5 mM) dissolved in DMSO- d_6 and D_2O (99.9%) and referenced to H_2O (4.79 ppm) and DMSO- d_6 (2.5 ppm). Coupling constants, J values were measured in Hertz (Hz) and chemical shift values in parts per million (ppm). Two-dimensional COSY, TOCSY (80 ms mixing time) and NOESY (500 ms mixing time) spectra were acquired at 298 K.

3.6.5 CHARACTERIZATION DATA

Ac-Asp-Ile-azaTyr-Glu-Thr-CONH₂ (2.36). Yield (15 mg, 50%), ^1H NMR (500 MHz, DMSO- d_6) δ 0.78 (m, 6H), 1.04 (d, $J = 6$ Hz, 3H), 1.38 (bs, 1H), 1.71 (bs, 1H), 1.82 (s, 3H), 1.84 (m, 1H), 1.96 (m, 1H), 2.25 (m, 2H), 2.44 (dd, $J = 8.5, 18$ Hz, 1H), 2.63 (dd, $J = 5, 20$ Hz, 1H), 3.91 (bs, 1H), 4.07 (d, $J = 7$ Hz, 2H), 4.13 (d, $J = 4.5$ Hz, 1H), 4.59 (d, $J = 6.5$ Hz, 1H), 6.67 (d, $J = 8.5$ Hz, 2H), 7.03 (d, $J = 8.5$ Hz, 2H), 7.11 (d, $J = 14.5$ Hz, 2H), 7.50 (bs, 1H), 8.07 (d, $J = 6.5$ Hz, 1H), 8.16 (s, 1H), 10.2 (bs, 1H); ESI-LCMS [2-90% MeOH in H_2O (0.1% FA), 15 min] RT = 9.95 min; [2-90% MeCN in H_2O (0.1% FA), 15 min] RT = 6.68 min; Calculated for $\text{C}_{29}\text{H}_{42}\text{N}_7\text{O}_{12}$ [M-H]⁻, 681.3 found m/z 681.2.

Ac-Asp-azaAla-Tyr-Glu-Thr-CONH₂ (2.37). Yield (22 mg, 51%), ^1H NMR (500 MHz, D_2O) δ 1.21 (m, 1H), 1.27 (d, $J = 6$ Hz, 3H), 2.04 (m, 1H), 2.08 (s, 3H), 2.15-2.19 (m, 1H), 2.42 (t, $J = 7$ Hz, 2H), 2.80 (dd, $J = 2, 6.25$ Hz, 2H), 2.97-3.01 (m, 1H), 3.05 (s, 3H), 3.10-3.16 (m, 1H), 4.31-4.35 (m, 2H), 4.41-4.74 (m, 2H), 4.60 (t, $J = 6$ Hz, 1H), 6.88 (d, $J = 8.5$ Hz, 2H), 7.15 (d, $J = 8$ Hz, 2H); ESI-LCMS [2-90% MeOH in H_2O (0.1% FA), 15 min] RT =

7.42 min; [2-90% MeCN in H₂O (0.1% FA), 15 min] RT = 5.26 min; Calculated for C₂₆H₃₆N₇O₁₂ [M-H]⁻ 638.3 found *m/z* 638.2.

Ac-Asp-azalle-Tyr-Glu-Thr-CONH₂ (2.38). Yield (27 mg, 55%), ¹H NMR (500 MHz, D₂O) δ 0.67-0.70 (m, 1H), 0.84-0.90 (m, 3H), 0.98-1.10 (m, 3H), 1.27 (dd, *J* = 2, 6.25 Hz, 3H), 1.40-1.47 (m, 2H), 2.06 (s, 3H), 2.11-2.15 (m, 1H), 2.39 (t, *J* = 5 Hz, 2H), 2.68-2.86 (m, 2H), 2.97-3.02 (m, 1H), 3.06-3.10 (m, 1H), 3.19-3.26 (m, 1H), 4.29-4.36 (m, 3H), 4.41-4.43 (m, 1H), 4.54-4.48 (m, 1H), 4.57-4.60 (m, 1H), 6.86-6.91 (m, 2H), 7.13 (d, *J* = 8.5 Hz, 1H), 7.22 (d, *J* = 8 Hz, 1H); ESI-LCMS [2-90% MeOH in H₂O (0.1% FA), 15 min] RT = 6.97 min; [2-90% MeCN in H₂O (0.1% FA), 15 min] RT = 5.13 min; Calculated for C₂₉H₄₂N₇O₁₂ [M-H]⁻ 680.3 found *m/z* 680.2.

Ac-Asp-azaGly-Tyr-Glu-Thr-CONH₂ (2.39). Yield (22 mg, 55%), ¹H NMR (500 MHz, D₂O) δ 1.27 (d, *J* = 6 Hz, 3H), 2.00-2.06 (m, 2H), 2.08 (s, 3H), 2.14-2.18 (m, 1H), 2.36-2.39 (m, 2H), 2.75 (dd, *J* = 2.5, 6.5 Hz 2H), 3.01 (dd, *J* = 8.5, 14 Hz, 1H), 3.12 (dd, *J* = 6, 14.5 Hz, 1H), 4.30-4.34 (m, 2H), 4.41 (dd, *J* = 5, 9.25 Hz, 1H), 4.49 (dd, *J* = 6, 8.5 Hz, 1H), 4.65 (t, *J* = 6.5 Hz, 1H), 6.85 (d, *J* = 8.5 Hz, 2H), 7.17 (d, *J* = 8.5, 2H); ESI-LCMS [2-90% MeOH in H₂O (0.1% FA), 15 min] RT = 6.99 min; [2-90% MeCN in H₂O (0.1% FA), 15 min] RT = 5.04 min; Calculated for C₂₅H₃₄N₇O₁₂ [M-H]⁻ 624.2 found *m/z* 624.2.

Ac-Asp-Ile-azaPhe-Glu-Thr-CONH₂ (2.40). Yield (17 mg, 43%), ¹H NMR (500 MHz, D₂O) δ 0.85 (m, 6H), 1.13 (m, 1H), 1.29 (d, *J* = 6.5 Hz, 3H), 1.35 (bs, 1H), 1.84 (bs, 1H), 2.05 (s, 3H), 2.18 (m, 1H), 2.39 (bs, 2H), 2.58 (dd, *J* = 8, 16.5 Hz, 1H), 2.69 (dd, *J* = 6.5, 16 Hz, 1H), 4.05 (bs, 1H), 4.34-4.39 (m, 3H), 4.63-6.65 (m, 1H), 7.37 (d, *J* = 7.5 Hz, 2H), 7.41-7.47 (m, 3H); ESI-LCMS [2-90% MeOH in H₂O (0.1% FA), 15 min] RT = 11.76 min; [2-

90% MeCN in H₂O (0.1% FA), 15 min] RT = 7.78 min; Calculated for C₂₉H₄₄N₇O₁₁ [M+H]⁺, 666.3 found *m/z* 666.2.

Ac-Asp-Ile-aza(DOPA)-Glu-Thr-CONH₂ (2.41). Yield (6 mg, 36%), ¹H NMR (500 MHz, D₂O) δ 0.82-0.89 (m, 6H), 1.06 (bs, 1H), 1.28 (d, *J* = 6.5 Hz, 3H), 1.82 (bs, 1H), 2.05 (s, 6H), 2.16 (bs, 2H), 2.31 (bs, 2H), 2.58 (bs, 1H), 2.67-2.70 (m, 1H), 4.05 (bs, 1H), 4.31-4.38 (m, 4H), 4.63-4.67 (m, 2H), 6.62-6.65 (m, 1H), 6.80 (d, *J* = 8.5 Hz, 1H), 6.88 (s, 1H), 6.92 (d, *J* = 8 Hz, 1H); ESI-LCMS [2-90% MeOH in H₂O (0.1% FA), 15 min] RT = 8.90 min; [2-90% MeCN in H₂O (0.1% FA), 15 min] RT = 6.33 min; Calculated for C₂₉H₄₄N₇O₁₃ [M+H]⁺, 698.3 found *m/z* 698.2.

Ac-Asp-Ile-Tyr-azaGlu-Thr-CONH₂ (2.42). Yield (16 mg, 42%), ¹H NMR (500 MHz, D₂O) δ 0.81-0.86 (m, 1H), 0.89-0.96 (m, 6H), 1.22 (d, *J* = 7 Hz, 3H), 1.47 (bs, 1H), 1.85-1.88 (m, 1H), 2.07 (s, 3H), 2.57 (dd, *J* = 9, 16 Hz, 1H), 2.70 (dd, *J* = 5.5, 16 Hz, 1H), 3.00 (m, 2H), 3.25 (dd, *J* = 6, 13 Hz, 1H), 3.66 (bs, 1H), 4.20 (d, *J* = 4 Hz, 1H), 4.23 (d, *J* = 8 Hz, 1H), 4.30 (t, *J* = 4 Hz, 1H), 4.41 (bs, 1H), 4.61 (dd, *J* = 5.5, 8.5 Hz, 1H) 6.91 (d, *J* = 8.5 Hz, 2H), 7.24 (d, *J* = 8 Hz, 2H); ESI-LCMS [2-90% MeOH in H₂O (0.1% FA), 15 min] RT = 9.61 min; [2-90% MeCN in H₂O (0.1% FA), 15 min] RT = 6.41 min; Calculated for C₂₉H₄₂N₇O₁₂ [M-H], 680.3 found *m/z* 680.2.

Ac-Asp-Ile-Tyr-Glu-Thr-CONH₂ (2.28). Yield (50 mg, 75%), ¹H NMR (500 MHz, DMSO-*d*₆) δ 0.60-0.67 (m, 6H), 0.85-0.91 (m, 1H), 0.96 (d, *J* = 6.5 Hz, 3H), 1.07 (bs, 1H), 1.58-1.61 (m, 1H), 1.71-1.74 (m, 1H), 1.76 (s, 3H), 1.89 (bs, 1H), 2.15-2.23 (m, 2H), 2.37-2.40 (m, 1H), 2.54-2.59 (m, 1H), 2.68 (bs, 1H), 2.86 (dd, *J* = 4, 14 Hz, 1H), 3.94-3.97 (m, 1H), 3.99-4.01 (m, 1H), 4.23 (dd, *J* = 8.5, 13 Hz, 1H), 4.34 (bs, 1H), 4.53 (dd, *J* = 7.5, 14 Hz, 1H), 4.77 (bs, 1H), 6.43 (bs, 1H), 6.55-6.57 (m, 2H), 6.95-7.01 (m, 4H), 7.45 (d, *J* = 8.5 Hz, 1H), 7.63

(bs, 1H), 7.90 (bs, 1H), 8.09 (bs, 1H), 9.04 (bs, 1H); ESI-LCMS [2-90% MeOH in H₂O (0.1% FA), 15 min] RT = 9.34 min; [2-90% MeCN in H₂O (0.1% FA), 15 min] RT = 6.55 min; Calculated for C₃₀H₄₅N₆O₁₂ [M+H]⁺, 681.3 found *m/z* 681.2.

3.7 REFERENCES

1. Aubry, A.; Marraud, M. *Biopolymers* **1989**, *28*, 109-122.
2. Thormann, M.; Hofmann, H.J. *J. Mol. Struct. (Theochem)* **1999**, *469*, 63-76.
3. Jeffrey, G.A. *J. Mol. Struct. (Theochem)* **1984**, *17*, 1-15.
4. Ramondo, F.; Bencivenni, L. *J. Chem. Soc. Perkin Trans. 2*, **1995**, 1797-1804,
5. Reynolds, C.H.; Hormann, E. *J. Am. Chem. Soc.* **1996**, *118*, 9395-9401.
6. Chakravorty, S.; Reynolds, C.H. *J. Mol. Graphics Mod.* **1999**, *17*, 315-324.
7. Lee, H.J.; Park, H.M.; Lee, K.B. *Biophys. Chem.* **2007**, *125*, 117-126.
8. Hutchinson, E.G.; Thornton, J.M. *Protein Sci.* **1994**, *3*, 2207-2216.
9. Sabatino, D.; Proulx, C.; Klocek, S.; Bourguet, C.B.; Boeglin, D.; Ong, H.; Lubell, W.D. *Org. Lett.* **2009**, *11*, 3650-3653.
10. Sabatino, D.; Proulx, C.; Pohankova, P.; Ong, H.; Lubell, W.D. *J. Am. Chem. Soc.* **2011**, *133*, 12493-12506.
11. Proulx, C.; Picard, É.; Boeglin, D.; Pohankova, P.; Chemtob, S.; Ong, H.; Lubell, W.D. *J. Med. Chem.* **2012**, *55*, 6502-6511.
12. Kato, M.; Abe, M.; Kuroda, Y.; Hirose, M.; Nakano, M.; Handa, T. *J. Pept. Sci.* **2009**, *15*, 327 – 33633.
13. Ranjbar, B.; Gill, P. *Chem. Biol. Drug. Des.* **2009**, *74*, 101-120.
14. (a) Greenfield, N.J. *Tr. Anal. Chem.* **1999**, *18*, 236-244, (b) Kelly, S.M.; Price, N.C. *Biochim. Biophys. Acta.* **1997**, *1338*, 161-185, (c) Kelly, S.M.; Price, N.C. *Curr. Protein Pept. Sci.* **2000**, *1*, 349-384, (d) Kelly, S.M.; Jess, T.J. *Biochim. Biophys. Acta.* **2005**, *1751*, 119-139.
15. Nikiforovich, G.V. *Int. J. Pept. Protein Res.* **1994**, *44*, 513-531.

16. Goodwin, C.R.; Fenn, L.S.; Derewacz, D.K.; Bachmann, B.O.; McLean, J.A. *J. Nat. Prod.* **2012**, *75*, 48-53.
17. Chakraborty, K.; Shivakumar, P.; Raghothama, S.; Varadarajan, R. *Biochem. J.* **2005**, *390*, 573-581.
18. Mirza, Z.; Pillai, V.G.; Zhong, W.Z. *Int. J. Mol. Sci.* **2014**, *15*, 4221-4236.
19. Ostermeir, K.; Zacharias, M. *J. Comput. Chem.* **2014**, *35*, 150-158.
20. (a) Hammerlin, C.; Cung, M.T.; Boussard, G. *Tetrahedron Lett.* **2001**, *42*, 5009 – 5012; (c) Andre, F.; Boussard, G.; Marraud, M.; Didierjean, C.; Aubry, A. *Tetrahedron Lett.* **1996**, *37*, 183 – 186; (d) Benatalah, Z.; Aubry, A.; Boussard, G.; Marraud, M. *Int. J. Pept. Protein Res.* **1991**, *38*, 603 – 606.
21. Ruggles, E.L.; Deker, P.B.; Hondal, R.J. *J. Pept. Sci.* **2014**, *20*, 349-360.
22. Jamieson, A.G.; Boutard, N.; Sabatino, D.; Lubell, W.D. *Chem. Biol. Drug Des.* **2013**, *81*, 148-165.
23. Zouikri, M.; Vicherat, A.; Aubry, A.; Marraud, M.; Boussard, G. *J. Pept. Res.* **1998**, *52*, 19-26.
24. Lee, H.J.; Choi, K.H.; Ahn, I.A.; Ro, S.; Jang, H.G.; Choi, Y.S.; Lee, K.B. *J. Mol. Struct.* **2001**, *569*, 43-54.
25. (a) Hubbard, S.R.; Wei, L.; Ellis, L.; Hendrickson, W.A. *Nature* **1994**, *372*, 746–754; (b) Hubbard, S.R. *EMBO J.* **1997**, *16*, 5572–5581.
26. Trott, O.; Olson, A.J. *J. Comp. Chem.* **2010**, *31*, 455-461.

CHAPTER 4. IRTK INHIBITORY ACTIVITY OF AZAPEPTIDES

4.1 ABSTRACT

In the absence of regulated tyrosine kinase activity of the insulin receptor, increased levels of gene expression and cell proliferation have been observed and associated with tumor progression. Thus, the inhibition of un-regulated tyrosine kinase phosphorylation of the insulin receptor may prove to be an effective form of cancer treatment. Towards this goal, synthetic pentapeptides, Ac-DIYET-NH₂ (**2.28**) derived from the activation loop of the insulin receptor and related analog, Ac-DIFET-NH₂ (**2.43**), were found to inhibit the autophosphorylation of the insulin receptor to about 80% and 20%, respectively, at 4 mM making them potential leads in the development of novel peptide-based anti-cancer drugs. Moreover, molecular docking simulation studies of the lead peptide ligand, **2.28**, bound within the active site of the IRTK revealed a folded peptide structure, reminiscent of a turn geometry that may contribute to binding affinity with its receptor target. In order to test this hypothesis, azapeptide derivatives of the Ac-DIYET-NH₂ sequence, and specifically encompassing aza-modifications within the IYE region were developed for structure activity relationship studies. CD and NMR spectroscopy proved that the Ac-DIazaYET-NH₂ sequence, **2.36**, adopted a β -turn conformation. In this chapter, the phosphorylation activity of the recombinant IRTK domain (residues 1005-1310) in the presence of ATP (1000 μ M) was initially validated by western blotting. The inhibitory activity of the peptides, Ac-DIYET-NH₂ (**2.28**) vs Ac-DIazaYET-NH₂ (**2.36**), was next evaluated by conducting the IRTK phosphorylation reactions with the addition of peptide ligands (400 μ M). In a single dose experiment, minimal inhibitory activity (<10%) was detected for the parent peptide, Ac-

DIYET-NH₂ (**2.28**), whereas, Ac-DIazaYET-NH₂ (**2.36**) displayed 50% inhibition of the IRTK autophosphorylation. The azapeptide analogs, DazaIYET, DazaGYET and DazaAYET exhibited about 25% - 40% inhibition of the IRTK phosphorylation at 400 μ M concentration. The azapeptide analogs, [aza-DOPA³] and [aza-Glu⁴] displayed slight stimulatory effect on the phosphorylation activity of the IRTK at similar concentration levels.

These results validate the importance of the peptide β -turn geometry on the inhibition of IRTK phosphorylation. This finding is not only important towards the development of potent azapeptide inhibitors of the IRTK for potential anti-cancer applications, but also in the design of novel peptide ligands that may function as useful probes for studying the mechanisms and kinetics associated with this important class of tyrosine kinases.

4.2 INTRODUCTION

4.2.1. SIGNALING ACTIVITIES OF THE RECEPTOR TYROSINE KINASES

Signal transduction is ubiquitous in all cell types and involves the transfer of information from within and in between cells in order to regulate their structure and function. Signaling activity is transmitted from a ligand to a protein receptor and converted into a cellular response, which in turn regulates a biochemical process such as metabolism. Signal transduction must be precisely integrated and coordinated for normal cell function. The human genome project has revealed that ~ 20% of the ~ 32,000 human coding genes encode proteins that are implicated in signal transduction.¹ These include the transmembrane G-coupled protein receptors, whose recently solved crystal structures have led to a better understanding of their signaling activities.² A Nobel Prize was recently awarded to Drs. Robert Lefkowitz and Brian Kobilka in 2012 for their contributions into the structure and

function of this important class of signaling receptors.³ Within this class of G-coupled protein receptors, more than 520 protein kinases and 130 protein phosphatases have been implicated in cell signaling activity by regulating protein phosphorylation.⁴ The protein kinases govern substrate phosphorylation with ATP, and are further divided into subgroups which define their target phosphorylation sites. The protein or receptor tyrosine kinases, PTK or RTK, respectively, promote substrate-level phosphorylation onto active site tyrosine residues, whereas the serine/threonine specific enzymes phosphorylate active site serine and threonine residues. The phosphorylation activity of kinases has crucial cellular effects. These are most often implicated with the activation of signaling pathways that control gene expression, protein production and function in addition to regulating cell metabolism which governs the cell cycle for proliferation. Thus, PTKs are among the most widely studied classes of enzymes for their important implications in regulated and oncogenic signaling.⁵

4.2.2. THE INSULIN RECEPTOR TYROSINE KINASE

The RTKs encompass a large family of membrane bound protein receptors with intrinsic phosphorylation signaling activity.⁶ Insulin receptor has associated RTK activity found within its cytoplasmic domain. The insulin receptor tyrosine kinase (IRTK) is a heterotetrameric transmembrane protein having two identical extracellular α -subunits that function as the binding site for the natural ligand insulin and intracellular β -subunits which encompass the RTK domain (**Figure 4.1**).⁷ Signal transduction of the IRTK is mediated by insulin binding to the extracellular α -subunit of the IRTK. This ligand:receptor binding interaction produces conformational changes within the cytosolic β -subunits, exposing the RTK for ATP binding and phosphorylation onto the active site tyrosine residues.^{7,8} There are 3 major phosphorylation sites found within the insulin receptor (**Figure 4.2**) including a juxta

membrane region having Tyr residues, 965 and 979, the activation loop at position, 1158, 1162 and 1163 and the C-terminal region at 1328 and 1334.⁹

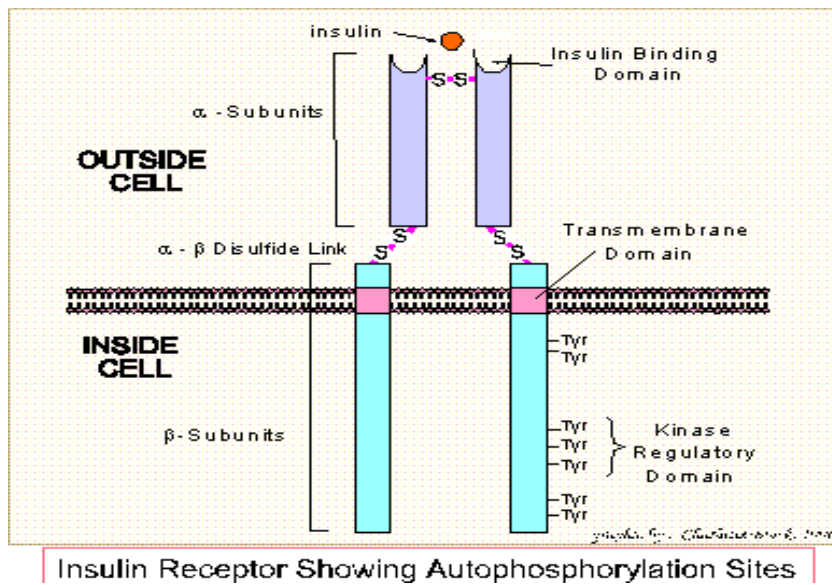


Figure 4.1. Figurative description of the IRTK. Figure adapted from: <http://grimwade.biochem.unimelb.edu.au/tutorial/s2730e.gif>

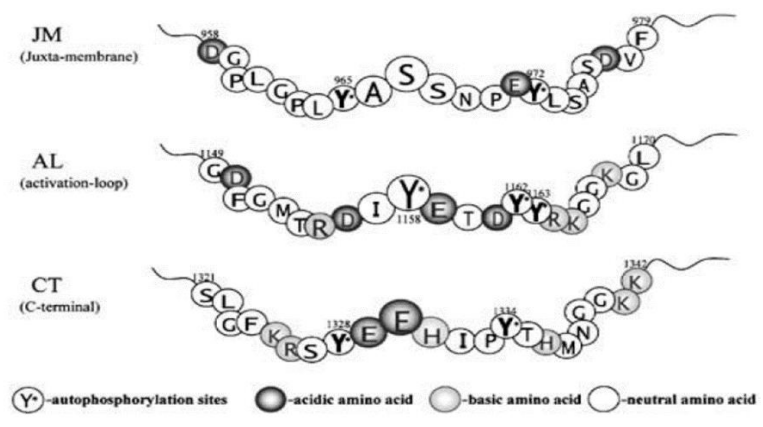


Figure 4.2. Phosphorylation sites of the IRTK. Figure adapted from: Hirose, M. *et al. Br. J. Pharm.* **2004**, *142*, 222 -228.¹⁶

This ligand:receptor binding interaction causes a change in IRTK conformation which subsequently leads to phosphorylation of the key tyrosine residues in the activation loop, Tyr1158, Tyr1162, Tyr1163 in the presence of ATP.⁷⁻⁹ Once these tyrosine residues are

phosphorylated, an additional conformational change occurs within the activation loop of the IRTK for additional phosphorylation which activates the receptor for intracellular signaling activity.⁷⁻⁹ The activated IRTK then dictates a myriad of signaling events, such as the PI(3)K, CAP/CbI and the Ras/MAPK pathways, respectively associated with glucose metabolism, protein synthesis, and cell proliferation.¹⁰⁻¹²

In order to maintain regulated IRTK signal transduction, the kinase activities of the RTKs must be precisely controlled. For example, when the receptor is in its inactive state the activation loop of the IRTK binds to its catalytic loop and inhibits the kinase domain by preventing ATP binding and phosphorylation of the active site Tyr residues.⁹ This conformation is stabilized by the hydrogen bonding interactions in between the Tyr 1162 residue in the activation loop of the insulin receptor and the Asp1132 residue in the catalytic loop of the RTK. Binding of insulin to the α -subunit reverses this process and activates tyrosine specific phosphotransferase activity with ATP. This leads to the autophosphorylation of the specific tyrosine residues in the cytoplasmic domain of the β -subunit. The phosphorylation of the Tyr 1158 Tyr 1162 and Tyr1163 residues is mainly responsible for activation of substrate phosphorylation.⁹ The introduction of three anionic phosphotyrosine residues forces a 30 Å change in the position of the activation loop away from the substrate binding site, making it available to bind to and phosphorylate a target protein as shown in Figure 4.3.¹³

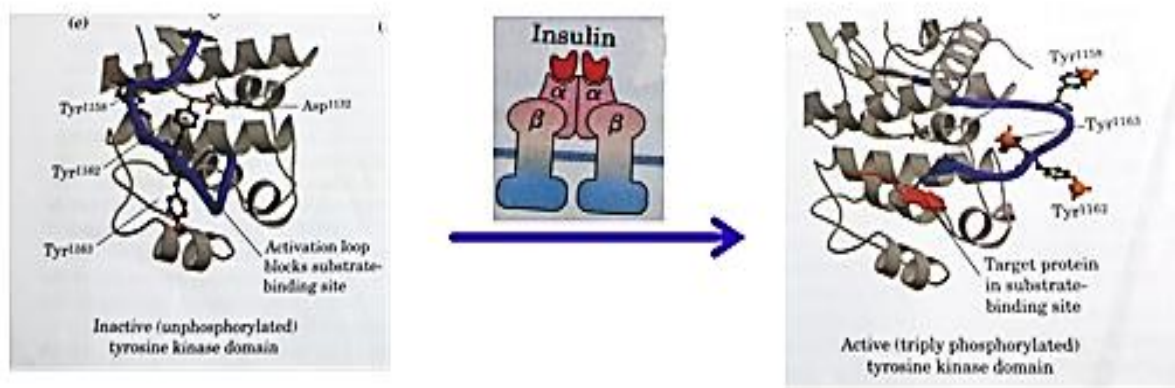


Figure 4.3. Phosphorylation mechanism of the IRTK. Figure adapted from: Nelson, D.L.; Cox, M.M. *Lehninger Principles of Biochemistry 5 ed.*, 2008, W.H. Freeman and Co. New York, NY, 440.¹³

Among the most important IRTK signal transduction pathways, the mitogen-activated protein, MAP kinase signaling cascade regulates gene expression and cell proliferation.^{12,13} This signaling pathway is triggered by insulin binding to the α -subunit of the IRTK leading to a series of substrate-level phosphorylation reactions which activates proteins that ultimately cause gene expression in the cells' nucleus (**Figure 4.4**). Initially, the phosphorylated IRTK stimulates phosphorylation and activation of the insulin receptor substrate 1, IRS-1, which in turn phosphorylates the growth factor receptor-bound protein, Grb2. Then the guanine nucleotide exchange factor, Sos binds to phosphorylated Grb2 and the Ras protein causing GTP binding to Ras and GDP release. Activated Ras then binds to Raf-1 and activates the so-called proto-oncogene serine/threonine protein kinase to phosphorylate the MEK serine residues. Activated MEK phosphorylates ERK which enters the nucleus and phosphorylates nuclear transcription factors Elk1 and SRF which stimulates mRNA transcription, protein translation and cell division.

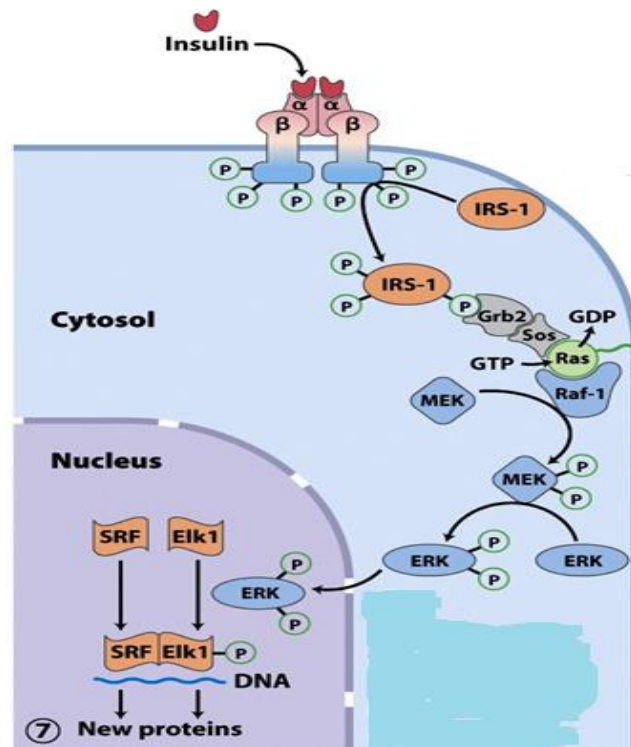


Figure 4.4 MAP kinase signaling cascade. Figure adapted from: Nelson, D.L.; Cox, M.M. *Lehninger Principles of Biochemistry 5 ed.*, 2008, W.H. Freeman and Co. New York, NY, 440.¹³

Normal IRTK MAP kinase signaling activity is found in epithelial cells that are expressed at lower basal levels.⁶ Unregulated IRTK MAP kinase signaling activity has been associated with uncontrolled gene expression, protein production and cell proliferation that are hallmarks of tumor growth.⁵ The overexpression and aberrant signaling activity of the IRTK have been found to occur in human breast, ovarian, colon and other epithelial tumors.¹⁴ It has been found that the IRTK may be directly related to oncogenic signaling activity by affecting cell metabolism and/or by working in synergy with other oncogenes that effect cell growth and differentiation. Moreover, genomic rearrangements such as chromosomal translocations, gain-of-function, GOF mutations, small deletions in PTKs, and gene amplification may each trigger oncogenic kinase signaling.⁵

4.2.3. INHIBITION OF IRTK PHOSPHORYLATION BY THE DIYET SEQUENCE

Considering their relevance in cancer, the selective regulation and potent inhibition of aberrant IRTK signaling activity may form the basis for effective forms of cancer treatment.¹⁵ Towards this goal, the pentapeptide, Ac-DIYET-NH₂ (**2.28**), derived from the activation loop of the IRTK (G¹¹⁴⁹DFGMTRDIY¹¹⁵⁸ETDY¹¹⁶²Y¹¹⁶³RKGGKGL¹¹⁷⁰) and specifically encompassing the autophosphorylation site (Y¹¹⁵⁸) was found to inhibit IRTK phosphorylation to about 80% at 4 mM.^{16,17} Moreover, competitive binding experiments in between ATP and Ac-DIYET-NH₂ (**2.28**) demonstrated that the pentapeptide was a competitive inhibitor of the IRTK domain, binding to the catalytic loop of the receptor and thereby preventing autophosphorylation of the IRTK in a non-ATP dependent manner.¹⁷ This mechanism was also confirmed by mass spectrometry, which indicated that the Ac-DIYET-NH₂ (**2.28**) sequence was phosphorylated at the tyrosine residue by the IRTK. Other peptide ligands were developed, of which Ac-DIFET-NH₂ (**2.43**), demonstrated modest inhibition (20% at 4 mM) illustrating the importance of the Tyr side chain on peptide activity. Moreover, molecular docking simulation studies in between the Ac-DIYET-NH₂ (**2.28**) sequence and the IRTK demonstrated a folded peptide geometry, which resembled a β -turn motif. These studies suggested that a peptide turn may be also responsible for IRTK binding and inhibitory activity. Thus, peptide mimics (peptidomimetics) that may stabilize the putative bio-active β -turn conformation responsible for IRTK binding may lead to the generation of more potent IRTK inhibitors. Towards this goal, azapeptide analogs of the parent pentapeptide Ac-DIYET-NH₂ (**2.28**) were synthesized by submonomer solid-phase synthesis to explore the importance of a turn conformation on IRTK inhibitory activity.

4.3. CHAPTER OBJECTIVES

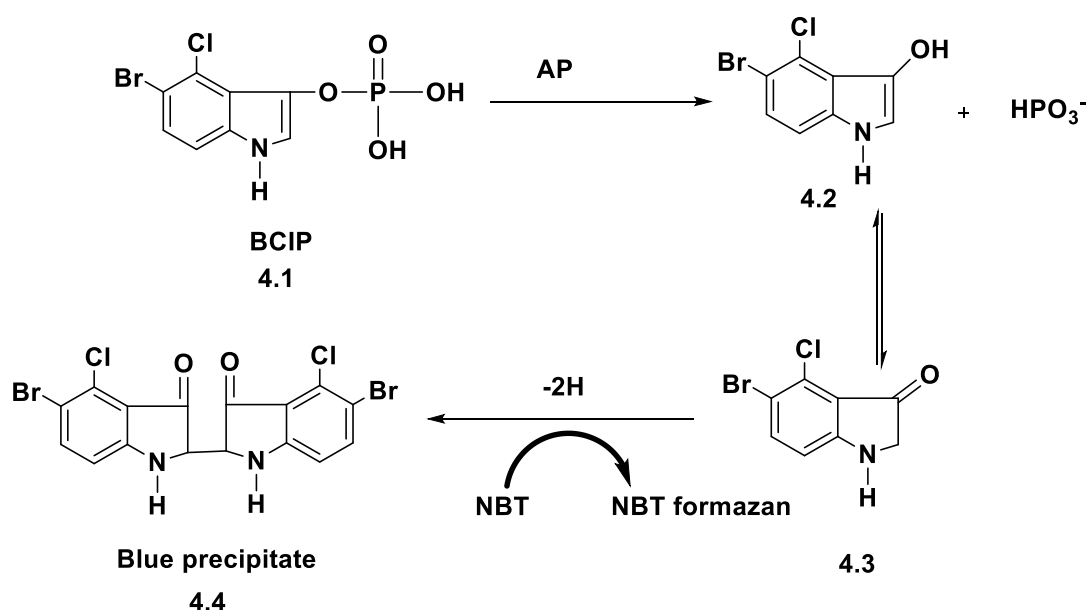
The biological activity of the peptides synthesized in Chapter 2 and characterized in Chapter 3 will be described in this chapter. More specifically, the azapeptide derivatives of the Ac-DIYET-NH₂ (**2.28**) sequence will be tested as inhibitors of IRTK autophosphorylation. The western blotting technique will be employed to determine the peptides' ability to inhibit IRTK phosphorylation. Briefly, the IRTK and ATP will be incubated with and without the peptides to determine their influence on IRTK phosphorylation. Following the IRTK phosphorylation reactions, the protein samples will be separated on by PAGE and the phosphorylated IRTK will be selected by a primary antibody which only binds to the phosphorylated form of the IRTK. A secondary antibody coupled with a detection probe is finally added to monitor the signal. In this manner, the effect of the peptides on IRTK phosphorylation can be tracked and evaluated quantitatively by densitometric analyses. This study will serve to validate the assumption that a biologically active turn conformation within the parent Ac-DIYET-NH₂ (**2.28**) sequence is responsible for IRTK binding and inhibition of phosphorylation in the presence of ATP. Azapeptides are perfectly suitable probes for testing the influence of turn conformations on peptide activity as the semicarbazide modification is known to restrain the ψ and ϕ dihedral angles leading to some types of β -turn conformations. Thus, azapeptide derivatives of the Ac-DIYET-NH₂ (**2.28**) sequence will be tested as potential inhibitors of IRTK phosphorylation en route towards the development of peptide-based anti-cancer agents (**Figure 2.5**).

4.4. RESULTS AND DISCUSSION

4.4.1 IRTK PHOSPHORYLATION STUDIES

A preliminary study on the inhibitory activity of the azapeptide Ac-DIazaYET-NH₂ (**2.36**) in comparison with the native sequence Ac-DIYET-NH₂ (**2.28**) was performed by western blot. The phosphorylation activity of the recombinant IRTK domain (residues 1005-1310) was initially determined with the IRTK (200 ng/mL) (**Figure 4.5, lane 1**), the IRTK (200 ng/mL) and ATP (1000 μM) (**Figure 4.5, lane 2**), and with the IRTK (200 ng/mL), ATP (1000 μM) and insulin (200 ng/mL) (**Figure 4.5, lane 3**), in a reaction buffer consisting of HEPES, NaCl, EDTA, MgCl₂, MnCl₂, DTT, and phenylmethylsulfonyl fluoride.

The phosphorylation reactions were performed in Eppendorf tubes at 37 °C for 20 minutes. The reactions were then quenched (Laemmli sample buffer) and heated at 70 °C for 10 minutes prior to gel electrophoresis. The samples were then resolved by denaturing 10% Bis-Tris PAGE and transferred to a PVDF membrane in a transfer buffer (25 mM Bicine, 25 mM Bis-Tris (free base, 1 mM EDTA, pH 7.2) at 30 V for 1 hour. The membrane was kept for overnight blocking in bovine serum albumin and Tris-buffered saline with Tween 20 (2% BSA in TBST) to prevent any non-specific binding. The membrane was then rinsed and treated with primary antibody, antiphospho-IR/IGFIR (Tyr 1158, 1162, 1163). The antigen-antibody complexes were then visualized with a goat anti-rabbit IgG antibody, alkaline phosphatase (AP) conjugate which catalyzed the colorimetric detection of the blue colored phosphorylated IRTK using 5-Bromo-4-chloro-3-indolyl phosphate/ Nitroblue tetrazolium (BCIP/NBT). The combination of NBT (nitro-blue tetrazolium chloride) and BCIP (5-bromo-4-chloro-3'-indolyphosphate p-toluidine salt) yields an intense, insoluble black-purple precipitate when reacted with alkaline phosphatase (**Scheme 4.1**).¹⁸



Scheme 4.1. Reaction mechanism for color development using BCIP/NBT.¹⁸

The substrate BCIP, **4.1**, is hydrolyzed by alkaline phosphatase to form an intermediate that undergoes dimerization to produce an indigo dye, **4.4**. The NBT is reduced to the NBT-formazan during the oxidation of **4.3** to **4.4**. This reaction proceeds at a steady rate, allowing for accurate control of detection during the reaction progress. The signal intensity may be then measured by densitometric analyses using Image J (<http://rsbweb.nih.gov/ij/download.html>).

Incubation of IRTK in a HEPES buffer without ATP did not produce any visible bands following immunoblotting (**Figure 4.5, lane 1**). This is an expected result, considering in the absence of ATP no IRTK phosphorylation can occur nor can be detected by the primary antibody used for binding phosphorylated IRTK. A band was observed when the IRTK was phosphorylated with ATP (**Figure 4.5, lane 2**) and a more intense signal, albeit with a modest increase of ~10% relative to the control IRTK + ATP sample was observed with additional insulin (**Figure 4.5, lane 3**). The latter result is somewhat surprising, since only a small

portion of the IRTK (residues 1005-1310) comprising the cytoplasmic β -subunit of the RTK domain and not the extracellular α -subunit insulin binding site was used for this study. These results suggests the presence of an allosteric binding pocket on the IRTK domain that may contribute towards insulin binding and activation of IRTK phosphorylation. This result may be noteworthy of further investigation, but falls outside the scope of this present study. Therefore, further analyses were performed without the addition of insulin.

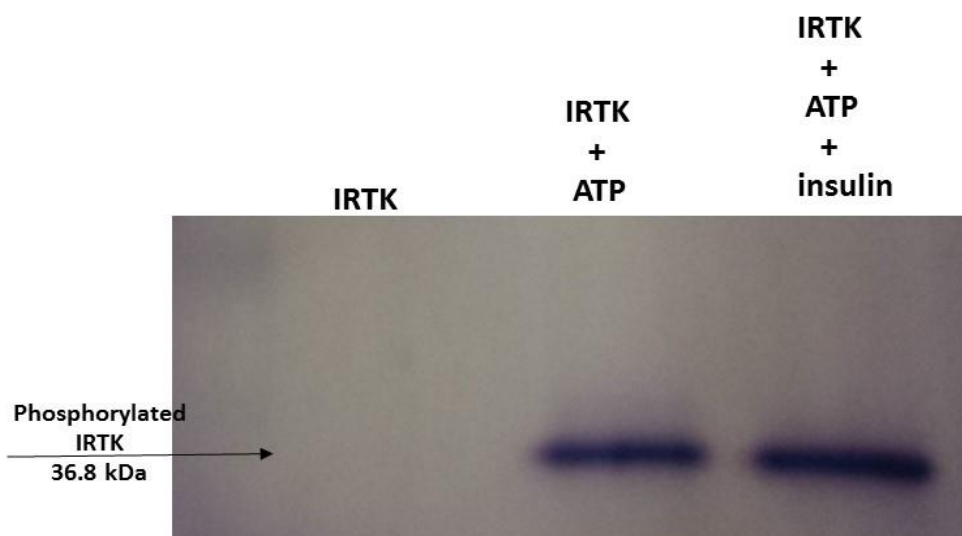


Figure 4.5. Western blot analyses of the IRTK phosphorylation activity. Samples were analyzed as: IRTK (200 ng/mL) (lane 1), IRTK (200 ng/mL) and ATP (1000 μ M) (lane 2), and with the IRTK (200 ng/mL), ATP (1000 μ M) and insulin (200 ng/mL) (lane 3), in a HEPES reaction buffer consisting of HEPES, NaCl, EDTA, MgCl₂, MnCl₂, DTT, and phenylmethylsulfonyl fluoride.

4.4.2 INHIBITION OF IRTK PHOSHORYLATION

The inhibitory activity of the peptides, Ac-DIYET-NH₂ (**2.28**) vs Ac-DIazaYET-NH₂ (**2.36**), was next evaluated by conducting the IRTK phosphorylation reactions as previously described, but with the addition of peptide ligands (400 μ M). Phosphorylation of the insulin receptor in the absence of the peptide ligands was considered to be 100%. In this single dose

experiment, minimal inhibitory activity (<10%) was detected for the parent peptide, Ac-DIYET-NH₂ (**2.28**), whereas, Ac-DIazaYET-NH₂ (**2.36**) displayed about 50% inhibition of the IRTK autophosphorylation (**Figure 4.6**). This result lends supporting evidence that the β -turn conformation adopted by the selected azapeptide, Ac-DIazaYET-NH₂ (**2.36**) may contribute to IRTK binding affinity and inhibitory activity within the catalytic loop of the RTK active site.

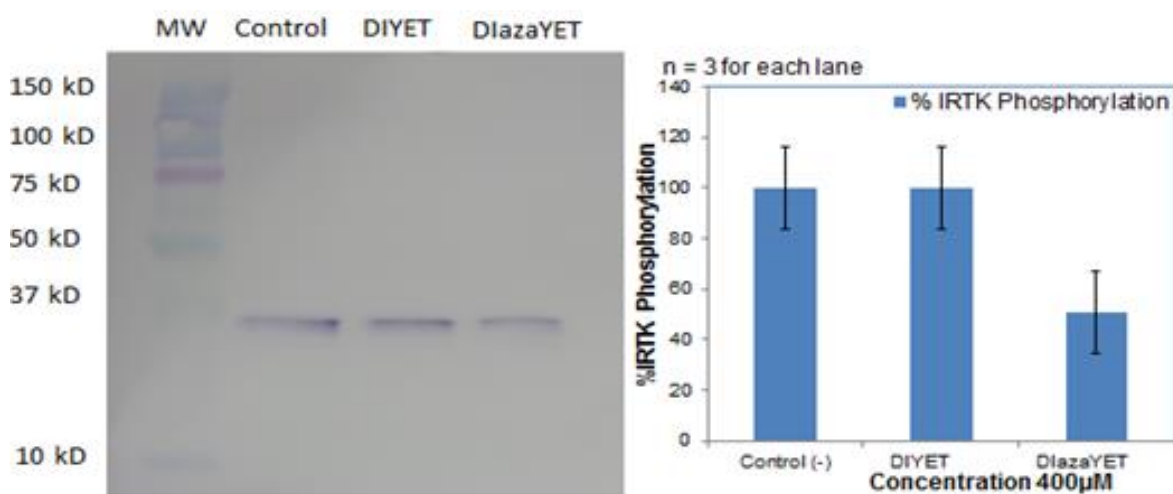


Figure 4.6. Western blot data for IRTK (200 ng/mL) phosphorylation inhibition with peptide ligands Ac- DIYET-NH₂ (**2.28**), and Ac-DIazaYET-NH₂ (**2.36**) at 400 μ M. Each experiment was conducted in replicate n=3 with standard deviations reported about the mean % IRTK phosphorylation.

A dose-response (0 - 400 μ M) assay was next conducted, comparing the inhibitory activity of the native sequence (**2.28**) with the azapeptide (**2.36**) and a known tyrophostin (AG1024) inhibitor of the IRTK was used as control.¹⁹ Three different concentrations of peptide ligands, 4, 40 and 400 μ M were used for this dose-response assay (**Figure 4.7**). In this experiment, Ac-DIazaYET-NH₂ (**2.36**), maintained about 50% inhibitory activity of the IRTK autophosphorylation at 400 μ M, albeit to a lesser extent relative to the tyrophostin inhibitor

(~80% inhibition at 40 μM) and without a dose-response correlation as depicted below. No significant inhibitory activity was noticed for the natural sequence with the conditions used in this study and which differ from the literature reported conditions, especially with the use of the IRTK.^{16,17}

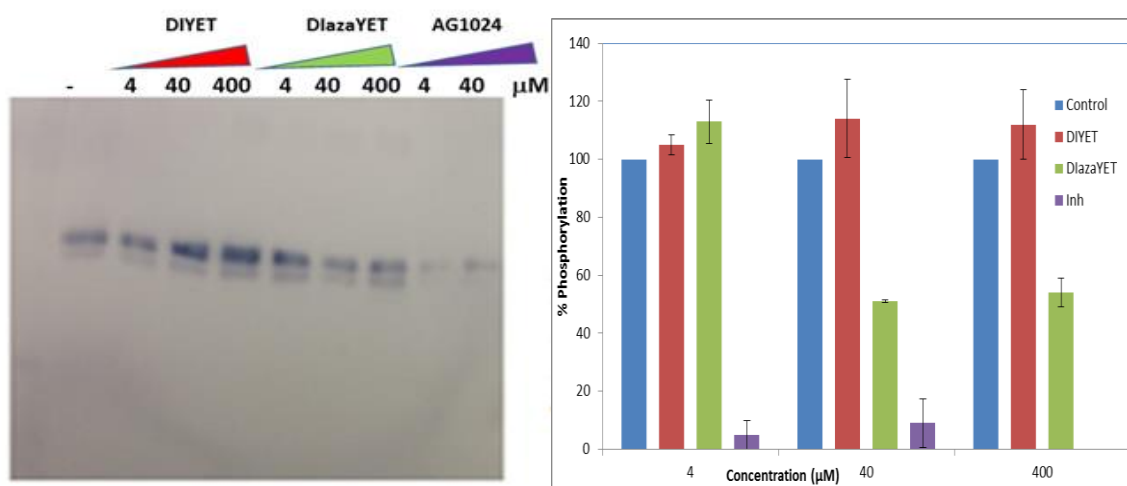


Figure 4.7. Western blot data for IRTK (200 ng/mL) phosphorylation inhibition with peptide ligands Ac-DIYET-NH₂ (**2.28**), and Ac-DIazaYET-NH₂ (**2.36**) in addition to tyrphostin inhibitor (AG1024) at 4, 40 and 400 μM . Each experiment was conducted in replicate $n=3$ with standard deviations reported about the mean % IRTK phosphorylation.

The inhibitory activity of the azapeptides on IRTK autophosphorylation was tested at 400 μM by western blot. A control sample consisting of the IRTK (200 ng) and ATP (1000 μM) was included in the phosphorylation reaction without the addition of any peptides and considered as 100% phosphorylation. The experimental results showed that the inhibitory activity of the azapeptides vary on the position and composition of the aza-residue. In this library, the Ac-DIazaYET-NH₂ sequence exhibited the most antagonistic activity (50-60%) on the autophosphorylation of the IRTK. Similarly, the azapeptide analogs DazaAYET, DazaGYET and DazaYET showed about 25% - 40 % inhibitory activity on the autophosphorylation of IRTK. Conversely, the azapeptide analog [azaDOPA³] displayed an increase (30%) in the autophosphorylation activity of IRTK. A similar effect was also observed for the azapeptide analog [azaE⁴], with a modest (10%) increase in IRTK

autophosphorylation activity. The modulatory effects of the azapeptide ligands on IRTK autophosphorylation are depicted in **Figure 4.8**.

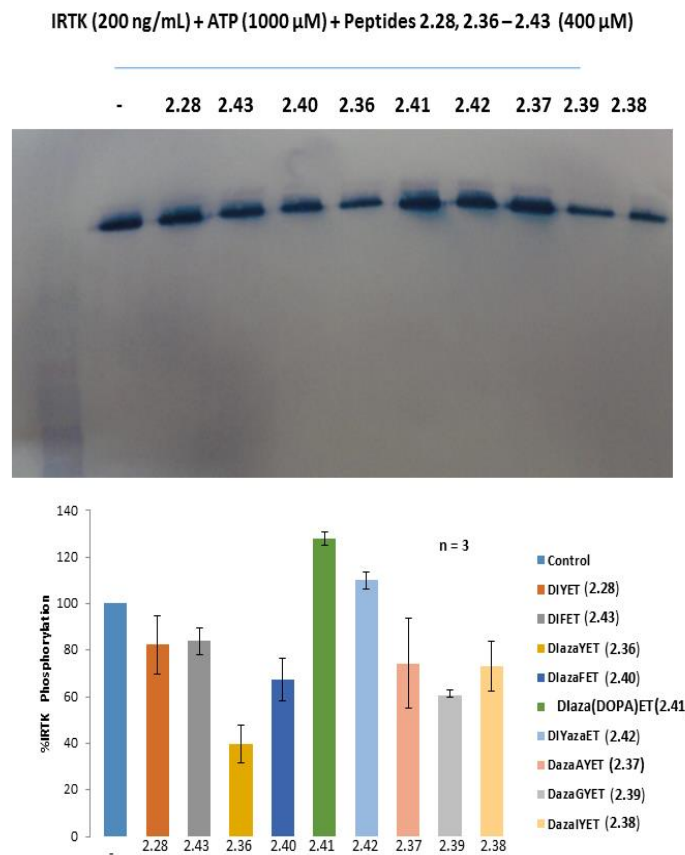


Figure 4.8. Western blot data for IRTK (200 ng/mL) phosphorylation inhibition with peptide ligands synthesized in this study at 400 μ M. Each experiment was conducted in replicate n=3 with standard deviations reported about the mean % IRTK phosphorylation.

Entry	Sequence (#)	% IRTK Phosphorylation
1	Ac-DIYET-NH ₂ (2.28)	82 ± 12
2	Ac-DIFET-NH ₂ (2.43)	84 ± 5.7
3	Ac-DIazaYET-NH ₂ (2.36)	40 ± 8.2
4	Ac-DIazaFET-NH ₂ (2.40)	67 ± 9.4
5	Ac-DIaza(DOPA)ET-NH ₂ (2.41)	128 ± 2.9
6	Ac-DIYazaET-NH ₂ (2.42)	110 ± 3.6
7	Ac-DazaAYET-NH ₂ (2.37)	74 ± 19
8	Ac-DazaGYET-NH ₂ (2.39)	61 ± 2.3
9	Ac-DazaIYET-NH ₂ (2.38)	73 ± 10

Table 4.1 IRTK Phosphorylation (%) in presence of peptides (400 μM) and ATP (1000 μM)

4.5 CONCLUSIONS

In sum, a new class of azapeptide inhibitors of the IRTK domain have been validated in this study. The selected azapeptide, Ac-DIazaYET-NH₂ (**2.36**), which demonstrated a stable β -turn geometry resulted in a ~5-fold increase in IRTK inhibitory activity relative to the parent pentapeptide (50 vs <10%). The azapeptide analogs, Ac-DazaIYET-NH₂ (**2.38**), and Ac-DazaAYET-NH₂ (**2.37**) exhibited about 25% and Ac-DazaGYET-NH₂ (**2.39**) exhibited about 40% inhibitory activity on the autophosphorylation of IRTK. Thus, azapeptide inhibitors of the IRTK may form new leads in the development of potent and selective Tyr kinase binding ligands for anti-cancer²⁰ and related applications in drug discovery.¹⁵

4.6 REFERENCES

1. Sierra, D.A.; Gilbert, D.J.; Householder, D.; Grishin, N.V.; Yu, K.; Ukidwe, P.; Barker, S.A.; He, W.; Wensel, T.G.; Otero, G.; Brown, G.; Copeland, N.G.; Jenkins, N.A.; Wilkie, T.M. *Genomics* **2002**, *79*, 177-185.
2. (a) Ring, A.M.; Manglik, A.; Kruse, A.C.; Enos, M.D.; Weis, W.I.; Garcia, K.C.; Kobilka, B.K. *Nature* **2013**, *502*, 575-579; (b) Tan, Q.; Zhu, Y.; Li, J.; Chen, Z.; Han, G.W.; Kufareva, I.; Li, T.; Ma, L.; Fenalti, G.; Li, J.; Zhang, W.; Xie, X.; Yang, H.; Jiang, H.; Cherezov, V.; Liu, H.; Stevens, R.C.; Zhao, Q.; Wu, B. *Science* **2013**, *341*, 1387-1390.
3. Lin, H.H. *Biomed. J.* **2013**, *36*, 118-124.
4. Hunter, T. *Cell* **1995**, *80*, 225-236.
5. Blume-Jensen, P.; Hunter, T. *Nature* **2001**, *11*, 355 – 365.
6. Schlessinger, J. *Cell* **2000**, *103*, 211 – 225.
7. (a) Hubbard, S.R.; Wei, L.; Ellis, L.; Hendrickson, W.A. *Nature* **1994**, *372*, 746–754; (b) Hubbard, S.R. *EMBO J.* **1997**, *16*, 5572–5581; (c) Lee, J.; Pilch, P.F. *Am. J. Physiol.* **1994**, *266*, C319-34.
8. Balotti, R.; Le Marchand-Brustel, Y.; Gammeltoft, S.; Van Obberghen, E. *Reprod. Nutr. Dev.* **1989**, *29*, 653-661.
9. White; M.F., Shoelson; S.E., Keutmann; H., Kahn; C.R. *J. Biol. Chem.* **1988**, *263*, 2969–2980.
10. Niswender, K.D.; Morrison, C.D.; Clegg, D.J.; Olson, R.; Baskin, D.G.; Myers, M.G.; Seeley, R.J.; Schwartz, M.W. *Diabetes* **2003**, *52*, 227-231.
11. Saltiel, A.R.; Kahn, C.R. *Nature* **2001**, *414*, 799–806.
12. Skolnik, E.Y.; Batzer, A.; Li, N.; Lee, C-H.; Lowenstein, E.; Mohammadi, M.; Margolis, B.; Schlessinger; J. *Science* **1993**, *260*, 1953–1955.
13. Nelson, D.L.; Cox, M.M. *Lehninger Principles of Biochemistry 5 ed.*, **2008**, W.H. Freeman and Co. New York, NY, 440.

14. Paonessa, F.; Foti, D.; Costa, V.; Chiefari, E.; Brunetti, G.; Leone, F.; Luciano, F.; Wu, F.; Lee A.S.; Gulletta, E.; Fusco, A.; Brunetti, A. *Cancer Res.* **2006**, *66*, 5085.
15. (a) Al-Obeidi, F.A.; Wu, J.J.; Lam, K.S. *Biopolymers* **1998**, *47*, 197–223; (b) Levitzki, A.; Gazit, A. *Science* **1995**, *267*, 1782–1788.
16. Hirose, M.; Kuroda, Y.; Sawa, S.; Nakagawa, T.; Hirata, M.; Sakaguchi, M.; Tanaka, Y. *Br. J. Pharmacol.* **2004**, *142*, 222 – 228.
17. Kato, M.; Abe, M.; Kuroda, Y.; Hirose, M.; Nakano, M.; Handa, T. *J. Pept. Sci.* **2009**, *15*, 327 – 336.
18. Smejkal, G.B.; Kaul, C.A. *J. Histochem. Cytochem.* **2001**, *49*, 1189-1190.
19. Parrizas, M.; Gazit, A.; Levitzki, A.; Wertheimer, E.; LeRoth, D. *Endocrinology* **1997**, *138*, 1427-1433.
20. Kim, M.H.; Tshako, A.L.; Co, E.W.; Aftab, D.T.; Bentzien, F.; Chen, J.; Cheng, W.; Engst, S.; Goon, L.; Klein, R.R.; Le, D.T.; Mac, M.; Parks, J.J.; Qian, F.; Rodriguez, M.; Stout, T.J.; Till, J.H.; Won, K.A.; Wu, X.; Yakes, F.M.; Yu, P.; Zhang, W.; Zhao, Y.; Lamb, P.; Nuss, J.M.; Xu, W. *Bioorg. Med. Chem. Lett.* **2012**, *22*, 4979-4985.

4.7 EXPERIMENTAL MEHODS

4.7.1. Materials and Methods

The insulin receptor tyrosine kinase domain, IRTK, (EMD Millipore, cat. no. 14-466) ATP (sigma) and insulin (calbiochem) were used directly as received. The reagents for preparing the reaction buffer, 4-(2-Hydroxyethyl)piperazine-1-ethanesulfonic acid, HEPES, (Sigma), NaCl (Macron), ethylenediaminetetraacetic acid, EDTA, (Sigma), MgCl₂ (Fisher), MnCl₂ (Fisher), dithiothreitol, DTT, (BRL) and phenylmethylsulfonyl fluoride (sigma aldrich) were mixed together in MilliQ grade water and adjusted at pH 7.4. Laemmli sample buffer (consisting of 106 mM Tris HCl, 141 mM Tris Base, 2% LDS, 10% Glycerol, 0.51 mM

EDTA, 0.22 mM SERVA Blue G250, 0.175 mM Phenol Red, pH 8.5) was purchased from (Life Technologies) and used to quench the phosphorylation reactions prior to PAGE and western blotting. The gels, 10% Bis-Tris PAGE were purchased from Life Technologies and transferred to a polyvinylidene fluoride, PVDF, membrane (Millipore) for immunoblotting. Bovine serum albumin in tris-buffered saline containing 20% Tween 20 (2% BSA in TBST) was purchased from GeneTex and used directly for membrane blocking. The antibodies for phosphor-IRTK detection antiphospho-IR/IGFIR (Tyr1158/Tyr 1162/Tyr 1163) (EMD Millipore, cat. no. 07-841) and goat anti-rabbit IgG antibody, Alkaline Phosphatase conjugate (EMD Millipore, cat. no. 12-448) were used directly as received. The colorimetric detection of the antigen:antibody complexes was determined using 5-Bromo-4-chloro-3-indolyl phosphate / Nitroblue tetrazolium (BCIP/NBT) purchased from Sigma Aldrich. The IRTK inhibitor, AG1024 (EMD Millipore, cat. no. 121767) was also used as a control inhibitor for the IRTK.

4.7.2 Phosphorylation reactions of the IRTK

The phosphorylation of the active insulin receptor tyrosine kinase domain, IRTK, encompassing residues 1005-1310 (EMD Millipore, cat. no. 14-466) was initially performed by treating the IRTK (200 ng) with ATP (1000 μ M) and insulin (2.6 μ g/mL) in 25 μ L of incubation buffer consisting of 50 mM HEPES pH 7.4, 125 mM NaCl, 1 mM EDTA, 10 mM MgCl₂, 5 mM MnCl₂, 5 mM DTT and 1 mM phenylmethylsulfonyl fluoride for 20 min at 37 °C. The reaction was quenched by addition of Laemmli sample buffer (8 μ L) and the IRTK was denatured at 70 °C for 10 minutes followed by separation and detection by western blotting.

4.7.3. Inhibition studies of the IRTK

The inhibitory activity of the peptides on the autophosphorylation of the insulin receptor was next evaluated by adding various concentrations (4-400 μM) of the peptides or control IRTK inhibitor, AG1024 (EMD Millipore, cat. no. 121767) to the IRTK (200 ng) and then proceeding with the phosphorylation reactions as previously described. The reactions were quenched by the addition of Laemmli sample buffer (8 μL) and the IRTK was denatured at 70 °C for 10 minutes and analyzed by western blotting.

4.7.4. Western blotting

The IRTK was then resolved by denaturing 10% Bis-Tris PAGE and transferred to a PVDF membrane for overnight blocking (2% BSA in TBST) and immunoblotting was performed with antiphospho-IR/IGFIR (Tyr1158/Tyr 1162/Tyr 1163). The antigen-antibody complexes were visualized with a goat anti-rabbit IgG antibody, Alkaline Phosphatase conjugate (EMD Millipore, cat. no. 12-448) which catalyzed the colorimetric detection of the complexes using 5-Bromo-4-chloro-3-indolyl phosphate / Nitroblue tetrazolium (BCIP/NBT). After addition of the color development solution (BCIP/NBT) the reaction was continued for 10 minutes to visualize the desired bands. The PVDF membrane was rinsed with deionized water and dried at room temperature. The band intensities were measured by Image J (<http://rsbweb.nih.gov/ij/download.html>). The autophosphorylation of the IRTK domain in the presence of 1000 μM ATP for 20 minutes at 37 °C was taken as control and considered to be 100%. A commercially available IRTK inhibitor, AG1024 (EMD Millipore, cat. no. 121767) was also used as a control inhibitor for the IRTK.

CHAPTER 5: CONCLUSIONS AND CONTRIBUTIONS TO KNOWLEDGE

5.1 CONCLUSIONS AND CONTRIBUTIONS TO KNOWLEDGE MADE IN THIS THESIS

5.1.1 DESIGN, SYNTHESIS AND CONFORMATIONAL ANALYSES OF AZAPEPTIDE INHIBITORS OF THE INSULIN RECEPTOR TYROSINE KINASE

Receptor tyrosine kinases play a crucial role in cell growth and differentiation. The phosphorylation activity of kinases is implicated in the activation of signaling pathways that governs the cell cycle for proliferation among other biological functions. Thus, kinase signaling activity must be highly regulated in order to maintain cellular homeostasis and avoid tumorigenesis. In cells that harbor mutations or genetic modifications leading to the overexpression of receptor tyrosine kinases, regulated cell division ceases to exist leading rise to cell division without restriction. As a result, the overexpression of receptor tyrosine kinases has been associated with oncogenic signaling and the growth of tumors. They have been vastly implicated in many epithelial tumor types, such as those belonging to breast, ovarian and prostate cancers. Thus, the selective inhibition of aberrant receptor tyrosine kinase signaling activity may lead to the development of effective forms of cancer therapy. Towards this goal, a synthetic pentapeptide, Ac-DIYET-NH₂, derived from the activation loop of the insulin receptor tyrosine kinase (IRTK) domain has been validated as a peptide lead for the inhibition of IRTK phosphorylation and activation of its signaling activity. The peptide sequence exhibited strong IRTK inhibition (~80%), albeit at high concentration levels (4 mM) which limits its applications *in vivo*. Moreover, molecular docking studies of the lead pentapeptide bound to the active site of the IRTK domain demonstrated a turn type peptide geometry that may contribute to binding affinity and inhibitory activity. Considering

azapeptides are a valid class of peptide mimics that are known to stabilize bio-active turn conformations, a small library (7) of azapeptide analogs of the Ac-DIYET-NH₂ sequence were synthesized, characterized and evaluated for IRTK inhibitory activity.

A submonomer approach was adopted for the synthesis of azapeptides belonging to the Ac-DIYET-NH₂ sequence in order to systematically introduce aza-residues within the IYE pharmacophoric region of the peptide sequence. In Chapter 2, the submonomer solid phase synthesis furnished a small library (7) of azapeptides featuring the introduction of new aza-Ile and aza-DOPA residues. Halogen exchange reactions were found to be particularly useful for the introduction of aza-Tyr and aza-DOPA residues at the Tyr³ position. These reactions were used to convert the poorly reactive benzyl chlorides to the more reactive iodides leading to azapeptides, **2.36** and **2.41** in 50 and 36% yields, respectively. The aza-isoleucine analog was synthesized using racemic 2-iodobutane as alkylating agent in the presence of BTPP. Although this resulted in diastereomeric Ac-DazaIYET-NH₂, **2.38**, RP-LCMS purification and analysis provided a single diastereomer, suitable for SAR studies. Azapeptides were isolated in sufficient yields (36-55%) and good purities (>95%) following submonomer synthesis and RP-LCMS purification. Thus, the submonomer approach for azapeptide synthesis proved to be an efficient method for the preparation of azapeptides useful for structure-function studies as described in Chapters 3 and 4.

A conformational analysis of the novel azapeptides synthesized in Chapter 2 was presented in Chapter 3 of this thesis. A molecular docking simulation study was initially performed to evaluate the propensity for the azapeptide analog Ac-DIazaYET-NH₂, **2.36**, to adopt a turn geometry at the active site of the IRTK. An interface between the molecular graphics system PyMOL and the molecular docking suite AutoDock Vina was used to demonstrate the combination of docking and visualization models. The Ac-DIazaYET-NH₂,

2.36, sequence was found to be in close proximity to the key IRTK binding site residues Asp 1132 and Arg 1136 found within the catalytic loop of the IRTK. Moreover, the azapeptide was found to project a turn-type conformation bound to the IRTK domain that may contribute to binding affinity. CD and NMR spectroscopy were used to lend additional support into the structural trends determined by computational analyses. The CD study was conducted in aqueous media (H₂O, phosphate buffered saline, PBS) to determine the influence of salt on peptide conformation. Moreover, the CD spectra of the peptides were also collected in DMSO, to support the NMR data. The CD curve for the parent peptide, Ac-DIYET-NH₂ was typical of a random coil or a disordered structure, characterized by the strong negative band at 190 nm. At the 2 position, the [aza-Ile²], [aza-Ala²] and the [aza-Gly²]-residues exhibited CD spectra that were respectively associated with random coils in water (**Figure 3.6**), a combination of helical and turn geometries in phosphate buffer (**Figure 3.7**) and folded conformations in DMSO (**Figure 3.8**). Thus, the solvent conditions were found to impact the azapeptide folds, indicating the influence of solvent and aza substitutions at the *i+1* position on the peptide conformations. At the 3 position, the [aza-Tyr³], [aza-DOPA³] and [aza-Phe³] modifications were found to exhibit CD spectra with characteristic positive bands near 215 nm and two negative ones near 230 and 190 nm. The observed CD traces are indicative of a β -turn geometry, with some proportion of random coil due to the sharp negative minima observed near 190 nm (**Figure 3.9**). The observed β -turn geometry was also maintained for the azapeptide dissolved in phosphate buffer (**Figure 3.10**), whereas peptide folds were observed in DMSO (**Figure 3.11**). Thus, the insertion of aza-residues at the *i+2* position were found to stabilize a turn conformation about the peptide backbone geometry. Moving to the 4 position, [aza-Glu³], **2.42**, displayed a CD spectrum in water, PBS and DMSO that failed to stabilize a peptide turn conformation. These results were based on the large proportion of

random coil observed in water and characterized by the negative minimum band at 190 nm (**Figures 3.12**). In phosphate buffer, the azapeptide displayed a large positive band near 190 nm that are typically consistent with helical type structures (**Figure 3.13**). In DMSO, a poorly folded peptide geometry indicated that the aza-Glu modification at the 4 position failed to stabilize the peptide secondary structure (**Figure 3.14**).

The NMR spectrum of the parent pentapeptide Ac-DIYET-NH₂, **2.28** was compared to azapeptide, **2.36**, in deuterated water and DMSO. In DMSO, the azapeptide displayed an NMR spectrum that was indicative of a β -turn. This azapeptide secondary structure was characterized by the disappearance of the Glu NH and down-field chemical shift of the Ile NH (δ : 8.2 vs 7.6) when compared to the parent peptide (**Figure 3.15 A and B**, respectively). This observation is consistent with the hydrogen bonding interaction found in between the carbonyl group of the Asp residue at the *i* position and the amino group of the Glu residue at the *i*+3 position to generate the turn conformation that is stabilized by the aza-Tyr residue at the *i*+2 position. Moreover, 2D NOESY confirmed multiple NOE correlations that were consistent with a folded azapeptide geometry that was absent within the parent peptide whose protons appeared to be solvent exposed with fewer NOE correlations (**Figure 3.16**).

After the confirmation of the peptide structures, biology was next examined towards the development of an azapeptide analog which may improve the inhibitory activity of the Ac-DIYET-NH₂ sequence towards the IRTK (Chapter 4).

5.1.2 BIOLOGICAL ACTIVITY OF AZAPEPTIDE ANALOGS

In Chapter 4 of this thesis, a preliminary study on the inhibitory activity of the azapeptide Ac-DIazaYET-NH₂ (**2.36**) in comparison with the native sequence Ac-DIYET-NH₂ (**2.28**) was performed by western blot. The phosphorylation activity of the recombinant

IRTK domain (residues 1005-1310) was initially determined with the IRTK (200 ng/mL) (**Figure 4.5, lane 1**), the IRTK (200 ng/mL) and ATP (1000 μ M) (**Figure 4.5, lane 2**), and with the IRTK (200 ng/mL), ATP (1000 μ M) and insulin (200 ng/mL) (**Figure 4.5, lane 3**), in a reaction buffer at pH 7.4, consisting of HEPES, NaCl, EDTA, MgCl₂, MnCl₂, DTT, and phenylmethylsulfonyl fluoride. The extent of the IRTK phosphorylation reactions was probed with an anti-phospho-IRTK primary antibody and a secondary one conjugated with alkaline phosphatase for detection. A band was observed when the IRTK was phosphorylated with ATP (**Figure 4.5, lane 2**) and a more intense signal, albeit with a modest increase of ~10% relative to the control IRTK + ATP sample was observed with additional insulin (**Figure 4.5, lane 3**).

In this single dose (400 μ M) experiment, minimal inhibitory activity (<10%) was detected for the parent peptide, Ac-DIYET-NH₂ (**2.28**), whereas, Ac-DIazaYET-NH₂ (**2.36**) displayed about 50% inhibition of the IRTK autophosphorylation (**Figure 4.6**). This result lends supporting evidence that the β -turn conformation adopted by, Ac-DIazaYET-NH₂ (**2.36**) may contribute to IRTK binding affinity and inhibitory activity at the IRTK active site. A dose-response (0 - 400 μ M) study with Ac-DIazaYET-NH₂ (**2.36**), maintained about 50% inhibitory activity of the IRTK autophosphorylation at 400 μ M, without a dose-response correlation.

In sum, a new class of azapeptide inhibitors of the IRTK domain have been validated in this thesis. The selected azapeptide, Ac-DIazaYET-NH₂ (**2.36**), which demonstrated a stable β -turn geometry resulted in a about 5-fold increase in IRTK inhibitory activity relative to the parent pentapeptide (50 vs <10%). Thus, azapeptide inhibitors of the IRTK may form new

leads in the development of potent and selective Tyr kinase binding ligands for anti-cancer and related medicinal chemistry applications.

5.1.3 FUTURE WORK

The submonomer approach for azapeptide synthesis is especially useful in the production of a library of structurally diverse azapeptides to further our SAR studies. As part of our ongoing SAR studies, future work will be geared towards additional biology experiments that will be used to evaluate the *in-vitro* IRTK phosphorylation inhibitory activity of the azapeptide ligands. Moreover, mechanistic insights can also be gained by the azapeptides that may function as valuable probes for elucidating their mechanisms of IRTK inhibitory activity. This enzyme-based study will pave the way for cell-based assays, in which a relevant tumor cell line model (*eg.* HepG2 cells) known to overexpress IRTK will be used to determine the potential of the azapeptides to inhibit IRTK signaling activity in cancer. A variety of molecular markers may be evaluated for this cell based assay, including IRTK phosphorylation levels and a number of downstream substrates (*i.e.* IRS-1, c-Raf, Ras and Sos) known to activate oncogenic signaling. Moreover, caspase activation and cell death measurements may be used to evaluate the anti-cancer potential of the azapeptides. These fruitful experiments will facilitate the selection of a lead azapeptide inhibitor that may be screened in multiple cell types to validate efficacy and selectivity. A medicinal chemistry approach may then be used to optimize the ‘drug-like’ properties of the azapeptide en route towards the development of a potent and selective peptidomimetic therapeutic.

5.2 PUBLICATIONS AND CONFERENCE PRESENTATIONS

- *Manuscript submitted for publication*

1. Lathamol A. Kurian, Tammy A. Silva and David Sabatino - **Submonomer Synthesis of Azapeptide Ligands of the Insulin Receptor Tyrosine Kinase Domain**. *Bioorganic and Medicinal Chemistry Letters* **2014**, *asaps*.

- *Poster Presentations*

1. Lathamol A Kurian and David Sabatino. **Submonomer Solid-Phase Synthesis of Azapeptide Inhibitors of the Insulin Receptor Tyrosine Kinase**. IBC 16th Annual TIDES Conference, Providence, RI, May 12, 2014.
2. Lathamol A Kurian and David Sabatino **Azapeptide Inhibitors of the Insulin Receptor Tyrosine Kinase**. AAPS Annual Meeting and Exposition, San Diego, CA. Nov 2 - 6, 2014 (Poster accepted # AM-14-0439).
3. Stesha Joseph, Lathamol Kurian, Mariana Phillips, Ivonne Martinez, Brittany Blackman[‡], Christopher Parronchi, Megan Kelly, Michael Beaury, Constantine Bitsaktsis, Allan Blake and David Sabatino, **Synthesis, Characterization and Biological Evaluation of Cancer-Targeting Peptides**. NYAS, Chemical Biology Discussion Year-End Symposium, New York, NY, June 3, 2014.
4. Stesha C. Joseph, Anthony Maina, Mariana Phillips, Lathamol A Kurian, Emily Borland, Ivonne Martinez, and David Sabatino, **Cancer-Targeting Peptides in**

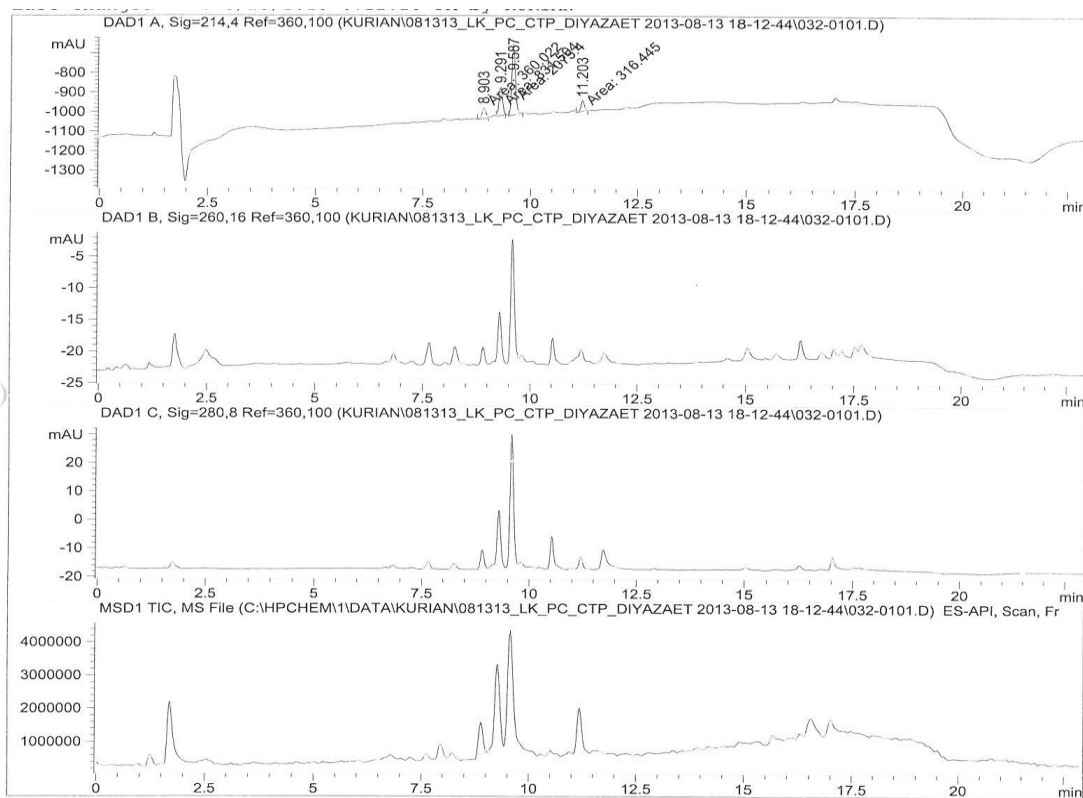
Cancer Therapy. 17th Annual Petersheim Academic Symposium, Seton Hall University, South Orange, NJ, April 23, 2013.

5. Stesha C. Joseph, Lathamol A Kurian, Leah R. Poland, Tammy A. Silva, and David Sabatino, **How do we make peptides in the lab?** 16th Annual Petersheim Academic Symposium, Seton Hall University.

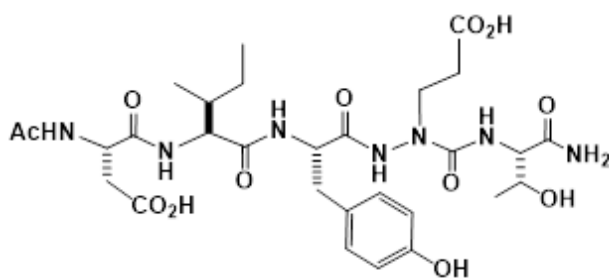
Figure A1	RP-HPLC analysis of crude Ac-DIYazaET-NH ₂ , 2.42 .	118
Figure A2	ESI-LCMS analysis of crude Ac-DIYazaET-NH ₂ , 2.42 .	119
Figure A3	RP-HPLC analysis of pure Ac-DIYazaET-NH ₂ , 2.42 .	120
Figure A4	ESI-LCMS analysis of pure Ac-DIYazaET-NH ₂ , 2.42 .	121
Figure A5	RP-HPLC analysis of pure Ac-DIYazaET-NH ₂ , 2.42 .	122
Figure A6	ESI-LCMS analysis of pure Ac-DIYazaET-NH ₂ , 2.42 .	123
Figure A7	RP-HPLC analysis of crude Ac-DazaAYET-NH ₂ , 2.37 .	124
Figure A8	ESI-LCMS analysis of crude Ac-DazaAYET-NH ₂ , 2.37 .	125
Figure A9	RP-HPLC analysis of pure Ac-DazaAYET-NH ₂ , 2.37 .	126
Figure A10	ESI-LCMS analysis of pure Ac-DazaAYET-NH ₂ , 2.37 .	127
Figure A11	RP-HPLC analysis of pure Ac-DazaAYET-NH ₂ , 2.37 .	128
Figure A12	ESI-LCMS analysis of pure Ac-DazaAYET-NH ₂ , 2.37 .	129
Figure A13	RP-HPLC analysis of crude Ac-DazaGYET-NH ₂ , 2.39 .	130
Figure A14	ESI-LCMS analysis of crude Ac-DazaGYET-NH ₂ , 2.39 .	131
Figure A15	RP-HPLC analysis of pure Ac-DazaGYET-NH ₂ , 2.39 .	132
Figure A16	ESI-LCMS analysis of pure Ac-DazaGYET-NH ₂ , 2.39 .	133
Figure A17	RP-HPLC analysis of pure Ac-DazaGYET-NH ₂ , 2.39 .	134
Figure A18	ESI-LCMS analysis of pure Ac-DazaGYET-NH ₂ , 2.39 .	135
Figure A19	RP-HPLC analysis of crude Ac-DazaIYET-NH ₂ , 2.38 .	136
Figure A20	ESI-LCMS analysis of crude Ac-DazaIYET-NH ₂ , 2.38 .	137

Figure A21	ESI-LCMS analysis of crude Ac-DazaIYET-NH ₂ , 2.38 .	138
Figure A22	ESI-LCMS analysis of crude Ac-DazaIYET-NH ₂ , 2.38 .	139
Figure A23	RP-HPLC analysis of pure Ac-DazaIYET-NH ₂ , 2.38 .	140
Figure A24	ESI-LCMS analysis of pure Ac-DazaIYET-NH ₂ , 2.38 .	141
Figure A25	RP-HPLC analysis of crude Ac-DIazaFET-NH ₂ , 2.40 .	142
Figure A26	ESI-LCMS analysis of crude Ac-DIazaFET-NH ₂ , 2.40 .	143
Figure A27	RP-HPLC analysis of crude Ac-DIazaFET-NH ₂ , 2.40 .	144
Figure A28	ESI-LCMS analysis of pure Ac-DIazaFET-NH ₂ , 2.40 .	145
Figure A29	ESI-LCMS analysis of pure Ac-DIazaFET-NH ₂ , 2.40 .	146
Figure A30	ESI-LCMS analysis of crude Ac-DIazaFET-NH ₂ , 2.40 .	147
Figure A31	RP-HPLC analysis of crude Ac-DIazaYET-NH ₂ , 2.36 .	148
Figure A32	ESI-LCMS analysis of crude Ac-DIazaYET-NH ₂ , 2.36 .	149
Figure A33	RP-HPLC analysis of pure Ac-DIazaYET-NH ₂ , 2.36 .	150
Figure A34	ESI-LCMS analysis of pure Ac-DIazaYET-NH ₂ , 2.36 .	151
Figure A35	RP-HPLC analysis of pure Ac-DIazaYET-NH ₂ , 2.36 .	152
Figure A36	RP-HPLC analysis of crude Ac-DIazaYET-NH ₂ , 2.36 .	153
Figure A37	RP-HPLC analysis of crude Ac-DIaza(DOPA)ET-NH ₂ , 2.41 .	154
Figure A38	RP-HPLC analysis of crude Ac-DIaza(DOPA)ET-NH ₂ , 2.41 .	155
Figure A39	RP-HPLC analysis of pure Ac-DIaza(DOPA)ET-NH ₂ , 2.41 .	156
Figure A40	ESI-LCMS analysis of crude Ac-DIaza(DOPA)ET-NH ₂ , 2.41 .	157
Figure A41	RP-HPLC analysis of pure Ac-DIaza(DOPA)ET-NH ₂ , 2.41 .	158

Figure A42	ESI-LCMS analysis of pure Ac-DIaza(DOPA)ET-NH ₂ , 2.41.	159
Figure A43	RP-HPLC analysis of crude Ac-DIYET-NH ₂ , 2.28.	160
Figure A44	ESI-LCMS analysis of crude Ac-DIYET-NH ₂ , 2.28.	161
Figure A45	RP-HPLC analysis of pure Ac-DIaza(DOPA)ET-NH ₂ , 2.41.	162
Figure A46	ESI-LCMS analysis of pure Ac-DIYET-NH ₂ , 2.28.	163
Figure A47	¹ H NMR spectra of Ac-DIaza(DOPA)ET sequence, 2.41.	164
Figure A48	¹ H NMR spectra of Ac-DIYazaET sequence, 2.42.	165
Figure A49	¹ H NMR spectra of Ac-DazaIYET sequence, 2.38.	166
Figure A50	¹ H NMR spectra of Ac-DazaGYET sequence, 2.39.	167
Figure A51	¹ H NMR spectra of Ac-DazaAYET sequence, 2.37.	168
Figure A52	¹ H NMR spectra of Ac-DIYazaET sequence, 2.42.	169
Figure A53	¹ H NMR spectra of Ac-DIazaFET sequence, 2.40.	170
Figure A54	¹ H NMR spectra of Ac-DIazaYET sequence, 2.36.	171
Figure A55	2D NOESY of Ac-DIYET-NH ₂ , 2.28.	172



Peak #	RetTime [min]	Type	Width [min]	Area [mAU*s]	Height [mAU]	Area %
1	8.903	MM T	0.1282	360.02173	56.61224	10.0470
2	9.291	MM T	0.0944	831.50415	146.80551	23.2045
3	9.587	MM T	0.0951	2075.40283	363.66449	57.9176
4	11.203	MM T	0.1197	316.44540	54.34470	8.8309



2.42

Figure A1. RP-HPLC analysis of crude Ac-DIYazaET-NH₂, **2.42**, using a linear gradient 2-90% CH₃OH/H₂O (0.1% FA) over 15 min using a Symmetry Shield C₁₈ reverse-phase column (150 × 4.60 mm, 3.5 μm) set at a temperature of 25 °C at a flow rate of 1 mL/min with detection at 214 nm.

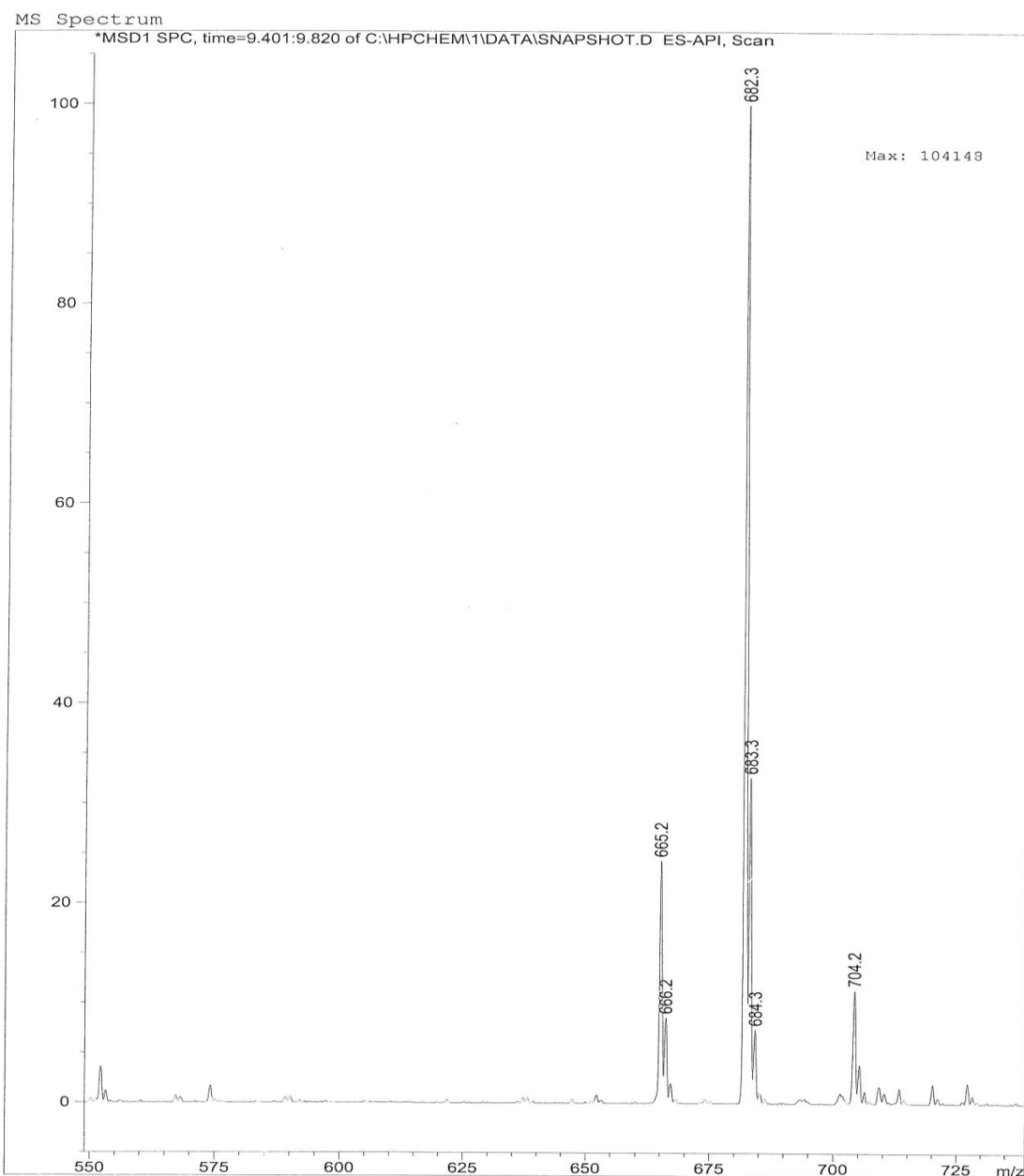
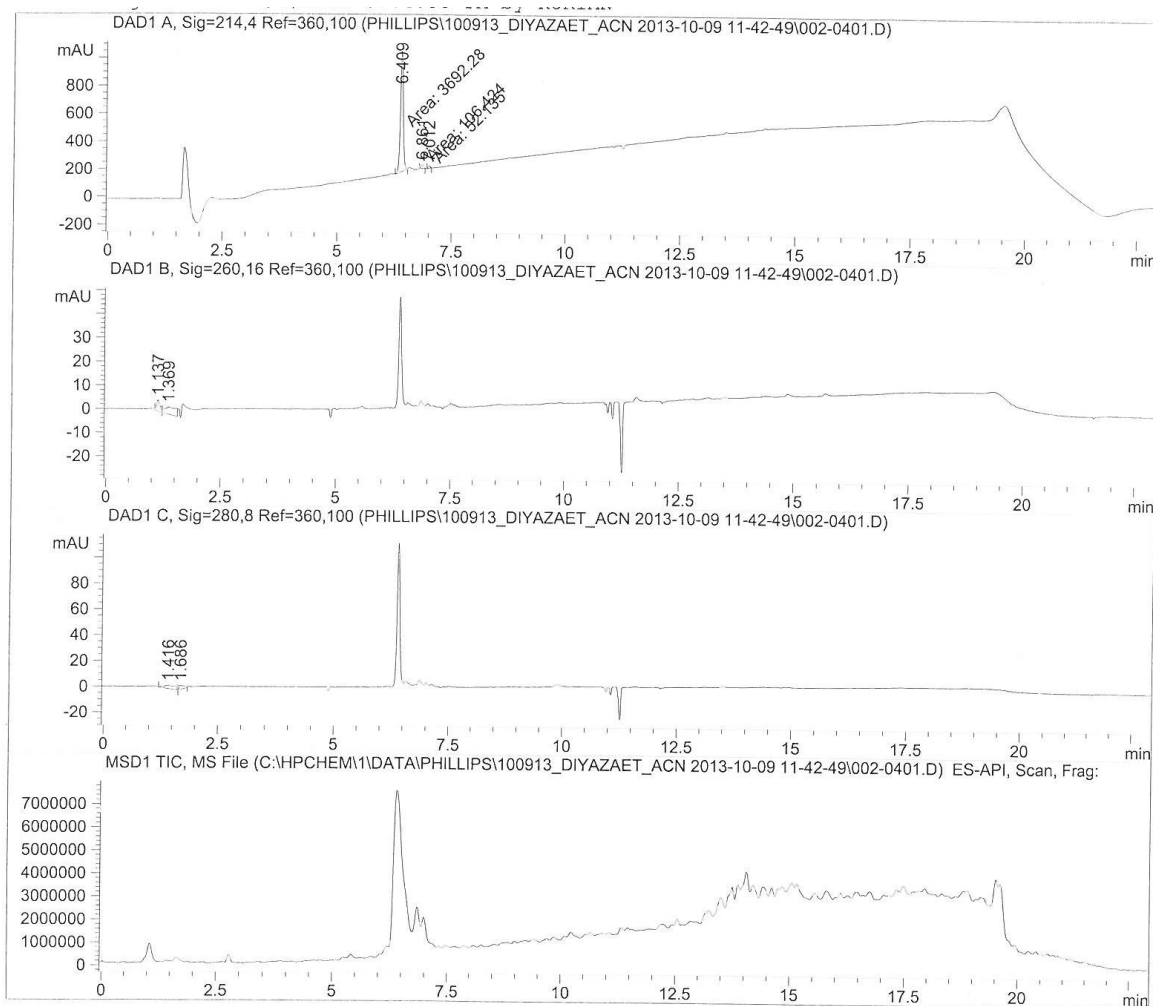


Figure A2. ESI-LCMS analysis of crude Ac-DIYazaET-NH₂, **2.42**, using a linear gradient 2-90% CH₃OH/H₂O (0.1% FA) over 15 min using a Symmetry Shield C₁₈ reverse-phase column (150 × 4.60 mm, 3.5 μm) set at a temperature of 25 °C at a flow rate of 1 mL/min with positive mode of detection.



Peak #	RetTime [min]	Type	Width [min]	Area [mAU*s]	Height [mAU]	Area %
1	6.409	MM T	0.0704	3692.28369	874.64838	95.8825
2	6.861	MM T	0.0623	106.42373	28.44954	2.7636
3	7.012	MM T	0.0551	52.13498	15.76332	1.3539

Figure A3. RP-HPLC analysis of pure Ac-DIYazaET-NH₂, **2.42**, using a linear gradient 2-90% CH₃CN/H₂O (0.1% FA) over 15 min using a Symmetry Shield C₁₈ reverse-phase column (150 × 4.60 mm, 3.5 μm) set at a temperature of 25 °C at a flow rate of 1 mL/min with detection at 214 nm.

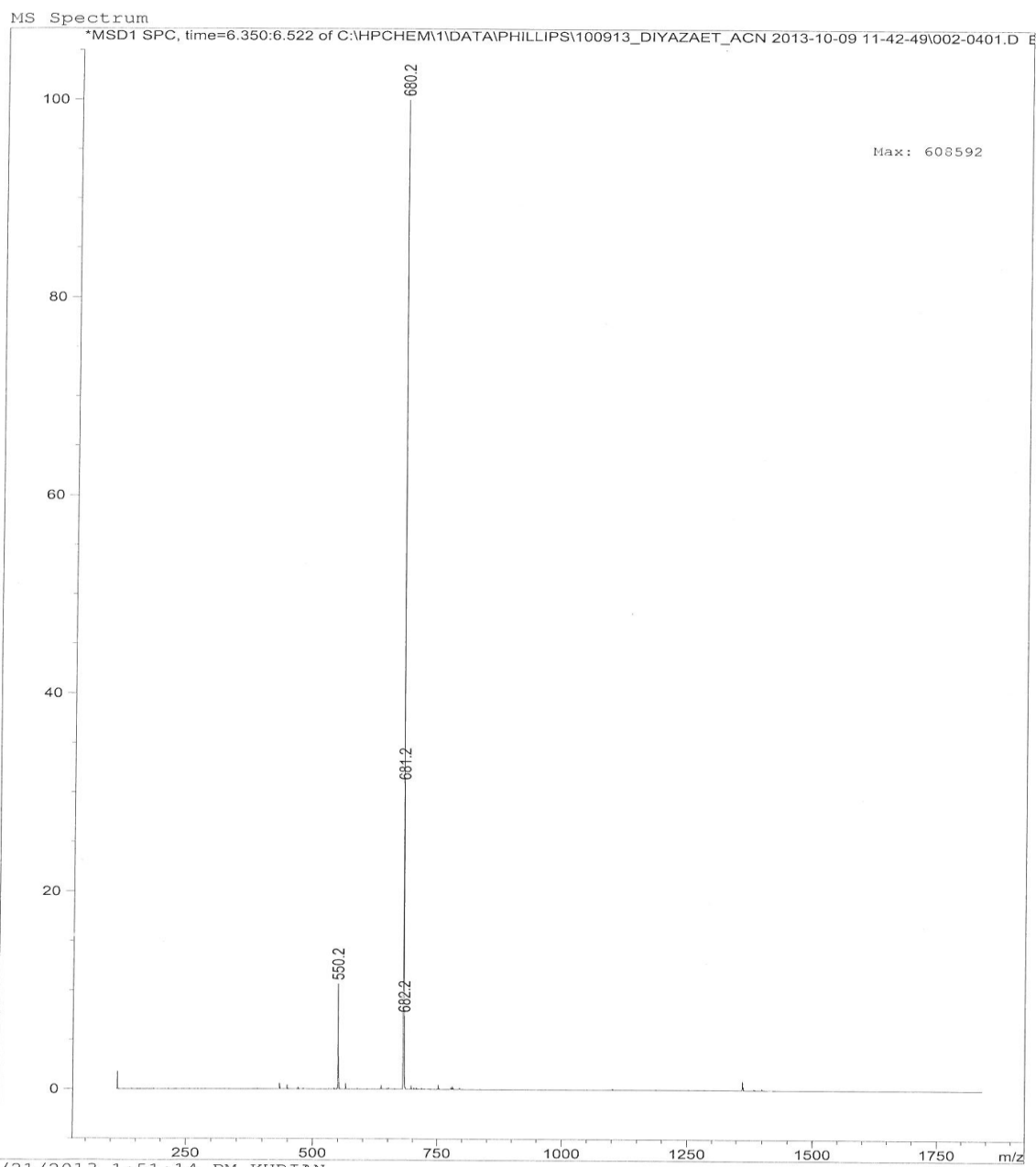
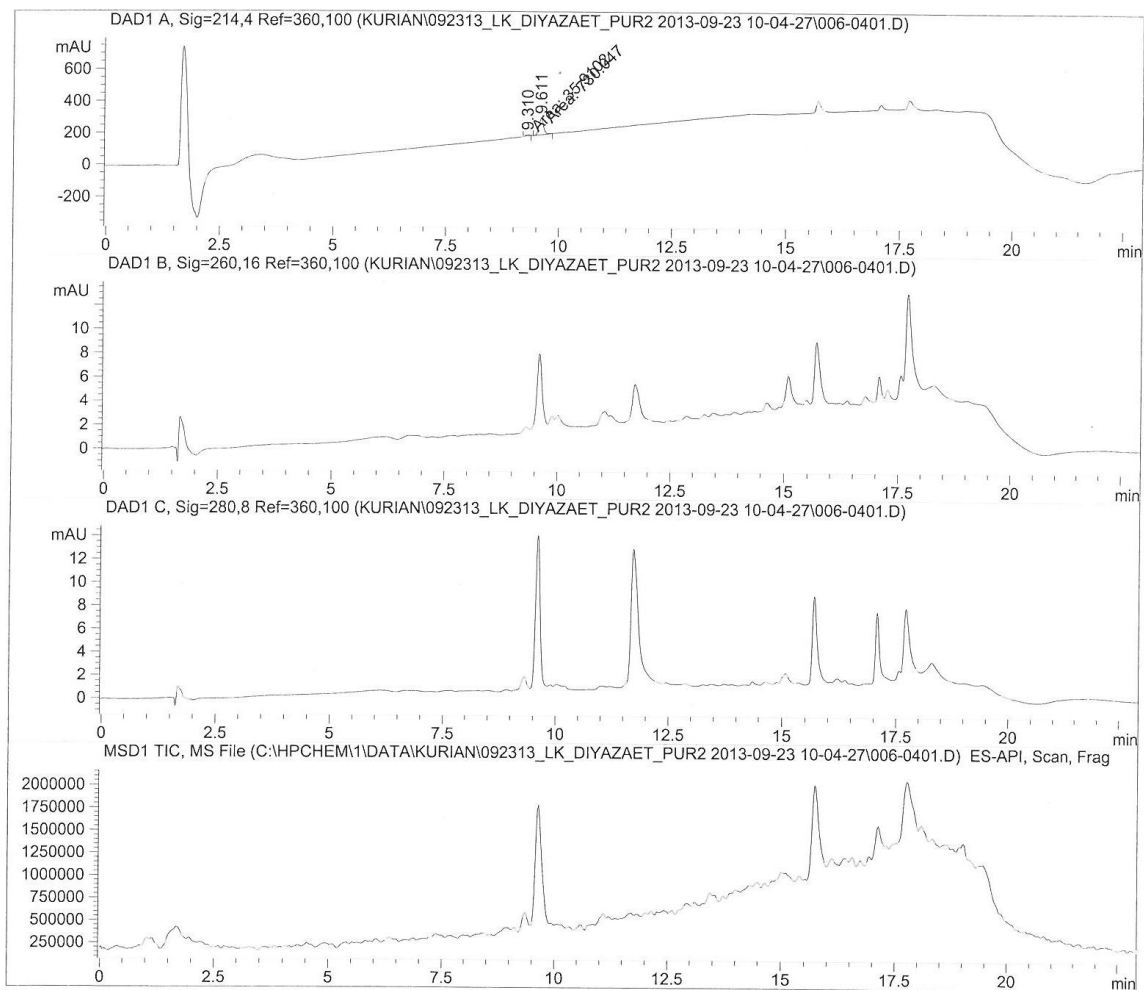


Figure A4. ESI-LCMS analysis of pure Ac-DIYazaET-NH₂, **2.42**, using a linear gradient 2-90% CH₃CN/H₂O (0.1% FA) over 15 min using a Symmetry Shield C₁₈ reverse-phase column (150 × 4.60 mm, 3.5 μm) set at a temperature of 25 °C at a flow rate of 1 mL/min with positive mode of detection.



Peak #	RetTime [min]	Type	Width [min]	Area [mAU*s]	Height [mAU]	Area %
1	9.310	MM T	0.0929	35.91018	6.43938	4.6883
2	9.611	MM T	0.1458	730.04669	102.78987	95.3117

Figure A5. RP-HPLC analysis of pure Ac-DIYazaET-NH₂, **2.42**, using a linear gradient 2-90% CH₃OH/H₂O (0.1% FA) over 15 min using a Symmetry Shield C₁₈ reverse-phase column (150 × 4.60 mm, 3.5 μm) set at a temperature of 25 °C at a flow rate of 1 mL/min with detection at 214 nm.

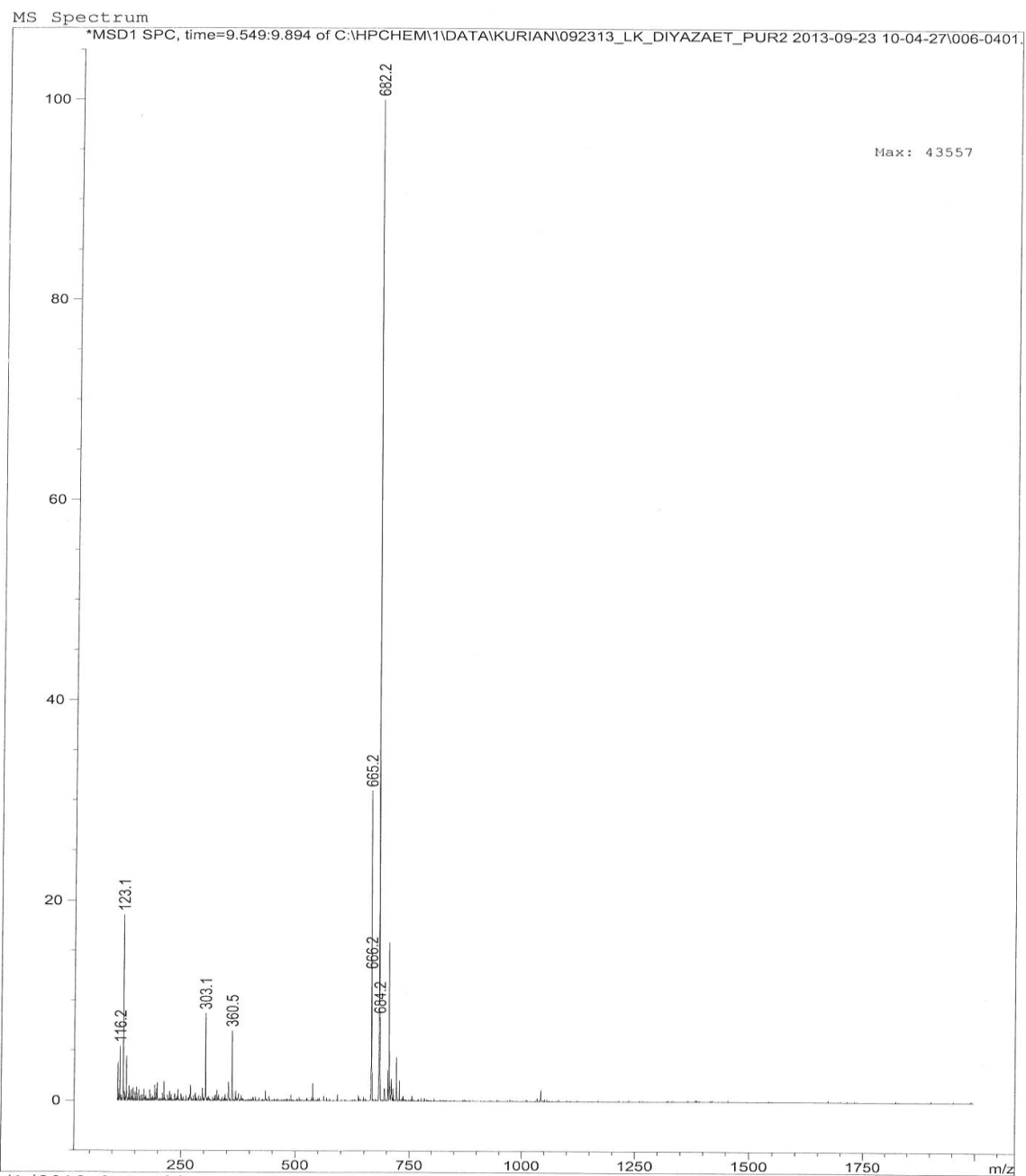
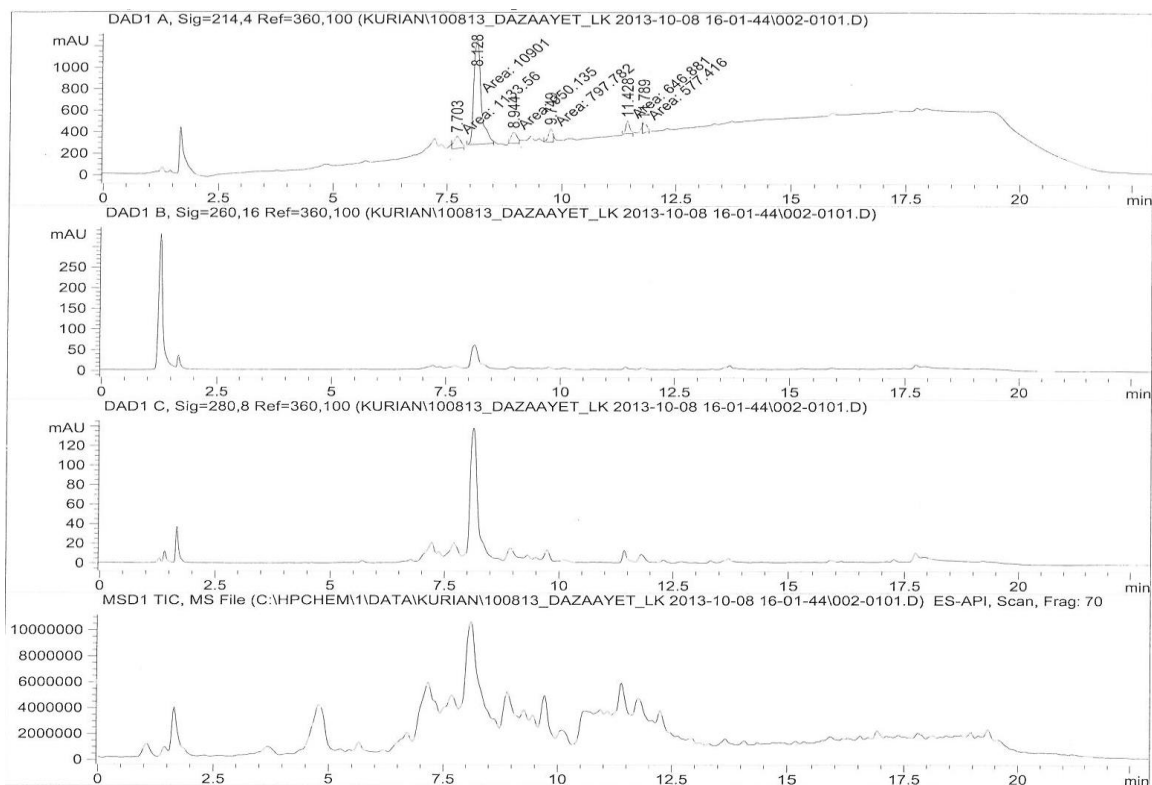


Figure A6. ESI-LCMS analysis of pure Ac-DIYazaET-NH₂, **2.42**, using a linear gradient 2-90% CH₃OH/H₂O (0.1% FA) over 15 min using a Symmetry Shield C₁₈ reverse-phase column (150 × 4.60 mm, 3.5 μm) set at a temperature of 25 °C at a flow rate of 1 mL/min with positive mode of detection.



Peak #	RetTime [min]	Type	Width [min]	Area [mAU*s]	Height [mAU]	Area %
1	7.703	MM T	0.1697	1133.55615	111.30363	7.5536
2	8.128	MM T	0.1881	1.09010e4	965.98920	72.6405
3	8.944	MM T	0.1498	950.13538	105.70071	6.3314
4	9.749	MM T	0.1064	797.78162	124.92185	5.3162
5	11.428	MM T	0.0920	646.88141	117.22967	4.3106
6	11.789	MM T	0.0991	577.41620	97.06461	3.8477

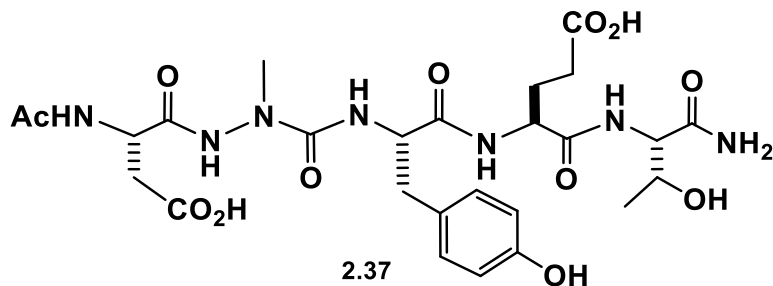


Figure A7. RP-HPLC analysis of crude Ac-DazaAYET-NH₂, **2.37**, using a linear gradient 2-90% CH₃OH/H₂O (0.1% FA) over 15 min using a Symmetry Shield C₁₈ reverse-phase column (150 × 4.60 mm, 3.5 μm) set at a temperature of 25 °C at a flow rate of 1 mL/min with detection at 214 nm.

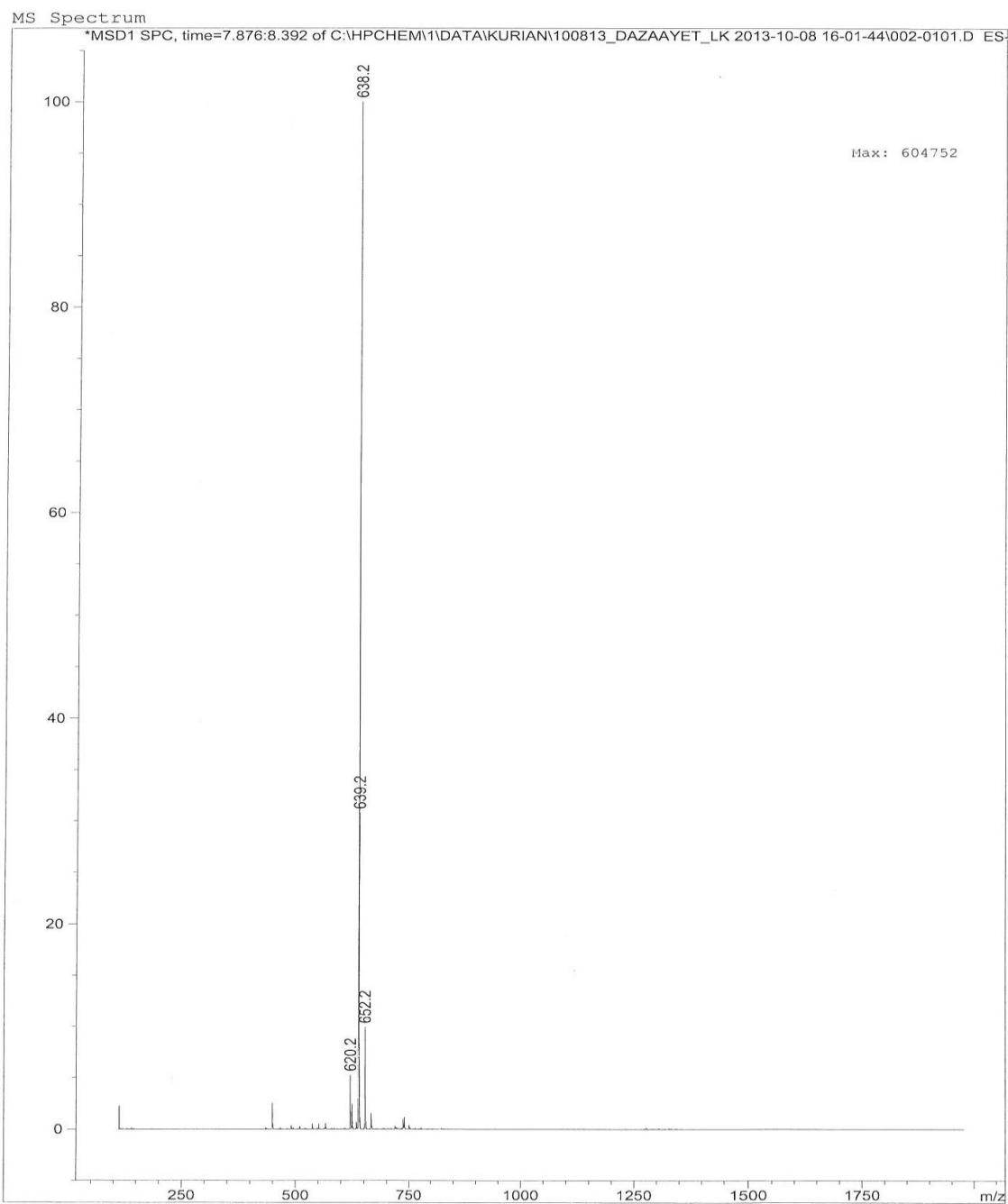
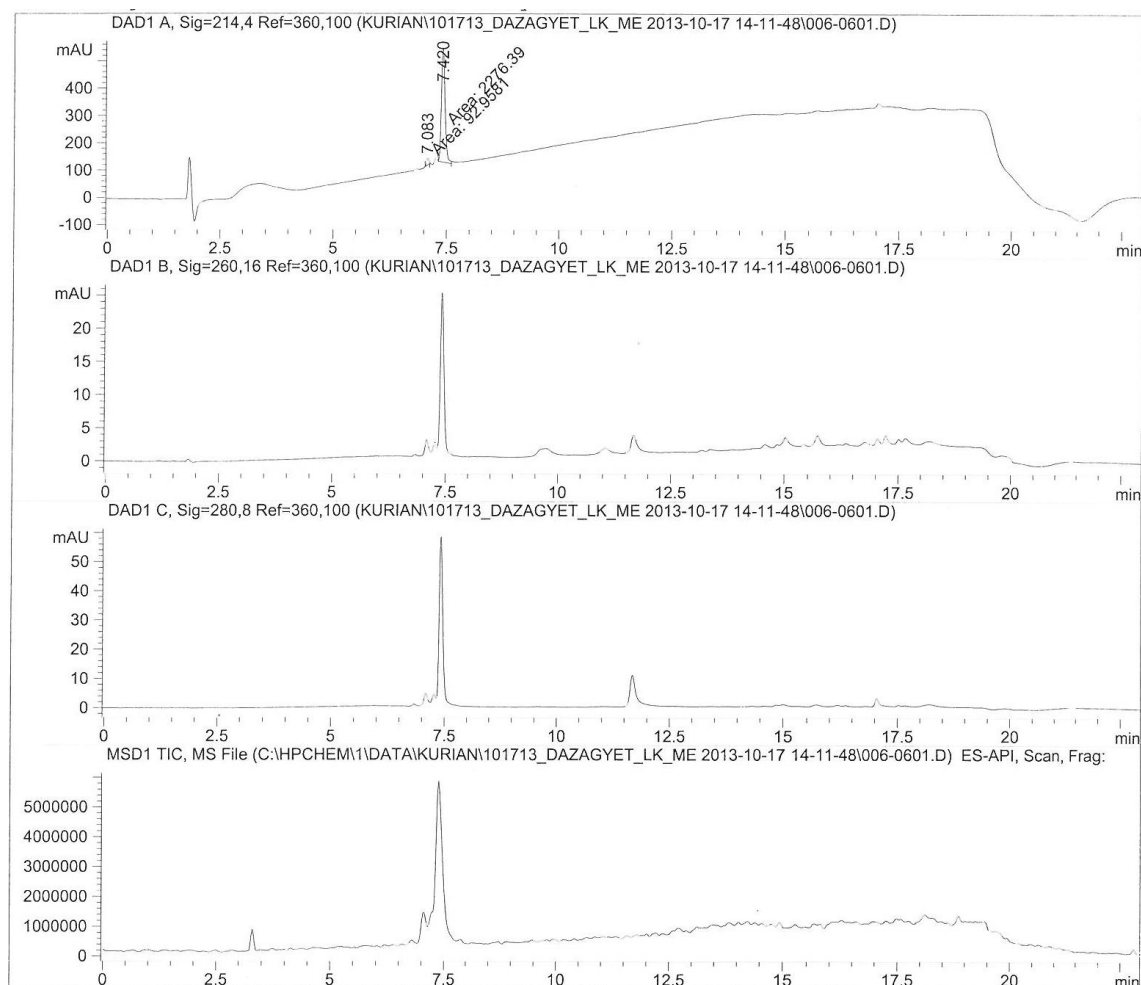


Figure A8. ESI-LCMS analysis of crude Ac-DazaAYET-NH₂, **2.37**, using a linear gradient 2-90% CH₃OH/H₂O (0.1% FA) over 15 min using a Symmetry Shield C₁₈ reverse-phase column (150 × 4.60 mm, 3.5 μm) set at a temperature of 25 °C at a flow rate of 1 mL/min with negative mode of detection.



Peak #	RetTime [min]	Type	Width [min]	Area [mAU*s]	Height [mAU]	Area %
1	7.083	MM T	0.0643	92.95805	24.09834	3.9234
2	7.420	MM T	0.0915	2276.39331	414.55161	96.0766

Figure A9. RP-HPLC analysis of pure Ac-DazaAYET-NH₂, **2.37**, using a linear gradient 2-90% CH₃OH/H₂O (0.1% FA) over 15 min using a Symmetry Shield C₁₈ reverse-phase column (150 × 4.60 mm, 3.5 μm) set at a temperature of 25 °C at a flow rate of 1 mL/min with detection at 214 nm.

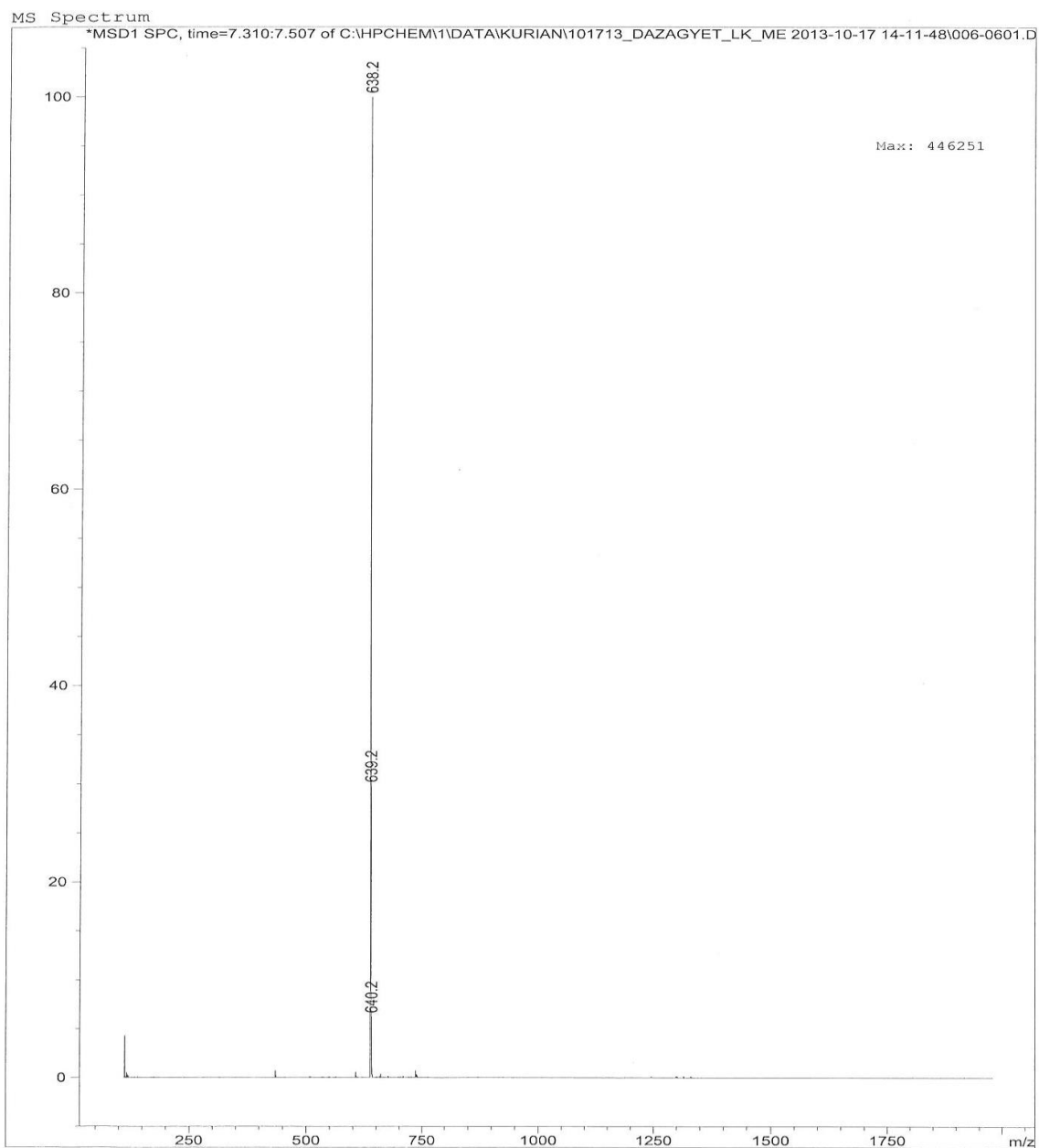


Figure A10. ESI-LCMS analysis of pure Ac-DazaAYET-NH₂, **2.37**, using a linear gradient 2-90% CH₃OH/H₂O (0.1% FA) over 15 min using a Symmetry Shield C₁₈ reverse-phase column (150 × 4.60 mm, 3.5 μm) set at a temperature of 25 °C at a flow rate of 1 mL/min with negative mode of detection.

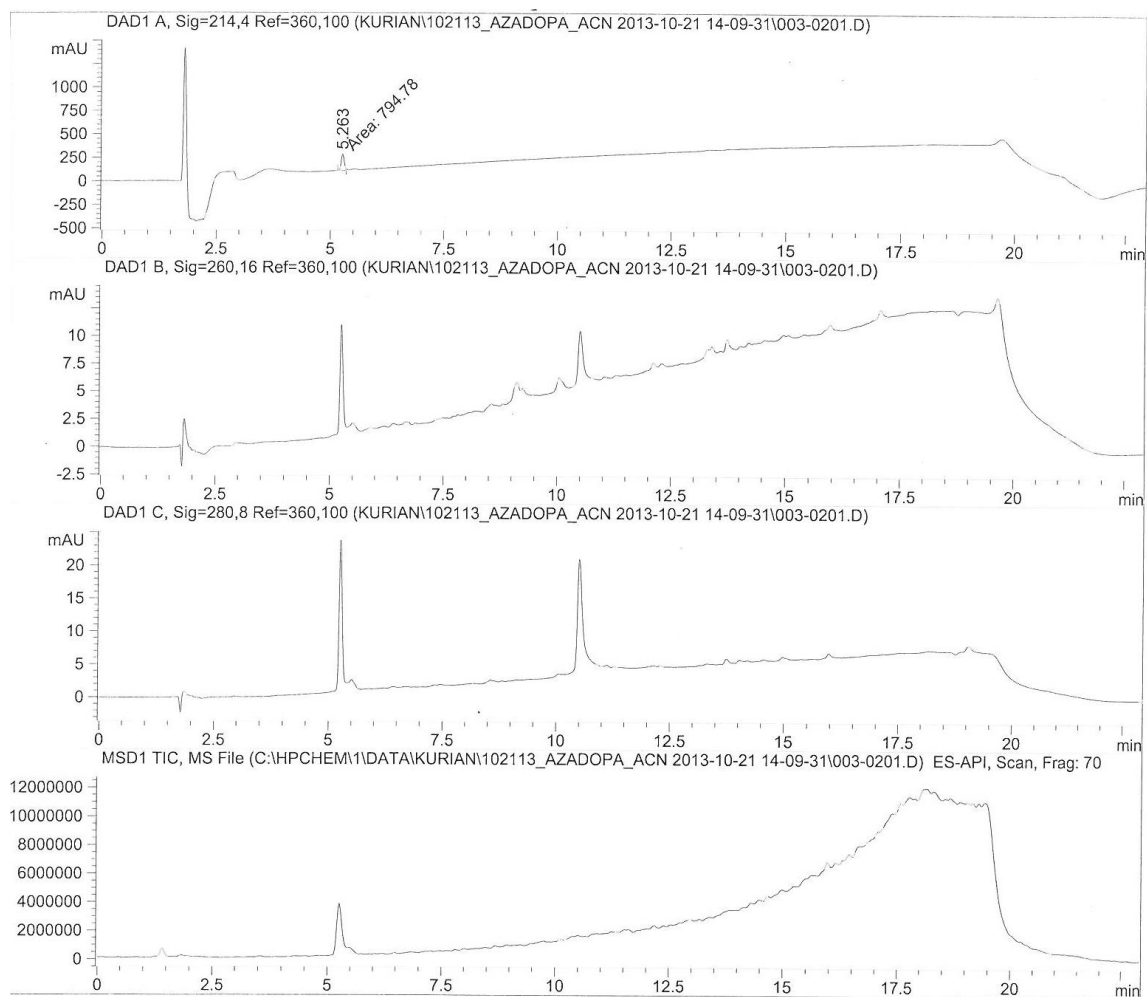


Figure A11. RP-HPLC analysis of pure Ac-DazaAYET-NH₂, **2.37**, using a linear gradient 2-90% CH₃CN/H₂O (0.1% FA) over 15 min using a Symmetry Shield C₁₈ reverse-phase column (150 × 4.60 mm, 3.5 μm) set at a temperature of 25 °C at a flow rate of 1 mL/min with detection at 214 nm.

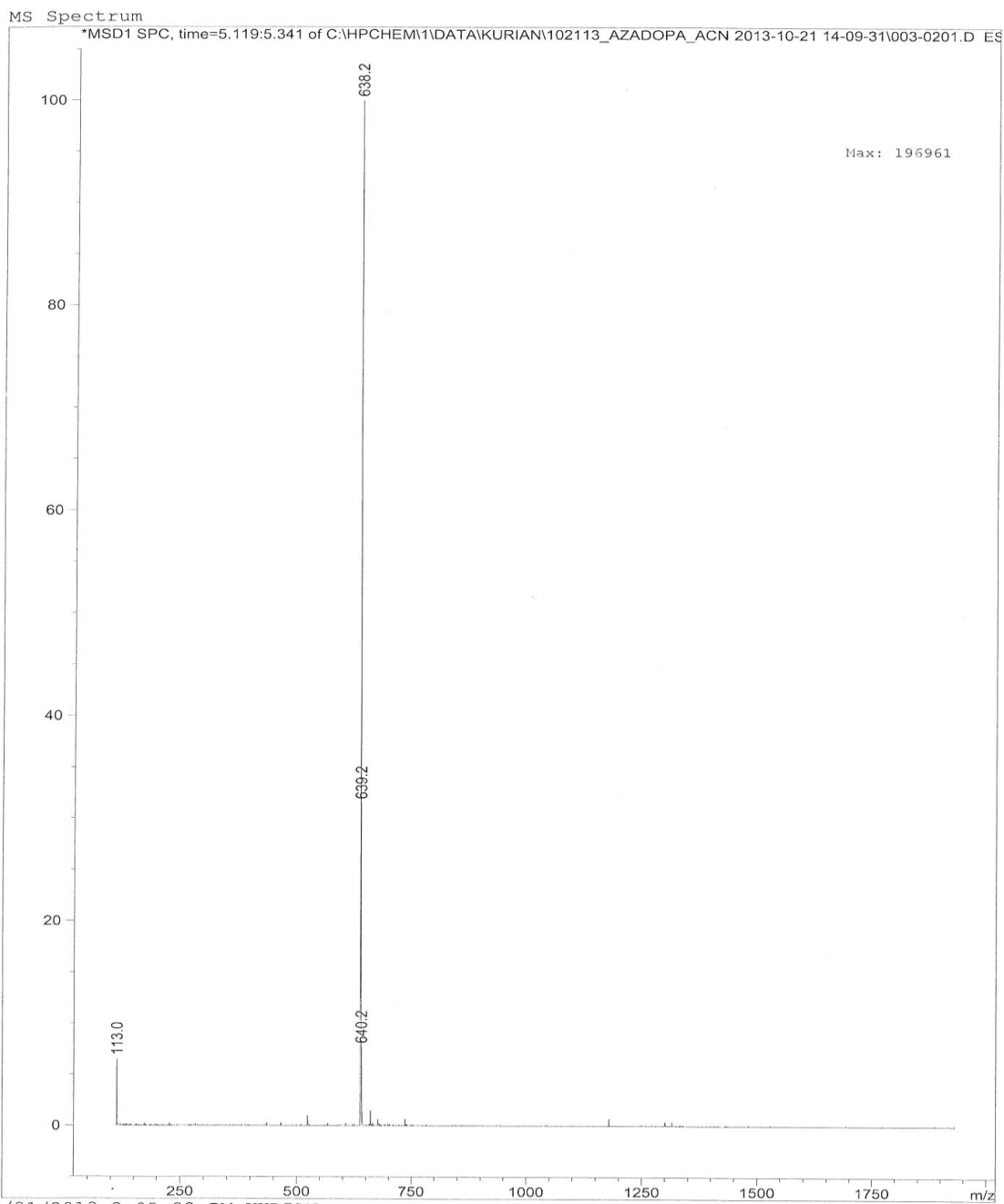
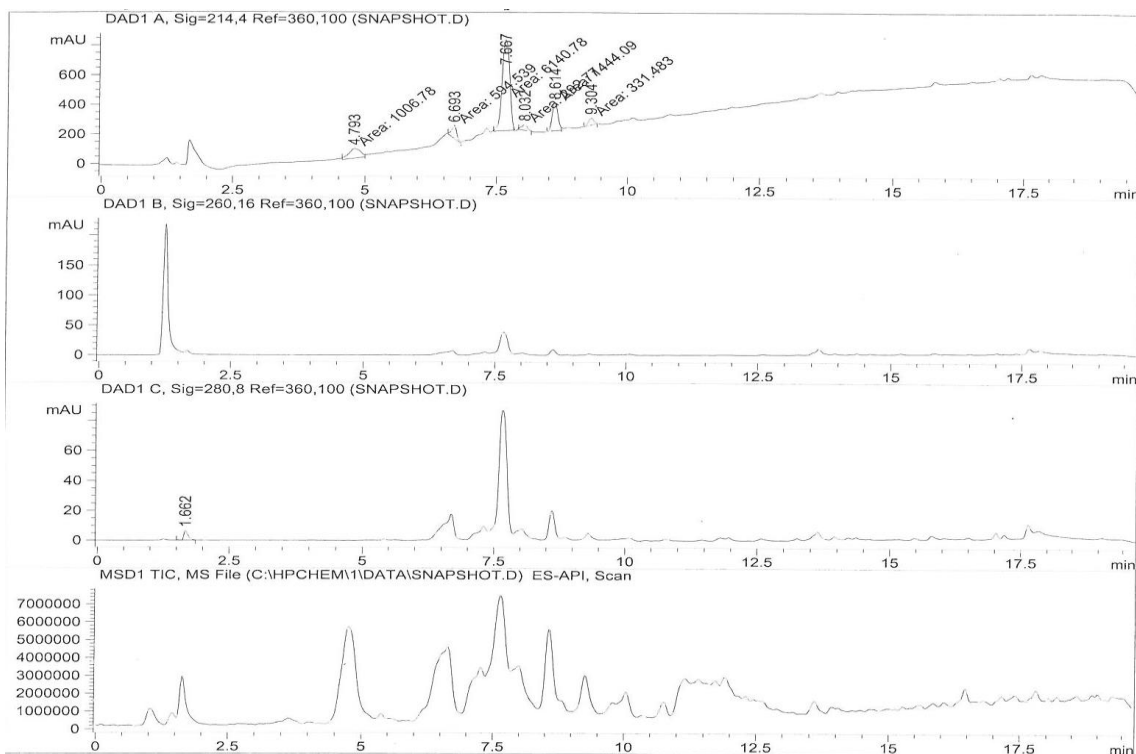


Figure A12. ESI-LCMS analysis of pure Ac-DazaAYET-NH₂, **2.37**, using a linear gradient 2-90% CH₃CN/H₂O (0.1% FA) over 15 min using a Symmetry Shield C₁₈ reverse-phase column (150 × 4.60 mm, 3.5 μm) set at a temperature of 25 °C at a flow rate of 1 mL/min with negative mode of detection.



Peak #	RetTime [min]	Type	Width [min]	Area [mAU*s]	Height [mAU]	Area %
1	4.793	MM T	0.2561	1006.77997	65.52070	10.2623
2	6.693	MM T	0.1126	594.53851	88.00694	6.0603
3	7.667	MM T	0.1677	6140.78125	610.15289	62.5943
4	8.032	MM T	0.1270	292.77036	38.43233	2.9843
5	8.614	MM T	0.1273	1444.09131	189.03102	14.7199
6	9.304	MM T	0.1175	331.48312	47.00021	3.3789

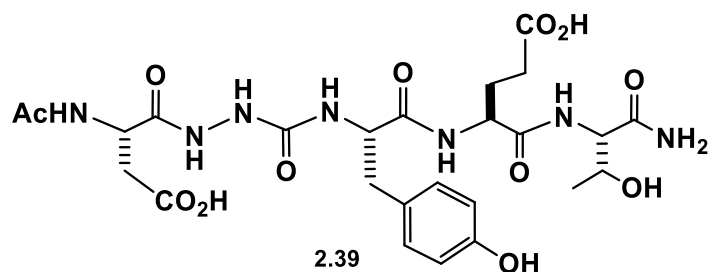


Figure A13. RP-HPLC analysis of crude Ac-DazaGYET-NH₂, **2.39**, using a linear gradient 2-90% CH₃OH/H₂O (0.1% FA) over 15 min using a Symmetry Shield C₁₈ reverse-phase column (150 × 4.60 mm, 3.5 μm) set at a temperature of 25 °C at a flow rate of 1 mL/min with detection at 214 nm.

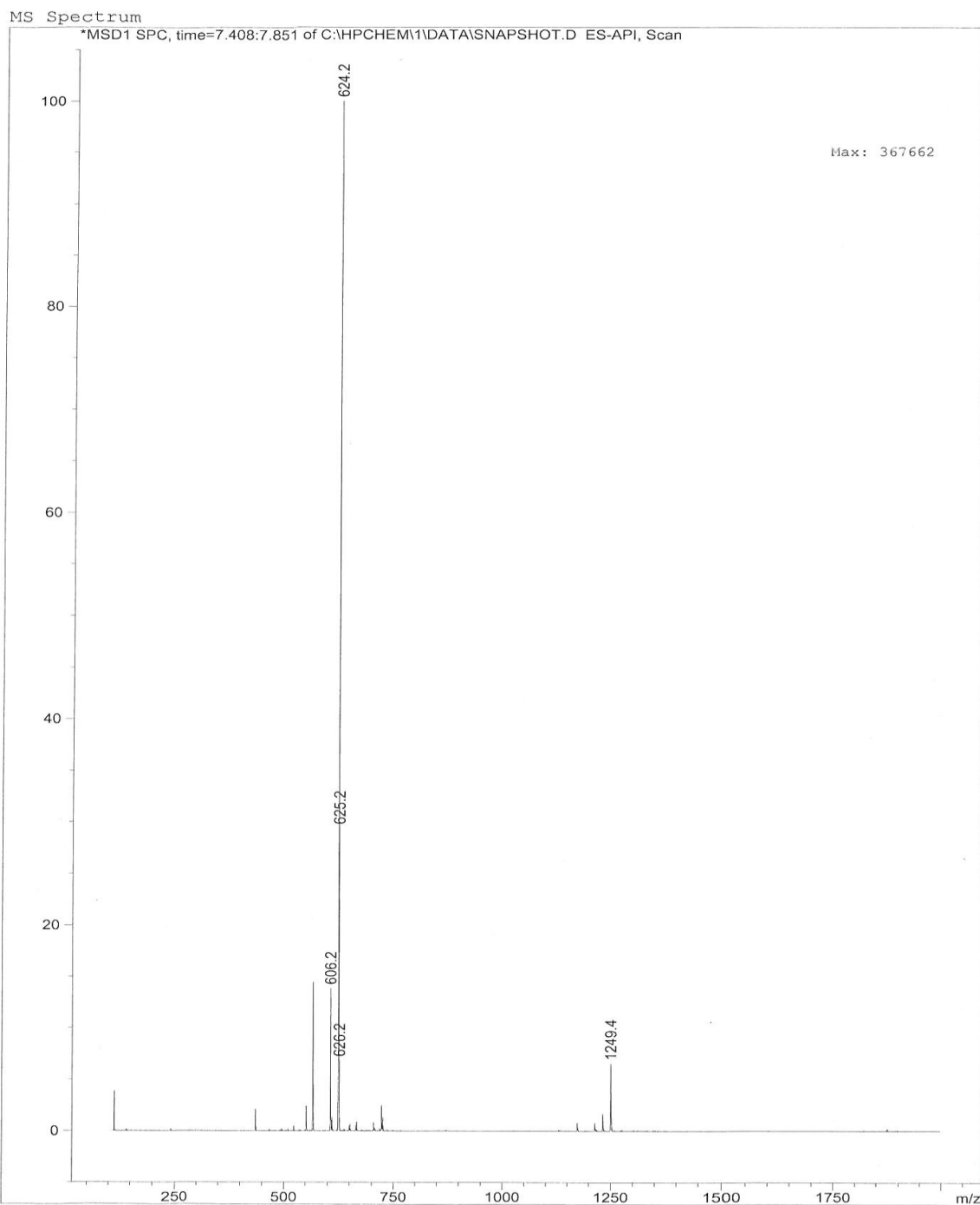
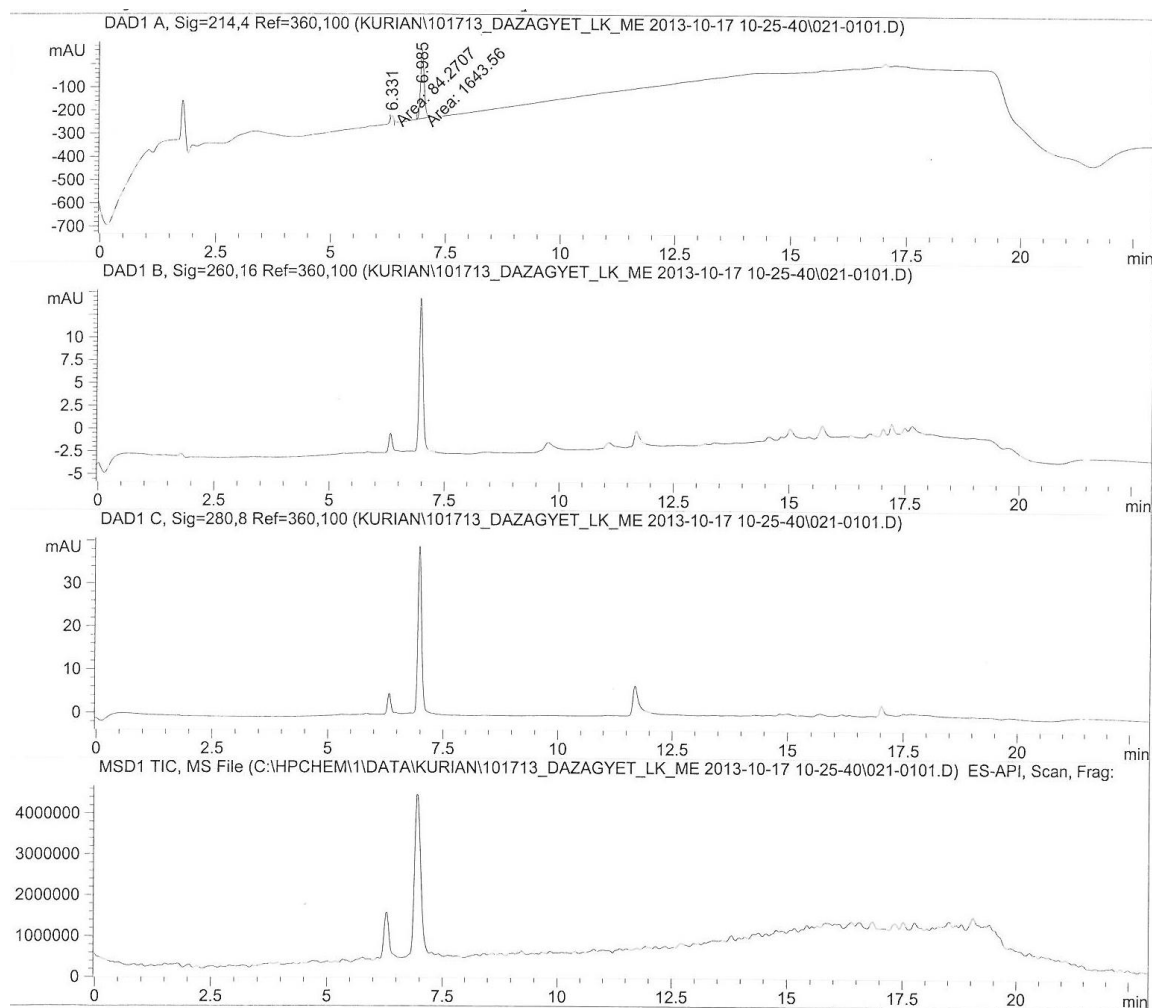


Figure A14. ESI-LCMS analysis of crude Ac-DazaGYET-NH₂, **2.39**, using a linear gradient 2-90% CH₃OH/H₂O (0.1% FA) over 15 min using a Symmetry Shield C₁₈ reverse-phase column (150 × 4.60 mm, 3.5 μm) set at a temperature of 25 °C at a flow rate of 1 mL/min with negative mode of detection.



Peak #	RetTime [min]	Type	Width [min]	Area [mAU*s]	Height [mAU]	Area %
1	6.331	MM T	0.0587	84.27070	23.91042	4.8773
2	6.985	MM T	0.0926	1643.55835	295.83331	95.1227

Figure A15. RP-HPLC analysis of pure Ac-DazaGYET-NH₂, **2.39**, using a linear gradient 2-90% CH₃OH/H₂O (0.1% FA) over 15 min using a Symmetry Shield C₁₈ reverse-phase column (150 × 4.60 mm, 3.5 μm) set at a temperature of 25 °C at a flow rate of 1 mL/min with detection at 214 nm.

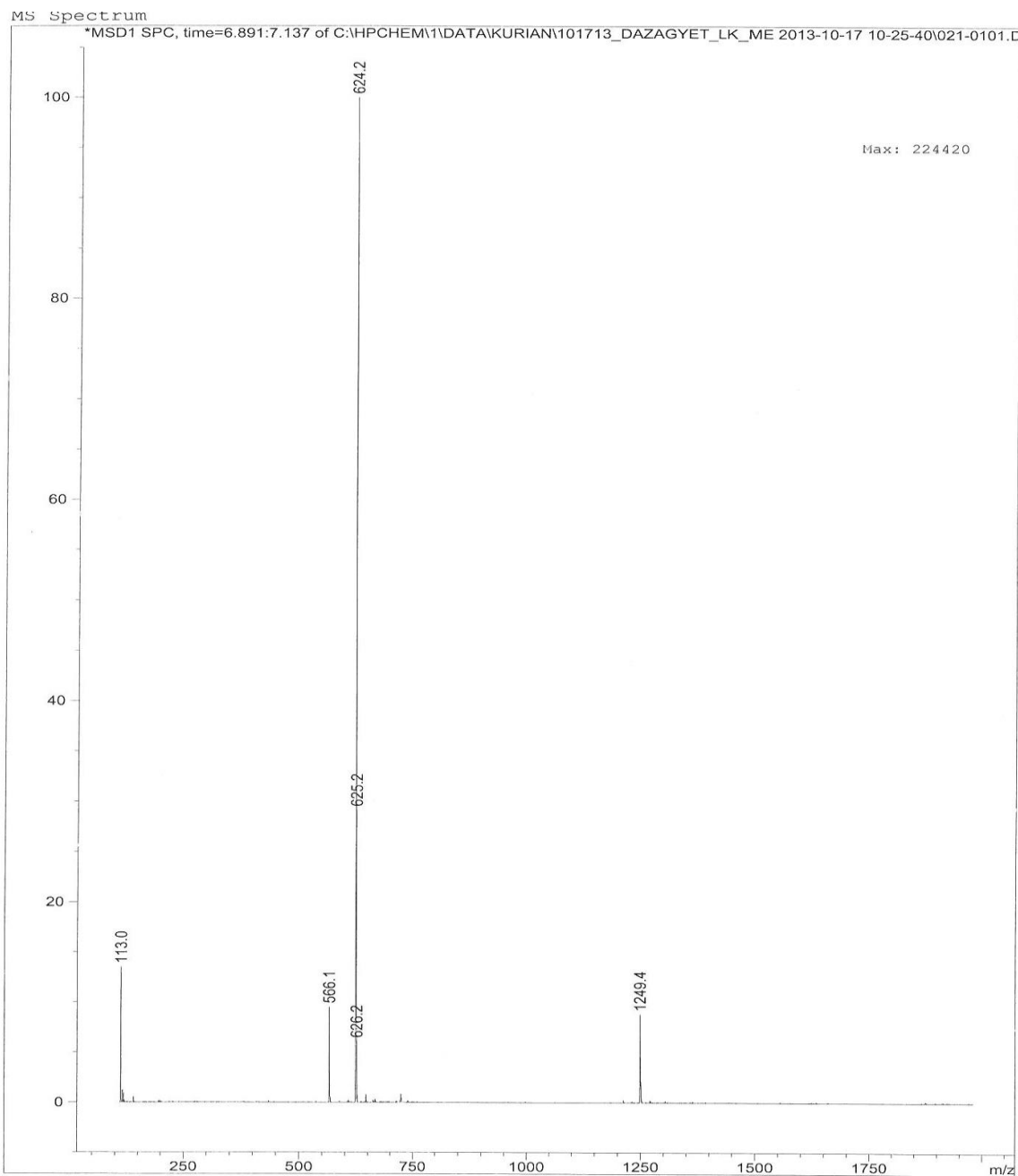
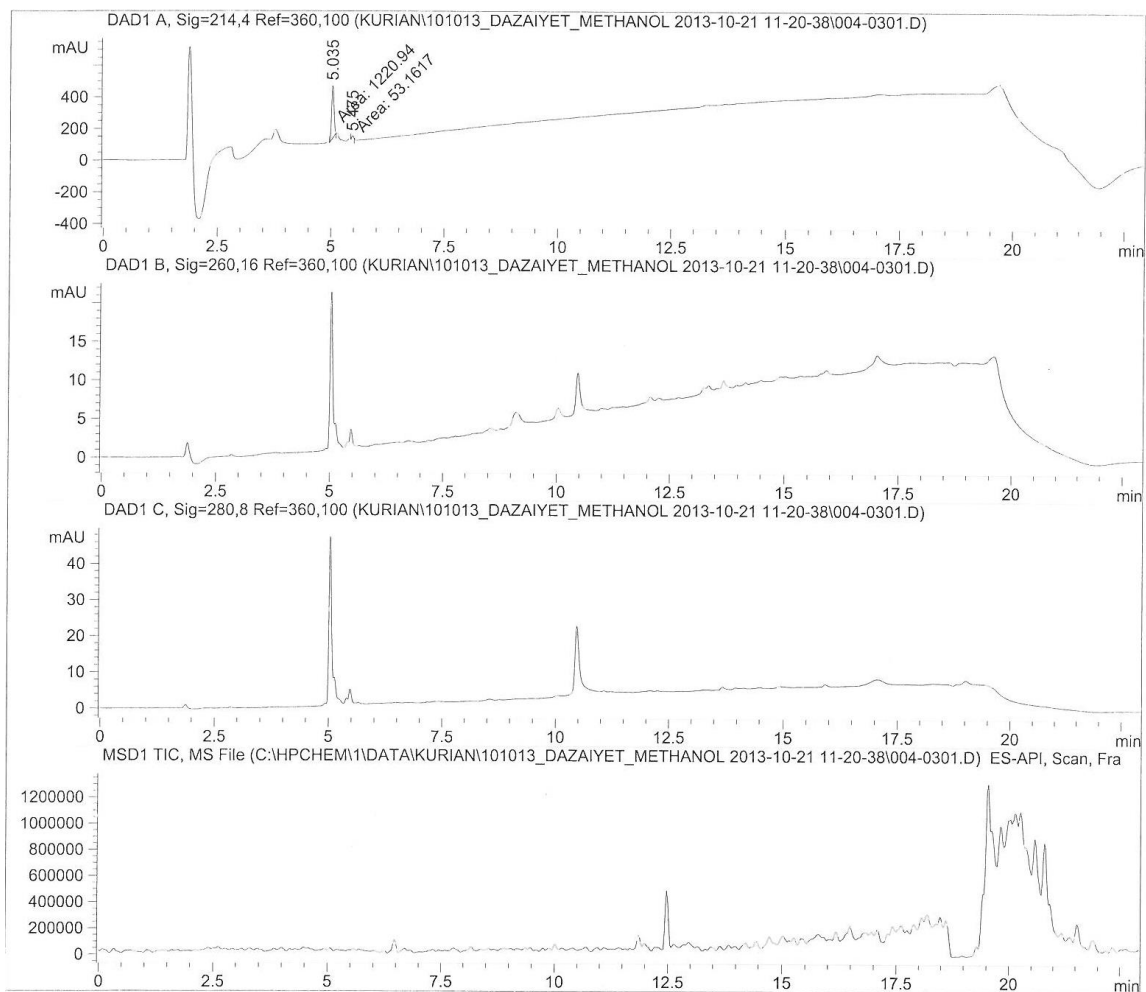


Figure A16. ESI-LCMS analysis of pure Ac-DazaGYET-NH₂, **2.39**, using a linear gradient 2-90% CH₃OH/H₂O (0.1% FA) over 15 min using a Symmetry Shield C₁₈ reverse-phase column (150 × 4.60 mm, 3.5 μm) set at a temperature of 25 °C at a flow rate of 1 mL/min with negative mode of detection.



Peak #	RetTime [min]	Type	Width [min]	Area [mAU*s]	Height [mAU]	Area %
1	5.035	MM T	0.0605	1220.94043	336.25366	95.8275
2	5.475	MM T	0.0442	53.16175	20.06745	4.1725

Figure A17. RP-HPLC analysis of pure Ac-DazaGYET-NH₂, **2.39**, using a linear gradient 2-90% CH₃CN/H₂O (0.1% FA) over 15 min using a Symmetry Shield C₁₈ reverse-phase column (150 × 4.60 mm, 3.5 μm) set at a temperature of 25 °C at a flow rate of 1 mL/min with detection at 214 nm.

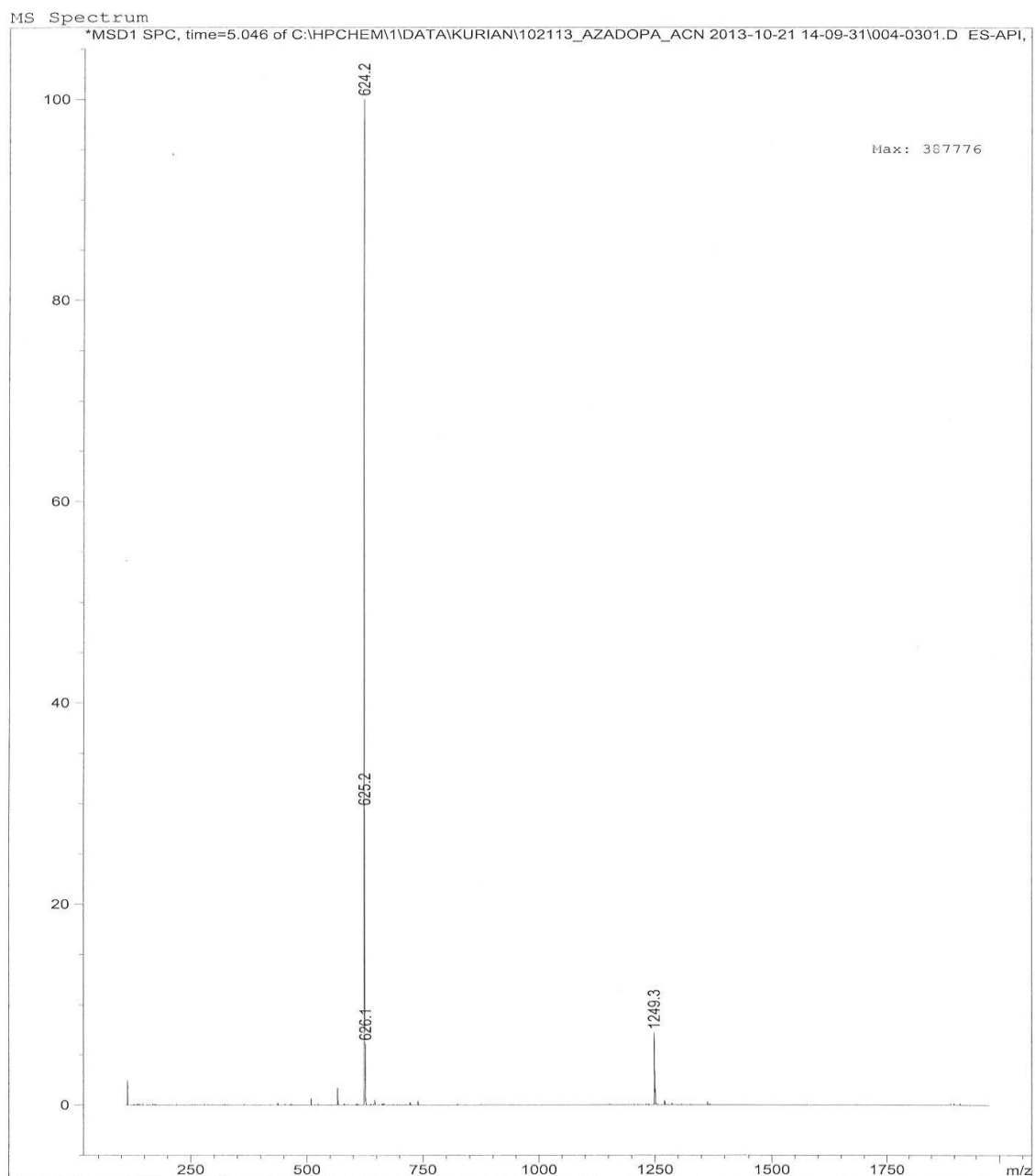
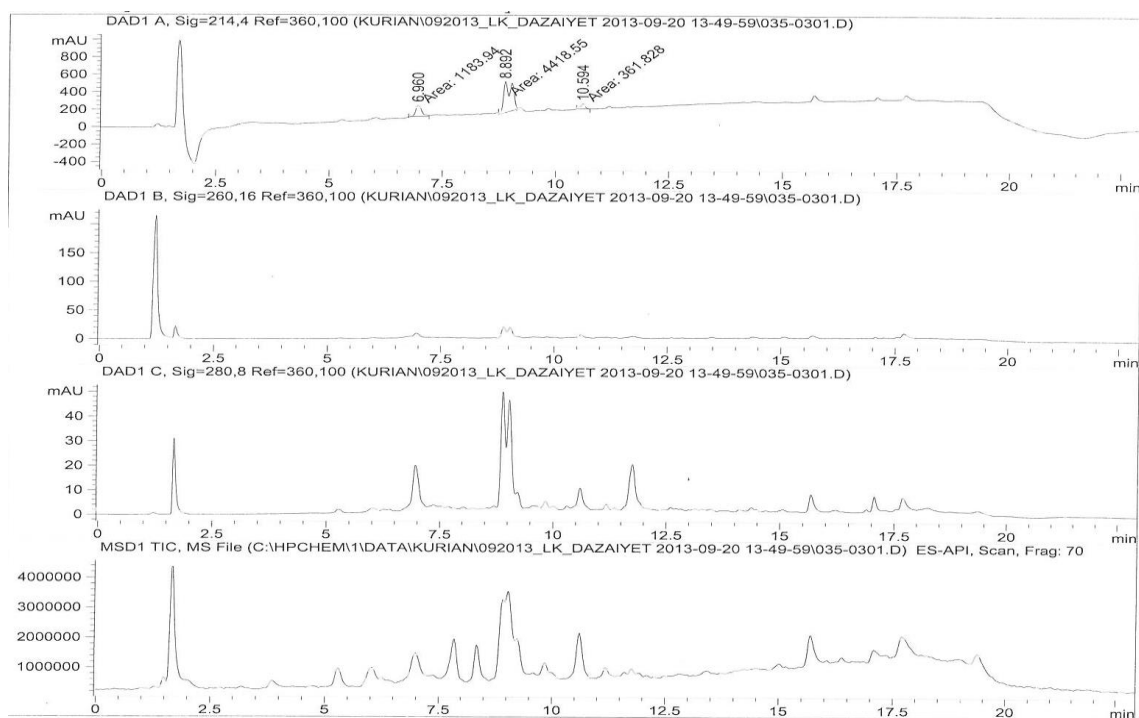


Figure A18. ESI-LCMS analysis of pure Ac-DazaGYET-NH₂, **2.39**, using a linear gradient 2-90% CH₃CN/H₂O (0.1% FA) over 15 min using a Symmetry Shield C₁₈ reverse-phase column (150 × 4.60 mm, 3.5 μm) set at a temperature of 25 °C at a flow rate of 1 mL/min with negative mode of detection.



Peak #	RetTime [min]	Type	Width [min]	Area [mAU*s]	Height [mAU]	Area %
1	6.960	MM T	0.1530	1183.94092	128.96533	19.8504
2	8.892	MM T	0.2019	4418.55469	352.03571	74.0831
3	10.594	MM T	0.1058	361.82816	56.99021	6.0665

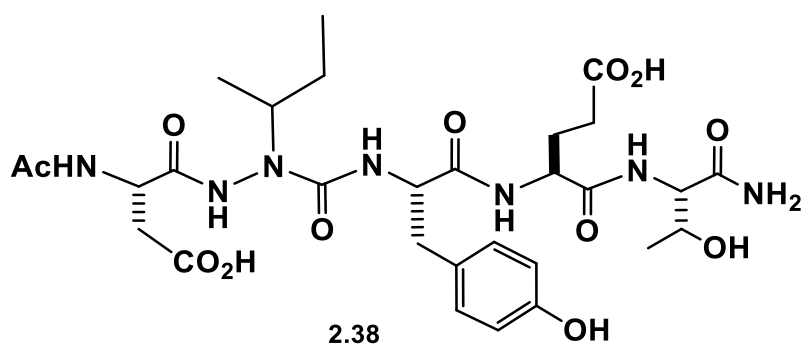


Figure A19. RP-HPLC analysis of crude Ac-DazaiYET-NH₂, **2.38**, using a linear gradient 2-90% CH₃OH/H₂O (0.1% FA) over 15 min using a Symmetry Shield C₁₈ reverse-phase column (150 × 4.60 mm, 3.5 μm) set at a temperature of 25 °C at a flow rate of 1 mL/min with detection at 214 nm.

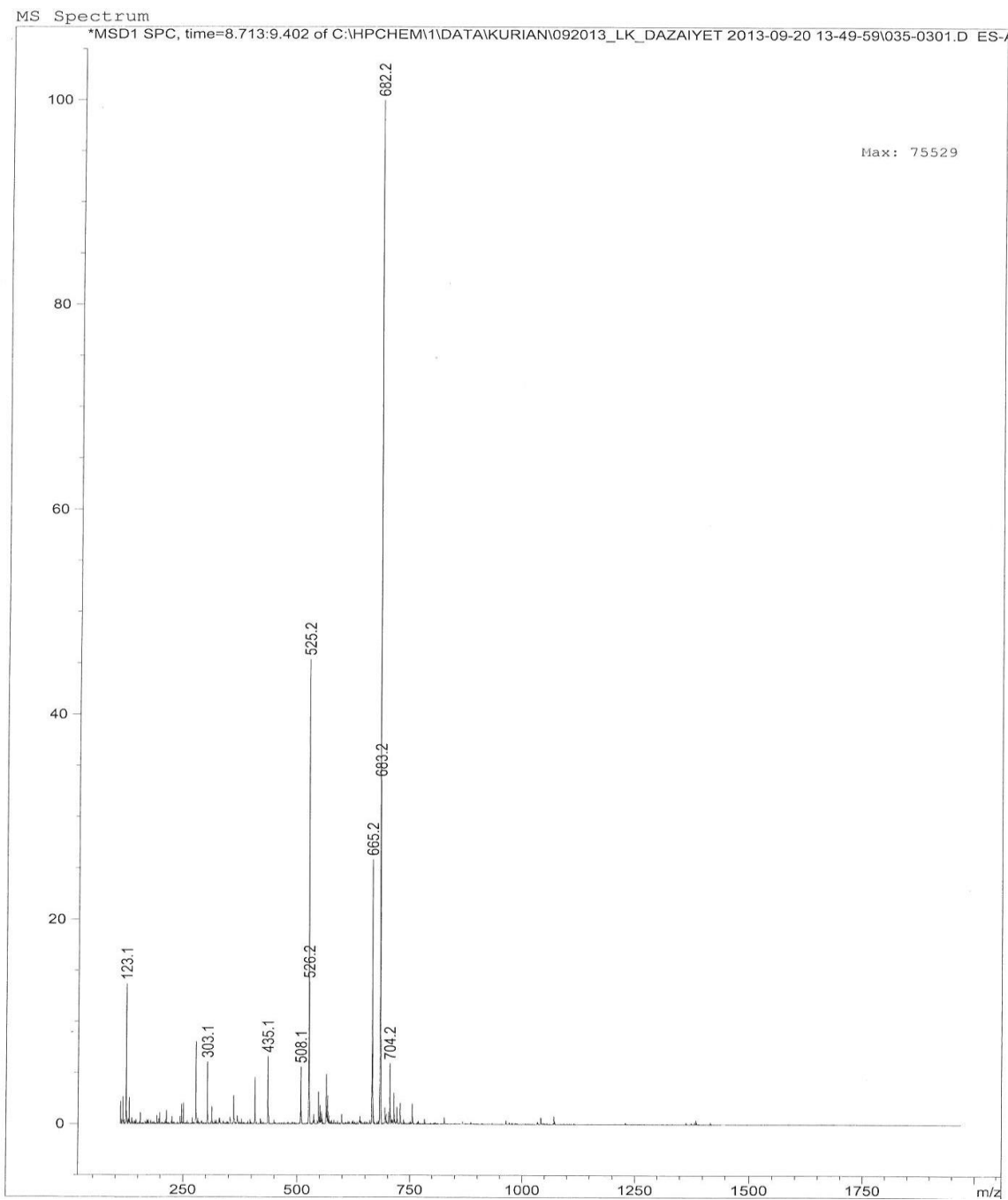


Figure A20. ESI-LCMS analysis of crude Ac-DazaiYET-NH₂, **2.38**, using a linear gradient 2-90% CH₃OH/H₂O (0.1% FA) over 15 min using a Symmetry Shield C₁₈ reverse-phase column (150 × 4.60 mm, 3.5 μm) set at a temperature of 25 °C at a flow rate of 1 mL/min with negative mode of detection.

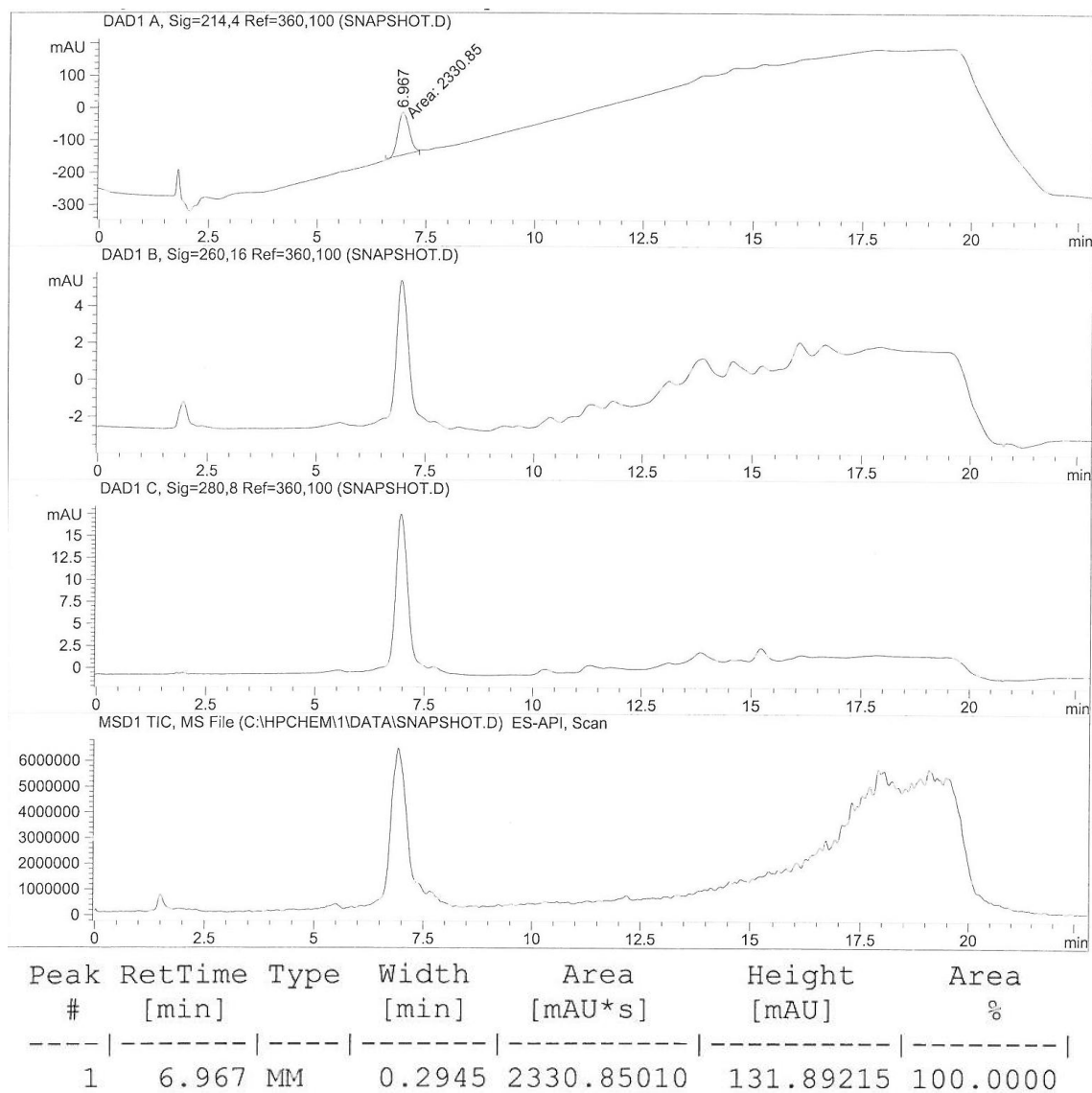


Figure A21. ESI-LC/MS analysis of crude Ac-DazalYET-NH₂, **2.38**, using a linear gradient 2-90% CH₃OH/H₂O (0.1% FA) over 15 min using a Symmetry Shield C₁₈ reverse-phase column (150 × 4.60 mm, 3.5 μm) set at a temperature of 25 °C at a flow rate of 1 mL/min with detection at 214 nm.

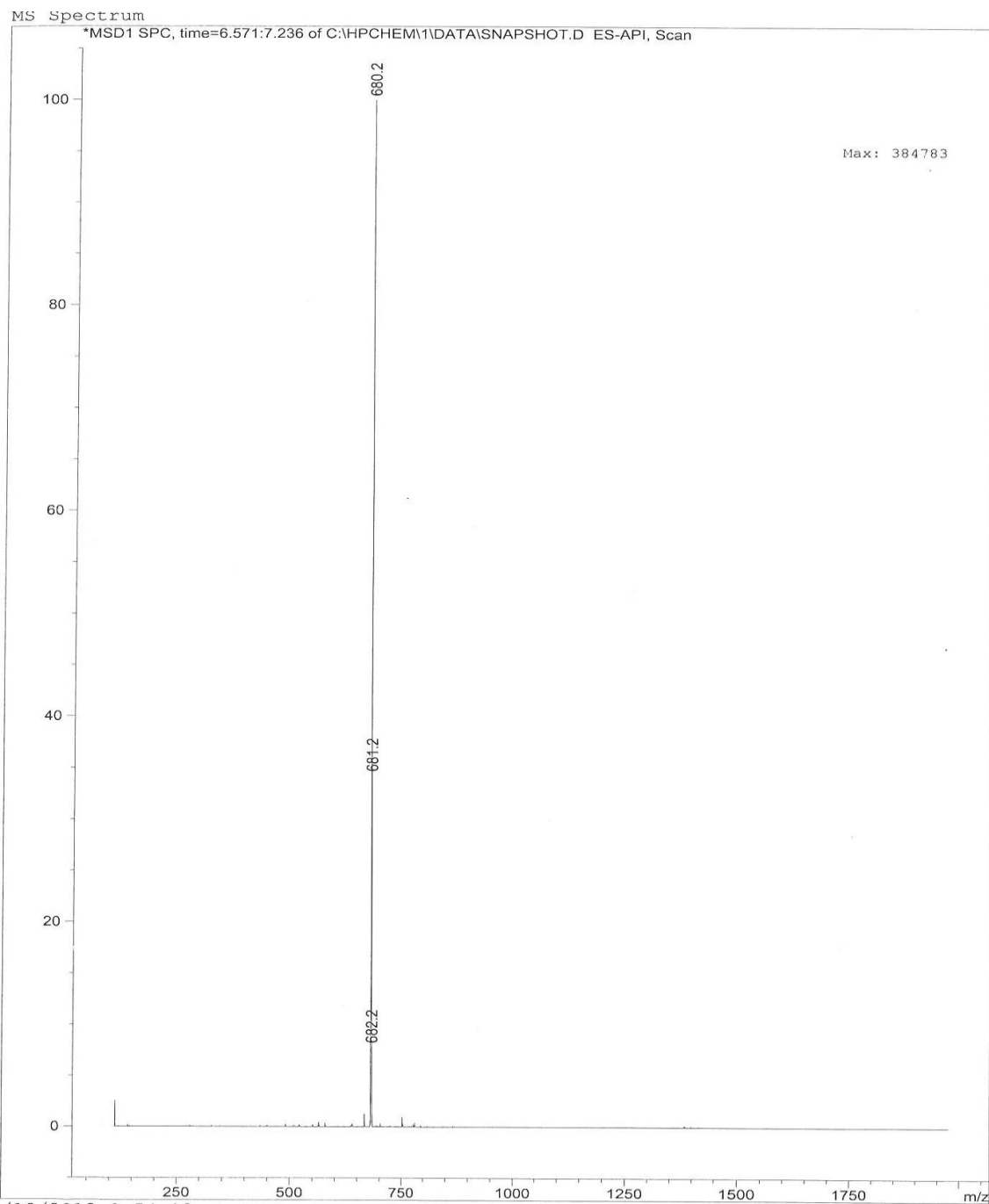


Figure A22. ESI-LCMS analysis of crude Ac-DazaiYET-NH₂, **2.38**, using a linear gradient 2-90% CH₃OH/H₂O (0.1% FA) over 15 min using a Symmetry Shield C₁₈ reverse-phase column (150 × 4.60 mm, 3.5 μm) set at a temperature of 25 °C at a flow rate of 1 mL/min with negative mode of detection.

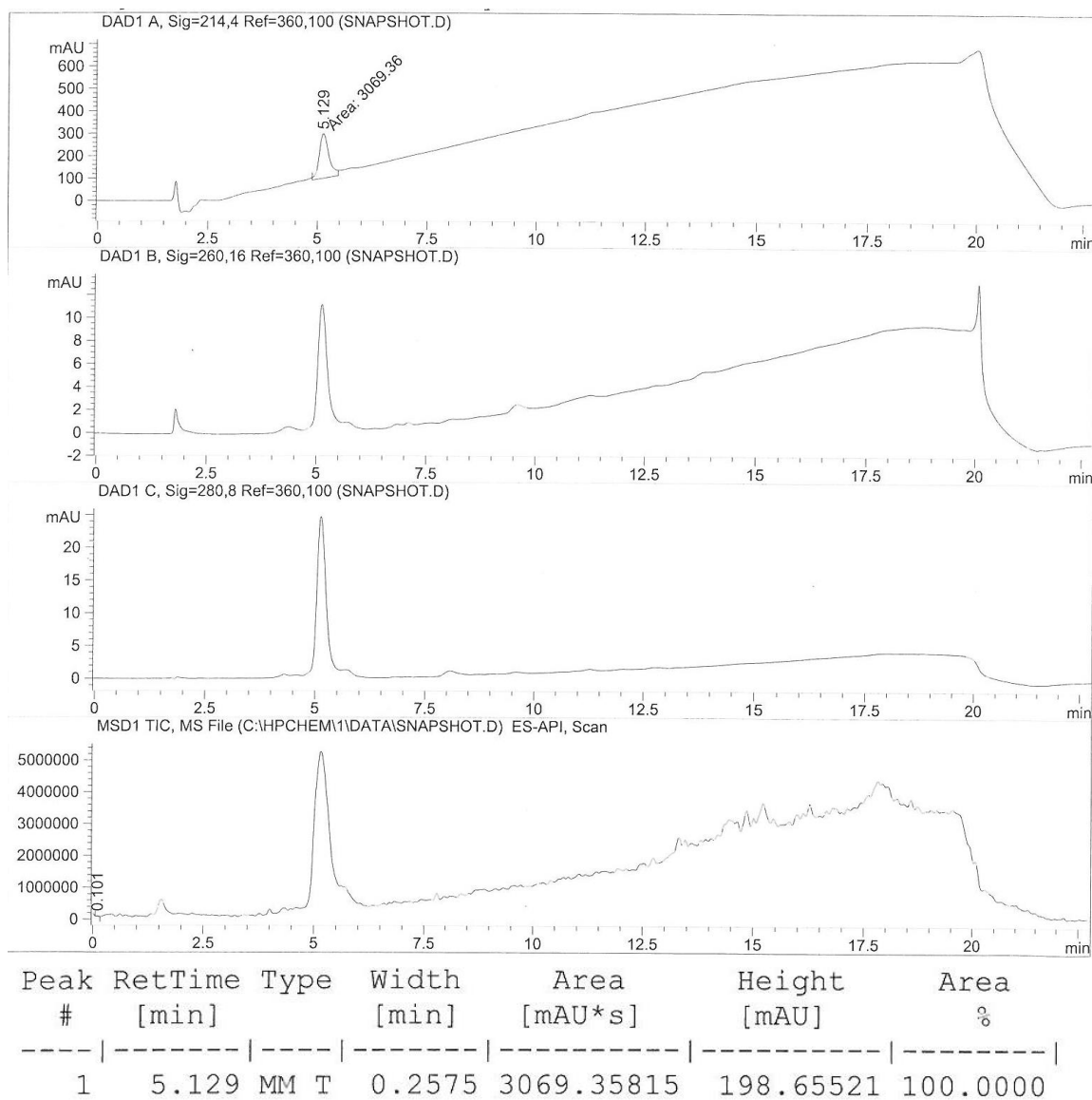


Figure A23. RP-HPLC analysis of pure Ac-DazalYET-NH₂, **2.38**, using a linear gradient 2-90% CH₃CN/H₂O (0.1% FA) over 15 min using a Symmetry Shield C₁₈ reverse-phase column (150 × 4.60 mm, 3.5 μm) set at a temperature of 25 °C at a flow rate of 1 mL/min with negative mode of detection.

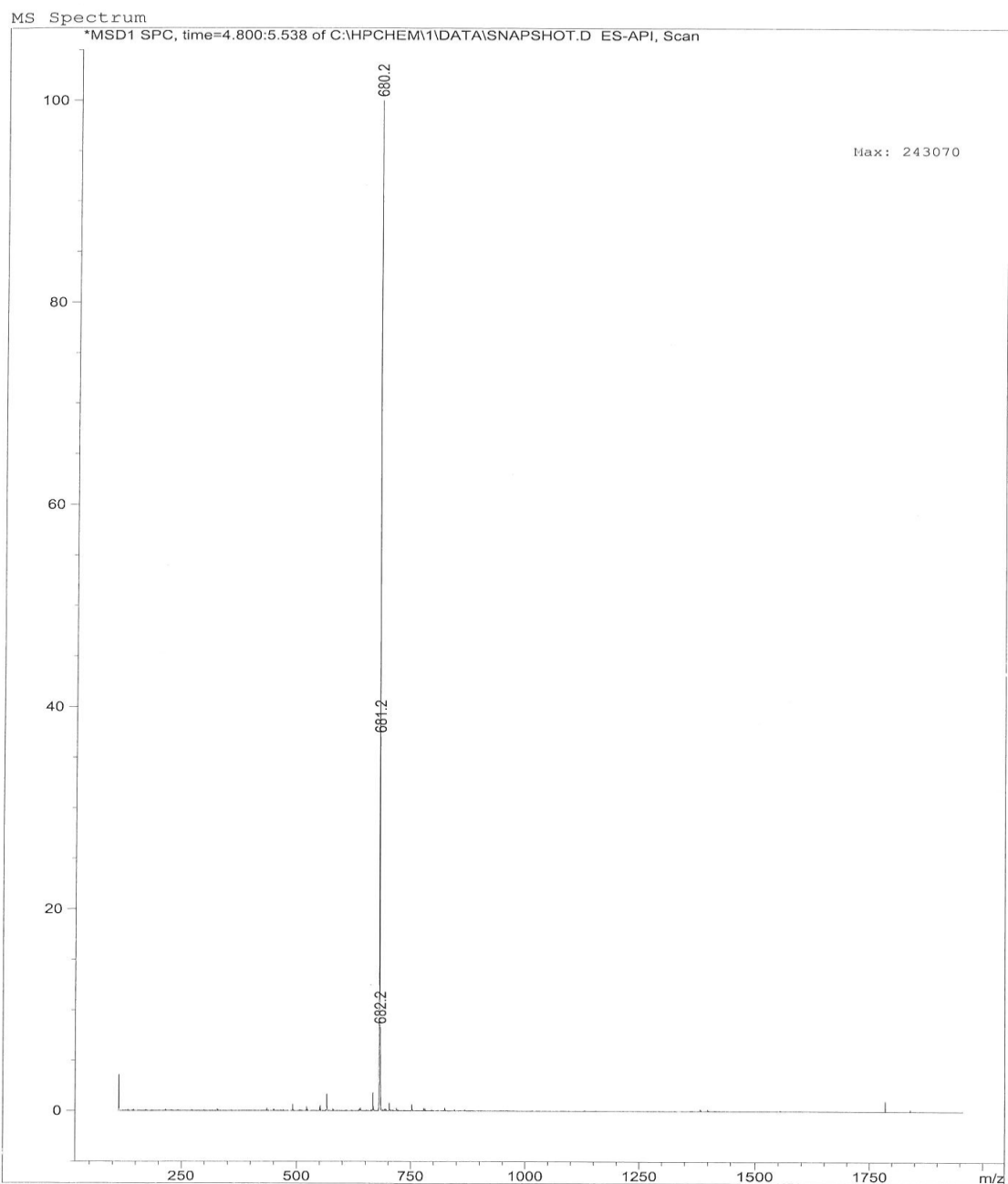
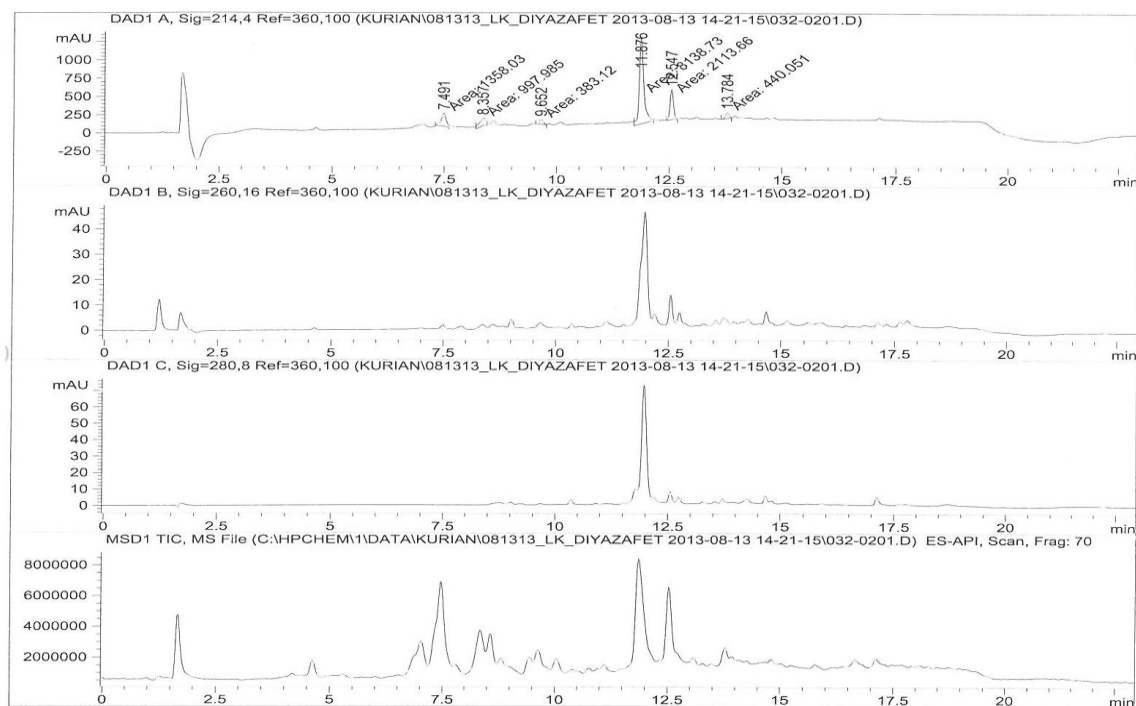


Figure A24. ESI-LCMS analysis of pure Ac-DazalYET-NH₂, **2.38**, using a linear gradient 2-90% CH₃OH/H₂O (0.1% FA) over 15 min using a Symmetry Shield C₁₈ reverse-phase column (150 × 4.60 mm, 3.5 μm) set at a temperature of 25 °C at a flow rate of 1 mL/min with negative mode of detection.



Peak #	RetTime [min]	Type	Width [min]	Area [mAU*s]	Height [mAU]	Area %
1	7.491	MM T	0.1220	1358.02588	185.48239	10.1107
2	8.357	MM T	0.1612	997.98456	103.21362	7.4301
3	9.652	MM T	0.0998	383.11984	64.00102	2.8524
4	11.876	MM T	0.1157	8138.72998	1172.60767	60.5940
5	12.547	MM T	0.0849	2113.65796	414.75897	15.7365
6	13.784	MM T	0.0862	440.05069	85.08654	3.2762

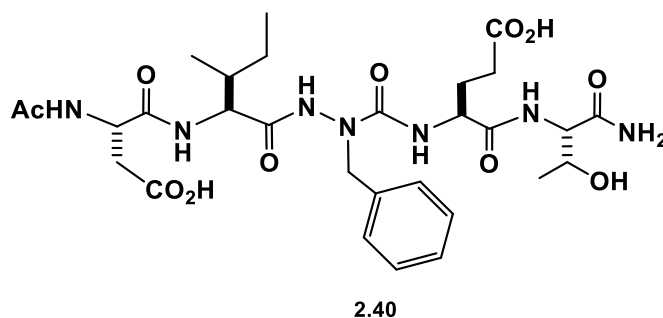


Figure A25. RP-HPLC analysis of crude Ac-DIazaFET-NH₂, **2.40**, using a linear gradient 2-90% CH₃OH/H₂O (0.1% FA) over 15 min using a Symmetry Shield C₁₈ reverse-phase column (150 × 4.60 mm, 3.5 μm) set at a temperature of 25 °C at a flow rate of 1 mL/min with detection at 214 nm.

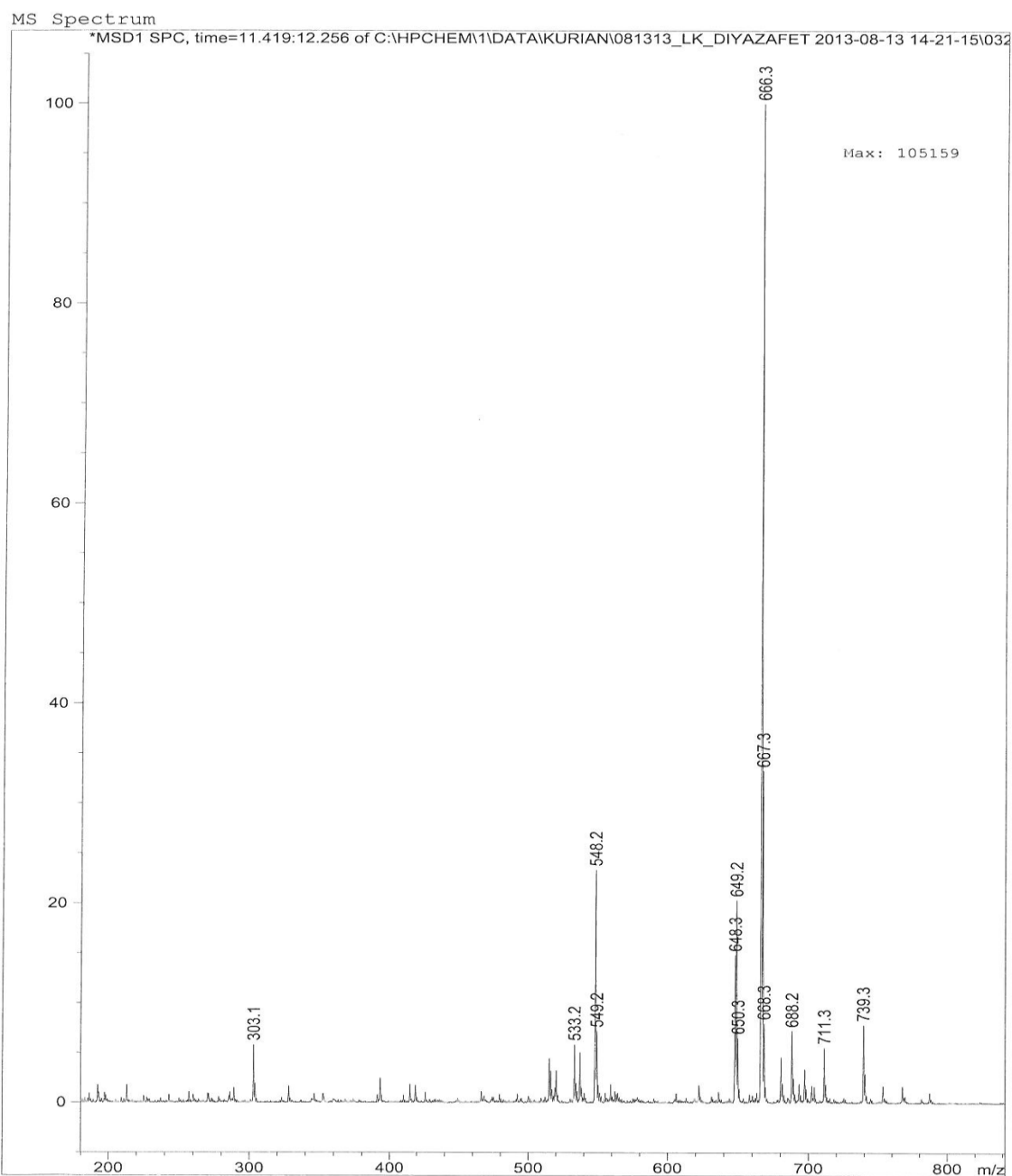
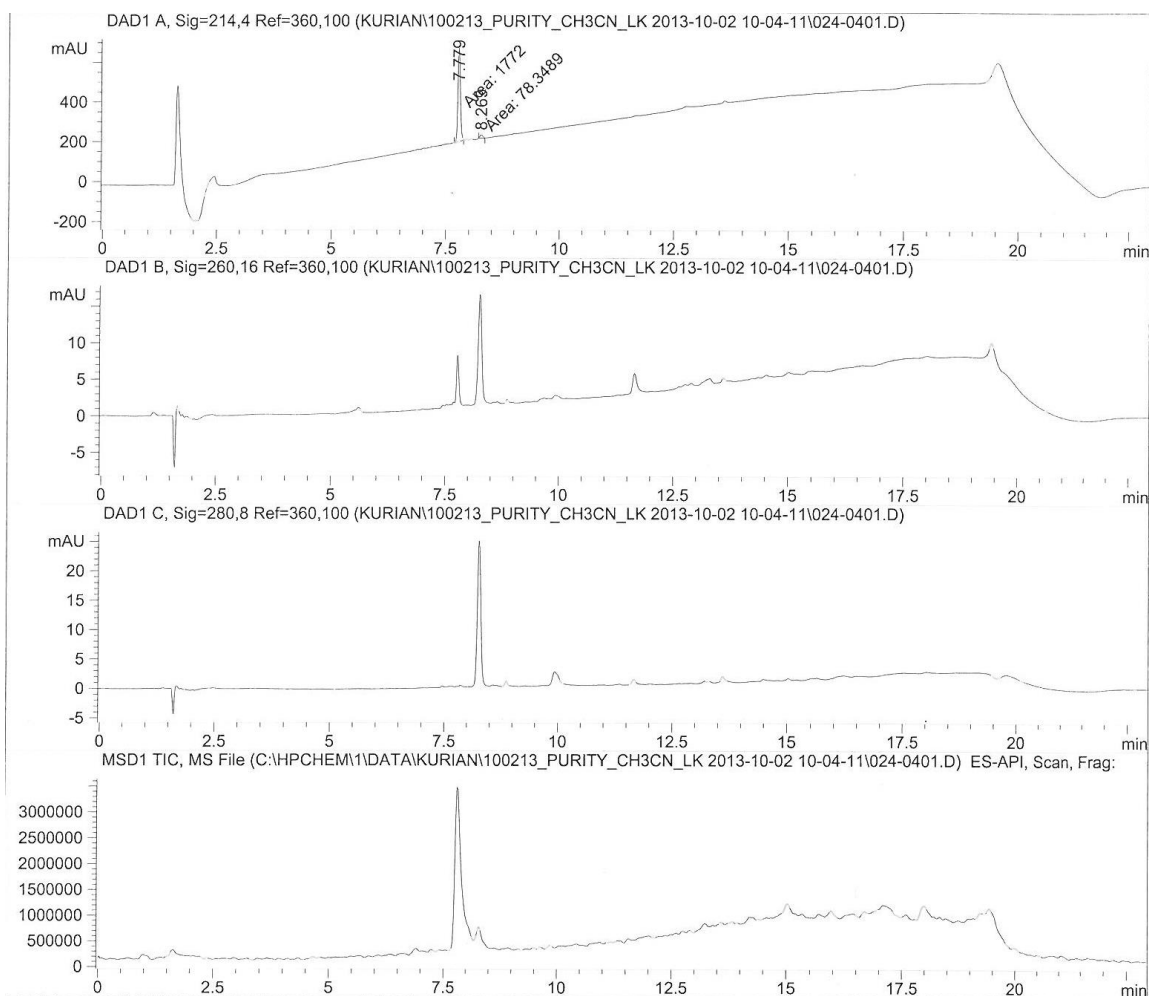


Figure A26. ESI-LCMS analysis of crude Ac-DIazaFET-NH₂, **2.40**, using a linear gradient 2-90% CH₃OH/H₂O (0.1% FA) over 15 min using a Symmetry Shield C₁₈ reverse-phase column (150 × 4.60 mm, 3.5 μm) set at a temperature of 25 °C at a flow rate of 1 mL/min with positive mode of detection.



Peak #	RetTime [min]	Type	Width [min]	Area [mAU*s]	Height [mAU]	Area %
1	7.779	MM T	0.0625	1772.00391	472.43219	95.7657
2	8.269	MM T	0.0770	78.34886	16.95910	4.2343

Figure A27. RP-HPLC analysis of crude Ac-DIazaFET-NH₂, **2.40**, using a linear gradient 2-90% CH₃CN/H₂O (0.1% FA) over 15 min using a Symmetry Shield C₁₈ reverse-phase column (150 × 4.60 mm, 3.5 μm) set at a temperature of 25 °C at a flow rate of 1 mL/min with detection at 214 nm.

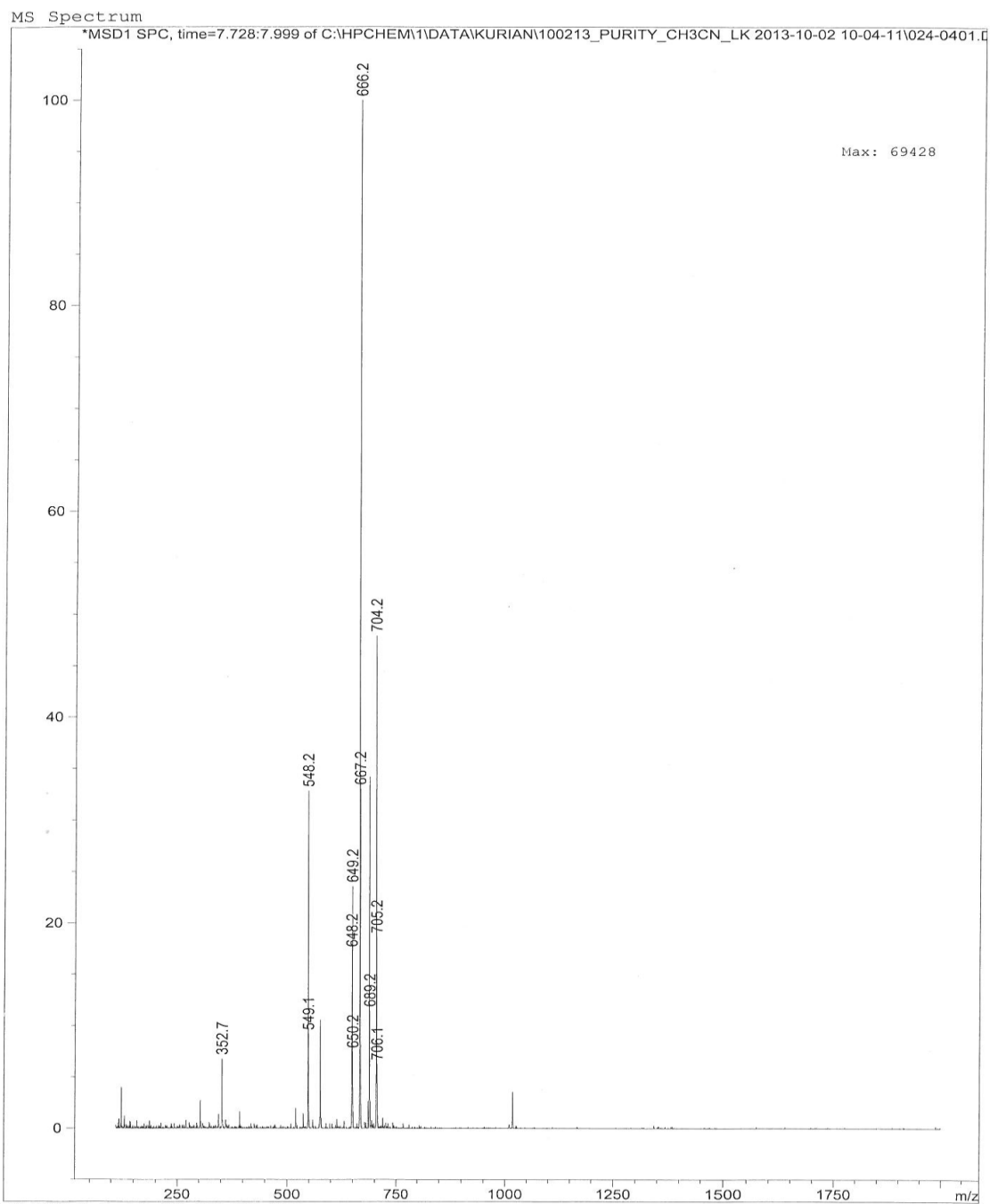
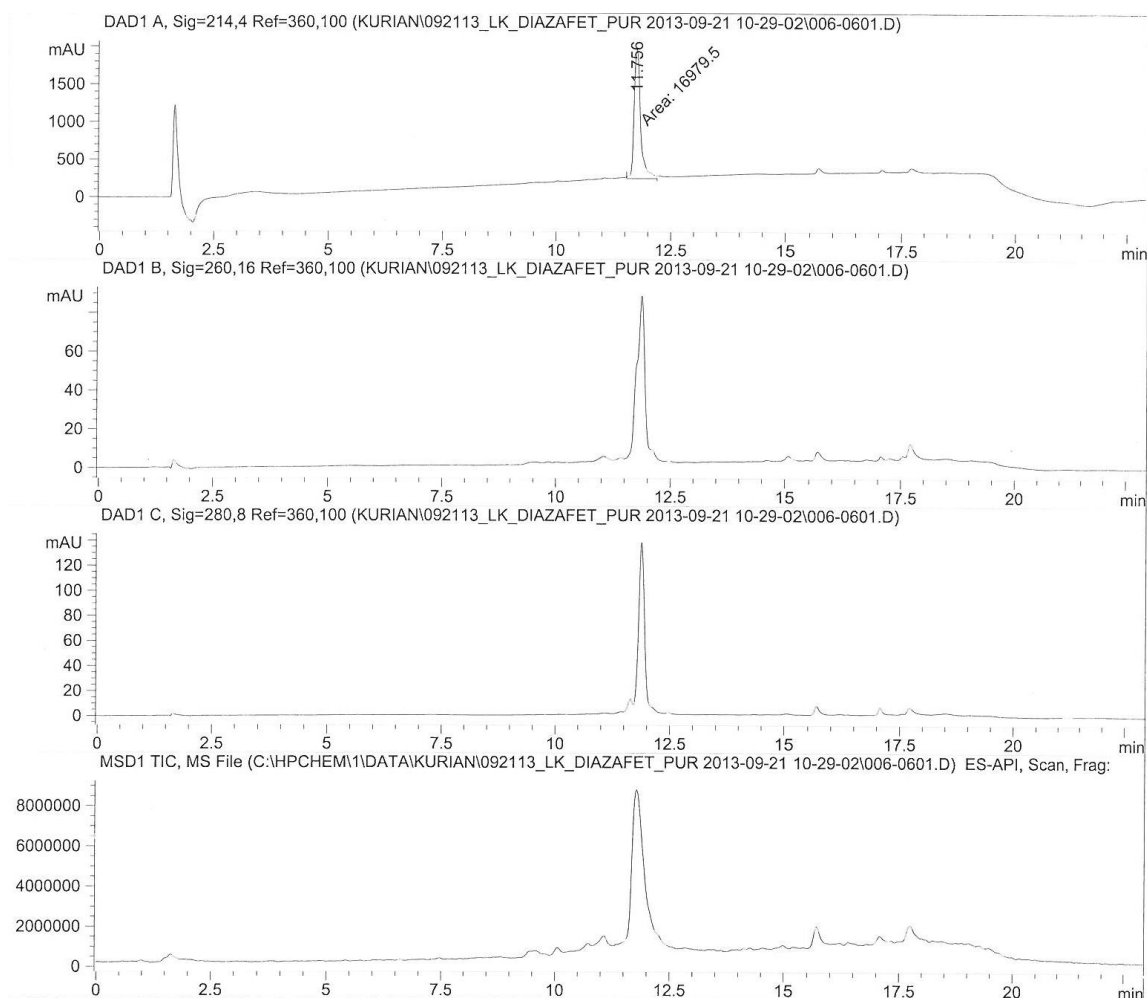


Figure A28. ESI-LCMS analysis of pure Ac-DIazaFET-NH₂, **2.40**, using a linear gradient 2-90% CH₃OH/H₂O (0.1% FA) over 15 min using a Symmetry Shield C₁₈ reverse-phase column (150 × 4.60 mm, 3.5 μm) set at a temperature of 25 °C at a flow rate of 1 mL/min with positive mode of detection.



Peak #	RetTime [min]	Type	Width [min]	Area [mAU*s]	Height [mAU]	Area %
1	11.756	MM T	0.1655	1.69795e4	1710.39392	100.0000

Figure A29. ESI-LCMS analysis of pure Ac-DiazaFET-NH₂, **2.40**, using a linear gradient 2-90% CH₃OH/H₂O (0.1% FA) over 15 min using a Symmetry Shield C₁₈ reverse-phase column (150 × 4.60 mm, 3.5 μm) set at a temperature of 25 °C at a flow rate of 1 mL/min with detection at 214 nm.

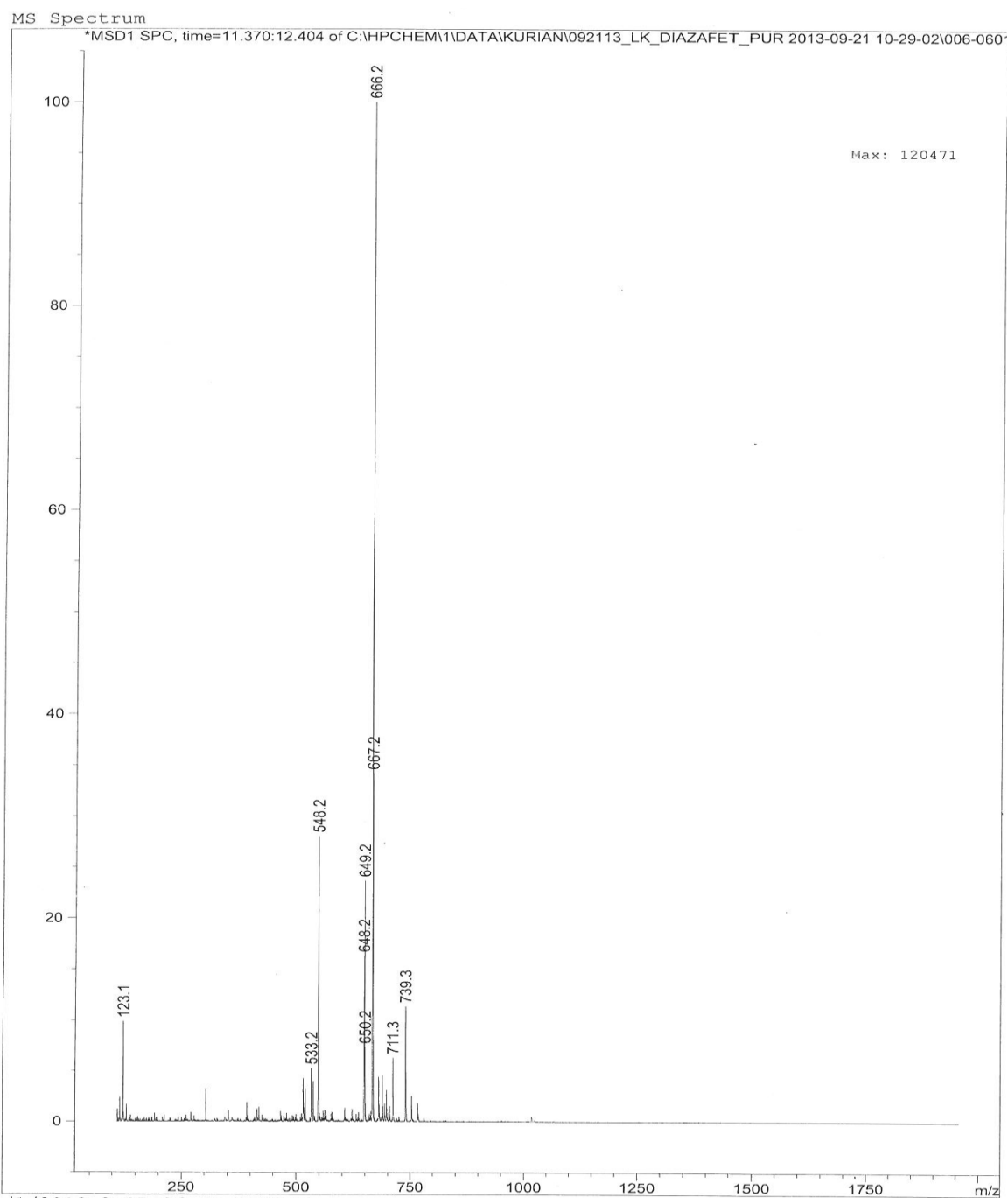
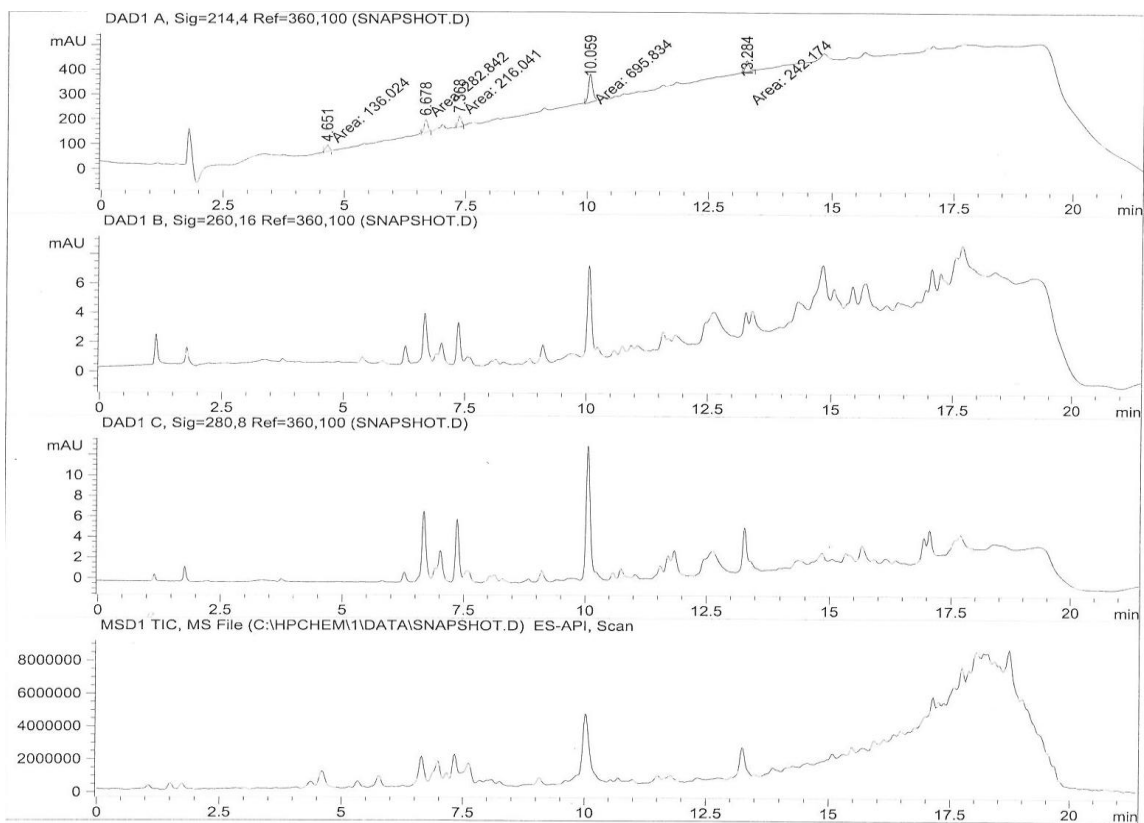


Figure A30. ESI-LCMS analysis of crude Ac-DIazaFET-NH₂, **2.40**, using a linear gradient 2-90% CH₃OH/H₂O (0.1% FA) over 15 min using a Symmetry Shield C₁₈ reverse-phase column (150 × 4.60 mm, 3.5 μm) set at a temperature of 25 °C at a flow rate of 1 mL/min with positive mode of detection.



Peak #	RetTime [min]	Type	Width [min]	Area [mAU*s]	Height [mAU]	Area %
1	4.651	MM T	0.0929	136.02400	24.39239	8.6479
2	6.678	MM T	0.0891	282.84171	52.90797	17.9820
3	7.368	MM T	0.0859	216.04060	41.91696	13.7350
4	10.059	MM T	0.1017	695.83435	114.05202	44.2385
5	13.284	MM T	0.0932	242.17407	43.30146	15.3965

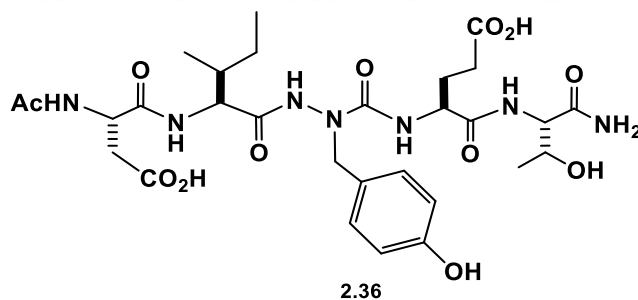


Figure A31. RP-HPLC analysis of crude Ac-DIazaYET-NH₂, **2.36**, using a linear gradient 2-90% CH₃OH/H₂O (0.1% FA) over 15 min using a Symmetry Shield C₁₈ reverse-phase column (150 × 4.60 mm, 3.5 μm) set at a temperature of 25 °C at a flow rate of 1 mL/min with detection at 214 nm.

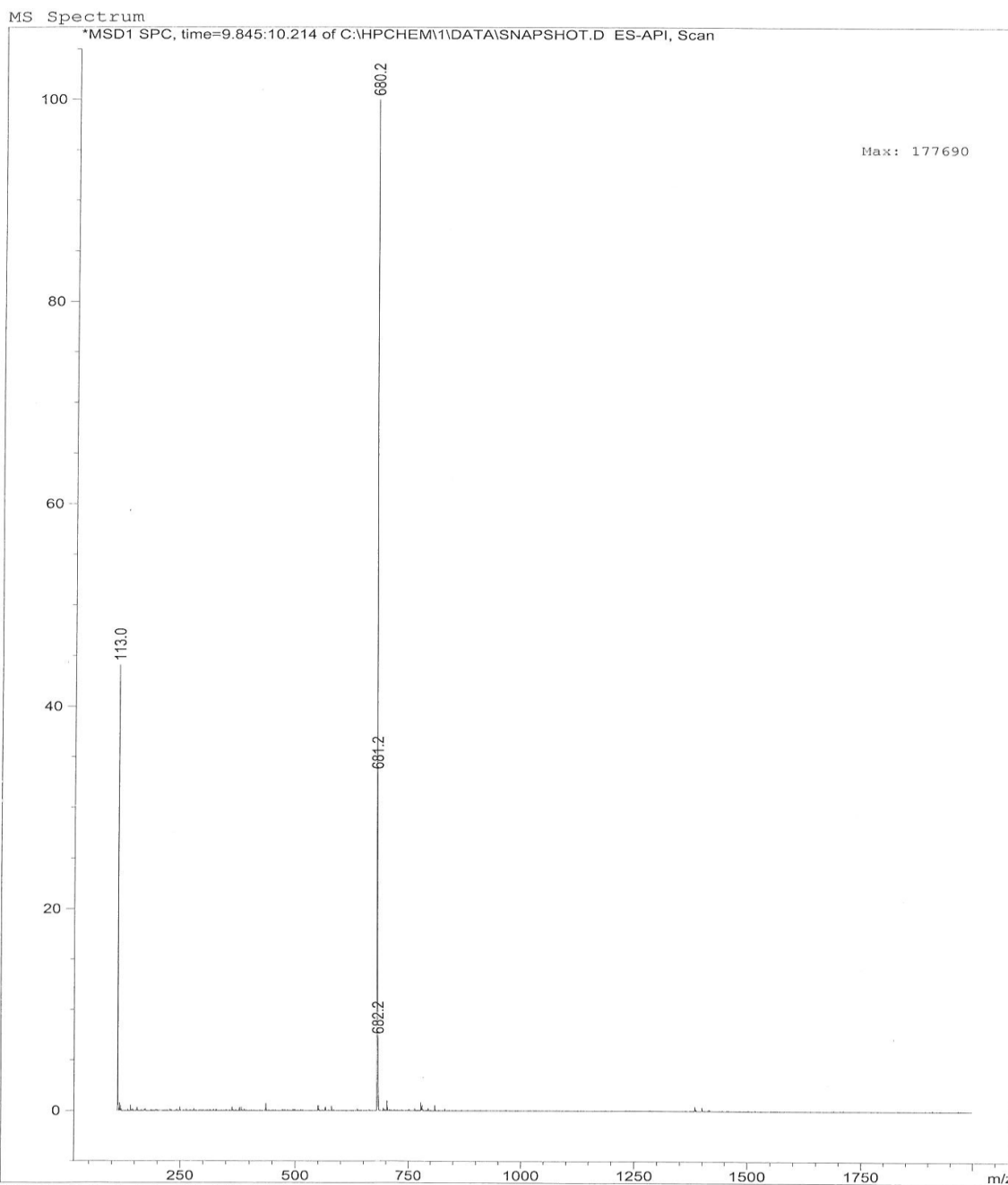
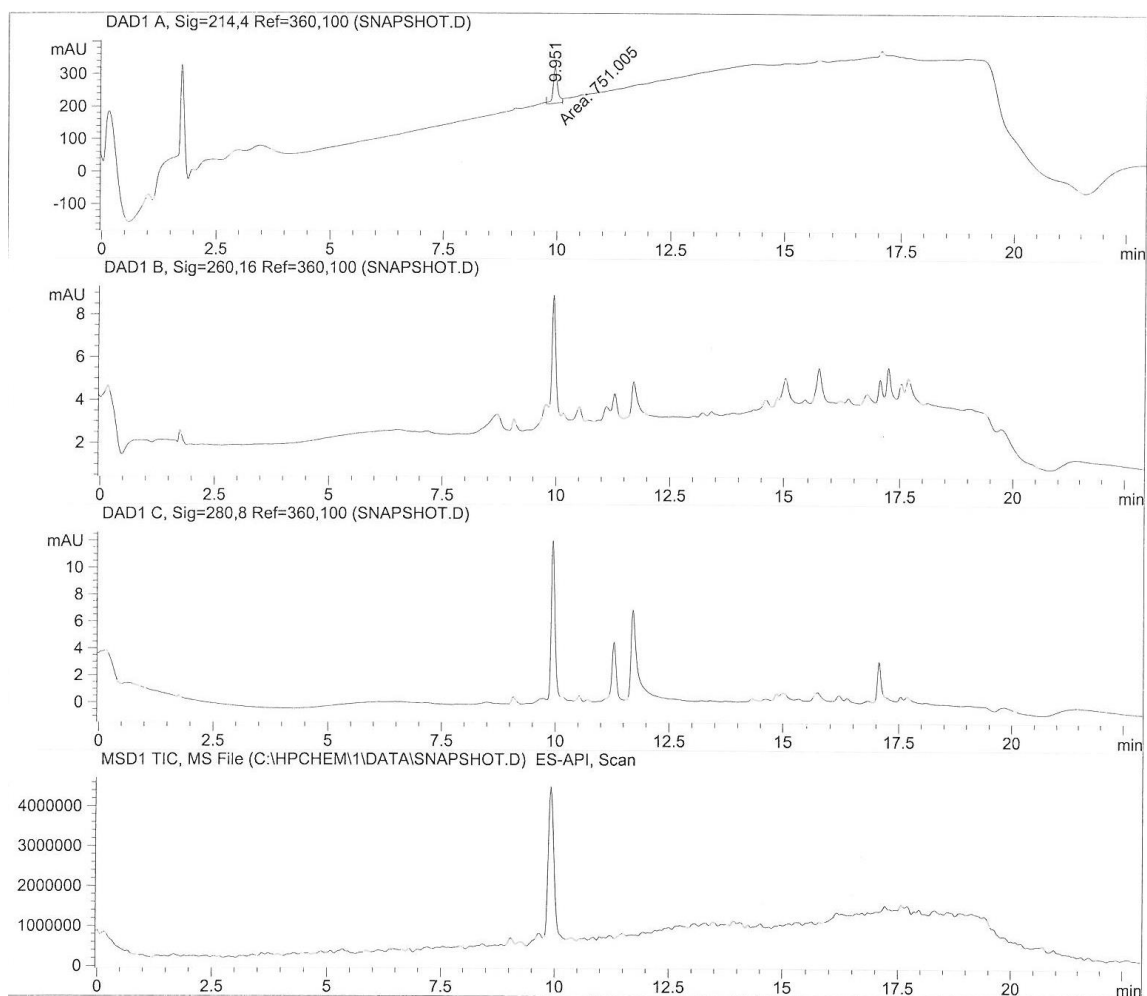


Figure A32. ESI-LCMS analysis of crude Ac-DIazaYET-NH₂, **2.36**, using a linear gradient 2-90% CH₃OH/H₂O (0.1% FA) over 15 min using a Symmetry Shield C₁₈ reverse-phase column (150 × 4.60 mm, 3.5 μm) set at a temperature of 25 °C at a flow rate of 1 mL/min with negative mode of detection.



Peak #	RetTime [min]	Type	Width [min]	Area [mAU*s]	Height [mAU]	Area %
1	9.951	MM T	0.1433	751.00537	110.21140	100.0000

Figure A33. RP-HPLC analysis of pure Ac-DIazaYET-NH₂, **2.36**, using a linear gradient 2-90% CH₃OH/H₂O (0.1% FA) over 15 min using a Symmetry Shield C₁₈ reverse-phase column (150 × 4.60 mm, 3.5 μm) set at a temperature of 25 °C at a flow rate of 1 mL/min with detection at 214 nm.

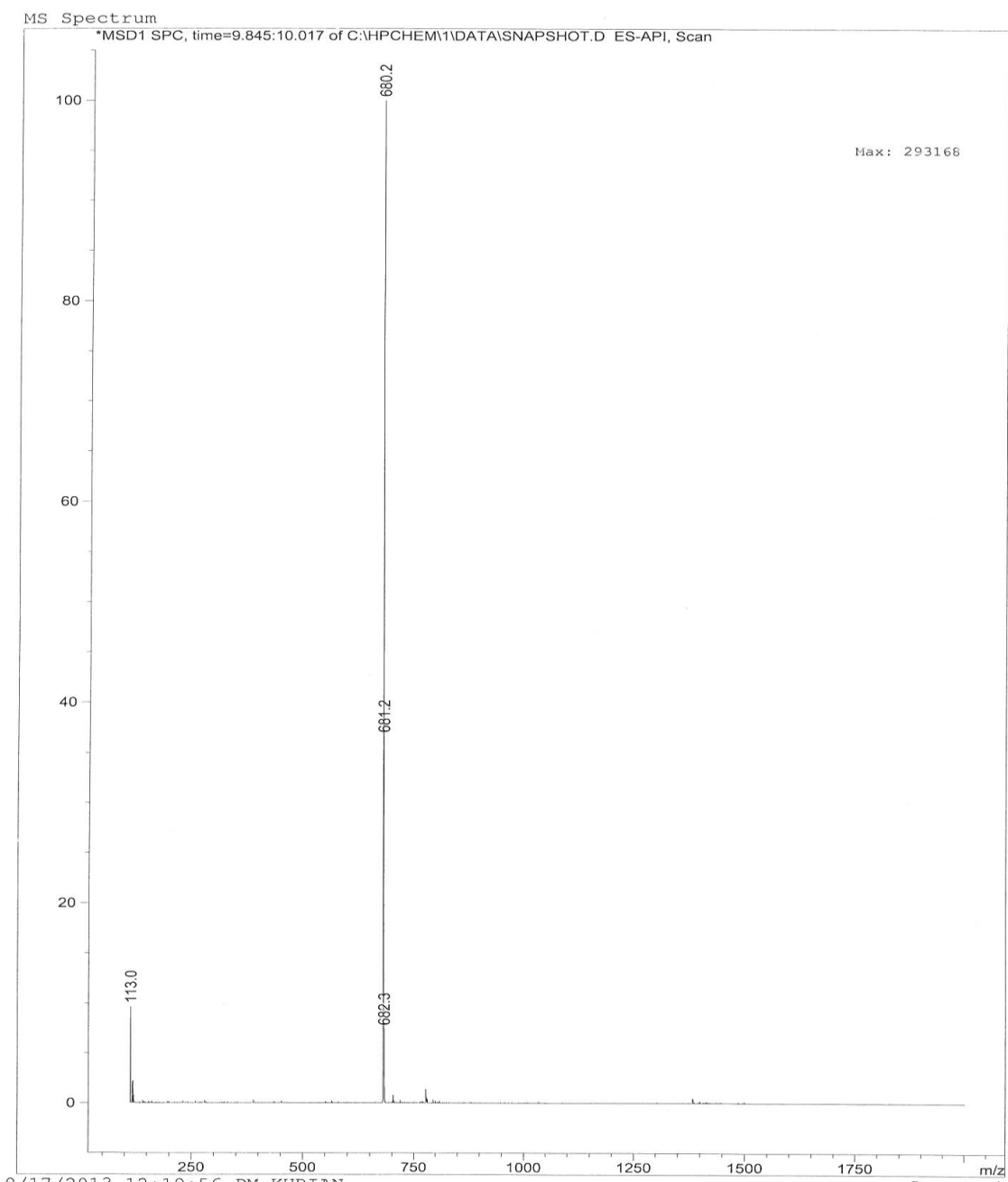
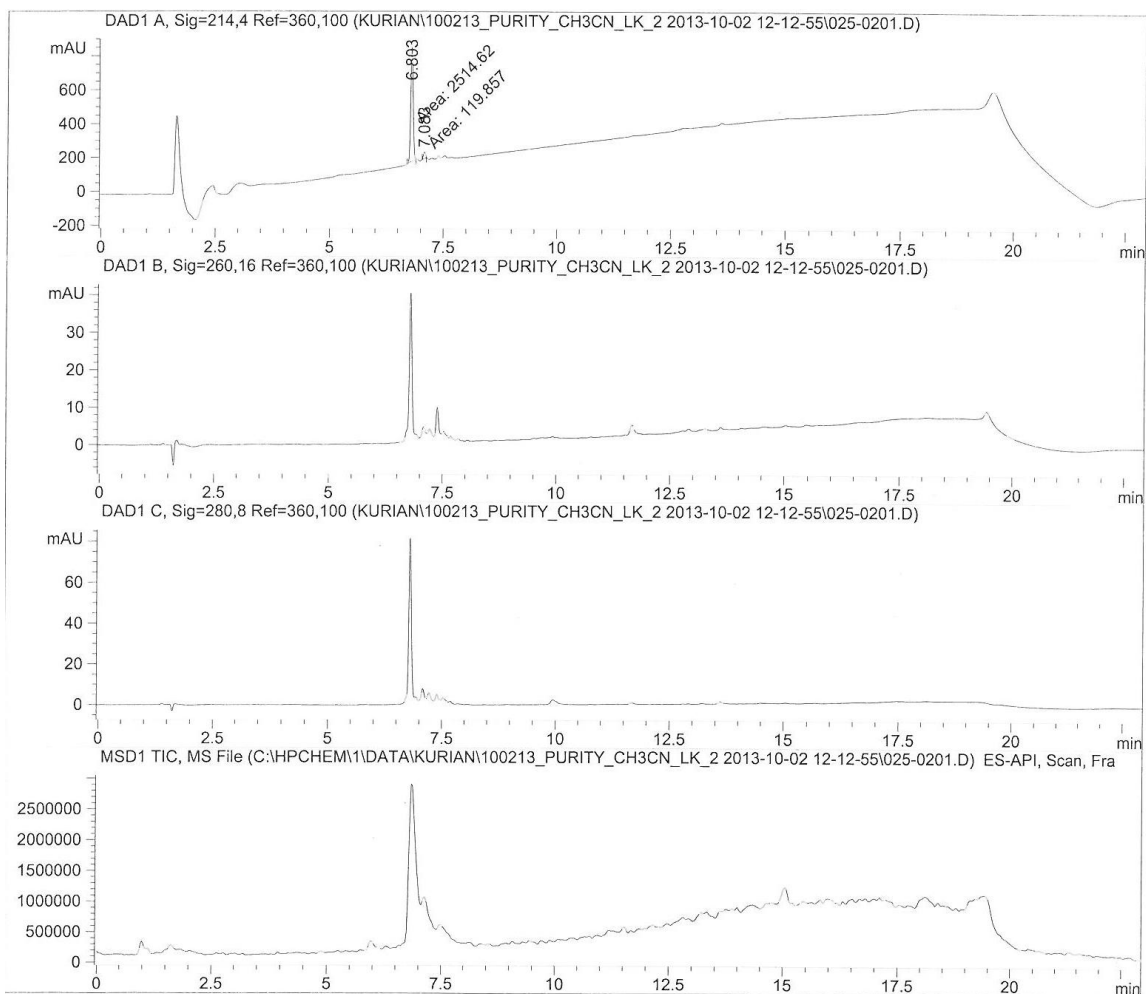


Figure A34. ESI-LCMS analysis of pure Ac-DIazaYET-NH₂, **2.36**, using a linear gradient 2-90% CH₃OH/H₂O (0.1% FA) over 15 min using a Symmetry Shield C₁₈ reverse-phase column (150 × 4.60 mm, 3.5 μm) set at a temperature of 25 °C at a flow rate of 1 mL/min with positive mode of detection.



Peak #	RetTime [min]	Type	Width [min]	Area [mAU*s]	Height [mAU]	Area %
1	6.803	MM T	0.0621	2514.62378	675.03735	95.4505
2	7.083	MM T	0.0518	119.85651	38.58495	4.5495

Figure A35. RP-HPLC analysis of pure Ac-DIazaYET-NH₂, **2.36**, using a linear gradient 2-90% CH₃CN/H₂O (0.1% FA) over 15 min using a Symmetry Shield C₁₈ reverse-phase column (150 × 4.60 mm, 3.5 μm) set at a temperature of 25 °C at a flow rate of 1 mL/min with detection at 214 nm.

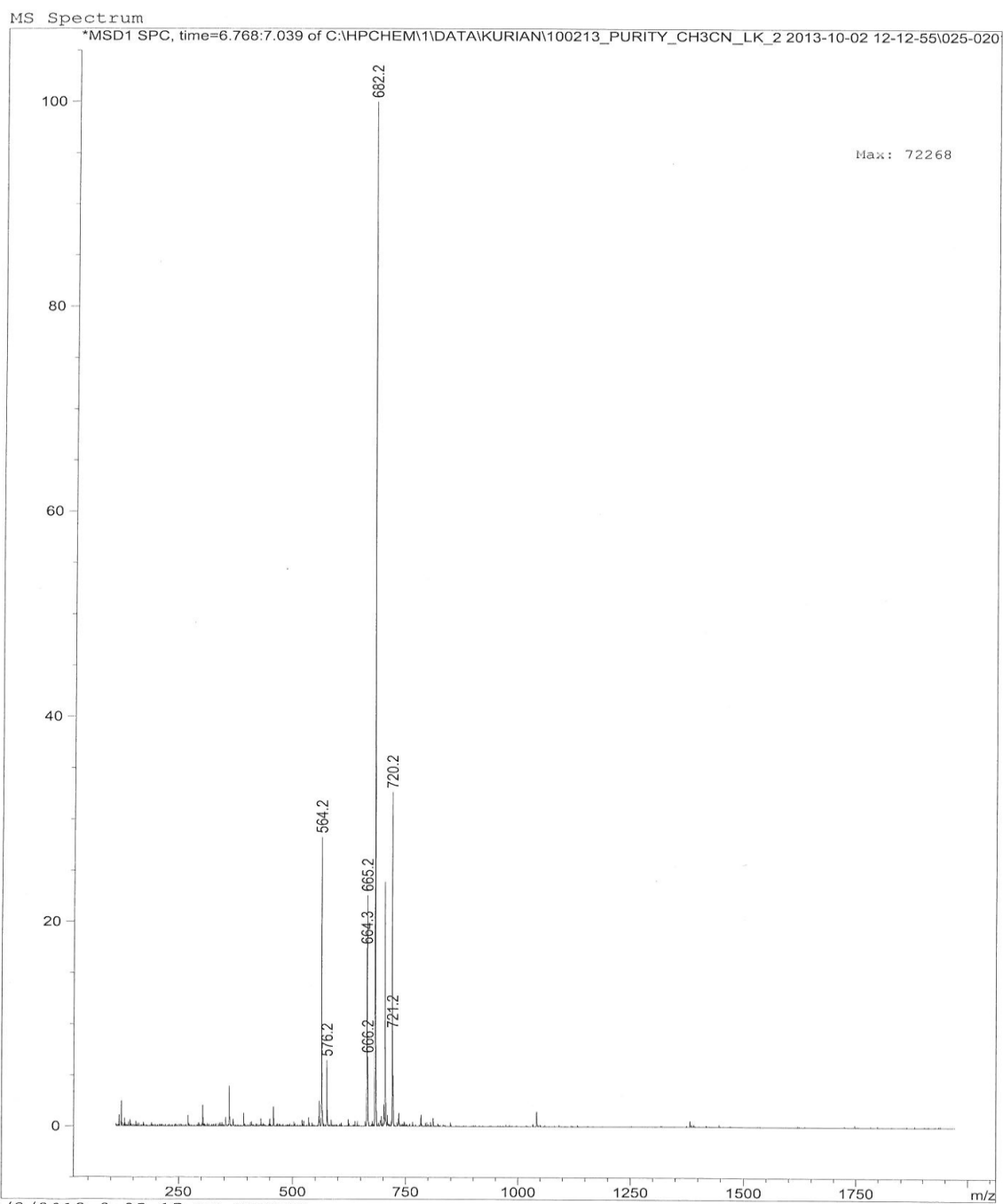


Figure A36. RP-HPLC analysis of crude Ac-DIazaYET-NH₂, **2.36**, using a linear gradient 2-90% CH₃CN/H₂O (0.1% FA) over 15 min using a Symmetry Shield C₁₈ reverse-phase column (150 × 4.60 mm, 3.5 μm) set at a temperature of 25 °C at a flow rate of 1 mL/min with positive mode of detection.

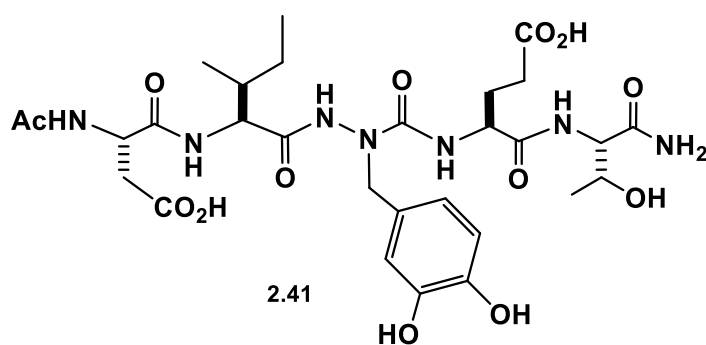
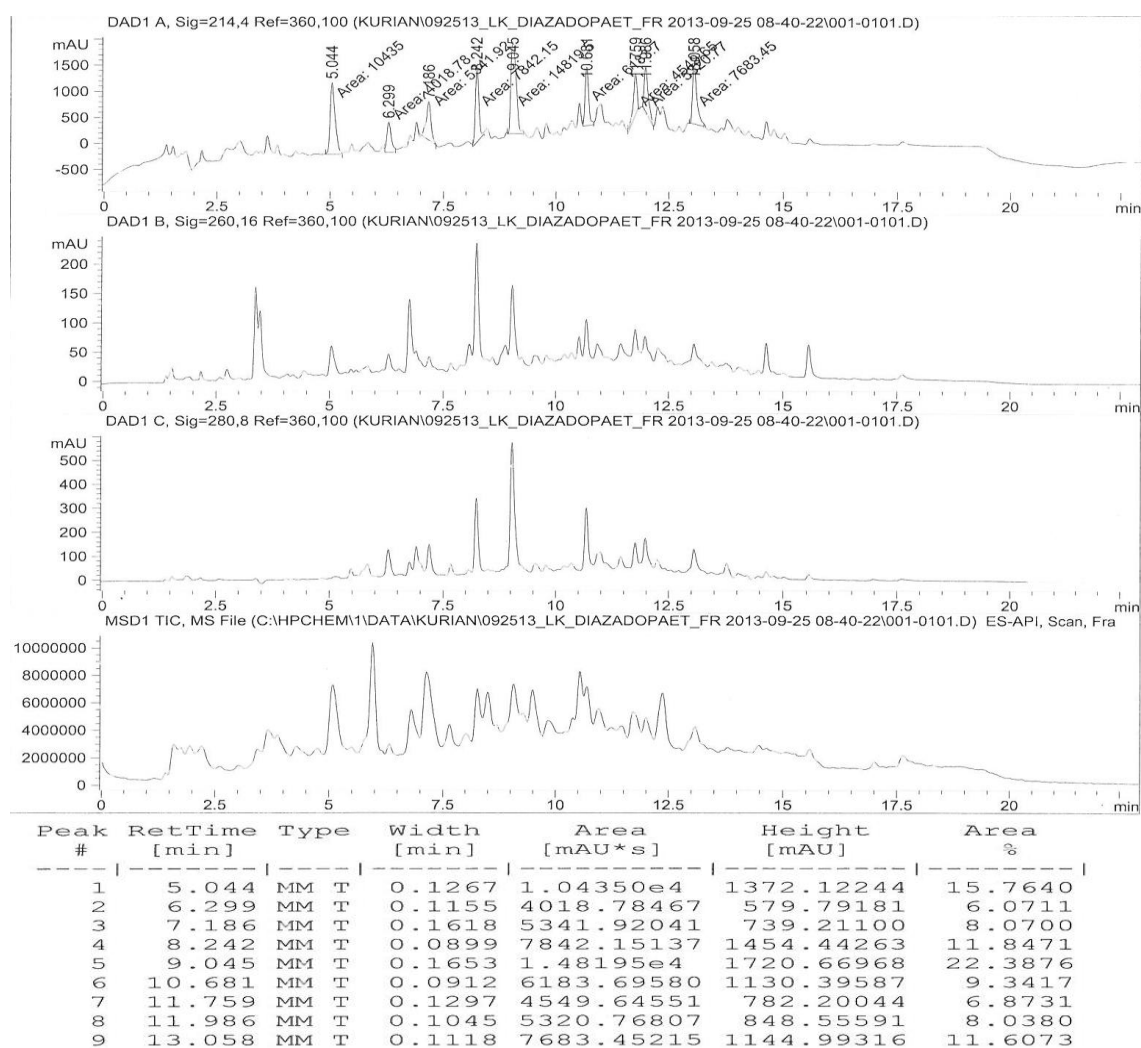


Figure A37. RP-HPLC analysis of crude Ac-DIaza(DOPA)ET-NH₂, **2.41**, using a linear gradient 2-90% CH₃OH/H₂O (0.1% FA) over 15 min using a Symmetry Shield C₁₈ reverse-phase column (150 × 4.60 mm, 3.5 μm) set at a temperature of 25 °C at a flow rate of 1 mL/min with detection at 214 nm.

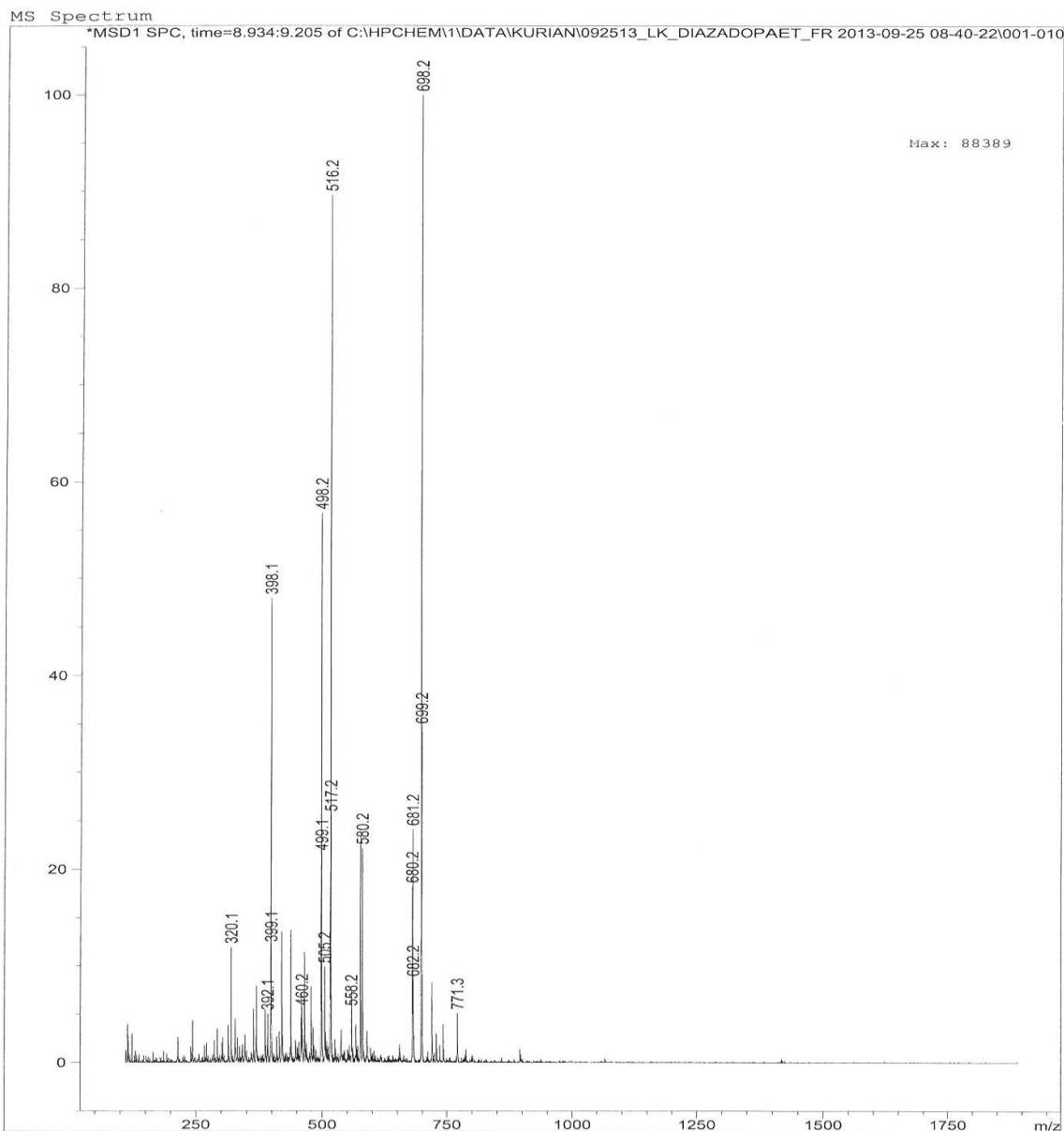
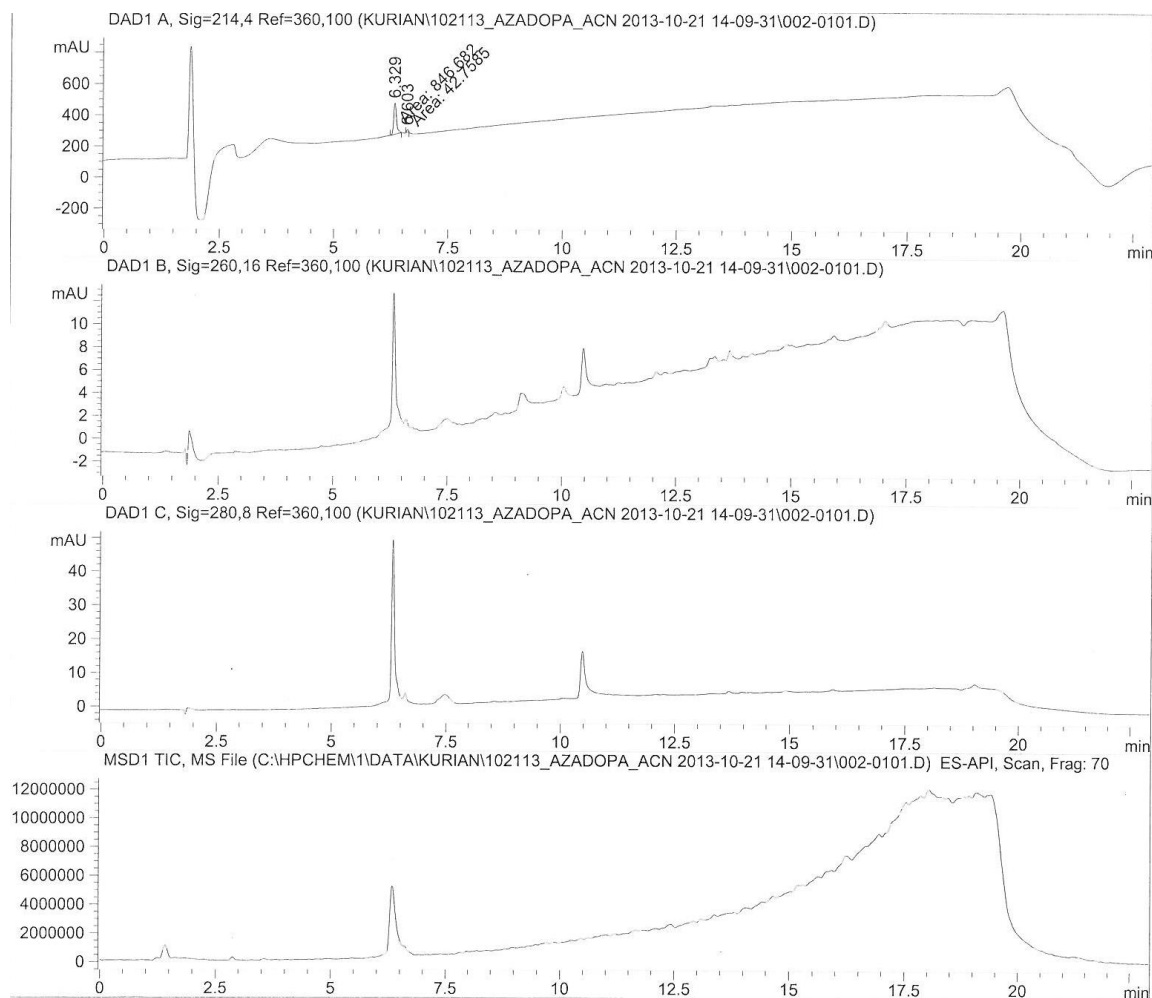


Figure A38. RP-HPLC analysis of crude Ac-DIaza(DOPA)ET-NH₂, **2.41**, using a linear gradient 2-90% CH₃OH/H₂O (0.1% FA) over 15 min using a Symmetry Shield C₁₈ reverse-phase column (150 × 4.60 mm, 3.5 μm) set at a temperature of 25 °C at a flow rate of 1 mL/min with positive mode of detection.



Peak #	RetTime [min]	Type	Width [min]	Area [mAU*s]	Height [mAU]	Area %
1	6.329	MM T	0.0697	846.68213	202.32498	95.1927
2	6.603	MM T	0.0437	42.75852	16.30388	4.8073

Figure A39. RP-HPLC analysis of pure Ac-DIaza(DOPA)ET-NH₂, **2.41**, using a linear gradient 2-90% CH₃CN/H₂O (0.1% FA) over 15 min using a Symmetry Shield C₁₈ reverse-phase column (150 × 4.60 mm, 3.5 μm) set at a temperature of 25 °C at a flow rate of 1 mL/min with detection at 214 nm.

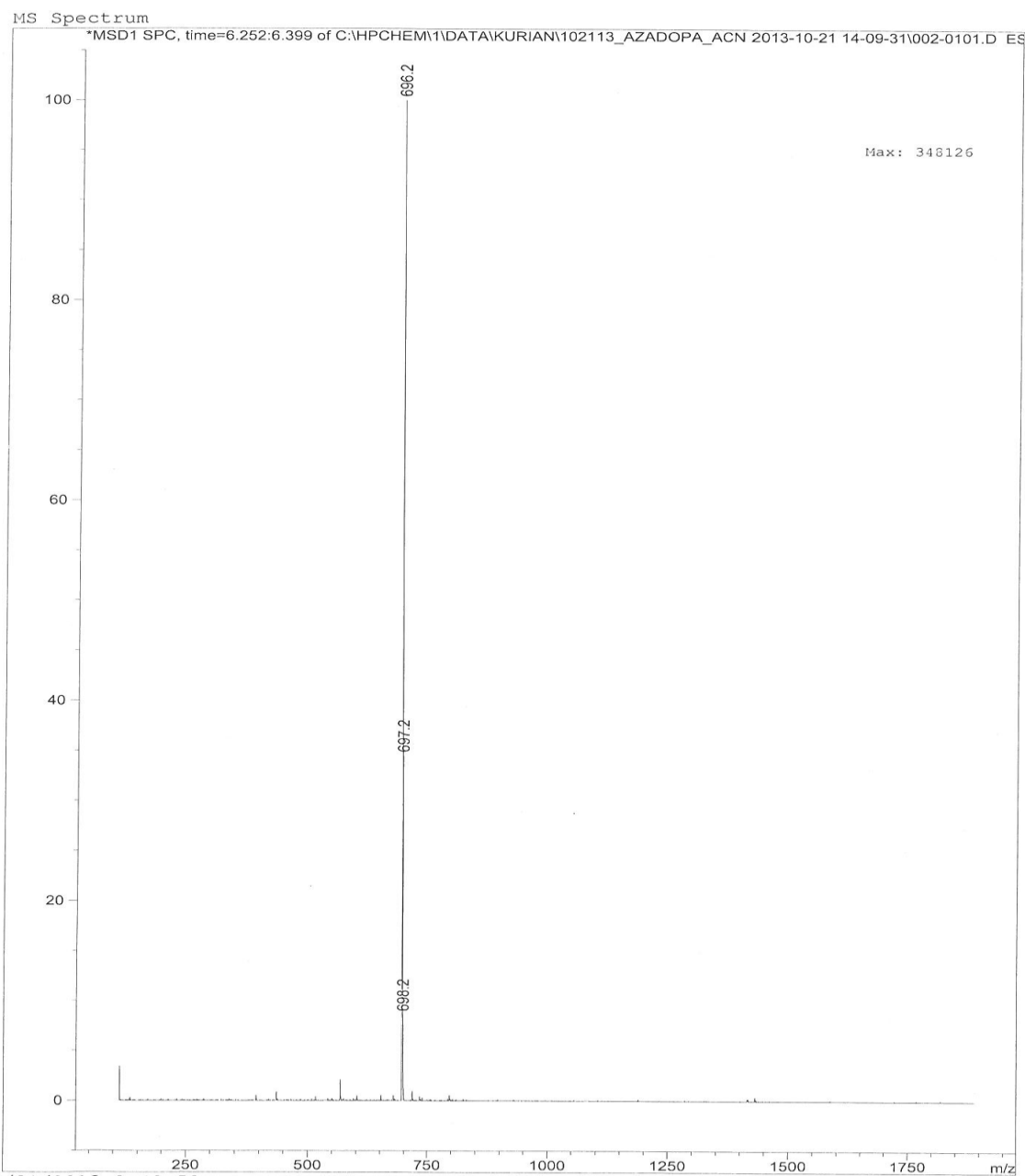


Figure A40. ESI-LCMS analysis of crude Ac-DIaza(DOPA)ET-NH₂, **2.41**, using a linear gradient 2-90% CH₃CN/H₂O (0.1% FA) over 15 min using a Symmetry Shield C₁₈ reverse-phase column (150 × 4.60 mm, 3.5 μm) set at a temperature of 25 °C at a flow rate of 1 mL/min with negative mode of detection.

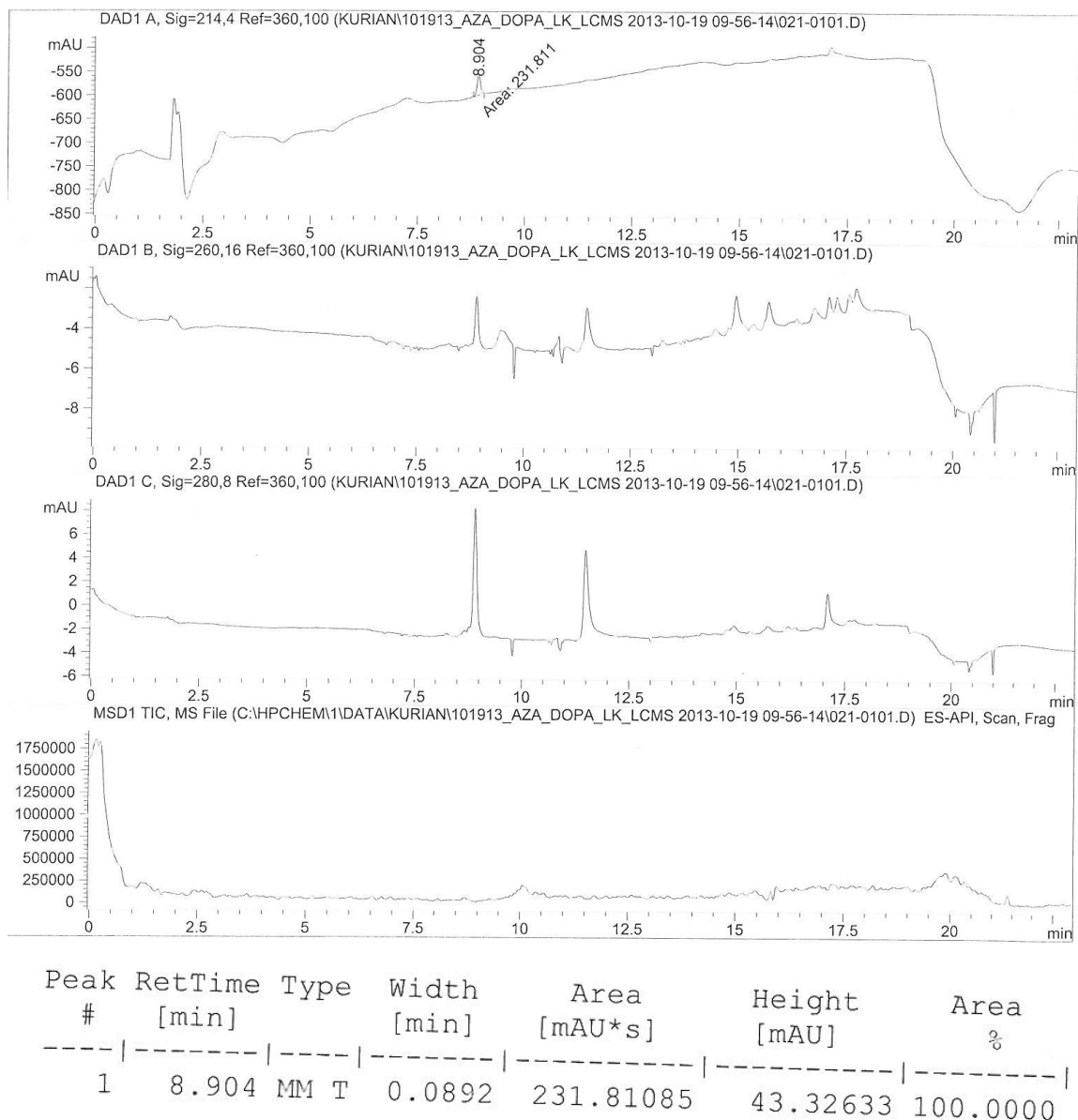


Figure A41. RP-HPLC analysis of pure Ac-DIaza(DOPA)ET-NH₂, **2.41**, using a linear gradient 2-90% CH₃OH/H₂O (0.1% FA) over 15 min using a Symmetry Shield C₁₈ reverse-phase column (150 × 4.60 mm, 3.5 μm) set at a temperature of 25 °C at a flow rate of 1 mL/min with detection at 214 nm.

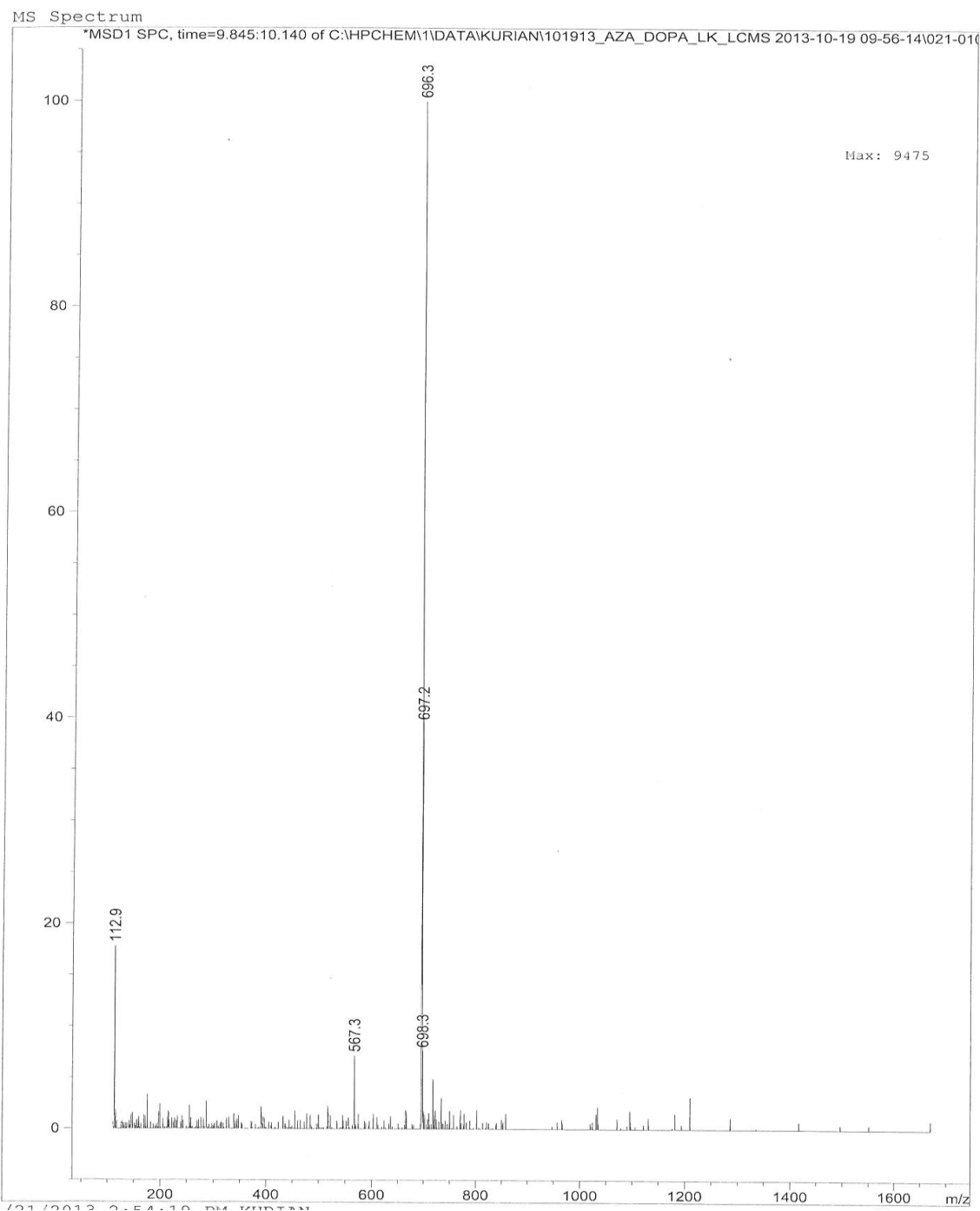
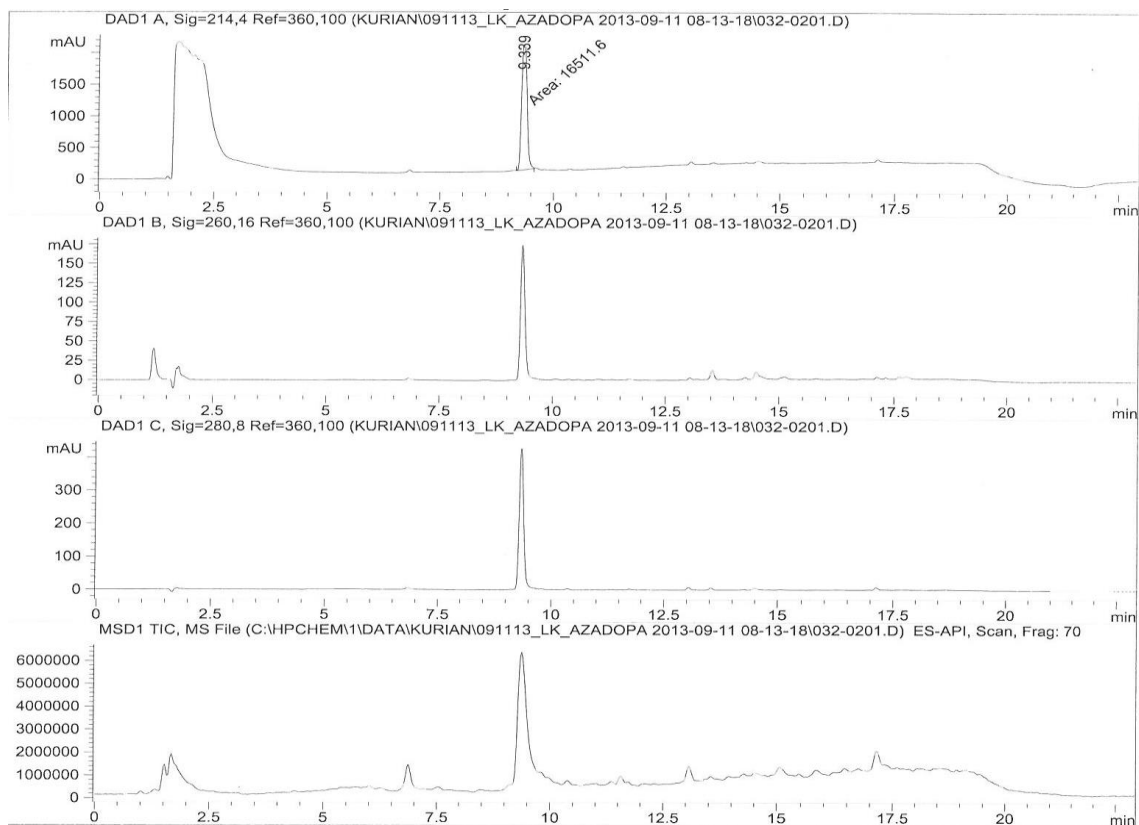
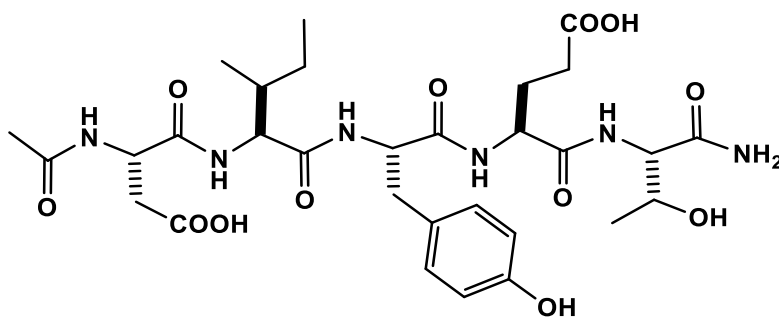


Figure A42. ESI-LCMS analysis of pure Ac-DIaza(DOPA)ET-NH₂, **2.41**, using a linear gradient 2-90% CH₃OH/H₂O (0.1% FA) over 15 min using a Symmetry Shield C₁₈ reverse-phase column (150 × 4.60 mm, 3.5 μm) set at a temperature of 25 °C at a flow rate of 1 mL/min with negative mode of detection.



Peak #	RetTime [min]	Type	Width [min]	Area [mAU*s]	Height [mAU]	Area %
1	9.339	MM T	0.1382	1.65116e4	1990.80884	100.0000



2.28

Figure A43. RP-HPLC analysis of crude Ac-DIYET-NH₂, **2.28**, using a linear gradient 2-90% CH₃OH/H₂O (0.1% FA) over 15 min using a Symmetry Shield C₁₈ reverse-phase column (150 × 4.60 mm, 3.5 μm) set at a temperature of 25 °C at a flow rate of 1 mL/min with detection at 214 nm.

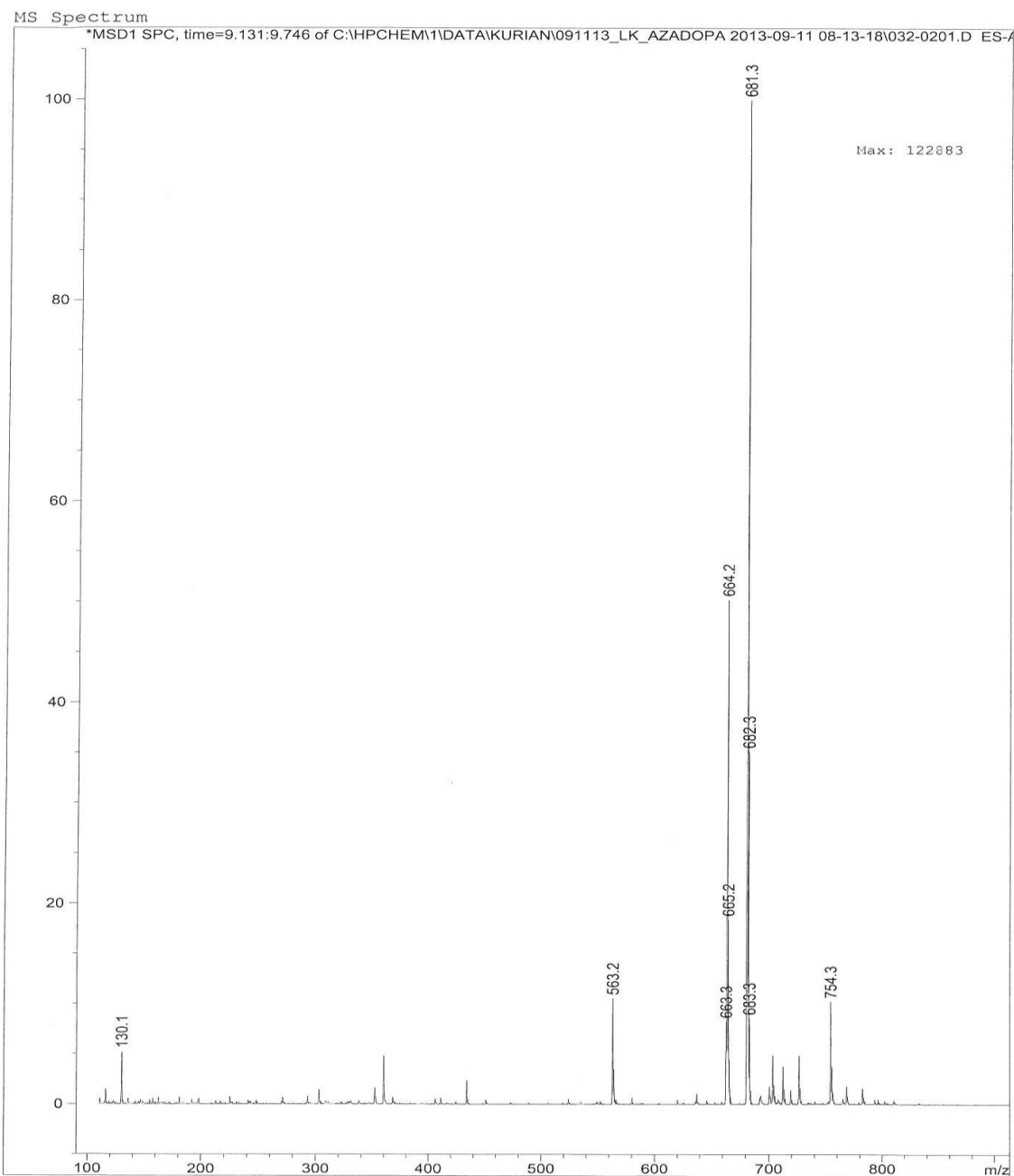
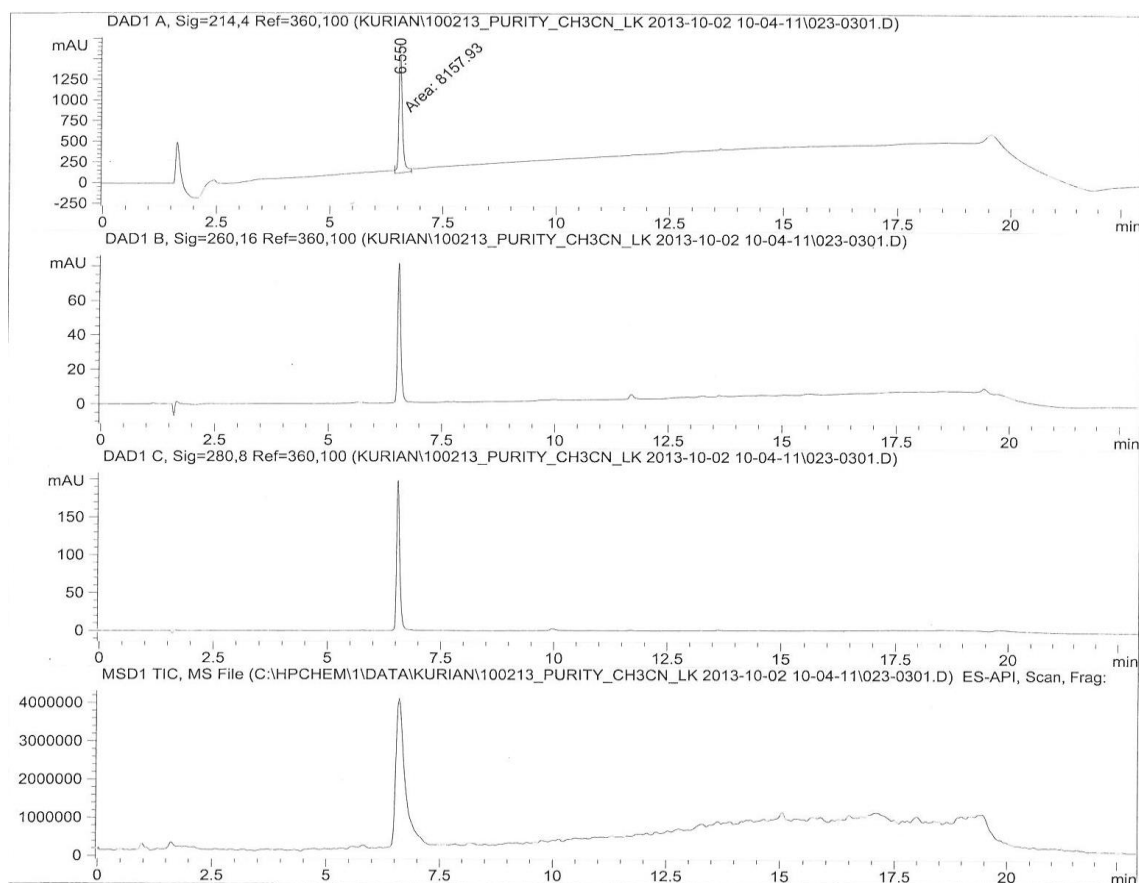


Figure A44. ESI-LCMS analysis of crude Ac-DIYET-NH₂, **2.28**, using a linear gradient 2-90% CH₃OH/H₂O (0.1% FA) over 15 min using a Symmetry Shield C₁₈ reverse-phase column (150 × 4.60 mm, 3.5 μm) set at a temperature of 25 °C at a flow rate of 1 mL/min with positive mode of detection.



Peak #	RetTime [min]	Type	Width [min]	Area [mAU*s]	Height [mAU]	Area %
1	6.550	MM T	0.0875	8157.92676	1553.75024	100.0000

Figure A45. RP-HPLC analysis of pure Ac-DIaza(DOPA)ET-NH₂, **2.41**, using a linear gradient 2-90% CH₃CN/H₂O (0.1% FA) over 15 min using a Symmetry Shield C₁₈ reverse-phase column (150 × 4.60 mm, 3.5 μm) set at a temperature of 25 °C at a flow rate of 1 mL/min with detection at 214 nm.

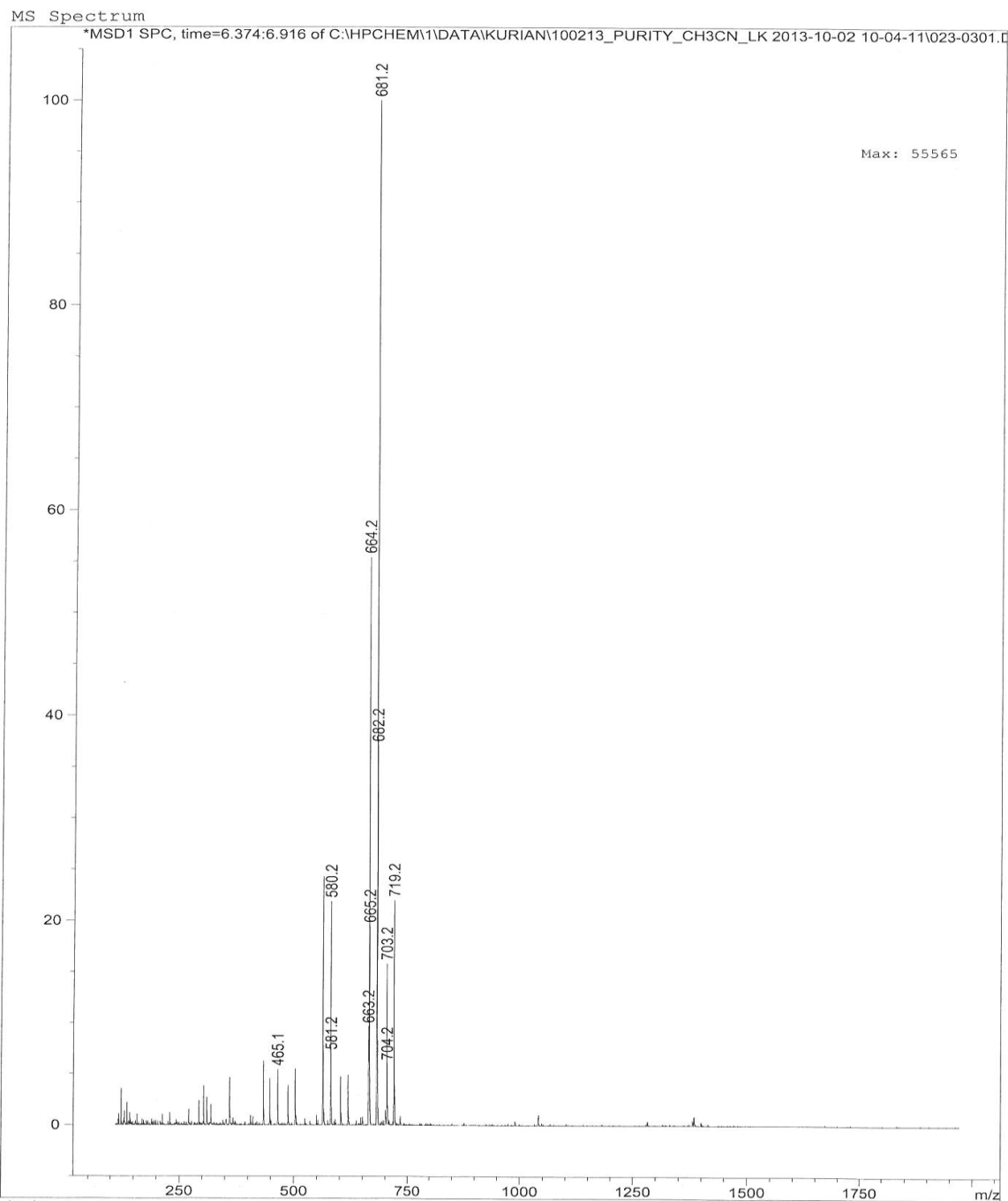


Figure A46. ESI-LCMS analysis of pure Ac-DIYET-NH₂, **2.28**, using a linear gradient 2-90% CH₃OH/H₂O (0.1% FA) over 15 min using a Symmetry Shield C₁₈ reverse-phase column (150 × 4.60 mm, 3.5 μm) set at a temperature of 25 °C at a flow rate of 1 mL/min with positive mode of detection.

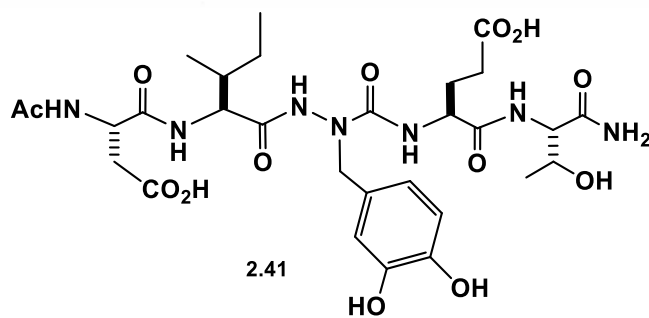
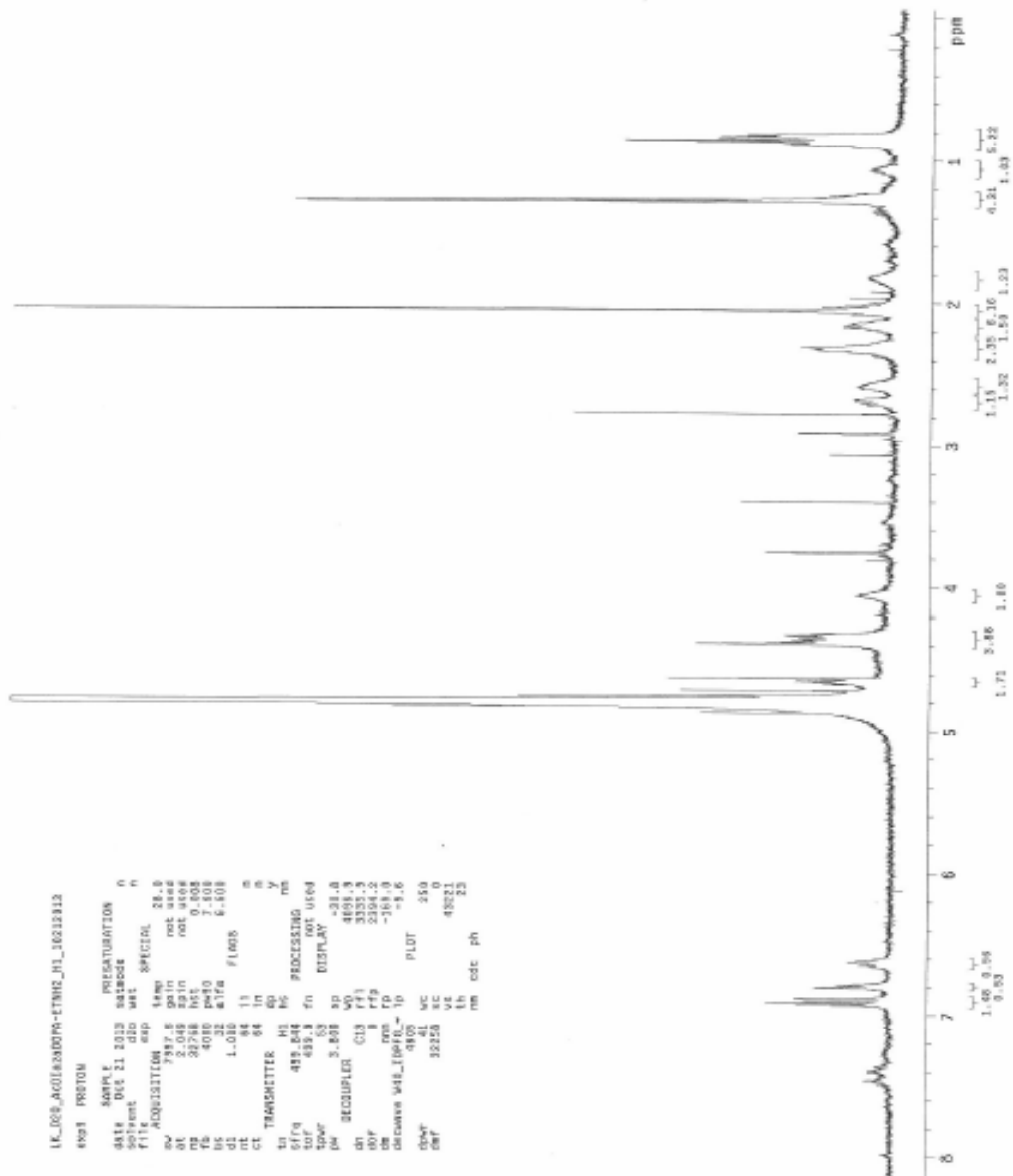
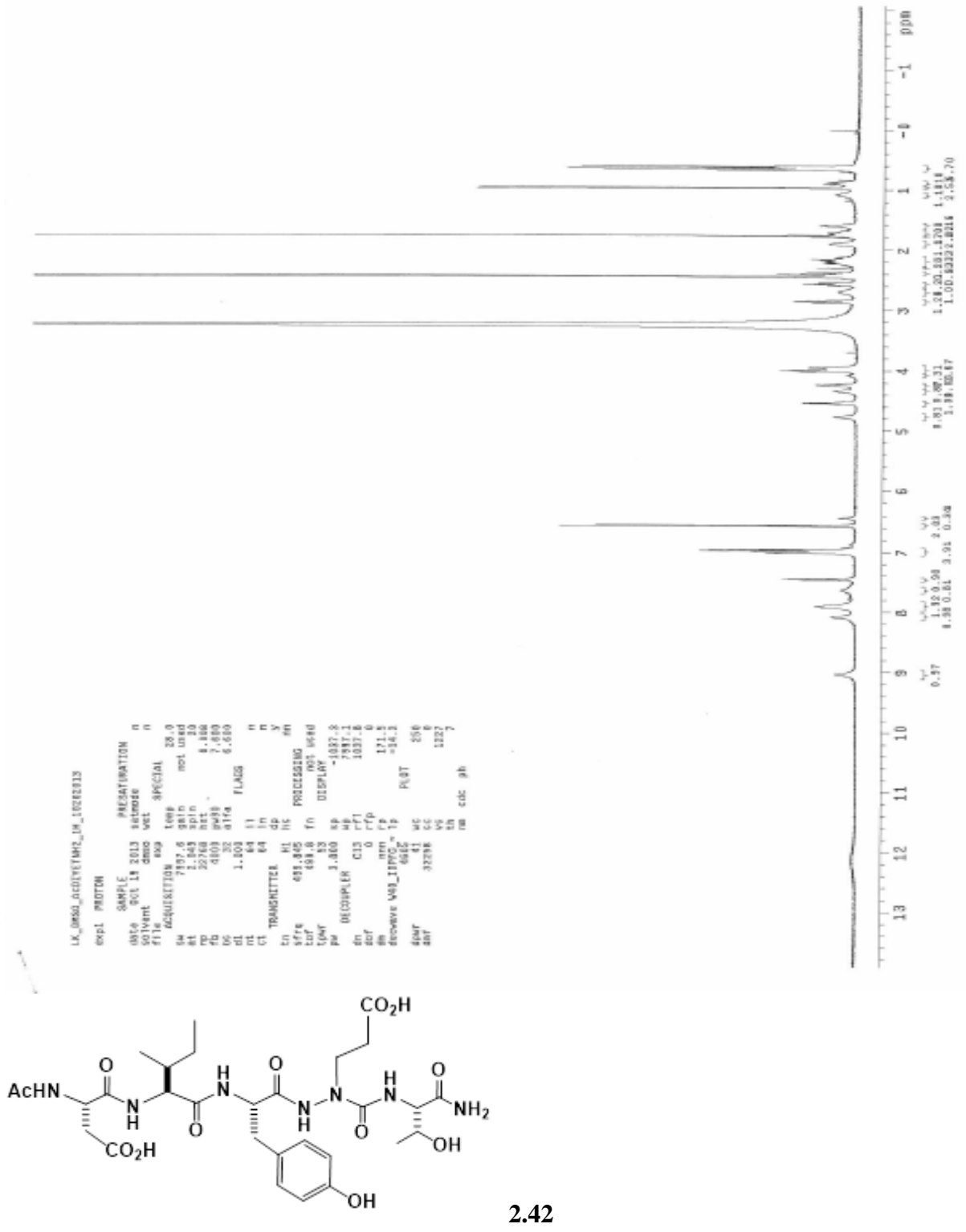


Figure A47. ^1H NMR spectra of Ac-DIaza(DOPA)ET sequence, **2.41**, (2 mM) in DMSO-d_6 .



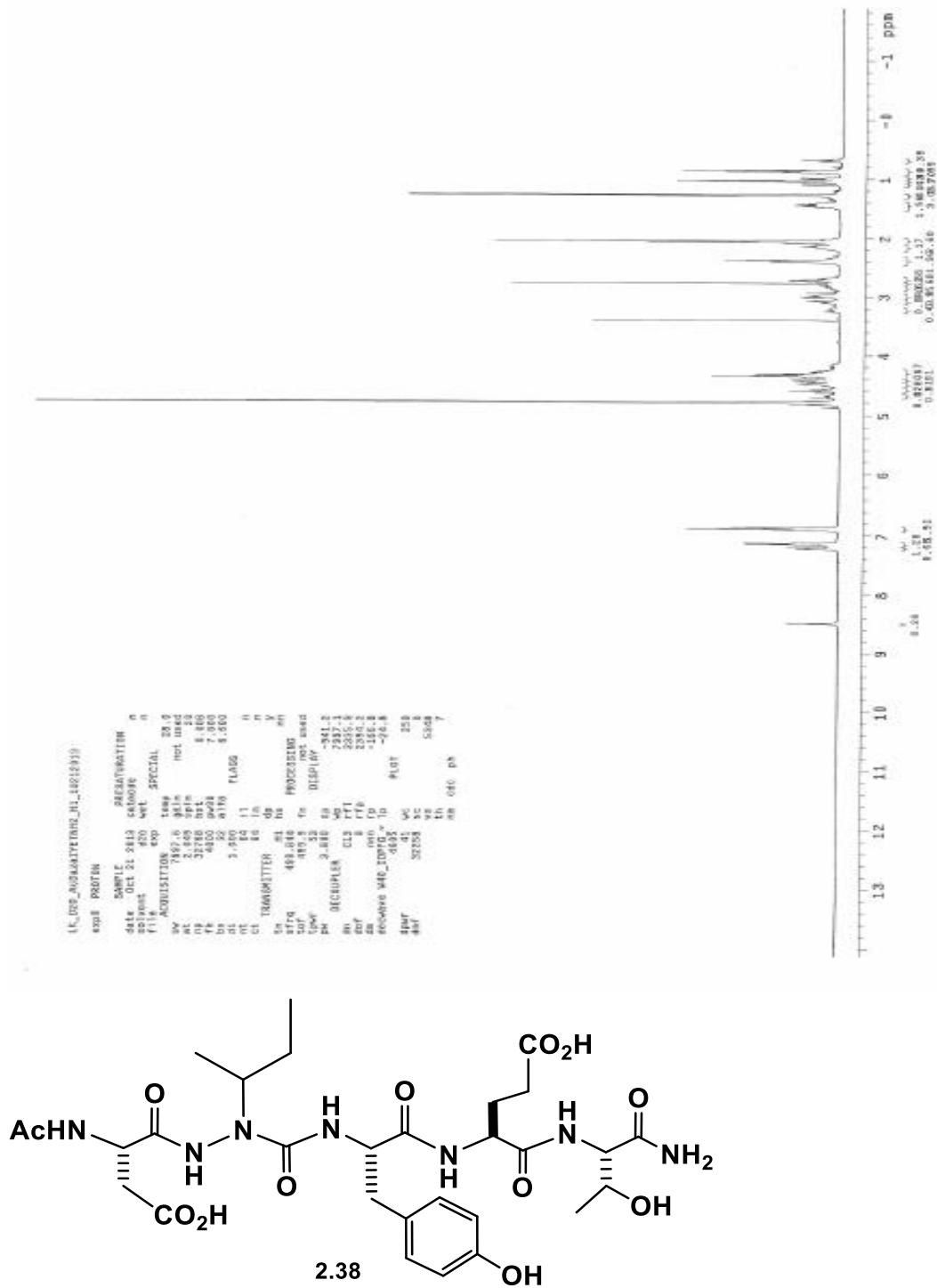


Figure A49. ^1H NMR spectra of Ac-DazaIYET sequence, **2.38**, (2 mM) in DMSO-d_6 .

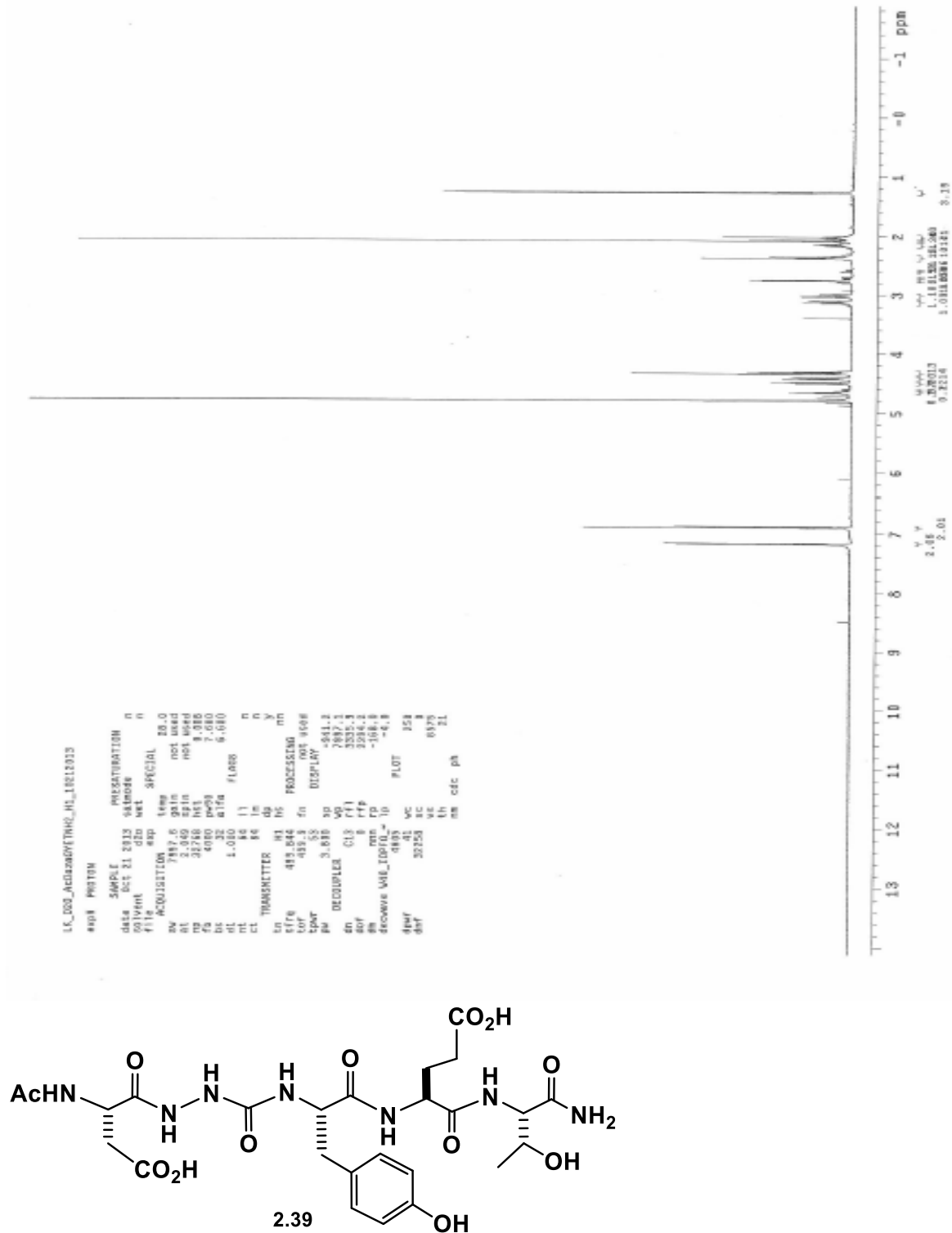


Figure A50. ¹H NMR spectra of Ac-DazaGYET sequence, **2.39**, (2 mM) in DMSO-d₆.

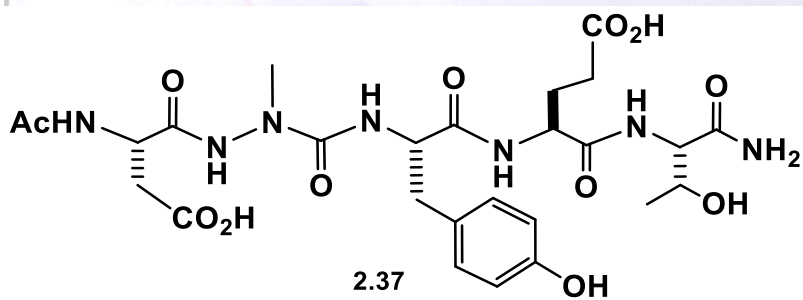
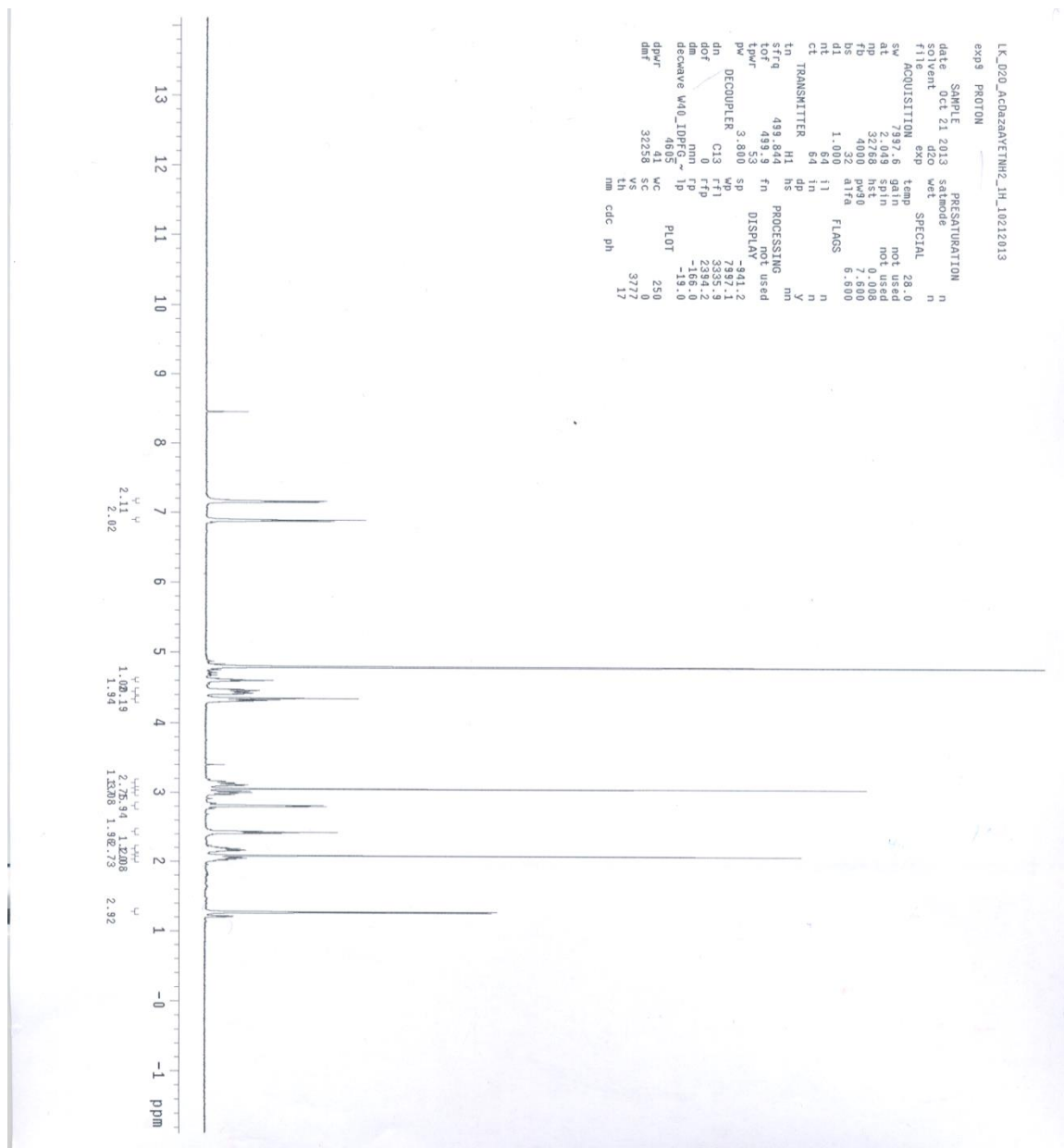


Figure A51. ^1H NMR spectra of Ac-DazaAYET sequence, **2.37**, (2 mM) in DMSO-d_6 .

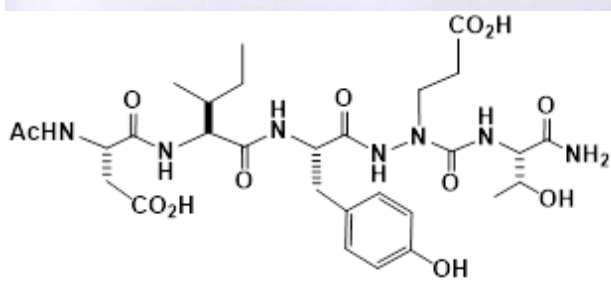
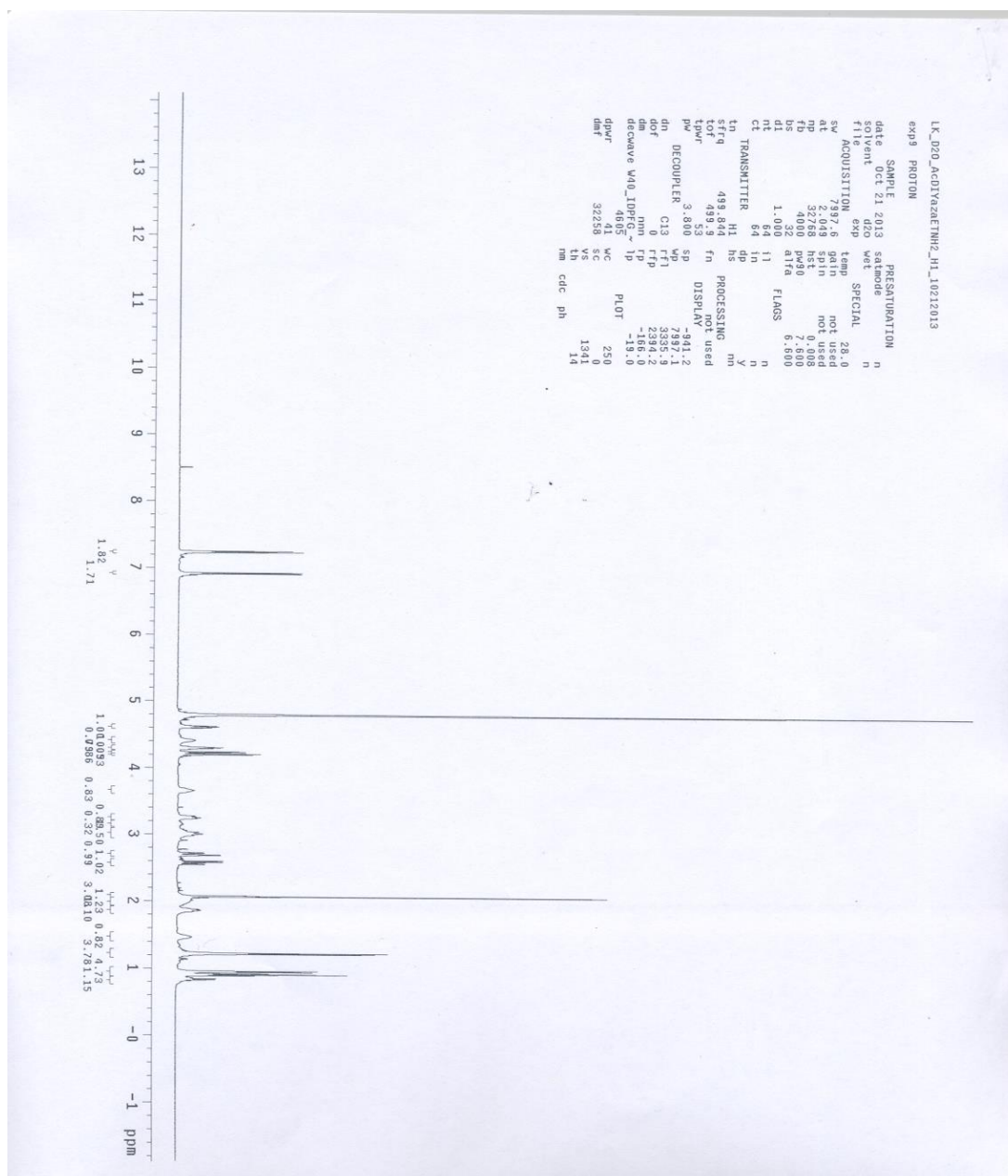


Figure A52. ¹H NMR spectra of Ac-DIYzaET sequence, **2.42**, (2 mM) in DMSO-d₆.

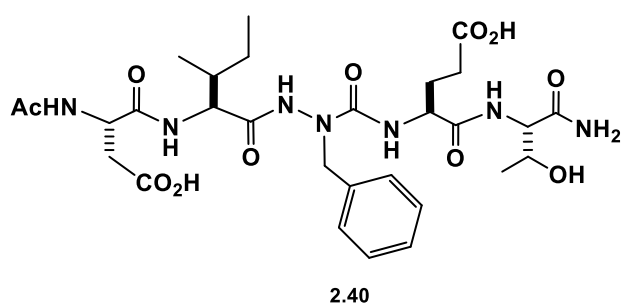
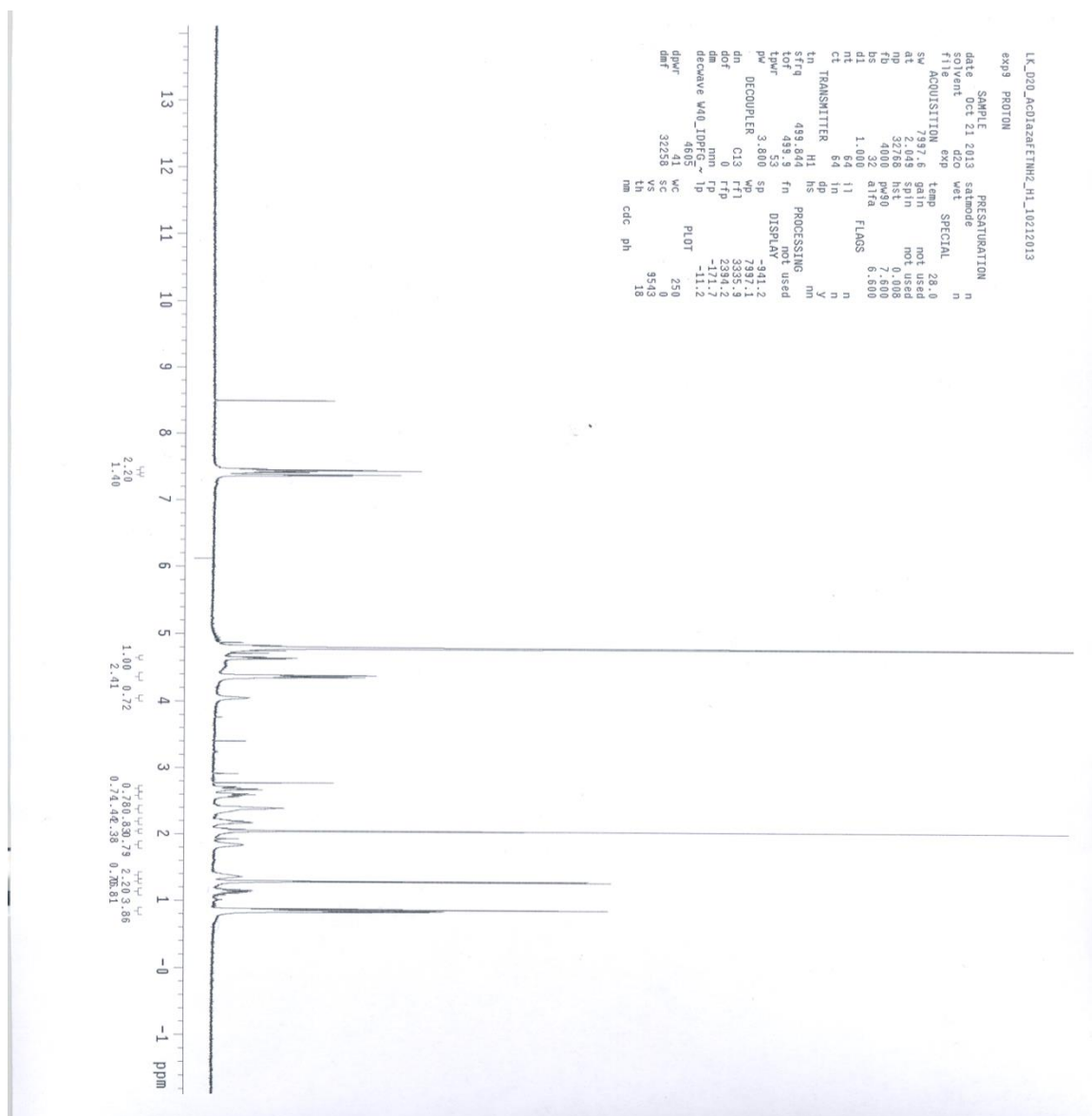


Figure A53. ^1H NMR spectra of Ac-DIazaFET sequence, **2.40**, (2 mM) in DMSO-d_6 .

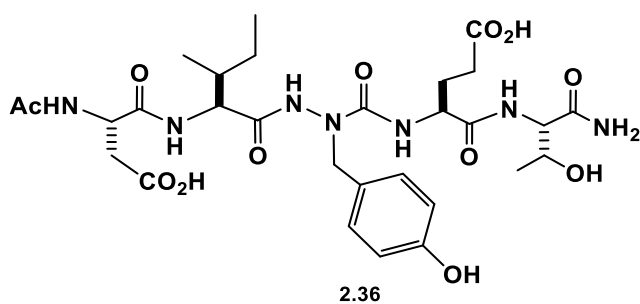
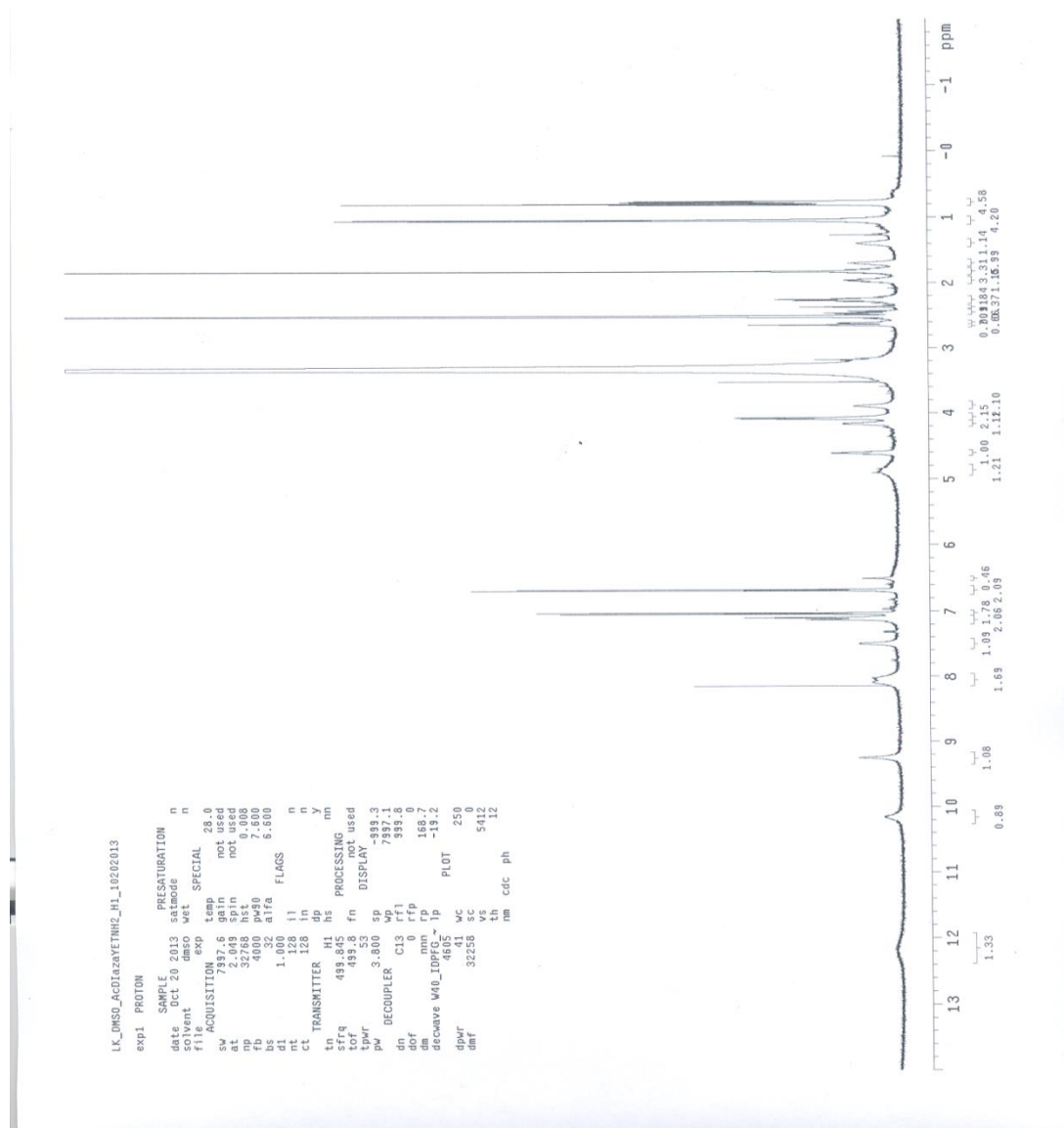


Figure A54. ¹H NMR spectra of Ac-DIazaYET sequence, **2.36**, (2 mM) in DMSO-d₆.

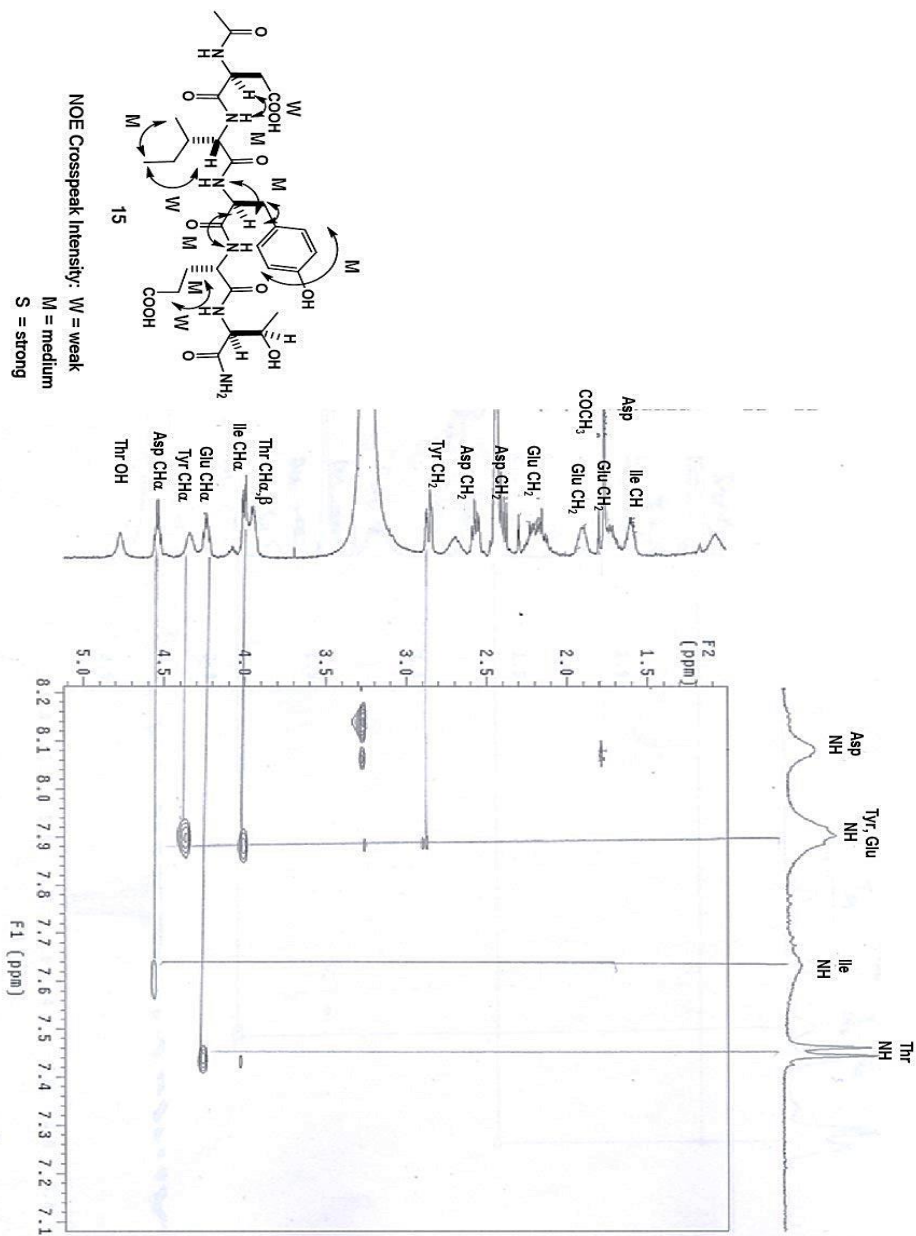


Figure A55. 2D NOESY spectrum and conformational analysis of Ac-DIYET-NH₂, **2.28**, (2 mM) in DMSO-d₆.